FADI ADNAN ABDULRAZZAQ

Doctor of Philosophy

Aston University

2016

Aston University

Title of thesis: Aquasomes as a drug delivery system for proteins and peptides
Name of candidate: Fadi Adnan Abdulrazzaq
Degree to be obtained: PhD in health sciences
Year of submission: 2016

Summary of Thesis

Aquasomes are nanocarrier systems consist of three distinctive layers; an inner core, a polyhydroxy carbohydrate layer and an outer layer of an API (Kossovsky *et al*., 1991). Aquasomes have a unique structure and ability to carry active molecules through a non-covalent bounding and provide superior stability, especially for proteins and peptides (Masatoshi and Yongning, 1998; Kim and Kim, 2002; Khopade *et al*., 2002). Different core and coating materials were used to prepare aquasomes under different conditions to investigate the relationship between preparation conditions and loading efficiency. In terms of loading efficiency, hydroxyapatite aquasomes, with either lactose or trehalose as a coating material, had the highest BSA loading (40%-60%) when compared to DSPA aquasomes. While DCPA aquasomes, with either lactose or trehalose as a coating material, had the lowest BSA loading (8%-16%). To investigate the interaction of the three layers of aquasomes, Surface analysis, docking and MD simulations were performed. Surface analysis performed by Discovery Studio showed that HA and trehalose interact by hydrogen bonding with the later acting as a hydrogen acceptor, while BSA displayed almost complete SAS and that there are numerous targets for trehalose attachments (no specific active site). MD simulations of BSA performed by AMBER 12 showed a stable MD simulation of BSA for 5 ns. Total energy analysis of BSA on the two conditions performed (300K and 280K) support the experimental data of lower BSA loadings of aquasomes prepared at 40^0C compared to those manufactured at 25^0C (p<0.05). This could be related to that BSA might have either started to denature/unfold or breaking up which eventually resulted in low BSA loadings obtained experimentally. The high loading efficiency highlights aquasomes as a promising carrier for the delivery of proteins and peptides. Following formulation Optimisation, two routes of delivery were investigated, pulmonary and oral routes. For pulmonary delivery of aquasomes, BSA-loaded aquasomes were successfully formulated as pMDI and DPI formulations. Both pMDI and DPI formulations were investigated to identify lung distribution of BSA-loaded aquasomes using NGI. *In vitro* release studies on the selected size fractions from NGI show a sustained release of BSA over a period of 6 hr. In order to complement the *in vitro* release data, cell culture studies were performed to demonstrate the controlled release effect of aquasomes with BEAS-2B cell lines. The release of salbutamol sulphate (model drug) from aquasomes post 2 hr started to slow gradually until it reached its highest difference at 6 hr (p<0.05) when compared to the control. For oral delivery of aquasomes, BSA-loaded aquasome tablets were successfully formulated with MCC as multifunctional excipient and talc as a lubricant. Various powder blends of varying aquasomes amounts (25, 37.5, 50, 62.5 and 75%) were prepared and compressed at increasing compression forces (0.5, 1, 2 and 3 tons). It was noticed that under high compression forces of 2 and 3 tons, BSA spreads out of BSA-loaded aquasomes as was presented with confocal microscopy images. Tablets compressed under 1 ton of compression force was therefore chosen for coating as it showed desirable tablet characteristics (hardness, disintegration etc.). Acrylic based coating was used to spray coat the tablets. The coated tablets were found to disintegrate in pH >5.5 and steadily release for 6 hr. Cell culture studies were conducted to demonstrate the controlled release effect of aquasomes using Caco-2 cell lines. The release of metronidazole (model drug) from aquasomes post 2 hr started to slow gradually until it reached its highest difference at 6 hr (p<0.05) when compared to the control.

Acknowledgment

Foremost, I would like to thank my supervisor Dr. Deborah Lowry for giving me the opportunity to conduct this project. I would also would like to thank her for the valuable advice, and willingness, which have contributed tremendously to this project.

I would like to express my sincere gratitude to Professor Yvonne Perrie for her constant support and assistance.

I would like to thank Dr. Lindsay Marshall for her help and support in cell culture work presented in chapter 3 and for her encouragement and insightful commentaries.

I would like to thank Dr. Defang Ouyang for his contribution and assistance in numerous ways to conduct molecular modelling presented in chapter 2.

I would like to thank Jiteen Kansara for his technical assistance and his on-going training throughout the project.

It is also a pleasure to express my thanks to my research group, my friends and lab colleagues who created a friendly atmosphere.

Lastly, yet importantly, I am indebted for the rest of my life to my family for their endless patience and support when it was most needed. My wife, thank you for your love, understanding and patience.

My Dad, you are my star, role model and best friend.

You will always be in my heart and thoughts.

Table of Contents

List of Figures

List of Tables

List of Abbreviations

(ε)	**True Volume Porosity**
ANOVA	**Analysis of Variance**
API	**Active Pharmaceutical Ingredient**
BSA	**Bovine Serum Albumin**
CYC	**Cysteine**
DCPA	**Di-Calcium Phosphate Anhydrous**
DSC	**Differential Scanning Calorimetry**
FDA	**Food and Drug Administration**
FTIR	**Fourier Transform Infrared Spectroscopy**
HA	**Hydroxyapatite**
HIS	**Histidine**
HPLC	**High Performance Liquid Chromatography**
J	**Joules**
K	**Kelvin**
Kg	**Kilogram**
KJ	**Kilojoules**
L	**Liter**
m	**Meter**
MCPA	**Mono-Calcium Phosphate Anhydrous**
mg	**Milligram**
min	**Minutes**
nm	**Nano Meter**
ns	**Nano Second**
P1	**Atmospheric Pressure**
P2	**Pressure Change During Determination**
RMSD	**Root-Mean-Square of Deviation**
RMSF	**Root-Mean-Square of Fluctuation**
SEM	**Scanning Electron Microscopy**

SIESTA	**Spanish Initiative for Electronic Simulation with Thousands of Atoms**
TEER	**Trans Epithelial Electric Resistance**

Research Participations and Papers

Selected list of conference participations

- CRS conference in Quebec, Canada 2012. Aquasomes as protein/peptide delivery system.
- CRS conference in Hawaii, USA 2013. Nanoceramic-based delivery systems for pulmonary drug delivery (DPI type formulation).
- APGI conference in Pisa, Italy 2013. Novel delivery route of ceramic-based nanoparticles for protein/peptide delivery.
- CRS conference in Chicago, USA 2014 (two accepted abstracts) Nanoceramic-based systems for the Oral delivery of Proteins and Peptides // Nanoceramic-based systems for the pulmonary delivery of Proteins and Peptides.
- GPEN conference in Helsinki, Finland 2014. Bio-based formulation of pulmonary delivery of protein and peptides.

List of research papers

- D Lowry and F Abdulrazzaq, 2012. Effect of temperature and time on the coating and loading process of aquasomes manufacture. CRS publications 29 (4).
- F Abdulrazzaq, Yvonne Perrie and D Lowry. pMDI formulation of nanosized ceramic-based self-assembly systems. Manuscript in preparation
- F Abdulrazzaq, Yvonne Perrie and D Lowry. Aquasomes for the delivery of protein and peptides: formulation and *in silico* modelling. Manuscript in preparation.

Chapter 1

Introduction

The process or method which involves the administration of a pharmaceutical compound to achieve a therapeutic effect in humans or animals is called drug delivery. Drug delivery systems (DDS) have been implemented because of their capability of sustaining the duration of therapeutic activity, controlling the rate of drug delivery and/or targeting the delivery of active pharmaceutical ingredient (API). Examples of DDS can include liposomes, gold nanoparticles and polymeric nanosystems. DDS can be classified into delayed release systems, sustained release systems, site-specific targeting systems and receptor targeting systems (Figure 1.1) (Tiwari *et al*., 2012; Ochekpe *et al*., 2009; Gothoskar, 2016).

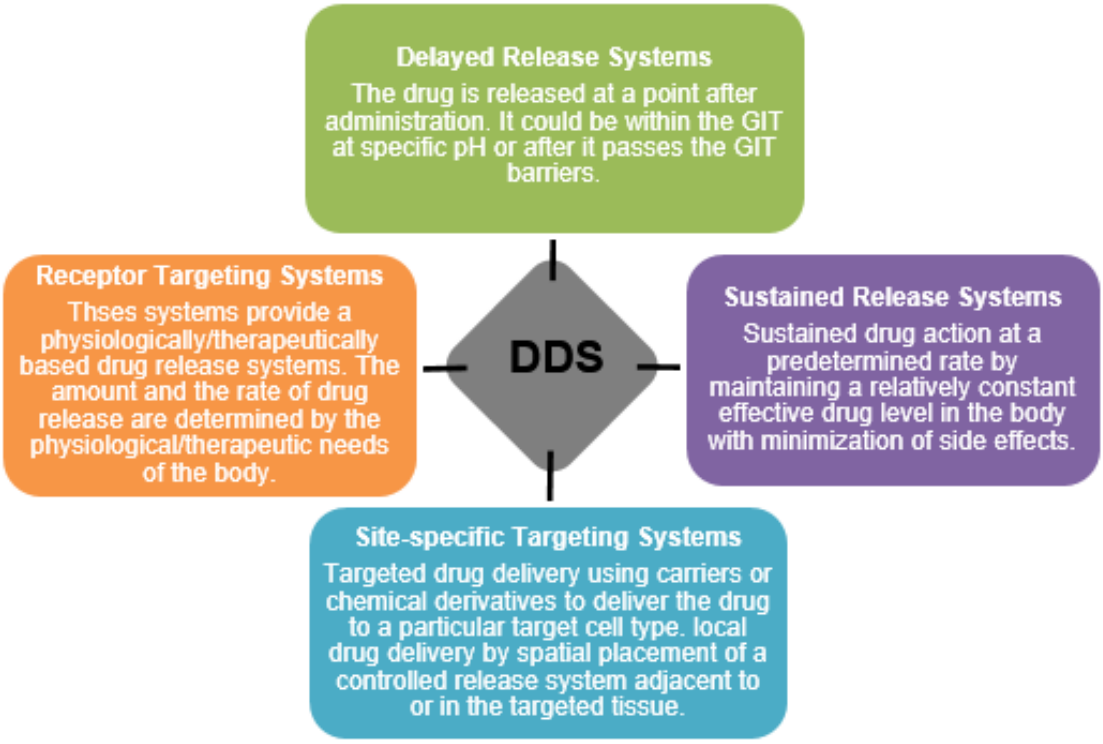

Figure 1.1. A diagram shows the descriptions of the different types of drug delivery systems (modified from: Gothoskar, 2016; Pathak and Thassu, 2007; Ochekpe *et al*., 2009).

The alteration of pharmacokinetics and pharmacodynamics of an API is considered as another tool to control the delivery of drugs besides changing the type of the DDS. Such alteration is achieved by the use of novel drug delivery system and/or the structural or physiological modification of the chosen route of delivery. When it comes to sustain the therapeutic action

of an API, it is preferable to tackle the approach as a design property of a rate controlled dosage form, and less preferable to tackle it as inherited kinetic properties of the drug. Therefore, to design an optimal controlled release system, a comprehensive understanding of pharmacokinetics and pharmacodynamics properties of an API is essential. Insuring patient safety, enhancing patient compliance and efficacy are the principal objectives for a controlled drug release. Precisely, the concentration of an API should reach the therapeutic window, below which no efficacy exerted and above which undesirable effects occur. The main parameter for developing a controlled delivery system for the nominated API is the therapeutic index (Ochekpe *et al*., 2009; Pathak and Thassu, 2007). Table 1.1 lists the main advantages and disadvantages of DDS.

Table 1.1. A table shows the advantages and disadvantages of drug delivery systems (modified from: Dixit *et al*., 2013; Patel, 2010).

Advantages of MDDs	Disadvantages of MDDs
patient compliance	Stability related issues
Less local side effects	Poor *in vitro – in vivo* correlation
Less fluctuation in drug levels which lead to enhanced bioavailability	Possibility of dose dumping. This is can happen outside the patients control such as food content, physiologic changes. It may also can occur when patients chew or grind the dosage form
Reduction in health care costs. The average cost of treatment over a period of time. This is could be to less dosing and side effects. Also the time for patient monitoring and administration is also reduced	The retrieval of dose after toxicity is problematic
	Higher fluctuation in drug levels which lead to reduced bioavailability
Minimize drug accumulation with chronic dosing	Require patient counselling and education
Improve efficiency in treatment	Increased cost.
Cures or controls condition more promptly	

Based on the recent statistics for the worldwide market concerning the top 10 DDS, the market shows an increase in the annual growth of about 113.6.5 $ bn in 2010 to an estimated 175.6 $ bn in 2016 (Figure 1.2). Moreover, the forecast of shares of generic market indicates a rise in the generic market (Table 1.3). The industrial investments in this market are highly competitive and innovative, this is why DDS are under the protection of a fundamental intellectual property. Occasionally, DDS development and manufacture requires a combination of technological acquaintance. Therefore, DDS industry usually requires both licensing practices and the collaboration with two or more parties with shared interests (The Medica, 2009).

Figure 1.2. The worldwide generic market ($ bn) in 2010. It is worth noted that US and Canada combined markets worth more than that of the rest of the world collectively (The Medica, 2009).

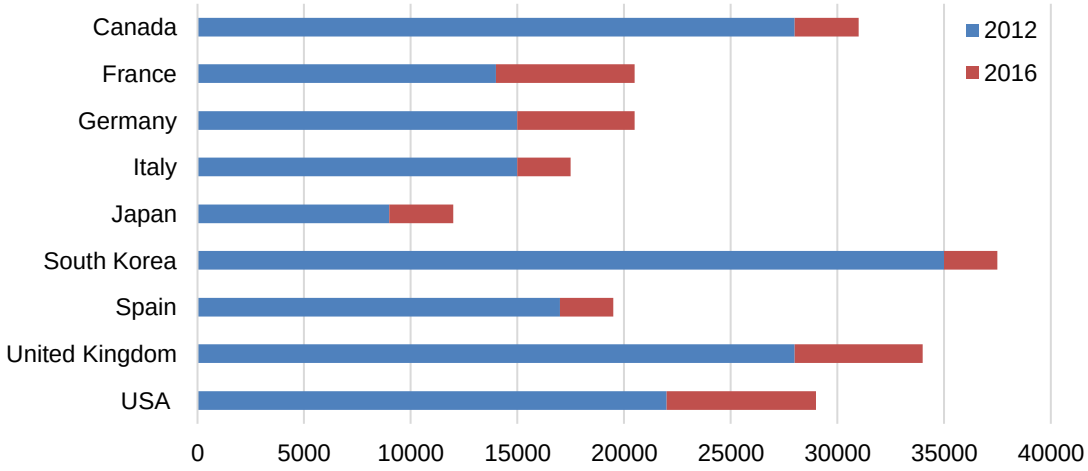

Figure 1.3. The forecast of shares of generic market in 2012 and 2016 (modified from: ReportLinker, 2015). The data highlight the driven interest in DDS by the major pharmaceutical companies and its importance in the pharmaceutical market.

1.1. Nanotechnology

Nanotechnology can be defined as the science at the scale of one-billionth of a metre. From a technological aspect, nanotechnology describes devices, materials and systems presenting new and enhanced physical, chemical and biological features. In general, distinguished properties of the materials are expressed in the nanoscale range of 1-100 nm. Such properties include the increase of the surface area and dominance of the quantum effect, the effect that are highly related with the large surface area and very small particle size to volume ratio. For instance, on a macroscale range copper is opaque however, it changes to transparent in the nanoscale range. A more significant change occurs with gold's physical properties. Based on the nanoparticle size of gold, the melting point ranges between 200-1068^{o}C, however the colour ranges from yellow to blue, pink, violet, and red. At the nanoscale the quantum effects influence the material's electrical, optical, thermal and magnetic properties (Ochekpe *et al*., 2009; Jain *et al*., 2006; Stylios *et al.*, 2005; Cortie, 2004). The importance of nanotechnology as a science and its wide spread benefits in both medical and non-medical areas is well defined by the yearly total spending in this field. Figure 1.4 shows the total spending on nanotechnology area in selected countries.

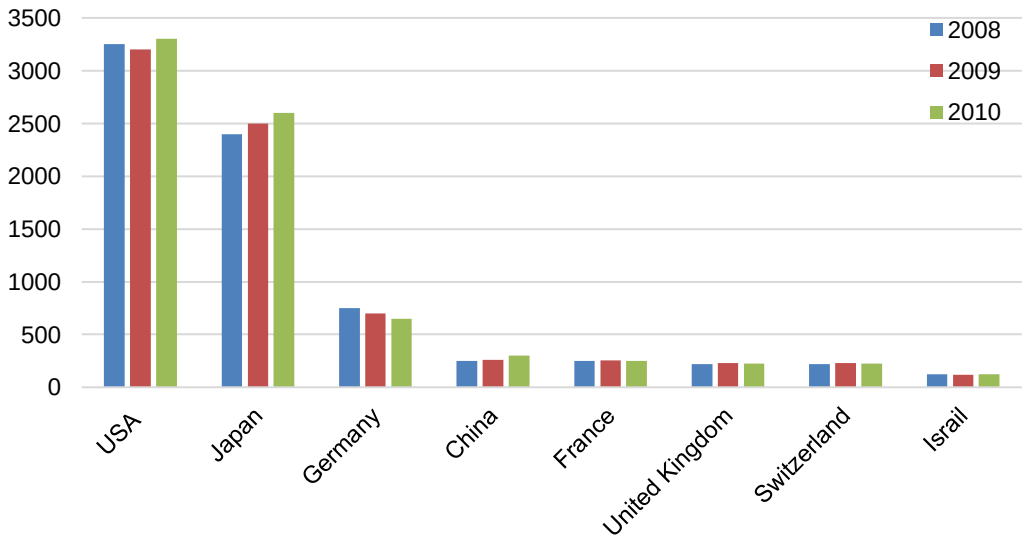

Figure 1.4. The total spending ($bn) on nanotechnology sciences in all areas 2008-2010. The annual increase in spending on nanotechnology hiighlight the importance ofthis field and its wide spread benefits in both medical and non-medical (modified from: Xue and Hwang 2011).

1.1.1. Nanotechnology in drug delivery

Multiple obstacles face nano drug delivery systems, for example the poor solubility/bioavailability of an API, *in vitro* and *in vitro* stability, intestinal absorptions, transmission to the targeted site of action, therapeutic efficacy and fluctuations of the API plasma concentration that either reaches values below the minimum effective concentrations (MEC) or exceeds the minimum toxic concentrations (MTC). The significance of nanotechnology lies with its beneficial employability to overcome the challenges faced in drug delivery, since the nanostructure fabrication at the nanoscale offers various advantages. It is necessary to highlight that the size limit in nanotechnology is meaningless, since DDS practicality and efficiency are not merely based on their size. The domain of DDS ranges from truly nanosystems (e.g. polymer micelles and drug-polymer conjugates) to micro-particles (within the range of 100 μm). Both the nano and micro systems have been highly essential in developing different clinically useful DDS. Highlighting the fact that nanotechnology implicates either nanofabrication or nanonamanufactre and its micro counterparts. Multiple attempts to use various nanoforms have been made to develop DDS, ranging from biological substances like albumin, phospholipids and gelatine for liposomes, to chemical substances such as solid metal-containing nanoparticles (NPs) and different polymers (Table 1.2). Such systems can be designed to contain or carry an API which either absorbed or conjugated onto the particle surface, engulfed or encapsulated inside the lipid/polymer or dissolved within the particle matrix. Such systems offer protection for the API when it faces critical environment or their undesirable biopharmaceutical properties can be disguised or substituted with the nanomaterials properties (Ochekpe *et al*., 2009; Stylios *et al*., 2005). In addition, nanocarriers can preferentially accumulate at inflammatory and infectious sites and tumour by virtue of improved permeability and retention (EPR) effect. Such effect employs site-specific features, which is not related with normal tissues or organs, thus results in increased target selectivity (Stylios *et al*., 2005; Kobayashi, 2014).

Table 1.2. A table shows selected DDS and their descriptions and applications (Gangwar *et al*., 2012).

Carrier	Description	Application
Archaeosomes	Vesicles composed of glycerolipids of Archaea with potent adjuvant activity	Potent adjuvant activity
Cryptosomes	Lipid vesicles with a surface coat composed of PC and of suitable polyoxyethylene derivative of phosphatidylethanolamine	Ligand-mediated drug targeting
Discomes	Niosomes solubilized with nonionic surfactant solution (polyoxyethylene cetyl ether glass)	Ligand-mediated drug targeting
Emulsomes	Nanosized lipid particles (bioadhesive nanoemulsions) consisting of microscopic lipid assembly with a polar core	Parenteral delivery of poorly water-soluble drugs
Enzymosomes	Liposomes designed to provide a mini bio-environment in which enzymes are covalently immobilized or coupled to the surface of liposomes	Targeted delivery to tumour cells
Ethosomes	Lipid-based soft, malleable vesicles containing a permeation enhancer and composed of phospholipids, ethanol, and water	Targeted delivery to deep skin layers
Genosomes	Artificial macromolecular complexes for functional gene transfer. Cationic lipids are most suitable because they possess high biodegradability and stability in the bloodstream	Cell-specific gene transfer
Novasomes	Consist of glyceryl dilaurate, cholesterol, and polyoxyethylene 10-stearyl ether at a weight-percent ratio of 57:15:28, respectively	Drug delivery to pilosebaceous compartment
Photosomes	Photolyase encapsulated in liposomes that release the contents by phototriggered changes in membrane permeability characteristics	Photodynamic therapy
Proteosomes	High-molecular-weight multi-subunit enzyme complexes with catalytic activity that is specifically due to assembly pattern of enzymes	Protein carrier
Transferosomes (elastic liposomes)	Modified lipid-based soft, malleable carriers tailored for enhanced systemic delivery of drugs	Noninvasive delivery of drugs into or across the deeper skin layers and systemic circulation

1.2.1.1. Liposomes

Liposomes are phospholipid bilayer vesicles with an empty centre (Figure 1.5). Liposomes can encapsulate high molecular weight molecules such as peptides and proteins and low molecular weight molecules such as glucose. Water-soluble compounds are present in the aqueous centre while lipid soluble compounds and amphiphilic compounds are imbedded in the phospholipid bilayer. The liposomal formulation can be administrated by many routes, such as intravenous, oral, inhalation, local and ocular applications. Liposomes can be classified according to size: multilamellar liposomes (MLVs) usually range from 500-10,000 nm and unilamellar liposomes. Unilamellar liposomes can be classified as small unilamellar vesicles (SUVs) and as large unilamellar vesicles (LUVs). In size, SUVs are smaller than 50 nm and LUVs are larger than 50 nm (Riaz, 1996; Goyal *et al*., 2005).

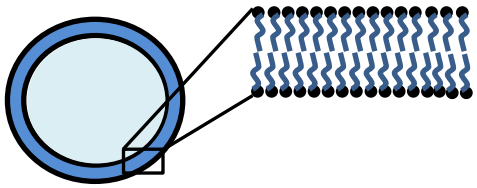

Figure 1.5. A figure shows the structure of liposomes which consists from outer phospholipid layer and inner aqueous core.

1.2.1.1.1. Mechanism of liposomal formation

Owing to their inherit characteristic, phospholipids spontaneously form closed vesicles when hydrated in aqueous media (Figure 1.6). This is because phospholipids are amphipathic in nature (has hydrophilic and hydrophobic tails). The self-assembling property of phospholipid molecules into bilayer sheets leads to the lowering of unfavourable interactions between the solvent and long hydrocarbon fatty chains. This acquires almost maximum stability at a lower energy state. To gain a stable state, the lipid sheets start folding or curl onto itself to form closed vesicles with a central aqueous core (Shehata *et al*., 2008; Goyal *et al*., 2005).

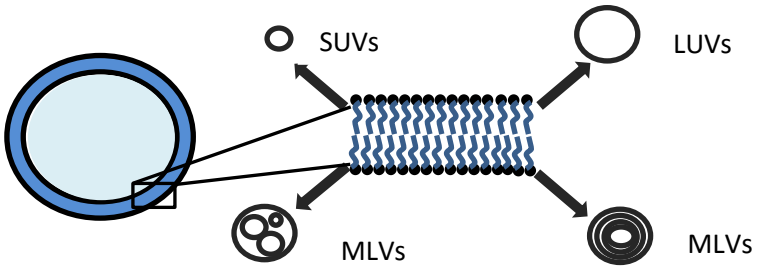

Figure 1.6. A figure shows the types of liposomes according to size (modified from: Riaz, 1996). Unilamellar vesicles are divided to SUVs and LUVs. Multilamellar vesicles are divided to MLVs of multiple size of engulfed liposomes.

1.2.1.2. Recent advances in liposomal research

For more than 40 years in the research area, liposomology has evolved tremendously (Table 1.3). One of the recent advances in liposomology is stimuli-sensitive liposome. These liposomes are triggered to release an API in response to various environmental triggers. Schroeder *et al* (2009) prepared perfluorocarbons gas loaded liposomes which when exposed to ultrasound waves resulted in the release of the loaded gas in the cytoplasm of the targeted cells. Another recent advance in liposomology are virosomes (Figure 1.7). Virosomes are composed from fusogenic viral envelope non-covalently attached to the liposomes. Influenza strain HVJ (hemagglutinating virus of Japan; Sendai virus) were loaded successfully on these liposomes as well as hepatitis B. Therefore, these virosomes could be a promising carrier for anti-cancer drugs (Kaneda, 2012).

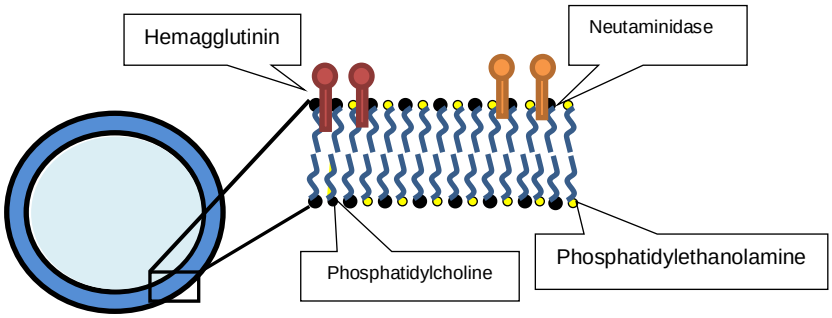

Figure 1.7. A schematic representation of a virosome. Viral envelope non-covalently attached to the liposomes outer lipid layer (modified from: Kaneda, 2012).

Table 1.3. A table shows the development in the liposomology field since first liposomes was proposed as a delivery system in 1965 by Bangham *et al*.

Year	Description of Liposomes	Description of use	Authors
1965	First reported lab made liposomes. The liposomes were made by lipid hydration method.	Liposomes were highlighted as a promotable carrier system.	Bangham *et al.*
1969	Liposomes were incorporated with ^{125}I-iodinated insulin and tested various tissues (e.g. perfused rat heart)	Establish a model system the features necessary for insulin binding	Caygill *et al.*
1979	Liposomes were radiolabelled with radionuclide (^{99}mTc)	Imaging system for lymph nodes and its potential in the detection of tumours.	Osborne *et al.*
1981	Inulin (^{14}C-labelled), entrapped in multilamellar immunoglobulin-G coated liposomes with ^{3}H-labelled cholesterol	Potential of liposomes as a carrier system via pulmonary route.	Shephard *et al.*
1988	Liposomes were encapsulated with different anti-inflammatory drugs glucocorticosteroids, nonsteroidal anti-inflammatory drugs, anti-oxidant enzymes and radioisotopes	A possible way to improve the therapeutic efficacy of these drugs through systemic administration.	Axelsson B.
1991	Liposomes consisting of lecithin and cholesterol were produced using a detergent dialysis technique. Indium was subsequently incorporated into these liposomes.	As a preoperative lymph node staining agent in dogs.	Hirnle *et al.*
1999	Liposomes were prepared by two different methods, the polyol dilution method and the proliposome method. Liposomes were encapsulated with clotrimazole and metronidazole	As a drug carrier system to treat vaginal infections.	Pavelić Z *et al.*
2000	Positivity charged liposomes were incorporated with decompression by lipid hydration method.	Potential of liposomes as a carrier system via intranasal route	Law *et al.*
2008	Multi lamellar liposomes were encapsulated with chitosan–aprotinin conjugate to protect against enzymatic and acidic degradation in stomach.	Potential of liposomes as a carrier system via oral route	Werle *et al.*

1.2.1.1.2. Clearance of liposomes in the body

After parenteral administration of liposomes, they become covered with circulating proteins in the blood stream. Some of these circulating proteins cause disruption to the integrity of the lipid bilayer and eventually results in rapid leakage of liposomal contents. Other liposomes may facilitate antibody recognition and subsequent elimination of liposomes from the blood. For instance, liposomes with unsaturated lipid bilayers (such as ethyl phosphatidylcholine) rapidly lose their membrane integrity and eventually disintegrate. This occurs after high-density lipoproteins insert ApoA1, an apolipoprotein, into the lipid bilayer, which eventually results in liposomal fragmentation (Patel, 1992; Semple *et al*., 1998). Mononuclear phagocyte system (MPS) can eliminate circulating liposomes. These Mononuclear phagocyte systems are present in the bone marrow, liver (Kupffer cells), lung and spleen (Semple *et al*., 1998; Semple *et al*., 1996).

1.2.1.1.3. Obstacles associated with liposomes as a carrier system

There are no doubts about how successful the liposomes are as a carrier system in the delivery of drugs, especially with clinically proven medicines such as DOXIL®. However, liposomes as of many other carrier systems have their own associated obstacles or limitations. For instance, fusion of liposomes can occur due to either an increase or decrease in pH or during storage (aging). This results in an uneven distribution of the dose within the system and eventually affects the system stability (Figure 1.8) (Maurer *et al*., 2001; Connor *et al*., 1985; Austin *et al.,* 1997). In addition, due to their lipid nature, liposomes are cleared by the reticuloendothelial system (RES), primarily in the liver, which results in reduced circulating time (Kamps *et al.,* 1997). Moreover, they are prone to destructive interactions between the drug and the lipid comprising the liposome, which can result in poor stability and eventually failure of therapy. Furthermore, recent studies suggest that liposomes could trigger an immune response, which can lead to serious consciences to the patient's health. (Moghimi and Hamad, 2008; Szebeni and Moghimi, 2009).

Figure 1.8. Two mechanisms (**A** and **B**) proposed for liposomal fusion, in which both results in fusion pore (modified from: Austin *et al*., 1997).

1.1.2.2. Aquasomes

It is well understood the stability of the chemical structure of an API is what provides this API with pharmacological activity. Hence, degradation, a shift or loss of its activity and an alteration in the physical or chemical properties can occur if the chemical structure of this API was affected. However, the spatial qualities are less considered in these circumstances, though it has a profound effect on the API pharmacological activity. The spatial qualities comprise of a freedom of internal molecular rearrangement, freedom of bulk movement and their unique 3D structure (Kossovsky *et al*., 1995; Kossovsky *et al*., 1990). As a nanodelivery system, aquasomes have advantages over other nanodelivery systems, Figure 1.9 highlights the advantages of aquasomes as a drug delivery system.

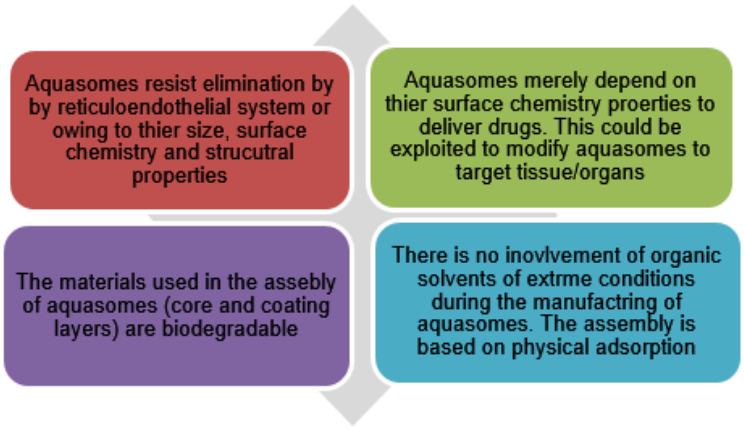

Figure 1.9. The main advantages of aquasomes as a drug delivery system (modified from: Umashankar *et al*., 2010; Jain *et al*., 2012; Kossovsky *et al*., 1995; Vengala *et al*., 2012). The advantages are merely based on the type of the materials that form aquasomes and the preparation method.

Numerous proteins and peptides have been used as therapeutic agents. In the last decade, the use of proteins or peptide-based drugs have increased the management of numerous diseases. It is challenging to deliver these sensitive protein and peptides systemically without the loose of their therapeutic effects (Pontiroli *et al*., 1990; Smith, 1997; Umashankar *et al*., 2010). Nir Kossovsky has proposed a nanocarrier carrier system for the delivery of protein and peptides named ‘’Aquasomes’’. Aquasomes consist of three distinct layers; an inner solid core, a polyhydroxy carbohydrate film and a layer of the active molecule with or without modification (Figure 1.10) (Kossovsky *et al.,* 1995). The unique ability of aquasomes to carry therapeutically active proteins and peptides non-covalently and it superior stability have highlighted them as potential nanocarriers for proteins and peptides (Vengala *et al*., 2012; Khopade *et al*., 2002).

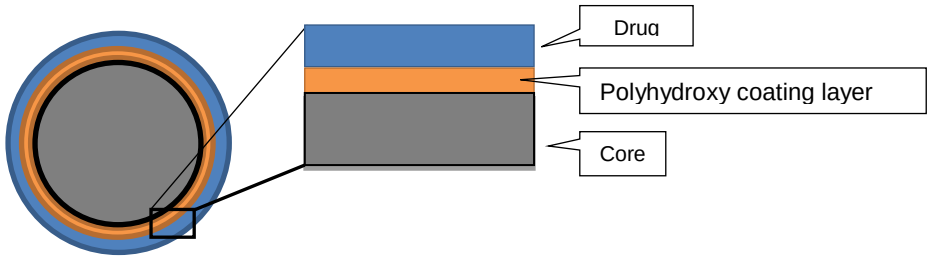

Figure 1.10. A figure shows the structure of aquasomes which consists from inner core, polyhydroxy carbohydrate layer and a drug layer.

1.1.2.2.1. Method of aquasomes preparation

Three main steps are needed to prepare aquasomes. The first step involves formulating the inorganic core, succeeded by core coating with polyhydroxy oligomer and the final step is the loading of the drug (Figure 1.11). The first step is based on ceramic core fabrication, which depends on the chosen materials. Calcium phosphate is the most commonly used ceramic core. The manufacture of calcium phosphate core is based on the use of inverted magnetron sputtering or colloidal precipitation and sonication. These materials are characterised for possessing a high degree of order in the crystalline state, thus ensuring only limited effects can affect the nature of the atoms during the performance of surface modification (adsorption). Moreover, ceramics are ovule shaped and biodegradable. Following the core fabrication, the cores are centrifuged and rinsed with deionised water to remove sodium chloride, which is generated during the reaction. Distilled water utilized to re-suspend the precipitates, which are later either sonicated or filtered using micro filters to collect the desired size. In the second

step of aquasomes preparation, the coating with polyhydroxy oligomer is carried out by adding the coating in an aqueous dispersion of the cores under constant mixing and then freeze-drying. Carbohydrates which are not absorbed are centrifuged in order to remove. During the last step, loading of the drug to the coated cores takes place. A known concentration solution of the drug is mixed with the coated cores and then Freeze-dried to obtain aquasomes (Umashankar *et al*., 2010; Jain *et al*., 2012; Oviedo *et al*., 2007; Vengala *et al*., 2012).

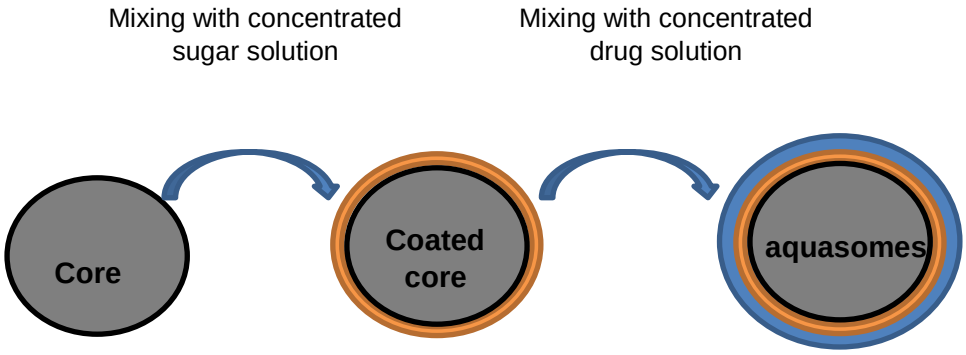

Figure 1.11. A Schematic diagram shows the steps of aquasomes preparation, which are coating the solid cores and loading the drug on the coated solid cores.

1.1.2.2.2. Recent research on aquasomes

He *et al.* (2000) compared the nanoparticulate adjuvant consisting of dihydrogen calcium phosphate anhydrous (DCPA) with the commonly used aluminium (alum) adjuvants concerning its capacity to stimulate immunity towards herpes simplex virus type 2 and Epstein-Barr virus infections. DCPA was observed to cause slight or no inflammatory reactions at the administration site, provide high immunoglobulin G2a (IgG2a) antibody accumulation, neutralize antibodies and ease a high protection percentage towards herpes simplex virus type 2 infections. The animal studies done investigating DCPA revealed that they are highly tolerated, absorbed and caused no side effects at high doses. DCPA are recommended by the authors as an adjuvant instead of aluminium to provide protection against the infection of herpes simplex virus type. Hydroxyapatite has been employed as a core by Khopade *et al.* (2002). Such core was formulated by the use of carboxylic acid-terminated half-generation poly(aminoamine) as templates. Trehalose was utilized to coat the cores and haemoglobin was loaded. The particle size was found to fall within the nanometre range, and the loading efficiency detected to approximately reach 13.7 mg of haemoglobin per gram of the core. Aquasomes were subjected to a study comparing their efficiency in carrying oxygen when

compared to the fresh blood and solutions of haemoglobin. Hill coefficient, an indicator for the binding of ligand to macrophages, was used as a parameter to compare haemoglobin carrying efficiency. The coefficient showed that haemoglobin properties and its oxygen carrying capacity using aquasomes were retained. Aquasomes were subjected to *in vivo* studies as well that showed their ability to retain their oxygen binding for a period over 30 days. Thus, the author deduced that aquasomes possess good potentials to be used as oxygen carriers.

Cherian *et al.* (2000) investigated aquasome employability for parenteral administration. They formulated aquasomes using calcium phosphate core to deliver insulin parentally. Different coatings were suggested such as cellobiose, pyridoxal-5-phosphate and trehalose. Drug loading was followed by the adsorption method. *In vivo* studies were carried out on albino rat for evaluating the different aquasomes formulations. All the formulation exhibited reduced glucose level except of the aquasomes coated with cellobiose, which might be reasoned by the high level of molecular preservation by the pyridoxal-5-phospate coating. These results led the authors to conclude that aquasomes hold a promising carriers for proteins and peptide when administered parentally.

1.1.2.2.3. Clearance of aquasomes

As previously mentioned, aquasomes comprise from three layers that are the core, polyhydroxy oligomer and the drug layer. Calcium phosphate ceramics are commonly used as core material. Monocytes and multicellular cells that are called osteoclasts are the main cells responsible for biodegrading aquasomes *in vivo*. Their efficiency in clearing the aquasomes results from their ability to first intervene at the site of biomaterial implantation during the inflammatory reaction. Biomaterials are reported to be exposed to two different types of phagocytosis, which is either dissolving the calcium phosphate crystals solely in the cytoplasm following the phagosome membrane disappearance or dissolution following the heterophagosomes formation. Calcium phosphate phagocytosis is harmonized with the autophagy and residual bodies accumulation within the cells (Vengala *et al*., 2012; Umashankar *et al*., 2010; Israelachvili, 2003). Other cytokines participate in the inflammatory mechanisms and may be engaged with the biodegradation process (Baumann and Gauldie, 1994). The fate of the carbohydrates layer depends on its type, they enter the metabolic cycles in the body to act as an energy source to breakdown the molecules to its subunits, such as gluconeogenesis and glycolysis (Umashankar *et al*., 2010; Kondoh *et al*., 2005; Vengala *et al*., 2012). The loaded drug on the aquasomes surface may not confront a difficulty with receptor recognition on the active site, thus producing the biological or pharmacological activity.

1.3. Pulmonary Drug Delivery

There are various routes for the delivery of DDS, such oral, pulmonary and parenteral routes. Pulmonary drug delivery has been employed for a long time to aid in treating lung diseases such as chronic obstructive pulmonary diseases (COPD) and asthma. The lungs provide a non-invasive route for systemic administration with the low enzymatic activity and no hepatic first pass effect. Such circumstances make the pulmonary route of administration suitable to deliver small and macromolecular drugs. The anatomy of the lungs offers good bioavailability for macromolecules due to the large surface area of absorption, which reach approximately 100 m^2, with a thin absorption membrane that ranges between 0.1 and 0.2 μm (Table 1.4). In the era of the 19^{th} century, many people were suffering from the asthma that used smoking roll-ups containing stramonium powder that is mixed with tobacco to relieve symptoms (Lenzer, 2006; Wolf, 1998).

Technically, the pulmonary drug delivery route is challenging. Multiple inhalation techniques can influence the extent of the delivered drug to the lungs. However, the pulmonary drug delivery route remains the favoured route for administering various drugs to manage various illnesses. The route is developed to be utilized to treat angina pectoris, bone disorders, diabetes, migraine, acute lung injury, tuberculosis and others. A safe and effective inhalational therapy does not solely depend on the active molecules but on the delivery systems and its application (Tortora and Grabowdki, 2003; Wolf, 1998).

Large quantities of biological and non-biological particulates target the respiratory tract that forms approximately 19,000 L of the inhaled air per day. In pulmonary drug delivery, the drug directly passes to the blood circulation. For instance, using the pulmonary drug delivery for treating obstructive respiratory diseases minimises the required dose and the systemic side effects with the benefit of a rapid response. In the case of the parental route, injections are associated with pain and with hygiene concerns and possible side effects. Nasal drug delivery approach in terms of quantity of the delivered drug to the site of action is insufficient, thus penetration enhancers must be incorporated which might cause local irritation. However, with pulmonary route the research has indicated many molecules are absorbed at the lower respiratory tract and diffuse to the bloodstream naturally with high bioavailability and without the aid of enhancers. Intra-dermal route provides less naturally permeable boundary for macromolecules if compared with the gastrointestinal tract. The device through which proteins are injected to the body like insulin has been available for years. However, such device did not meet acceptance with doctors and the patients as well because of the discomfort accompanied and the possibility of splash back that might transmit blood-borne diseases. The dosage form that serves this purpose is known as aerosols. These dosage forms contain

therapeutically active ingredients, which are dispensed under pressure in a sealed containers and upon the activation of an appropriate valve system a fine mist is released (Aulton and Wells, 1998; Hickey, 1996; Karhale, 2012).

Table 1.4. A table shows the advantages and disadvantages of drug delivery via the pulmonary route (Shaikh *et al*., 2010; Patil and Sarasija, 2012; Karhale, 2012).

Advantages of Pulmonary Drug Delivery	Disadvantages of Pulmonary Drug Delivery
It requires no need of needle to deliver the dose	local side effect due to oropharyngeal deposition during dose administration
It requires minimum dose to achieve therapeutic effect compared to oral delivery	Incorrect use of delivery device which lead to failure of therapy
Local/targeted delivery to the lungs	The mucus layer could limit absorption of drugs.
Compared to oral delivery, onset of action is quicker	Sever Lung condition could limit therapy.
Avoid first pass effect by the liver	Require the use of complex delivery devices specially for DPI formulations

1.3.1. Anatomy of lungs

The nose symbolizes the beginning of the respiratory tract, which terminates deep in the lungs at the alveolar sac. The lungs comprise of more than 40 types of cells, among which more than six line the airways (Figure 1.12). The pulmonary epithelia diversity can be elucidated by the examining the lungs structure from three main levels (Steinhoff, 2013).

1.3.1.1. Nasopharyngeal region

Upper airways are a term used to describe the nasopharyngeal region as well. This region includes respiratory airways, which start with the nose and end with the larynx (Inner Body, 2016).

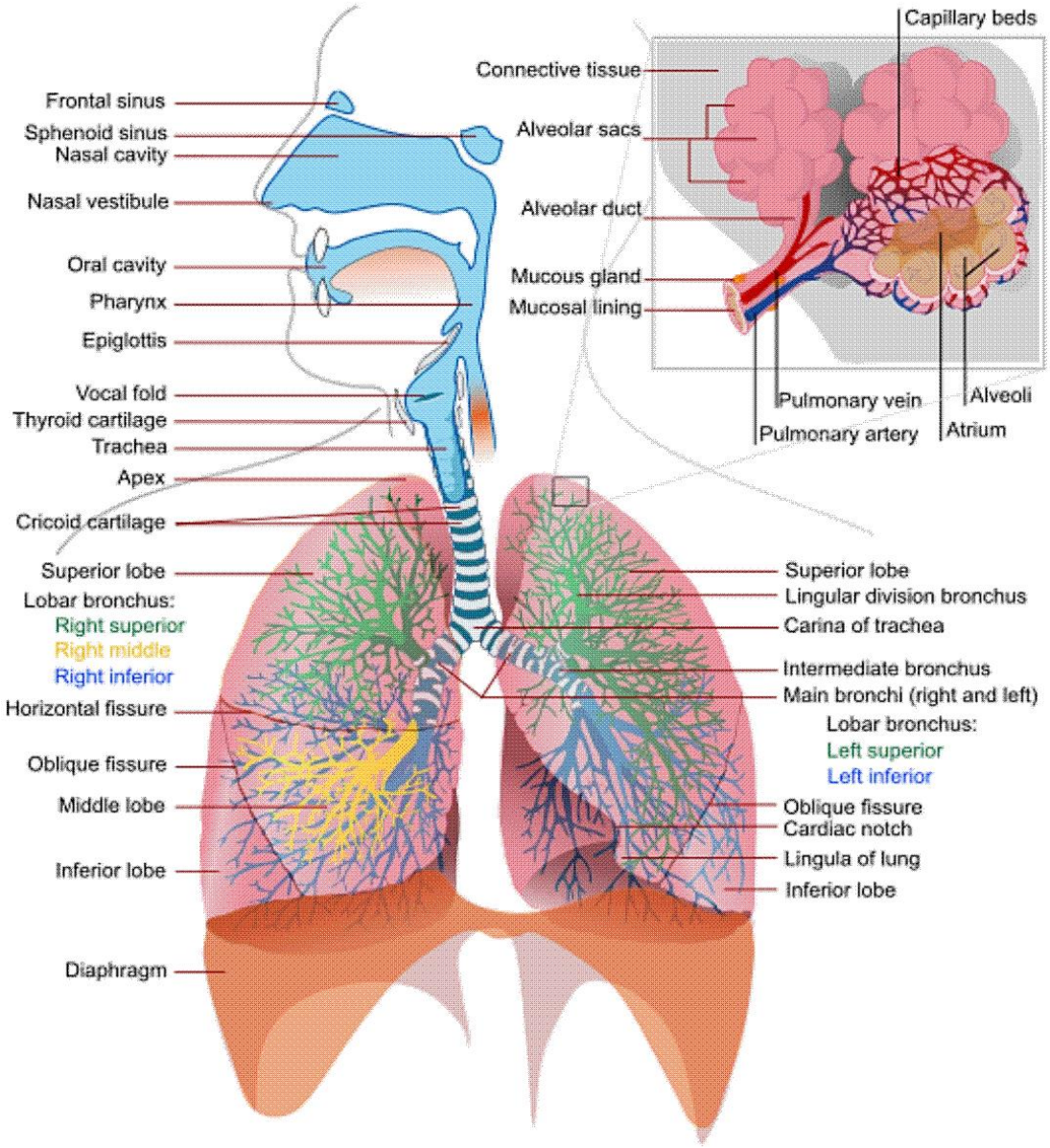

Figure 1.12. A diagram shows the anatomy of the human respiratory system (Health, Medicine and Anatomy Reference Pictures, 2013).

1.3.1.2. Tracheo-bronchial region

The central airways denote the trachea-bronchial region. This region begins with the larynx and goes through the trachea, bronchi and bronchioles then ends with the terminal bronchioles. This region is chiefly lined with ciliated and goblet cells. Some serous cells, clara cells and brush cells are also found with little kulchitsky cells (Dail and Hammar, 2013).

Clara cells secrete uteroglobin, which exerts anti-inflammatory functions and classified as secretoglobins. Despite clara cells abundancy in lungs, their mechanism of function remains vague. Bronchial Kulchitsky cells are disseminated specific cells and recognised by its adjacency to the basement membrane. Multiple studies denoted that they are comprised from electron-dense granules. These granules exhibit similarity with the cells of endocrine function. In addition, the degranulation studies done on these cells claim that such cells have either endocrine or paracrine nature (Dail and Hammar, 2013; Rocicki *et al*., 2016).

1.3.1.3. The bronchioles

Ciliated cuboidal cells predominantly line the bronchioles. The occurrence of serous and goblet cells along the progression of airways decreases while the Clara cells number increases (Dail and Hammar, 2013; Karhale, 2012).

1.3.1.4. Alveolar region

Peripheral airways, respiratory airways or pulmonary regions are all terms that refer to the alveolar region. This region comprises from the respiratory bronchioles, alveolar ducts and alveoli. The alveolar region is characterised by the absence of mucous and has a flatter epithelium, thus becoming the simple squamous type of thickness ranging between 0.1 and 0.5 µm. Type-I pneumocytes and Type-II pneumocytes are the principal cells of the alveolar region. Type-I pneumocytes are characterised by their short length of the airways-blood path in which the drug molecules and gases are diffuses. These cells represent approximately 93% of the alveolar sac surface area; however, their number is less than that of the type-II pneumocytes. Type-II pneumocytes cells have a cuboidal shape. They secret and store pulmonary surfactants. Within the alveolar region the alveolar macrophages account approximately reaches 3% of cell population. These phagocytic cells functions by scavenging and transporting particulate matters to mucociliary escalator and lymph nodes (Dail and Hammar, 2013; Hiralal, 2012; Karhale, 2012). At the level of alveoli, the gases are transferred across the respiratory surface in opposite directions, this biological process is called gas exchange. Oxygen and carbon dioxide are essentially required and generated through the cellular and metabolic reactions. Thus, the existence of an efficient exchange system is essential. The gas exchange results from the diffusion down the concentration gradient (the passage of gaseous molecules from the area of high concentration to the lower concentration) (Dail and Hammar, 2013; Curoservice, 2015; Karhale, 2012).

Oxygen contained within the inhaled air diffuses through the alveolar walls to near capillaries into blood stream, which then carried to the rest of the body by the pulmonary arteries. Carbon dioxide generated through the metabolic processes returns back to the lungs through the blood of the pulmonary veins, which are later diffuses across the capillary and alveoli walls into the air to exhaled (Dail and Hammar, 2013; Karhale, 2012).

1.3.2. Cell culture models for assessment of pulmonary drug absorption

The airways epithelium structure is characterised by being inaccessible and heterogeneous which makes the mechanical evaluation of pulmonary cellular integrity and physiological functions difficult. In order to investigate the mechanisms, which govern drug transportation, precise sampling and dosing, in addition defining the exposed surface area and the local drug concentrations, are considered as essential parameters that are required to be controllable and reproducible. Thus, various airway and alveolar epithelial cell culture models of human and animal origin have been employed as an *in vitro* absorption models (Foster *et al*., 2000; Morimoto *et al*., 1993; Winton *et al*., 1998; Shen *et al*., 1997). These models are comprised from both cell lines (airway) and primary cell cultures (airways and alveolar).

Cultures of primary cells resemble more closely native epithelia. However, these models are more time-consuming and less reproducible if compared with cell line models that decrease their suitability for the permeability screening. Two immortalized human bronchial cell line models have been proposed to investigate the barrier functions of airway epithelia, which are Calu-3 and 16HBE14o- (Winton *et al*., 1998). The adenocarcinoma epithelial cells Calu-3 are of a serous origin obtained from the bronchial airways. They are composed from mixture of phenotypic ciliated and secretory cells (Mathias *et al*., 2002) and from polarized, tight and well differentiated monolayer cells with apical microvilli in air-liquid interface culture (Foster *et al*., 2000; Mathias *et al*.,2002). Recently, cell line models have been employed in experiments investigating the airway drug transport mechanisms (Borchard *et al*., 2002; Florea *et al*., 2001; Hamilton *et al*., 2001a; Hamilton *et al*., 2001b; Mathias *et al*., 2002; Pezron *et al*., 2002). At present, there are no available epithelial cell lines to investigate the functions of the alveolar barrier. Instead, type II alveolar cells that are isolated from healthy human lungs, rabbits and rats in primary cultures have demonstrated to differentiate into type I cells and to produce tight epithelial barriers that exhibit morphological similarity to the *in vivo* alveolar epithelium (Matsukawa *et al*., 1997; Shen *et al*., 1997).

1.3.3. Components of the aerosol system

1.3.3.1. Containers

Glass, plastic, metal or combination of these material are usually utilized to manufacture the aerosol containers. For glass containers, precise designs are essential to give a maximised pressure capacity, impact resistance and safety. Plastics provide a coating either for the glass containers to enhance the safety features or to coat metal containers to increase the corrosion resistance and to improve the formulation stability. Metals usually used to manufacture aerosol containers include stainless steel, aluminium or tinplated steel (Shaik, 2016; Newman, 2005).

1.3.3.2. Propellants

Propellants exert an essential function for the pressurized metered dose inhalers, which is propel contained materials from the container by providing the required pressure within the aerosol system. Propellants are either liquefied or mixture of gases, in which the vapour pressure is utilized to obtain the necessary delivery by spraying the content from the aerosol container (Shaik, 2016; Newman, 2005).

1.3.3.3. Valves

Valves are the components that regulate the active ingredients and propellant flow from the container and determine the aerosol spray characteristics. Rubber, aluminium, stainless steel and plastic are the commonly used materials to manufacture the aerosol valves. Aerosols for oral or nasal application necessitate the use of metered-dose valves in order to ensure uniform dispensation of spay and an accurate dose of the active ingredients. Such function is expected within limited variability at each activation of the valves (Shaik, 2016; Newman, 2005).

1.3.3.4. Actuators

The actuator or adaptor is the device fitted to the stem of the aerosol valve. Upon depression or any other assigned movement, the valve opens and leads the spray to the desired direction (Figure 1.13). The actuator design comprises of an orifice that comes in various sizes and shapes with an expansion chamber. The design is very essential as it affects the physical features of the spray or foam, especially with the inhalation aerosols, since the delivery of the active ingredients must be achieved within a suitable particle size. Usually a proportion of the active ingredients deposit on the inner surface of the actuator indicating that the amount available is less than the released amount by actuating the valve (Shaik, 2016; Newman, 2005; Gothoskar, 2016)

Figure 1.13. A diagram shows MDIs and it valve function. It can be noticed that the actuator is designed to prevent continuous propellant gas exit after a successful puff (modified from Ramteke, 2012).

1.3.4. Inhalers used in pulmonary drug delivery

1.3.4.1. Pressurised metered dose inhalers (pMDIs)

Metered dose inhalers are considered the most commonly used devices in aerosol manufacturing. Propellant is used to disperse the micronized drug. If needed, surfactants are added to avoid agglomerations. The system operates upon actuation which expose the propellant to the atmospheric pressure, which causes aerosolisation of the formulation. The air warms up the aerosol causing the propellant to evaporate, thus reducing the particle size to fall within the desirable range (Finlay, 2001; Gothoskar, 2016).

1.3.4.2. Dry powdered inhalers (DPIs)

Most of the DPIs are designed to contain a blend of micronized drugs and carrier particles to prevent aggregation and enhance aerosolisation. Aerosol DPI activation occurs when the patient inhale and the airflow enters the device to generate turbulence and shear. The air fluidizes the blend of the static powder, thus facilitating the entry to the patient's airway. At the level of airways, the drug's particles dissociate from the carrier particles are travel deep into the lungs, while the large carrier particles collide on the oropharynx and cleared. Therefore, the efficiency of the system drug delivery to the lungs depends on the variable inspiratory airflow of the patient. The main challenge in case of DPIs is dose uniformity. Such challenge

is of a great concern with powders due to the discrete nature and size of the particulates (Gothoskar, 2016; Swain *et al*., 2012; Finlay, 2001).

1.4. Oral Drug Delivery

In addition to the delivery of DDS via pulmonary rout, the delivery of an API via the oral route are considered one of the most used route of delivery compared to all other routes whether the delivery of API was for local or systemic therapeutic effect. The preference of oral delivery over other routes of delivery because it's many advantages. Such advantages include patient acceptance, safe, convenient and relatively simple administration of oral drug formulations. The majority of oral delivery formulations are intended for immediate release rather than controlled or delayed release of an API, because of the fast absorption and metabolism via this route. (Figure 1.16) (Allen *et al*., 2011; Aulton, 2007).

1.4.1. Oral controlled drug delivery systems

Oral controlled release drug delivery system is a system, which releases an API in a constant manner until the API depletion, whether the API release intended for immediate or delayed release, in the GI tract. Such systems can be targeted for a specific part of the GI tract or intended for systemic delivery. For a successful oral delivery formulation, there are main aspects needed to be understood and examined before the formulation process. These factors include pharmacokinetic, physicochemical and pharmacodynamics of the API of interest. In addition to these factors, the anatomy and physiology of the GI tract has an influencing role (Figure 1.14) (Zaman et al., 2016; Aulton, 2007).

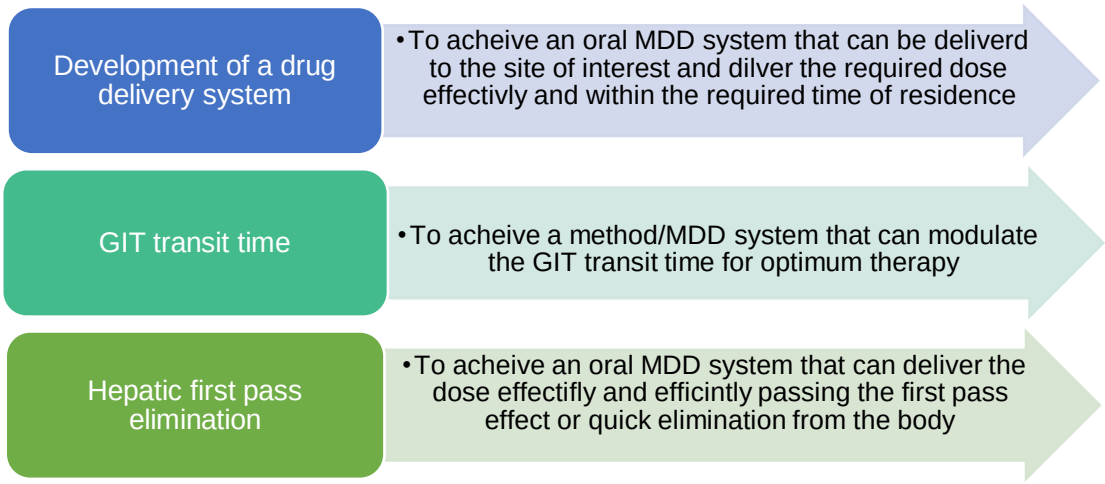

Figure 1.14. A diagram shows the main areas of potential challenge in the development of oral controlled drug delivery systems (modified from: Chien, 1992).

1.4.2. Anatomy of GIT

The gastrointestinal (GI) tract is the system that comprises of organs that receive food, digests it and absorb the nutrients, and expels waste material (Figure 1.15). The GI tract performs four distinct processes ingestion, digestion, absorption and excretion.

1.4.2.1. The Mouth

The first part of the GI tract is the mouth. It includes teeth, tongue, buccal mucosa and the salivary glands. The saliva is secreted in the mouth from exocrine glands. The exocrine glands are parotid, submandibular, and sublingual glands. The saliva secreted in the mouth can be either thick or thin. Thick saliva contains high amounts of digestive enzymes (lipase and amylase), where the thin saliva is mainly for food wetting (Philschatz, 2016; Inner Body, 2016).

1.4.2.2. The Pharynx

The pharynx is located in the region between the throat and neck. It has a dual function in the respiratory and digestive systems, as it prevents the food from directing towards the bronchi through the activation of receptor present on the surface of the pharynx. The pharynx is subdivided into three regions oropharynx, hypopharynx and nasopharynx. (Philschatz, 2016; Inner Body, 2016).

1.4.2.3. The Oesophagus

After the food passes from the pharynx region, the food enters the oesophagus, a muscular hallow tube. The oesophagus is lined with mucous membrane to allow easy passage/swallowing of the food. There are two types of muscles lining the oesophagus, circular and longitudinal layers of muscles. This creates a peristaltic action to help direct the food toward the stomach (Philschatz, 2016; Inner Body, 2016).

1.4.2.4. The Stomach

One the main part of the digestive system and where the food starts to digest by the effect of hydrochloric acid, which is secreted from oxyntic cells. It is a hollow muscular organ. It is positioned above the small intestine and just below the diaphragm. The stomach is connected to the oesophagus via the oesophageal sphincter and to the duodenum via the pyloric sphincter. There are two nerve supplies to the stomach, parasympathetic (stimulant action) and orthosympathetic (inhibitory action). At rest, the volume of the stomach can go low as 50 mL, while at feeding it can go up to 4L (Philschatz, 2016; Inner Body, 2016).

1.4.2.5. The Small Intestine

The majority of the food is digested in the small intestine. The small intestine can be subdivided to the duodenum, the jejunum, and the ileum. The length of the small intestine varies from individual to another; though the range of the length is between 4-6 m. Plicae circulars are permanent folds in the small intestine, which contains numerous villi. The villi are composed from microvilli, which are responsible for food absorption, while the digestive enzymes are secreted from the gallbladder and the pancreas (Philschatz, 2016; Inner Body, 2016).

1.4.2.6. The Large Intestine

The length of the large intestine is approximately 2 m, and it is divided into caecum, the ascending colon, transverse colon, descending colon and sigmoid colon. It is from large intestine where Water is largely absorbed and the food is completely digested by the time it reaches it. However, water-soluble vitamins are absorbed from the large intestine, which generated from the action of the floral bacteria (Philschatz, 2016; Inner Body, 2016).

Figure 1.15. A diagram shows the anatomy of the human GIT tract (Adapted from midlandstech, 2015).

1.4.3. Biological models for assessment of oral drug absorption

1.4.3.1. Human epithelial colorectal adenocarcinoma cell line (CaCo-2)

The typically used model in cell culture studies to represent oral drug absorption are Caco-2 cells. They model the epithelial cells which are the predominant cell type of the GI tract. Caco-2 cells form monolayers when seeded on to cell culture wells or into Transwells®. Oral drug transport studies and nanoparticle release studies are the typical studies performed with Caco-2 cells. Typically, the cells are seeded on to cell culture well plates or into Transwells® which have two compartments filled with media required for the growth of the cells. After cell confluency (18-21 days), the media is replaced with fresh media and cells are ready for the proposed study (Mi *et al*., 2008; Lin *et al*., 2008).

1.4.3.2. Human adenocarcinoma cell line (HT29)

The presence of the mucus layer lining the GI tract has defensive mechanisms. It protects from direct friction of the food to the cells as well as from harmful particles or substances. The mucous layer, therefore, constitutes a barrier in limiting the transport of nanoparticles across the epithelia cell. HT29 cells when seeded with Caco-2 cells, the former differentiate to goblet mucous screening cells. Hence, the model is more representative to the lumen of the GI tract compared to Caco-2 alone (Leibovitz, 1976).

1.4.4. Manufacturing of tablets

There are three methods to manufacture tablets, direct compression, dry granulation and wet granulation. The choice mainly depends on the API. For instance, acetylsalicylic acid cannot be prepared by wet granulation because it hydrolysed to acetic acid and salicylate and eventually leads to loss of therapeutic action. Of the three methods, direct compression remains an attractive option for many reasons. Direct compression methods, by comparison to the other methods, is time efficient, involves less steps and is economically viable (DFE, 2014).

1.4.4.1. Direct compression

Direct compression is by far the easiest method of tablet manufacturing. It comprises from three main steps of lubrication, powder blending, and compaction. The use of excipients is necessary to improve powder flowability (e.g. fillers and binders). Conversely, these excipients are not needed in dry and wet granulation because flow and compaction is enhanced by the flowability of granules. Other excipients such as superdisintegrants are generally used for tablet manufacturing by both wet or dry granulation. Regardless of the accessibility of these materials, direct compression has disadvantages. For instance, it is not suitable for

hygroscopic APIs and high compression forces can trigger physical/chemical interactions or degradation which eventually affect the stability of the APIs (DFE, 2014).

1.4.4.2. Dry granulation

Dry granulation has been increasingly used in the manufacturing of tablets, though it is not a modern technique. The method enhances the flowability of poorly flowable tablets through increasing the particle size prior to direct compression. The same steps in the manufacture of tablets by direct compression are required, with addition of a slug formation step, milling and sieving to the required size. (Stahl, 2014; DFE, 2015).

1.4.4.3. Wet granulation

The use of wet granulation is similar in purpose to the use of dry granulation in that it improves the flowability of poorly flowable powders ready to be tableted using direct compression. The API powder (mixed with tablet excipients) is mixed with water or any binding solution to form large agglomerates/paste. Then, after allowing the powder to dry, the resulted agglomerates/paste are then sieved or milled to the required particle size. Afterwards, the powder is mixed with lubricants, pigments or disintegrants and compressed to form tablets (Figure 1.16) (DFE, 2015; Stahl, 2014).

Figure 1.16. A Schematic diagram shows the process of tablet manufacture using wet granulation method (modified from: Pharm Tips, 2011).

1.4.5. Types of orally controlled release systems

1.4.5.1. Reservoir type

In this delivery system, the API is encapsulated in a polymer. The polymer controls the release of the API. By modifying the polymer type and thickness, multiple reservoir systems can be achieved. For instance, pulse delivery systems are systems in which the first layer is made from fast dissolving polymers which give a bolus effect, where the rest of the system is made of a polymer which dissolves/disintegrates slowly to allow for a delayed release effect (Kost and Langer, 2001; Aulton, 2007; Nokhodochi *et al*., 2012).

1.4.5.2. Matrix type

Matrix delivery systems are the most widely used delayed release systems because the preparation of the APIs and polymer dispersion is relatively easy. In addition, it can be further adjusted for pulse delivery using varying amounts of channelling agents (Kost and Langer, 2001; Aulton, 2007; Nokhodochi *et al*., 2012).

1.4.5.3. Ion Exchange matrix

The API is exchanged from these systems by an exchange process. Ions present in the GI tract get exchanged with resin, which in turn loses its structure and the API starts leaching slowly to the GI tract and gets adsorbed (Kost and Langer, 2001; Aulton, 2007; Nokhodochi *et al*., 2012).

1.4.6. Factors Affecting Oral Drug Delivery

1.4.6.1. Biological half-life

The choice of an API for delayed release formulations depends mainly on its half-life ($t_{1/2}$). This is because an API has to be released in the body at a rate similar to its rate of excretion. If the half-life of an API (such as digoxin $t_{1/2}$=8 hr) is long, the therapy would fail and could cause serious side effects. However, if the half-life of the API such as levodopa ($t_{1/2}$=3 hr), delayed effect can be beneficial in reducing the dose frequency and maintaining a prolonged therapeutic effect (Choudhary, 2014; Song, 2014).

1.4.6.2. Absorption

In the formulation of delayed release systems, the API release should not be faster nor slower than its absorption rate. For instance, if the API were released faster than the absorption rate, it would cause both local and systemic side effects, such as the case with furosemide. Conversely, if the API release was slower than its absorption, the minimum therapeutic dose would not be met (Choudhary, 2014; Song, 2014).

1.4.6.4. Distribution

The volume of distribution (V_d) is another factor that influences the choice of an API to be formulated in delayed release formulations. For instance, an API with a high V_d is not suitable to be formulated for delayed release formulations (such as Chloroquine) (Choudhary, 2014; Song, 2014).

1.4.6.5. Protein Binding

The therapeutic effect of an API greatly depends on the concentration of unbound API in the body. Some APIs have a tendency to highly bind to plasma proteins and this eventually results in a long half-life. Such APIs are not suitable for delayed release formulations (such as Digoxin) (Choudhary, 2014; Song, 2014).

1.5. *In Silico* Biological Modelling

In order to understand how DDS are performing either *in vitro* or *in vivo* situations, molecular modelling can be used to visualise such performance. *In Silico* modelling or molecular modelling is a process by which the energy of a structure is calculated based on the nuclear motion of the atoms. However, the electrons are not included directly in the energy calculation. The main reason to why electrons are not included directly is that electrons are self-arranged according to the position of their parent nuclei. The self-arrangement is based on Born-Oppenheimer approximation. In Born-Oppenheimer approximation, the electrons movement is governed by their weight, heavy electrons move faster compared to slow electrons (Leech, 2001; Richon, 1994).

Molecular modelling process molecules as groups of dots, which are connected by links. Therefore, a separate programming package called force fields are required. Force fields are used to identify molecular geometry and calculate the energy. Force fields are files which contain list of atoms and atom parameters and logarithmic equations for energy calculations. Depending on the use, several force fields can be created. For instance, sp^2-Hybridized and sp^3-Hybridized carbons (tetrahedral) are found in ethyl benzene. The C-C bond present in the benzene ring differs from that in the ethyl chain. Hence, to measure the energy of a molecule, each force potential is calculated separately and the energy of the molecule is the sum total all force potential. (Leech, 2001).

1.5.1. System coordination

It is crucial to specify the atoms and/or molecules positions in the system to a modelling programme. This can be carried out by using two different methods. The first method is to

specify the atoms and/or or molecules using Cartesian coordinates (x, y, z). The other method is to specify the locations of the atoms and/or molecules in relation to other atoms present in the system, such written language is called the Z-matrix (Figure 1.17). System coordination of the Cartesian can be converted to the Z-matrix and vice versa. However, the Z-matrix is usually preferred because it provides a more insight into the location of atoms in relation to each other. Hence, it is the writing method of choice in Quantum Mechanics, where the molecules are studied at the atomic scale. Furthermore, the number of lines that describes a linear molecule are written by Cartesian is less than that of the Z-matrix. Such differences occur therefore because in the Cartesian method, the atoms and/or molecules can be described with liberty (free to translate and rotate) within the Cartesian space without changing their positions (Leech, 2001; Clark, 1985; Richon, 1994).

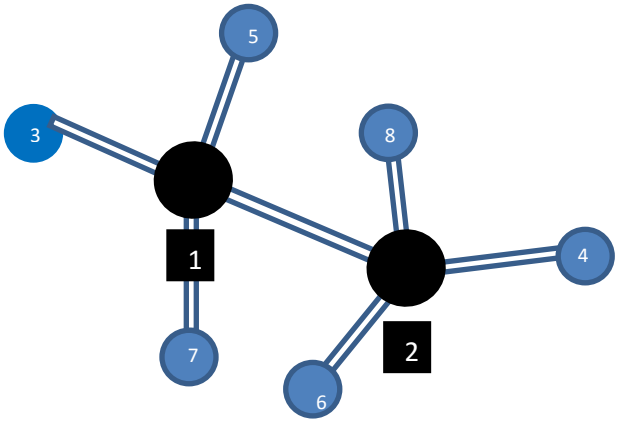

1	C						
2	C	1.54	1				
3	H	1.0	1	109.5	2		
4	H	1.0	2	109.5	1	180	3
5	H	1.0	1	109.5	2	60	4
6	H	1.0	2	109.5	1	-60	5
7	H	1.0	1	109.5	2	180	6
8	H	1.0	2	109.5	1	60	7

Figure 1.17. Z-matrix coordinates of ethane. Z-matrix provide a detailed method of coordination as it provides a more insight into the location of atoms in relation to each other (modified from: Leach, 2001).

1.5.2. Potential energy calculations

Molecular modelling has been used in the study of biomolecules and in bimolecular applications. An X-ray crystallography is necessary to perform molecular modelling. In the

case of the X-ray crystallography is not available, then the data gathered from NMR are combined with raw data from molecular mechanics to build a X-ray crystallography. Molecular modelling studies have proven their value in the study of SARS, binding affinities, nucleic acids and proteins stability that cannot be achieved from still models. A suitable example is the state of thiocamphor/cytochrome P450 complex during oxidation has determined with molecular modelling. (Gelin and Karplus, 1977; Paulsen and Ornstein, 1993).

Despite the valuable advantages of molecular modelling, the method is time consuming. For instance, the pharmacologically active conformation can be missed during the search for the global minima of the structure. This is further exploited if the molecule of interest is an agonist or antagonist. In this case, all low energy conformations have to be examined because not necessarily the conformation of lowest energy is the correct conformation. However, the search of the global minima in the case of small molecules with less numbers of rotating bonds is less time consuming. As shown in Figure 1.18, the torsion angle is driven stepwise with a rotation angle of 360^0 (Leach, 2001; Richon, 1994).

Figure 1.18 A diagram shows the various conformations of butan generated and their energies during a simulation (Richon, 1994).

As the simulation run time increases, the conformations generated for a given molecule, defined as the "non-identical arrangements of the atoms in a molecule obtainable by rotation about one or more single bonds" increases. The hypothetical number of conformation, which

could be generated during simulation, can be calculated using the equation 1 shown below (Smit, 1997; Jensen, 1999).

$$Number\ of\ Conformers = \left(\frac{360}{angle\ increment}\right)^{No.of\ rotatable\ bonds} \quad \text{..... (1)}$$

1.5.3. Mathematical and graphical representations

Molecular structures can be represented by means of graphical model presentations that show atomic geometry and electronic distribution (Figure 1.22). Models vary in simplicity and complexity. To choose between different graphical representations merely depends on the amount of information needed to comprehend and predict the chemical activity. For instance, the models shown in Figure 1.22 are correct. However, each graphical representation provides a different understanding. CH_4O is the simplest representation of methane. However, such representation provides all the necessary information to determine the quantity of CO_2 that is going to be released after burning methane. However, this representation is not sufficient for calculating the hydrogen bonding which could be resulted between molecules. In this case, the Lewis structure representation, which displays the non-bonding pairs of electrons of the oxygen atom, is preferable. Molecules represented by Lewis structures are shown in skeleton, which consist of atoms and their outer shell valence electrons. The importance of Lewis representations is that these representations are simple to draw and the amount of the information concluded from is adequate (Leach, 2001; Smit, 1997; Jensen, 1999).

1.5.4. Software and hardware tools

The performance and price of hardware and software, which are used in molecular modelling, has increased dramatically in the last few years. The speed at which electrical signals can be transmitted is what determines the computer speed. Therefore, there will come a time when no additional improvements can be made to machines with single-processor serial architectures, when the parallel computers will play an important role. A parallel computer couples processors together in such a way that the calculation is divided into small pieces with the results being combined at the end. Some calculations are more amenable to parallel processing than others, and a significant amount of effort is being spent converting existing algorithms to run efficiently on parallel architectures. Graphics processing units (GPUs) have been advanced to contain co-processors for high output to perform high volumes of computational loads. Currently, the crystal structure of biomolecules are large and the time scale used to study them have increased dramatically. Consequently, the community of molecular modelling were the pioneers to adapt computing with GPU. Early efforts to develop

molecular modelling algorithms using GPU computing was a total success. In 2000, semiconductor and microprocessor advances have provided a performance with an exponential growth curve, which eventually increasing molecular modelling applications and widen its capabilities. Although such success in using GPU computing in molecular modelling was valuable, it came to standing point as the demand on high throughput GPU increased. Heat dissipation and power consumption set the limitations for single-core microprocessors. Hence, the molecular modelling community begin the development of multi-core processors to satisfy the increasing demands. Data-parallel co-processors coupled to the usage of GPUs have provided a unique opportunity to increase the efficacy and workloads of desktop workstations and computers and laptops and their softwares, without the need of using remote supercomputers (Figure 1.19) (Leech 2001; Frenkel and Smit, 1997; Jensen, 1999).

Figure 1.19. The advantage of using GPU over CPU in reducing the simulation time for up to a half (modified from: Resse *et al*., 2011).

1.6. Aim and Objectives

The aim of the work included in the thesis is to investigate aquasomes as a nanoparticulate delivery system for the delivery of proteins and peptides via pulmonary and oral routes. To achieve this aim, the following objectives have been sought:

- Optimise a method for the preparation of aquasomes through investigating the effect of variables such as temperature and mixing time and perform MD to understand the assembly of aquasomes at the molecular level.
- Formulate BSA-loaded aquasomes as pMDI and DPI formulations and Investigate the aerodynamic behaviour of the formulations to identify lung distribution of aquasomes.
- Perform cell culture studies with salbutamol-loaded aquasomes in pMDI and DPI formulations as a model drug to demonstrate the controlled release effect of aquasomes with BEAS-2B cell lines (pulmonary route).
- Formulate BSA-loaded aquasomes as direct compression tablet formulations and investigate the effect of compression forces (0.5, 1, 2 and 3 tons) on BSA-loaded aquasomes.
- Perform cell culture studies with metronidazole-loaded aquasome formulations as a model drug to demonstrate the controlled release effect of aquasomes with Caco-2 cell lines (oral route).
- Perform stability studies to establish an understanding of the stability of BSA-loaded aquasome tablets, pMDI and DPI formulations.

CHAPTER 2

Optimisation of Aquasomes Manufacture

2.1. Introduction

Aquasomes consist of three distinct layers; inner solid core, polyhydroxy carbohydrate film and a layer of the active molecule with or without modification (Kossovsky *et al.,* 1995). Various core materials are available to manufacture aquasomes, such as ceramics, gold and diamond. Ceramics are widely used and have a safe profile, hence ceramics was selected to be used as core material. Ceramics can include dicalcium hydrogen phosphate (DCPA), monocalcium dihydrogen phosphate (MCPA) and hydroxyapatite (HA). To investigate their suitability, the three types of ceramics were used in the manufacture of aquasomes DCPA, MCPA and HA. DCPA (CaHPO4) is a natural occurring mineral. DCPA is widely used as an abrasive in medical applications, as a pharmaceutical excipient and in the food industry to increase calcium content (Gbureck *et al*., 2005; Miyazaki *et al*., 2009). MCPA [Ca(H2PO4)2] is a white, odorless, crystalline powder. MCPA can be obtained by heating calcium dihydrogen phosphate monohydrate (MCPM) to temperatures above 100°C. The compound is stable up to around 200°C and decomposes at higher temperatures. MCPA is mainly used in the production of fertilizers (Bohner *et al*., 1995). HA [Ca5(PO4)3(OH)] is a naturally occurring mineral from the family of calcium apatites. Hydroxyapatite is the main constituent of bone matrix (around 90%). Most of the remaining 10% are formed by carbonated apatites. Therefore, hydroxyapatite is the candidate of interest for many types of bone implants. It has the highest hardness when compared to DCPA and MCPA (Furlong *et al*., 1991).

Various disaccharides can be used in the coating step, such as lactose, trehalose, mannose and cellobiose. Lactose is a disaccharide sugar formed from galactose and glucose units. It is a yellowish powder and is soluble in water (216 mg/mL). Lactose is used as filler in capsule and tablet pharmaceutical formulations and as a carrier in dry powder inhalation devices. There are two isomeric forms of lactose, beta and alpha lactose. These isomeric forms are inter-changeable depending on various conditions such as temperature and pH. The beta form is obtained as an anhydrate phase, which has no tendency to form any hydrate phases. On the contrary, the alpha has anhydrous and hydrate forms, from which the anhydrous form is very hygroscopic and unstable (Nickerson T.A., 1979; Zhou *et al*., 2011). Trehalose is a disaccharide sugar formed from two glucose units joined by an alpha glucoside linkage. It is colourless and is soluble in water (68.9 g/100 g). It is very stable under high temperatures and acidic pH environments. The primary use of trehalose is in the processing of foods, other uses include cosmetic production, pharmaceutical preparation and antibacterial sheets (Miller and York, 1998; Schlichter *et al*., 2001). Cellbiose is formed from two joint glucose unites by beta glycosidic linkage. The water solubility of Cellbiose is 5.86 g/L and it is usually prepared from cellulose hydrolysis. It has medical uses such as an agent to indicate malabsorption syndrome

and intestinal permeability in Crohn's disease (HMDB, 2016).

2.1.1. Mechanisms of Self-assembly

If the components of a disordered system form an organized assembly or pattern reversibly as a result of specific or local interactions without external intervention, this is called self-assembly (Jain *et al*., 2006). There are three self-assembly mechanisms electrostatic interaction, hydrogen bonding and Van der Waals forces.

2.1.1.1. Electrostatic interaction

It is the interactions of charged groups such as sulphate, carboxyl and phosphate groups. An example of electrostatic interactions is the interactions of between charged groups of DNA double helixes, which maintain the stability of the tertiary structures of folded proteins (Yang *et al*., 2008; Tam *et al*., 2009).

2.1.2.2. Hydrogen bonding

Hydrogen bond formation is one of the most abundant form of mechanism of self-assembly. As the case with electrostatic interactions, hydrogen bond formation has an important role in the maintain of the stability of the tertiary structures of folded proteins. If hydrophobic molecules are surrounded with water molecules, the molecules tend to repel water molecules and bond together. This tendency to join together decreases the overall level of disorder/ entropy of the surrounding, thus the molecules become self-assembled. In this case, the inability to form hydrogen bonds resulted in the self-assembly of the hydrophobic system. (Gancia *et al*., 2001; Arunan and Mani, 2015)

2.1.1.3. Van der Waals forces

Dipole moment occur when molecules carry less charge than formally charged groups. Van der Waals forces are the forces related with dipole moment. The Van der Waals forces are fundamentally responsible for softness or hardness of a material. (Britanica, 2016; Tavares *et al*., 2004). Van der Waals forces are weaker than chemical bonds and hydrogen bonds. For instance, thermal activity at ambient temperature can disrupt the interactions based on Van der Waals forces (Senese, 2010).

To understand self-assembly at molecular level, molecular modelling (MD) can be used. MD is everything that requires the usage of a computer to draw, label or calculate the properties of the molecules in interest (Pensak, 1989). MD also embraces all methods used in

computational chemistry such as energy minimisation, energy calculation, and molecular dynamics. The identification of moieties responsible for the interaction with an active site allow having an understanding of the mechanisms responsible for the biological activity at the molecular level. The acquired knowledge is aimed at designing new active molecules that can be successfully used as APIs. The calculations are strictly based on the structure being investigated. Therefore, the generated data should normally be supported by experimental results, as MD data could be misleading or inaccurate (Sanchez, 1999).

The energy of a molecule can be calculated using two approaches, quantum mechanics and molecular mechanics. In quantum mechanics, the system is represented as nuclei where electrons spread around the system (electron cloud or electron density). There are many equations that are involved in the calculation of energy in quantum mechanics, such as the Schroedinger equation and the Hartree-Fock equation. The Hartree-Fock equation with the Born-Oppenheimer approximation are preferred method for energy calculations of biomolecules, as the motion of electrons are separated from the motion of nuclei. In the case of molecular mechanics, the electrons of the systems are not taken into consideration and energy calculation of the complex is based on the positions of the nuclei. Hence, the equations set and constraints, which describe the potential surface of a molecule, is called force field (Sanchez, 1999; Morin, 2015).

Energy minimisation or function optimisation in molecular modelling is to find the minimum energy of a given structure or collection of atoms. The reason for finding the energy minimum prior MD simulation is that the energy at this level is equal to the energy of the global minimum. Although it seems an easy step, the minimum energy calculated can score higher than that of the global minima and eventually lead to unreliable MD data. Physically, the process of energy minimization resembles an instantaneous localization of the system at which the atoms are exposed to a net force corresponding to a temperature of 0 K (Steinbach 2010; Sanchez, 1999).

2.1.2. Aim and Objectives

The aim of the work in this chapter is to investigate the various cores, coatings and manufacturing conditions to reach a high loading efficiency of BSA and to provide an understanding of how aquasome layers are assembled at a molecular level using molecular modelling. To achieve this aim, the following objectives were performed:

- Optimise a method for the preparation of aquasomes through investigating the effect of process variables such as temperature, concentration and mixing time.

- Manufacture of BSA-loaded aquasomes using multiple cores and coating materials to reach a high loading efficiency of BSA and optimum release profiles.
- Perform *in vitro* release studies with simulated intestinal fluid to examine the release profiles of the aquasomes.
- Perform stability studies to establish understanding of the stability of aquasomes formulations.
- Determine the forces responsible for aquasome assembly by performing docking experiments using suitable software for the three layers of aquasomes.
- Execute MD simulations to elaborate and investigate the self-assembly of the layers of aquasomes.
- Relate the data generated from MD and docking studies with the experimental data to provide enhanced understanding of aquasomes as a nanocarrier system.

2.2. Materials and Methods

2.2.1. Materials

Anhydrous calcium hydrogen phosphate (99%), lactose anhydrous powder (99%), trehalose powder (99%), mannitol powder (99%), potassium bromide powder (99%) D-Mannose powder (99%), Avicel powder (99%) D-galactose powder (99%), xylitol powder (99%), silicon nanoparticles (99%) D-sucrose powder (99%), cellobiose powder (99%), D- arabinose powder (99%) D-galactose powder (99%), D-ribose powder (99%), D-fucose powder (99%), D-mannose and lyophilized Bovine Serum Albumin powder (99%) were purchased from Sigma Aldrich, UK. HPLC grade acetonitrile and trifluoroacetic acid (TFA) of 99% purity were also purchased form Sigma Aldrich, USK. All materials were used as received unless otherwise specified. Ultra-pure grade water was used when required.

The materials section also includes the software used in molecular modelling and the computers used to operate them.

2.2.1.1 Scigress 7.7

Scigress 7.7 is one of the programmes used in the docking studies, primarily for docking ligands into active sites of proteins. It can also be used to measure other important features that describe the interaction between two molecules such as heat of energy, energy of interaction and optimization energy (FQS, 2016). The Scigress 7.7 software was used to draw and perform minimisation of HA and BSA, preparation of the HA and BSA for MD simulation in AMBER and to perform docking studies.

2.2.1.2. Assisted model building and energy refinement (AMBER) 12

AMBER is a range of force fields package designed for molecular dynamics of biomolecules. The AMBER package was first developed by Peter Kollman's group at the University of California, USA, Case *et al.*, 2012. AMBER was used to perform MD simulations of HA and BSA protein.

2.2.1.3. Accelrys discovery studio v3.5

Discovery studio has numerous uses such as visualising and editing biomolecules and perform modelling and simulation for macro and micro molecules using the CHARM force field (Accelrys, 2015). Discovery Studio was used to visualise HA, BSA and for the analysis of their interactions. Discovery Studio was also used for surface analysis which includes solvent accessibility surface (SAS), surface charge and hydrogen bond.

2.2.1.4. Visual molecular dynamics (vmd) v19.1

VMD is a visualisation computer programme at the molecular level and it is used for animating, displaying, and analysing systems using three-dimensional (3D) graphics and built in scripts (William, 1996). The VMD programme me was used to extract the compounds conformations from the AMBER MD trajectory.

2.2.1.5. Computer systems

For the modelling and other related work, two high-speed computers were used

- **MSI** based computer which was equipped with 8 nodes CPU at 3000 MHz clocking, 8 Gb of RAM, 2 Gb high definition video card (Nvidia GTX 670 GPU) running on Linux operation system (Ubuntu version 12.04).
- ***HP*** based computer which was equipped with 8 nodes CPU at 2000 MHz clocking, 8 Gb of RAM, 1 Gb high definition video card (Intel chipset) running on Windows 7 operation system.

2.2.2. Preparation of Aquasomes

2.2.2.5. Solid cores

2.2.2.5.1. DCPA cores

10 mL of Ultra-pure water was placed in eight glass containers (Batch No. 1, 2, 3, 4, 5, 6, 7 and 8) which contained 480 mg of DCPA powder followed by vigorous shacking. The samples were further sonicated at amplitude of 10.0 for 30 min using a Soniprep 150 Plus disintegrator (MSE, UK). The samples were then centrifuged at 3000 rpm for 3 min using a Universal 32 centrifugation system (Hettich Zentrifugen, Germany). The supernatants were then discarded and the recovered pellets were taken forward to the coating stage.

2.2.2.5.2. MCPA cores

10 mL of Ultra-pure water was placed in eight glass containers (Batch No. 1, 2, 3, 4, 5, 6, 7 and 8) which contained 480 mg of MCPA powder followed by vigorous shacking. The samples were further sonicated at amplitude of 10.0 for 30 min using a Soniprep 150 Plus disintegrator (MSE, UK). The samples were then centrifuged at 3000 rpm for 3 min using a Universal 32 centrifugation system (Hettich Zentrifugen, Germany). The supernatants were then discarded and the recovered pellets were taken forward to the coating stage.

2.2.2.5.3. HA cores

10 mL of Ultra-pure grade water was placed in eight glass containers (Batch No. 1, 2, 3, 4, 5, 6, 7 and 8) which contained 480 mg of HA powder followed by vigorous shacking (Figure 2.1). The samples were further sonicated at amplitude of 10.0 for 30 min using a Soniprep 150 Plus disintegrator (MSE, UK).

2.2.2.2. Coating stage

The samples containing the solid cores (DCPA, MCPA and HA) powder were divided into sets of eight samples. The first four sets were mixed with a lactose solution of concentration of 0.1 M for 1 hr (at 4°C and 25°C) or for 2.5 hr (at 4°C and 25°C). The recovered coated cores were then centrifuged at 3000 rpm for 3 min, washed to remove unadsorbed lactose and then freeze-dried. The previous procedure was repeated to the other set of four samples to coat with trehalose.

2.2.2.3. Loading stage

The coated solid cores were mixed with 10 mL of BSA solution (1 mg/mL) for 2.5 hr at 4°C and 24 hr at 25°C. The loaded cores were then centrifuged at 3000 rpm for 3 min, washed to remove unadsorbed BSA and then freeze-dried.

2.2.2.4. Freeze-drying Protocol

In the preparation of aquasomes, freeze-drying process was used. The freeze-dryer used was Vir Tis Advantage Plus, USA. A freeze-drying cycle of 24 hr was performed. The cycle consisted of four stages; pre-stage (60 min at -45ºC/no vacuum), primary drying (720 min at -45ºC under vacuum of 400 mbar) stage, secondary drying stage (460 min at -20ºC under vacuum of 400 mbar) and final stage (240 min at 25 ºC). The condenser temperatures set to - 76ºC. Freeze-drying vials and lids were used when required.

2.2.3. Characterisation of BSA-loaded aquasomes

2.2.3.1. Particle size analysis

Size measurements were performed using a Sympatek particle size analyser (Brookhaven Instruments, Germany). A quantity of 100 µg of aquasomes diluted with ultra-pure water were placed in the specified cuvette (4 clear sides cuvette). All measurements were performed in triplicate (n=3) at ambient temperature. The values are reported as mean ± standard deviation.

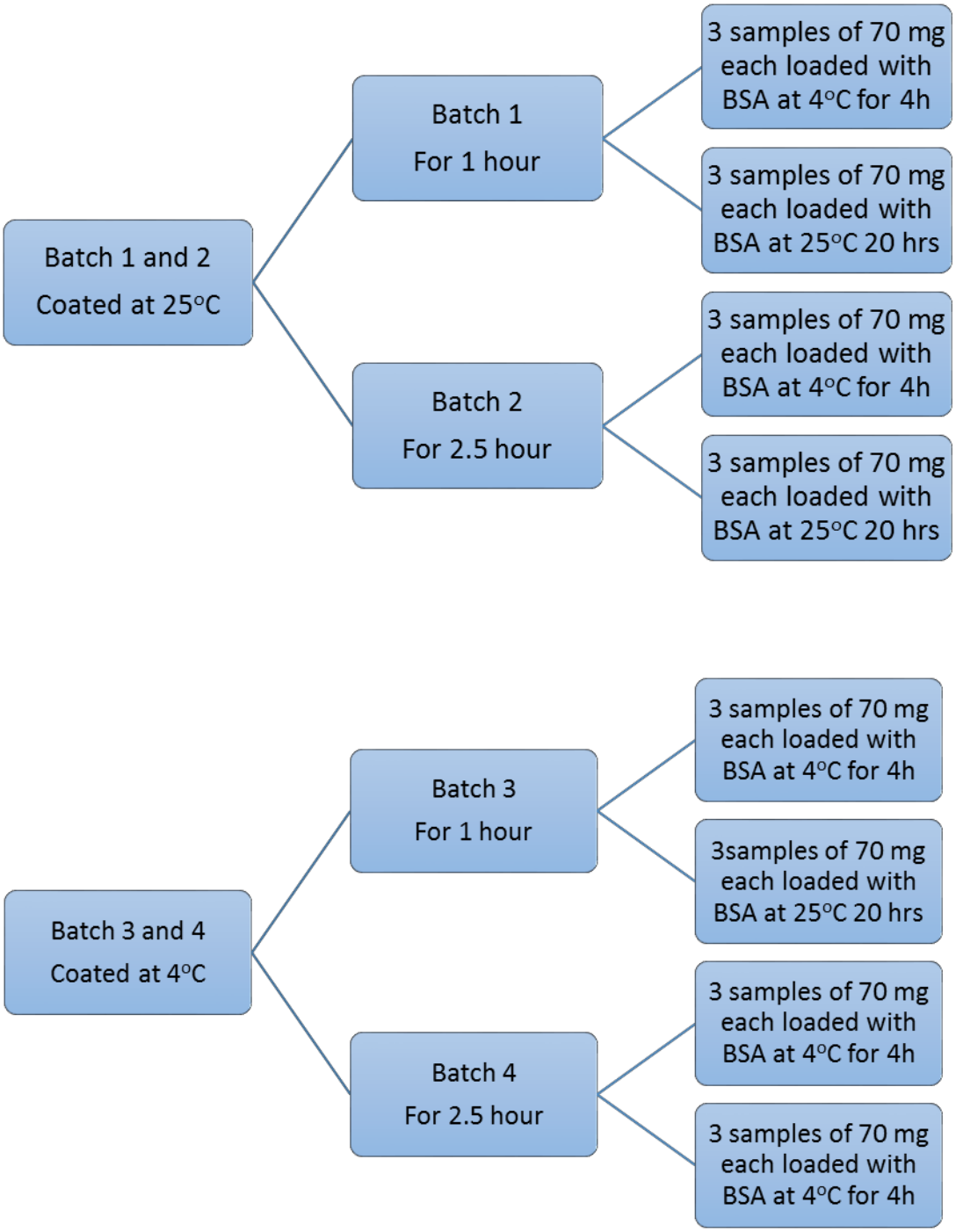

Figure 2.1. Flow chart of the method used to prepare aquasomes with DCPA, MCPA and HA cores with lactose and trehalose as coating materials.

2.2.3.2. Zeta potential measurements

Zeta potential measurements were carried out using a Zetaplus (Brookhaven Instruments, Germany). A quantity of 100 µL sample was placed in the specified cell with an electrode attached to it. All measurements were performed in triplicate (n=3) at ambient temperature. The values are reported as mean ± standard deviation.

2.2.3.3. DSC analysis

DSC analysis was carried out after the coating and loading stages. An amount of 1.2 mg of sample was placed in T*zero* low mass aluminum pan. The samples were then heated from 0°C-350°C at a scanning rate of 3°C/min under nitrogen purge using Q200 scanning calorimetry (TA instruments, USA). All measurements were performed in triplicate (n=3) at ambient temperature. The values are reported as mean ± standard deviation.

2.2.3.4. FTIR analysis

FTIR was used for structural analysis using potassium bromide (KBr) disc method. The KBr disks were prepared using KBr powder (200 mg) with 1% w/w of API. The mixed powders were then compressed at 8 tons for 10 min under vacuum. Infrared spectra were recorded in the wavenumber range of 4000–400 cm^{-1} using IR 2000 spectrophotometer (Thermal Electron Corporation, USA). All measurements are performed at ambient temperature.

2.2.3.5. SEM imaging

The samples were attached onto an aluminum pin stubs with adhesive surface (12.5 mm). The pin stubs were coated with a thin layer of gold using a gold coater Polaron SC500, Polaron Equipment, UK. The samples on the pin stubs were then examined using a Stereoscan 90, Cambridge Instrument. A High vacuum with an accelerating voltage of 20 KV was used to operate the SEM and at 12 mm of working distance in the presence of argon gas, Polaron Equipment, UK.

2.2.3.6. *In vitro* release studies

In vitro release studies were performed on BSA loaded aquasomes formulations. The samples were redistributed in 10 mL of phosphate buffer solution (pH 7.4) and placed in a shaking water bath (37^{o}C/100 rpm). A quantity of 0.3 mL was taken for analysis at a number of time points (1, 2, 3, 4, 5, 6, 7, and 24 hr). A fresh 0.3 mL of PBS was placed back into the samples to maintain sink conditions. Samples were analysed using HPLC with UV and fluorescent detection (section 2.2.3.7).

2.2.3.7. HPLC analysis

Drug analysis from the *in vitro* release studies was measured using an Agilent 1200 series HPLC System with UV and fluorescence detectors (Germany). Analysis was performed at ambient temperatures. For HPLC analysis of BSA, a C18-ODS Jupiter column (4.6 mm x 250 mm / 5 µm / 300 Å (Phenomenex, USA) was used. The injection volume of the sample was set at 100 µL. Fluorescent detection method was used with excitation wavelength was set at 220 nm and emission wavelength was set at 312 nm. A gradient elution method was used during which the proportion of solution B (acetonitrile) in the eluent increased from 5% to 65% solution against solution A (0.01%, v/v trifluoroacetic acid in ultra-pure water) at 1 mL/min a flow rate. BSA eluted with a retention time of 17.0 min. A standard calibration curve was established by the use of BSA standard solutions (r^2 = 0.998), which the concentration of BSA in unknown solutions was determined. The HPLC method was adapted from Umerthia *et al*., (2010).

2.2.3.8. Stability studies

BSA-loaded aquasomes powder were stored at 4ºC ±1ºC/60% RH ±2% RH, 25ºC ±1ºC/60% RH ±2% RH and 40ºC ±1ºC/75% RH ±2% RH in accelerated stability studies cabinet. At interval time points of 0, 7, 14, 21 and 28 days, samples were taken for in vitro release studies (section 3.2.3.6). Visual inspection was performed on the samples, which include changes in colour and peeling. Stability methods were adopted from FDA guidelines Q1A (R2). All measurements were performed in triplicate (n=3). The values are reported as mean ± standard deviation.

2.2.3.9. Statistical analysis

A one-way analysis of variance with Tukey–Kramer multiple comparisons test was used statistically compared the results obtained from performed experiments. The significance level of analysis was $p<0.05$.

2.2.4. Methods of molecular modelling

2.2.4.1. HA cell and HA surface

The structure of HA (ID R100225) was transferred from the American Mineralogist Data Base (AMDB). The structure was then beautified (valence, hyperdization and geometry) using Scigress workstation and then saved as a PDB file.

In order to perform MD simulation with AMBER 12, xLeap was used to build the library of the three atoms comprising the cell of HA (Ca, OH and P) as it was not provided by default. A cell was assembled later on using these libraries. An alternative method was used to build the xLeap library, which are detailed below:

Set up the starting file:
$AMBER HOME/EXE/ANTICHAMBER -i alpha.pdb –fi pdb –o acd.prepin –fo prpi
$AMBER HOME/EXE/ANTICHAMBER –I acd.pripen –f prepi –o acd.frcmod
Setting the library:
$AMBER HOME/EXE/xLeap –s –f leaprc ft99SB
Source leaprc.gaff
LoadAMBER prep acd.prepin
LoadAMBER params acd.frcmod
Complex = copy acd
Edit complex

The coordinates of the cell at this step were ignored, since the purpose is to generate a readable PDB file by xLeap. After file generation, the coordinates were imported for the first PDB file and entered manually to the PDB file generated by xLeap. The final step was to load the PDB file to xLeap and generate a library of the cell unit in order to build a surface of repeated cell units. After the HA surface build, the HA surface was minimized using the Sander programme of the AMBER package. The system was then taken into the first stage of the MD simulation (MD 1). After MD 1 completion, the system was progressed to MD 2 step. The conditions of each step mentioned previously are summarized below.

Stage: Minimization step
Cycles No. 2,000
Minimization method: Initial descent method (conjugate gradient after 1,000 cycles)
Explicit water mode
Cut of distance of 12 Å
Igb (Born approximation) =0
ntb (Periodic boundaries) =1
Fixing the position of coordinated residues
150
RES 1-500

Stage: MD 1
Heating 0 to 300K over 20
ps &cntrl
imin (Minimization) = 0,
irest (Restart simulation) = 0,
ntx (Read of information saved) = 1,
ntb (Periodic boundaries) = 1,
cut (Cut off distance) = 12,
ntr (Flag restrained atoms) = 0,
ntc (System shake) = 1,
ntf (Force evaluation) = 1,
igb (Born approximation) = 0
tempi (Temperature initiation) = 0.0,
temp0 (Temperature maintained) = 300.0,

ntt (Temperature scaling) = 3,
gamma_ln (Collision frequency) = 1.0,
nstlim (Number of MD steps) = 20000, dt (Time of step) = 0.001
ntpr (Frequency of printing) = 1000, ntwx (Write of coordinate) = 1000, ntwr (Write to *restrt* file) = 1000
Fixing the position of coordinated residues
150
RES 1-500

Stage: MD 2
MD run constant pressure
&cntrl
Imin (Minimization) = 0,
irest (Restart simulation) = 1,
ntx (Read of information saved) = 7,
ntb (Periodic boundaries) = 2,
cut (Cut off distance) = 12,
ntr (Flag restrained atoms) = 1,
ntc (System shake) = 1,
ntf (Force evaluation) = 1,
igb (Born approximation) = 0
ntp (Constant pressure dynamics) = 1
tempi = 300.0,
temp0 = 300.0,
ntt (Temperature scaling) = 3,
gamma_ln (Collision frequency) = 1.0,
nstlim (Number of MD steps) =500000, dt (Time of step) = 0.001
ntpr (Frequency of printing) = 1000, ntwx (Write of coordinate) = 1000, ntwr (Write to *restrt* file) = 1000
Fixing the position of coordinated residues
150
RES 1-500

2.2.4.2. Trehalose

The crystal structure of trehalose was drawn using Scigress workstation. After setting the structure, the structure was first beautified and an Augmented MM2 geometry was performed to determine energy minima.

2.2.4.3. BSA

The crystal structure of BSA (ID 3V03) was downloaded from the website of Protein Data Bank (Majorek K.A. *et al*., 2012). The PDB file was processed to be readable by AMBER 12 using Wordpad. The processing of the file includes deleting water molecules, ligands, co- factors and ions and renaming disulphide bridges (CYS-CYS) to (CYX-CYX). The parameter and topology files (PREPIN and FRCMOD) were created using the ANTECHAMBER programme in the AMBER package for BSA. Using the xLeap programme, PREPIN and FRCMOD files of BSA were loaded and the charge of BSA model was neutralised by adding 17 sodium ions. The system was then solvated in an 8-Å (at starting of the protein surface) truncated octahedron of transferable intermolecular potential 3P water molecules (TIP3P). Afterwards, BSA topology and parameter files were generated. BSA was then minimized using the Sander

programme of the AMBER package. The BSA was then processed to the first stage of the MD simulation (MD 1). After MD 1 completion, the system was then progressed to MD 2 step. The conditions of each step mentioned previously are summarized below.

Step: Minimization step
Cycles No. 2,000
Minimization method: Initial descent method (conjugate gradient after 1,000 cycles)
Cut of distance of 12 Å
Igb (Born approximation) =0
ntb (Periodic boundaries) =1

Step: MD 1
MD heating 0 to 300K over 20
ps &cntrl
imin (Minimization) = 0,
irest (Restart simulation) = 0,
ntx (Read of information saved) = 1,
ntb (Periodic boundaries) = 0,
cut (Cut off distance) = 12,
ntr (Flag restrained atoms) = 1,
ntc (System shake) = 1,
ntf (Force evaluation) = 1,
igb (Born approximation) = 1
tempi (Temperature initiation) = 0.0,
temp0 (Temperature maintained) = 300.0,
ntt (Temperature scaling) = 3,
gamma_ln (Collision frequency) = 1.0,
nstlim (Number of MD steps) = 20000, dt (Time of step) = 0.001
ntpr (Frequency of printing) = 1000, ntwx (Write of coordinate) = 1000, ntwr (Write to *restrt* file) = 1000
Step: MD 2
MD run constant pressure
&cntrl
imin (Minimization) = 0,
irest (Restart simulation) = 1,
ntx (Read of information saved) = 7,
ntb (Periodic boundaries) = 0,
cut (Cut off distance) = 12,
ntr (Flag restrained atoms) = 1,
ntc (System shake) = 1,
ntf (Force evaluation) = 1,
igb (Born approximation) = 1
tempi (Temperature initiation) = 0.0,
temp0 (Temperature maintained) = 300.0,
ntt (Temperature scaling) = 3,
gamma_ln (Collision frequency) = 1.0,
nstlim (Number of MD steps) = 20000, dt (Time of step) = 0.001
ntpr (Frequency of printing) = 1000, ntwx (Write of coordinate) = 1000, ntwr (Write to *restrt* file) = 1000

2.2.4.4. Docking of HA and trehalose

The FastDock programme within the Scigress workstation was used to perform docking experiments of HA and trehalose. The conditions of docking are as follows:

Docking method: Rigid active site side and flexible ligands.
Method of docking: Lamarckian genetic algorithm
AMBER van der Waals: Grid Spacing 0.30000 (Å)
Scoring Function: PMF
Size of pop: 50
Rate of Crossover: 0.80000
Maximum Generations: 3000
Rate of mutation: 0.20000
Convergence: 1.0000
Elitism: 5

2.3. Results and Discussion

2.3.1 Manufacture of aquasomes with DCPA cores

2.3.1.1. Preparation of DCP cores

DCPA cores have a high density of 2.89 g/cm^3 and calcium to phosphate ratio of 1.0. A high sonication amplitude was therefore required to break the DCPA cores (Kalita *et al*., 2007). A study carried out by Oviedo *et al*. (2007) prepared DCPA aquasomes loaded with indomethacin. In their study, a sonication amplitude of 90.0 for a duration of 90 min was needed to reduce the mean particle size of DCPA to <400 nm.

In the current study, the size distribution of the DCPA raw powder was heterogeneous and had a mean particle size of 60 µm ±11.5. To reduce the particle size of DCPA powder, DCPA powder was sonicated for a period of 30 min (intermittent) under sonication amplitude of 10.0. After sonication, two particle distributions were obtained (4 µm and 20 µm). Further sonication of 30 min did not result in more reduction in particle size. Alternative techniques such as increasing the depth of the probe and reducing the aqueous medium were employed, but their effect on particle size reduction was not noticeable. Due to the limitation of the machine to achieve higher sonication times (>10.0), the sonicated DCPA cores were used without modification.

2.3.1.2. Coating of DCPA cores

It is known that the higher the concentration of a coating results in higher adsorption onto the cores (Dormant and Adamson, 1968). In the current study, a concentration of 0.2M was used to coat the solid cores. Coating of solid cores at concentration above 0.2M was not desirable, due to viscosity and crystal formation (Crowe *et al*., 1996; Gharsallaoui *et al*., 2008).

The assembly of aquasomes is based on physical adsorption. The method of Oviedo *et al*. (2007) was followed with modifications. The coating was carried out at two different temperatures (25^{o}C and 4^{o}C) and two different mixing times (1 hr and 2.5 hr). The reason for choosing these two variables was to study the effect of coating time and coating temperature on aquasomes preparation.

2.3.1.3. Loading of DCPA cores

BSA has been used widely in research as a module for proteins (Gelamo and Tabak, 2000; Jun *et al*., 2011). In the literature, loading conditions for preparation of aquasomes varied. However, the method of Oviedo and co-workers was followed with modifications as described in section 2.2.2. Two loading conditions were used, 2.5 hr at 4^{o}C or 20 hr loading at 25^{o}C.

2.3.1.4. Size Analysis

Size analysis is a useful tool to measure the particles' size of a given sample before and after modification. Specifically, an increase in the mean particle size of a powder after the coating process is an indication of the presence of a coat covering the particles (Oviedo *et al*., 2007; Keck, 2010).

After sonication of the DCPA powder, two particle distributions were obtained (40 μm and 60 μm). Therefore, it was difficult to relate the effect of different coating and loading conditions to the increase in the mean particle size. In general, all size measurements recorded were above the mean particle size of the DCPA core before coating (51.2 μm ±11.5) (Table 2.1).

Table 2.1. Mean particle size measurements of DCPA cores before and after coating.

Formulation No.		Mean Particle Size (μm)	Formulation No.		Mean Particle Size (μm)
Lactose	1	69.8 ±10.9	Trehalose	5	69.3 ±12.8
	2	66.7 ±12.8		6	68.7 ±12.7
	3	68.4 ±12.8		7	70.5 ±12.3
	4	67.3 ±12.5		8	69.7 ±11.6

2.3.1.5. Zeta potential measurements

Zeta potential is widely used for the quantification of the magnitude of the electrical charge at the surface of a particle. When a molecule undergoes a surface molecular modification, the magnitude of the zeta potential changes. Hence, zeta potential has been used as a tool to confirm coating and loading processes of nanoparticles (Lyklema J., 1995; Borges *et al*., 2005).

Due to the variability in the mean particle size in the samples, the zeta potential measurements were also varied accordingly (Table 2.2). The effect of different coating and loading conditions could not be linked to the increase or decrease in zeta potential measurements. Such variability in zeta potential measurements occur because zeta potential is affected by the size of the particle. For instance, a larger particle will carry more charge when compared to a smaller one (Lyklema J., 1995; Horiba, 2009).

Table 2.2. Zeta potential measurements of DCPA cores before and after coating.

Formulation No.		Zeta Potential	Formulation No.		Zeta Potential
Lactose	1	13.8 ±0.7	Trehalose	5	16.1 ±1.2
	2	14.2 ±0.4		6	15.4 ±0.9
	3	13.2 ±0.8		7	13.2 ±0.8
	4	15.4 ±1.1		8	14.9 ±0.7

2.3.1.6. DSC analysis

DSC is a thermo-analytical technique in which the heat necessary to increase the temperature of a sample is calculated as a function of temperature. It has been used extensively to study polymorphism and glass transition (T_g) (Deangelis *et al*., 2006).

In the current study, Tzero technology and Tzero low-mass pans were used to achieve the most sensitive analysis possible. DCPA powder has high melting and decomposition temperatures (380^{o}C) which could not be measured due to instrument limitation (maximum of 350^{o}C can be measured on the TA Q200). However, both coating materials, lactose and trehalose, decompose at temperatures of 235^{o}C and 150^{o}C respectively (Taylor and York, 1998; Lefort *et al*., 2004).

The DSC peak recorded from the samples show that coatings of lactose or trehalose did not reveal any measured peak at the decomposition temperature of both lactose and trehalose. This could be related to the argument that DSC is unable to detect impurities if it is less than 0.1% (Figure 2.2 and 2.3) (Ceschel *et al*., 2003; Deangelis *et al*., 2006).

However, if the pan lids are removed after the DSC analysis is finished, it can be noticed that the cores are brownish in colour in the case of lactose as it was caramelized at high temperature (>120^{0}C) (Kroh, 1994). However, in the case of trehalose as a coating, the colour was the slightly off white, as trehalose dose not undergo caramelisation at high temperatures (Figure 2.4) (Takanobu, 2002).

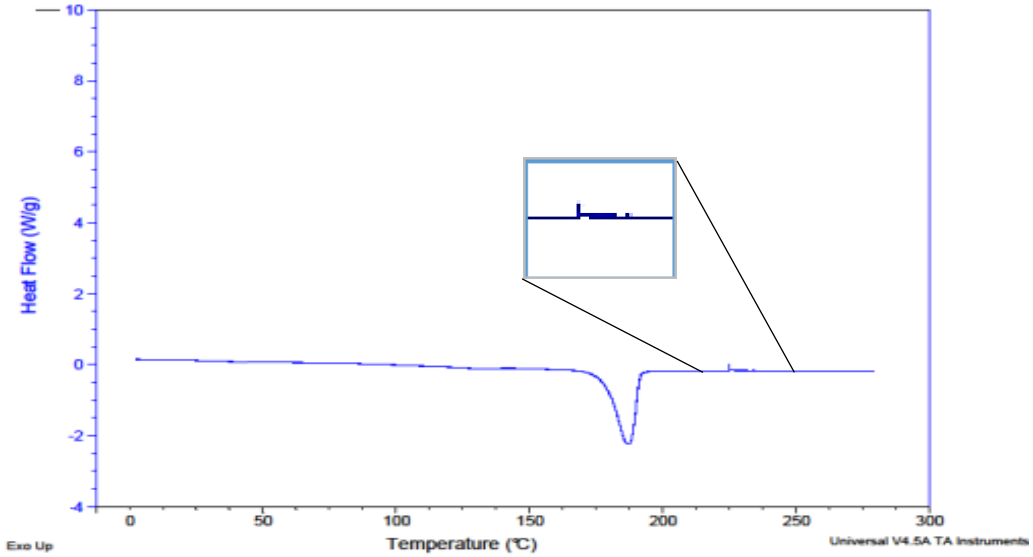

Figure 2.2. DSC analysis of aquasomes with DCPA cores coated with lactose. The arrow indicates the recorded peak at the lactose decomposing temperature.

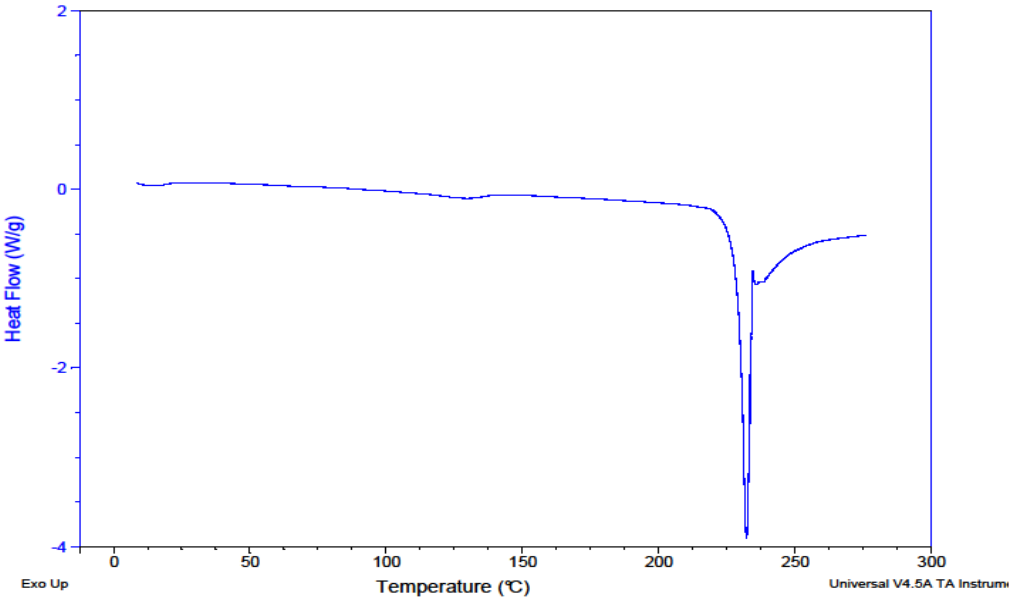

Figure 2.3. DSC melting curve of lactose, which decomposes at 235^{o}C.

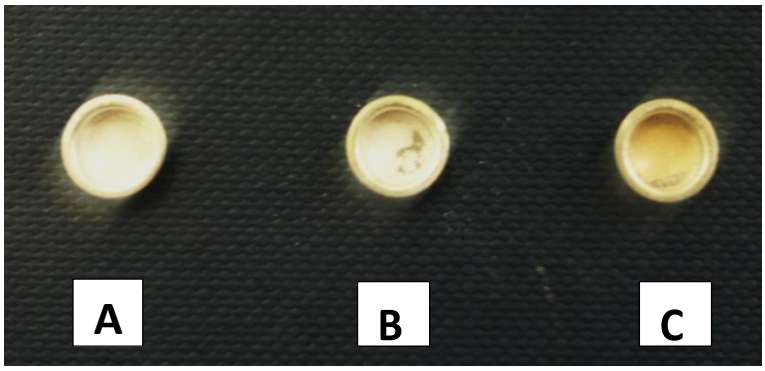

Figure 2.4. T*zero* low mass DSC pans: (A) aquasomes with DCPA cores before DSC analysis, (B) aquasomes with DCPA cores coated with trehalose after DSC analysis and (C) aquasomes with DCPA cores coated with lactose after DSC analysis (the lactose coating was decomposed (caramelised).

2.3.1.7. FTIR analysis

FTIR is the absorption measurement of a sample under different IR frequencies. It is an essential spectroscopic technique in organic and inorganic chemistry (Bertoluzza *et al*., 1995). For instance, Rawat *et al.* (2008) used FTIR to measure HA cores after coating with alginate as an indication for complete coating. Goyal *et al.* (2005) used FTIR to confirm the adsorption of Antigen T helper (Th1 and Th2) after loading them on liposomes. Such techniques allow easy identification of the compounds with minimal sample and in a non-destructive way.

FTIR analysis was carried out by the KBr disk method. According to the Beer-Lambert law, the IR spectrum is the sum of the IR spectrum of the materials present in the sample. It also states that the signal level is usually low for the trace material, since the infrared absorbance is proportional to concentration (Chan and Kazarian, 2005).

(Beer-Lambert Law) $\mathbf{A = \log_{10} (I_0/I) = abc}$

Where,

A= Absorbance (dimensionless)

I_0 = source radiation intensity

I = transmitted radiation intensity

a = co-efficient of absorptivity

b = Path length or thickness, and

c = Concentration of the absorber

In the current study, the samples did not reveal any identifying peaks of lactose and trehalose. This may be due to the low concentrations of both coating materials present when compared to the DCPA, which has the predominant absorbance. Moreover, similar results occurred when measuring the presence of BSA after the loading step.

However, the three identifying peaks of DCPA (3000 cm^{-1}, 2270 cm^{-1}, and 1050 cm^{-1} - 1125 cm^{-1} for OH, P-O and P=O stretching vibrations respectively which are indicated by red arrows were all clearly overlapped with lactose peaks (Figure 2.5) (Miller and Wilkins 1952). The low-absorbance peaks recorded at (2289 cm^{-1}) can be identified as lactose. After loading with BSA, these peaks were absent; this is may be due to overlapping with the BSA absorbance. Conversely, with trehalose the same was observed as lactose in terms of DCPA overlapping peaks. However, no identifying peak for trehalose was recorded. The presence of lactose, trehalose and BSA can therefore be detected by their overlapping effect with the IR spectrum of the DCPA cores but not by their identifying peaks. This is due to low concentrations of

sample present. Decreasing the path between the detector and the sample was carried out to try to increase the sensitivity of the detection, however no change was observed.

Figure 2.5. FTIR spectrums of aquasomes manufactured with DCPA cores. (**A**) IR spectrum of DCPA cores before coating, (**B**) IR spectrum of DCPA coated cores (**C**) IR spectrum of aquasomes with DCPA cores coated with lactose.

2.3.1.8. SEM analysis

SEM is an electron microscope that images a sample by scanning it with a beam of electrons. It provides valuable information, such as structural and thickness characterization, elemental analysis and electrical conductivity properties. (Barkay *et al*., 2009; Nouri *et al*., 2012).

SEM images of DCPA show DCPA cores are spherical in shape and have a rough surface (Figure 2.6). However, after coating with lactose and loading with BSA, the surface morphology changes (Figure 2.7). The DCPA cores after loading appear to have a smoother surface, which indicates the presence of layers coating them. This finding was parallel to what Oviedo *et al.* (2007) carried out; they used SEM images to confirm the presence of both layers (API and sugar layers).

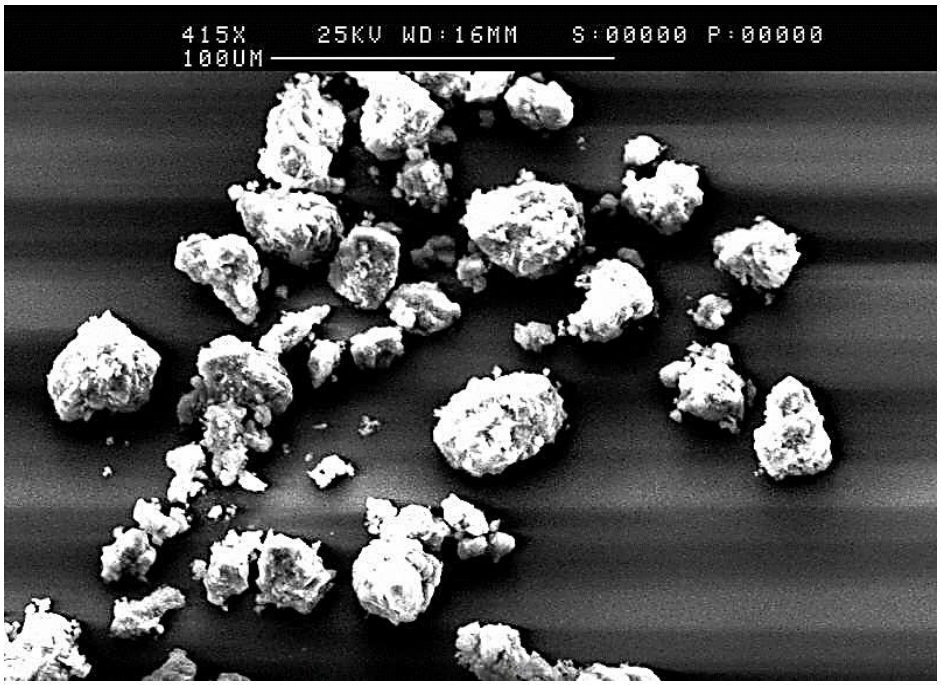

Figure 2.6. SEM image of DCPA cores before coating.

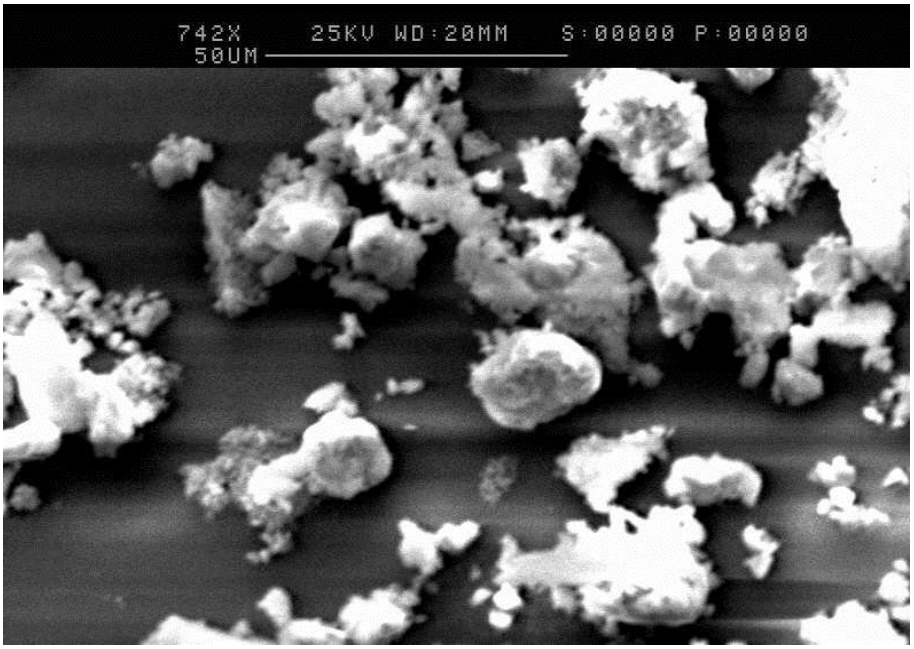

Figure 2.7. SEM image aquasomes with DCPA cores coated with lactose, which has a smoother surface when compared to uncoated DCPA cores.

2.3.1.9. *In vitro* release studies of aquasomes with DCPA cores

In vitro release studies were performed on the final aquasome formulations (Table 2.3 and Table 2.4). The samples were redistributed in 10 mL of phosphate buffer solution (pH 7.4) and placed in a shaking water bath (37^{o}C/100 rpm). Phosphate buffer solution (pH 7.4) was used to simulate the pH environment present in the intestine, where the aquasomes are targeted for delivery. A quantity of 0.3 mL was taken for analysis at a number of time points (1, 2, 3, 4, 5, 6, 7, and 24 hr). Samples collected from the *in vitro* release studies were analysed with HPLC using a gradient method for BSA reported by Umrethia *et al*. (2010). The method was tested and gave a correlation co-efficient of 0.998, a limit of detection of 0.15 µg/ml and limit of quantification of 0.40 µg/mL. It was challenging to place a relationship between the BSA released from the DCPA aquasomes (in both lactose and trehalose as coating materials) and the effect of different manufacturing conditions used. This is related to the high variability in the mean particle sizes between the samples after locating and coating steps. Such findings were anticipated, since both sizing analysis and zeta potential measurements varied across the samples, and hence, different loading efficiencies were obtained (Table 2.3). However, the total BSA loading efficiency of DCPA formulations coated with trehalose was approximately 2-3% less than those coated with lactose, though it is statistically not significant (p>0.05) (Figures 8-11).

It was observed from the cumulative release of BSA from the DCPA aquasomes, that all the formulations show a controlled release of BSA over the first 6 hr with no burst effect noticed. This is could be related to the fact that the number of OH groups on both sides of trehalose the same (the number of OH groups on each side is 4), while lactose has not uneven number of OH groups. Hence, trehalose has a more controlling effect (attachment to BSA) over the release of BSA. The coating and loading conditions of each formulation are listed in Table 2.4.

Table 2.3. Zeta potential measurements of aquasomes with DCPA cores after coating and loading steps.

Formulation No.	Coating material	Coating Conditions	Zeta Potential After Coating	Loading material	`Loading Conditions	Zeta Potential After Loading
1	Lactose	2.5 hr/4ºC	-1 ±0.2	BSA	2.5 hr/4ºC	-13 ±0.2
2					20 hr/25ºC	-9.5 ±0.3
3	Lactose	1 hr/4ºC	0.5 ±0.2		2.5 hr/4ºC	-9.1 ±0.1
4					20 hr/25ºC	-15 ±0.8
5	Lactose	2.5 hr/25ºC	-1.7 ±0.5		2.5 hr/4ºC	-18.3 ±0.5
6					20 hr/25ºC	-16.5 ±0.4
7	Lactose	1hr/25ºC	-1.2 ±0.5		2.5 hr/4ºC	-20.1 ±0.2
8					20 hr/25ºC	-17.7 ±0.2
9	Trehalose	2.5 hr/4ºC	-2.9 ±0.1		2.5 hr/4ºC	-11.2 ±0.3
10					20 hr/25ºC	-17.9 ±0.8
11	Trehalose	1 hr/4ºC	-2.1 ±0.2		2.5 hr/4ºC	-13.6 ±0.4
12					20 hr/25ºC	-12.4 ±0.1
13	Trehalose	2.5 hr/25ºC	-3.15 ±0.2		2.5 hr/4ºC	-12.2 ±0.3
14					20 hr/25ºC	-17.3 ±0.2
15	Trehalose	1hr/25ºC	-1.0 ±0.1		2.5 hr/4ºC	-13.4 ±0.33
16					20 hr/25ºC	-12.6 ±0.33

Table 2.4. The percentage BSA loading of aquasomes coated with lactose and trehalose.

Coating material	Formulation No.	% of BSA loading
Lactose	Formulation 1	14.10% ±1.7
	Formulation 2	8.69% ±1.2
	Formulation 3	11.78% ±1.4
	Formulation 4	14.92% ±1.5
	Formulation 5	15.77% ±1.4
	Formulation 6	13.42% ±2.8
	Formulation 7	12.77% ±1.8
	Formulation 8	9.62% ±1.3
Trehalose	Formulation 9	14.14% ±1.9
	Formulation 10	8.65% ±0.9
	Formulation 11	13.15% ±1.1
	Formulation 12	12.62% ±1.1
	Formulation 13	14.56% ±0.9
	Formulation 14	13.02% ±1.2
	Formulation 15	13.72% ±1.3
	Formulation 16	8.42% ±1.9

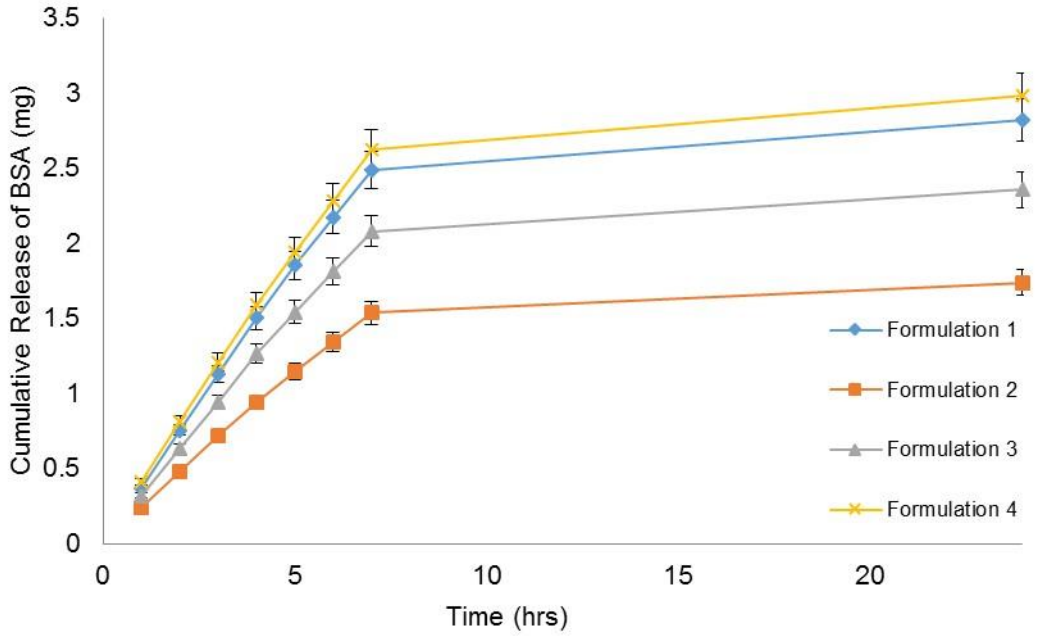

Figure 2.8. *In vitro* cumulative release of BSA (mg) from DCPA cores coated with lactose (formulations 1-4) over 20 hr.

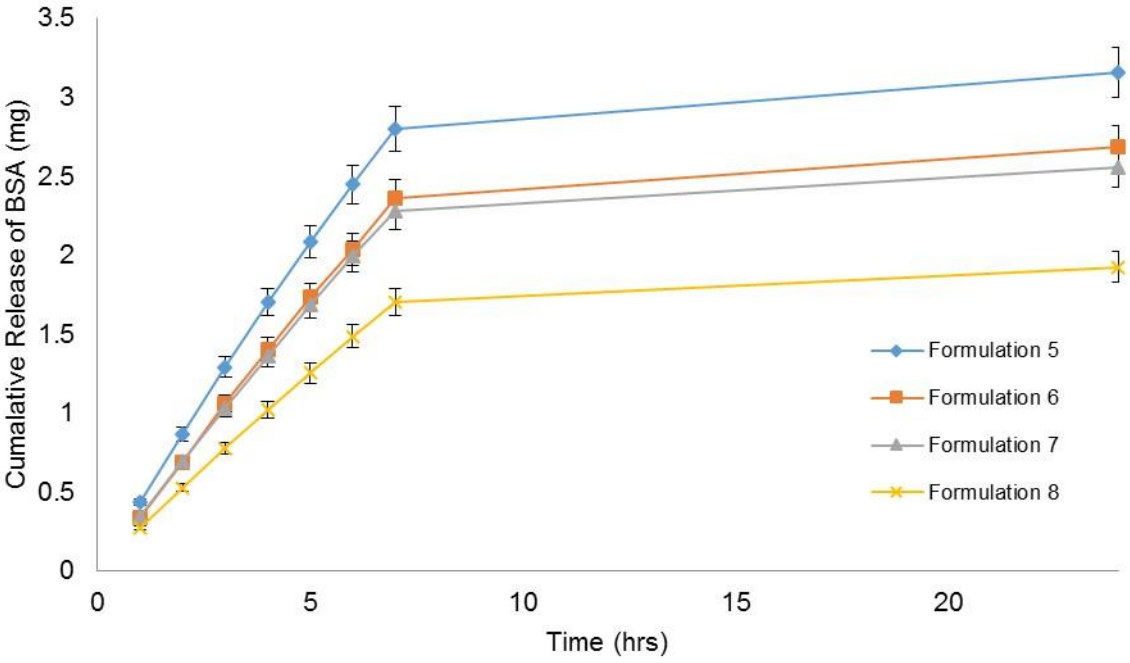

Figure 2.9. *In vitro* cumulative release of BSA (mg) from DCPA cores coated with lactose (formulations 5-8) over 20 hr.

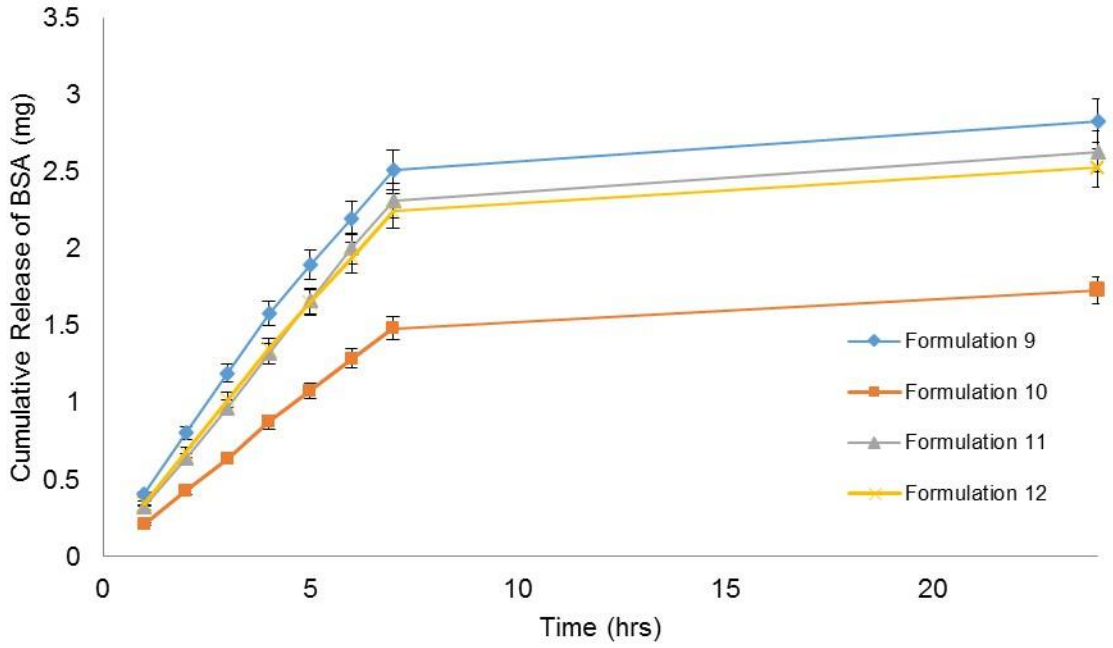

Figure 2.10. *In vitro* cumulative release of BSA (mg) from DCPA cores coated with trehalose (formulations 9-12) over 20 hr.

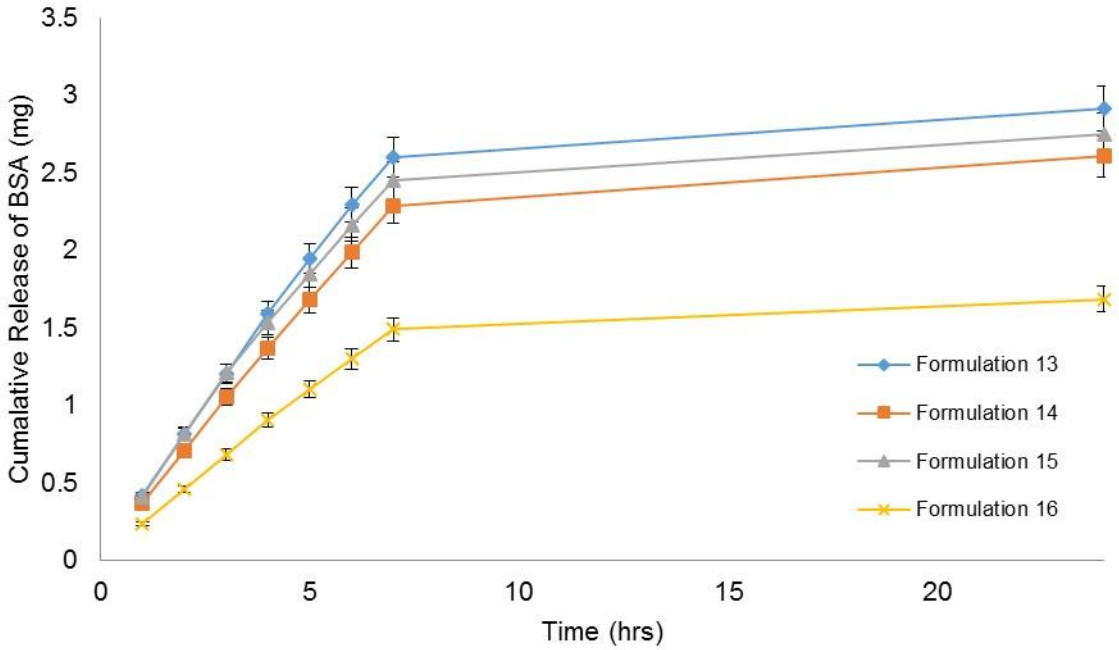

Figure 2.11. *In vitro* cumulative release of BSA (mg) from DCPA cores coated with trehalose (formulations 13-16) over 20 hr.

2.3.2. Manufacture of aquasomes with MCPA cores

2.3.2.1. Preparation of MCPA cores

MCPA powder has a density of 2.58 g/cm^3 and calcium/phosphate ratio of 0.5, therefore less sonication force was required to reduce the particle size of the MCPA particles (Fernandez et al., 1999). There is no evidence that MCPA has previously been used as a solid core material for aquasome preparation. However, the choice to investigate MCPA as a core material was based on its physical properties such as particle morphology (form spherical cores after size reduction with sonication) and biocompatibility (MCPA is a biodegradable material with safe toxicity profile).

To reduce the particle size of MCPA powder, MCPA powder was sonicated for a period of 30 min (intermittent) under sonication force of 10.0. After sonication, the size population of powder obtained was 4 µm. Sonication for an extra 30 min did not result in a further reduction in particle size. Other alternative techniques such as increasing the depth of the probe and reducing volume of the medium was employed, but did not result in a further reduction in particle size

2.3.2.2. Zeta potential measurements

The zeta potential measurement revealed that MCPA powder is slightly negative in charge (-3.9 ±0.32). This encourage the adsorption of both lactose and trehalose, because lactose is neutral to positively charged in pH 7.4 and trehalose is slightly negative at the same pH.

2.3.2.3. DSC analysis

According to DSC analysis (Figure 2.12), two peaks were recorded. The first peak is recorded at 150ºC, which is a rehydration peak. The second peak was recorded at 190ºC, which is the decomposition temperature of MCPA. It was not possible to analyse the coated particle with DSC as the decomposing peaks of trehalose and lactose would be overlapping with the rehydration peak and the decomposition peak of MCPA respectively.

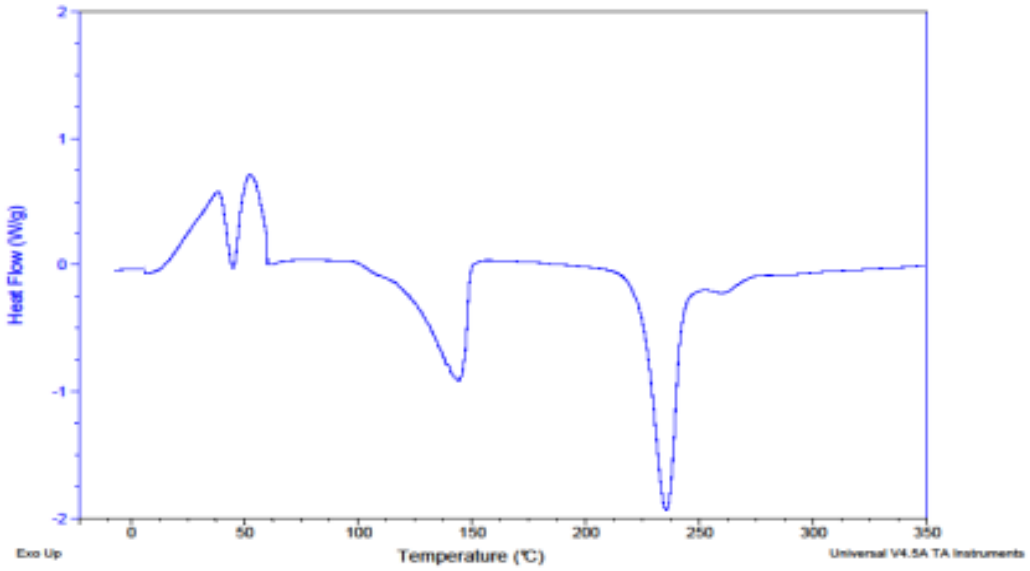

Figure 2.12 DSC analysis of MCPA cores, it shows the crystallization peaks (45ºC), the dehydration peak (150ºC) and the melting peak (240ºC).

2.3.2.4. SEM analysis

SEM studies show that MCPA particles have a rhombus shape with a semi smooth surface. However, after sonication the particles become spherical in shape, Figure 2.13. It can be noticed that sonication had reduced the size significantly compared HA and DCPA. This is related to the fact that MCPA has the lowest calcium to phosphor ratio (2.58 g/cm^3) when compared to HA and DCPA.

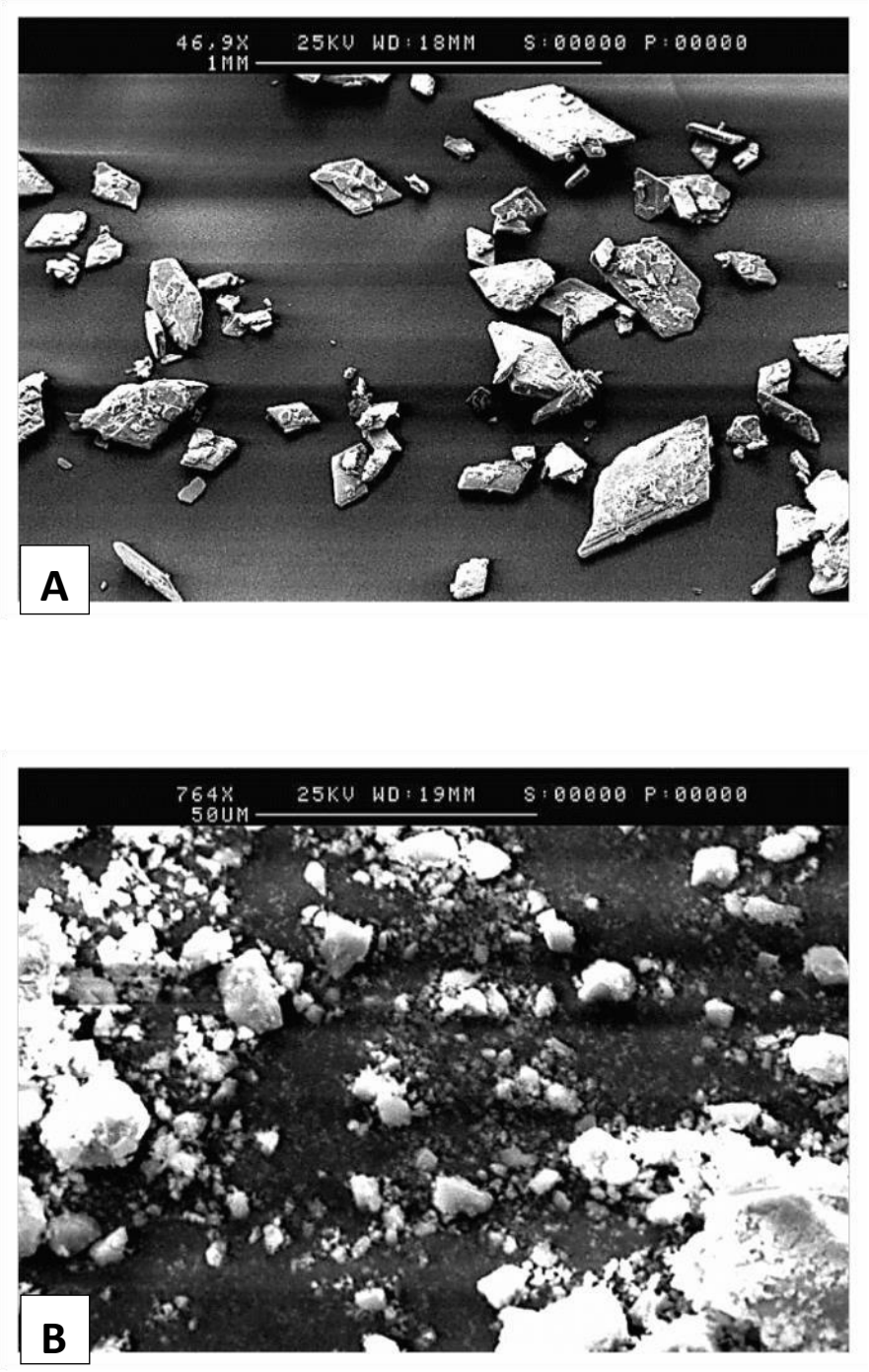

Figure 2.13. SEM images of MCPA powder: (**A**) shows MCPA cores before coating, (**B**) shows the morphology of the MCPA cores after sonication.

Initially, MCPA particles showed the characteristics of a good core material. Since it is slightly negative, has a spherical shape, a rough surface and small mean particle size. This suggests that MCPA could be used as a core material to prepare aquasomes. However, it is found that after coating with lactose and freeze-drying; it forms a gum upon contact with the air (Figure 2.14). These were very difficult to handle and it was difficult to characterize them. In addition, it was not ideal to load them as well as the gum was not distributed in the BSA solution. Hence, MCPA was not taken forward as core material for aquasomes preparation.

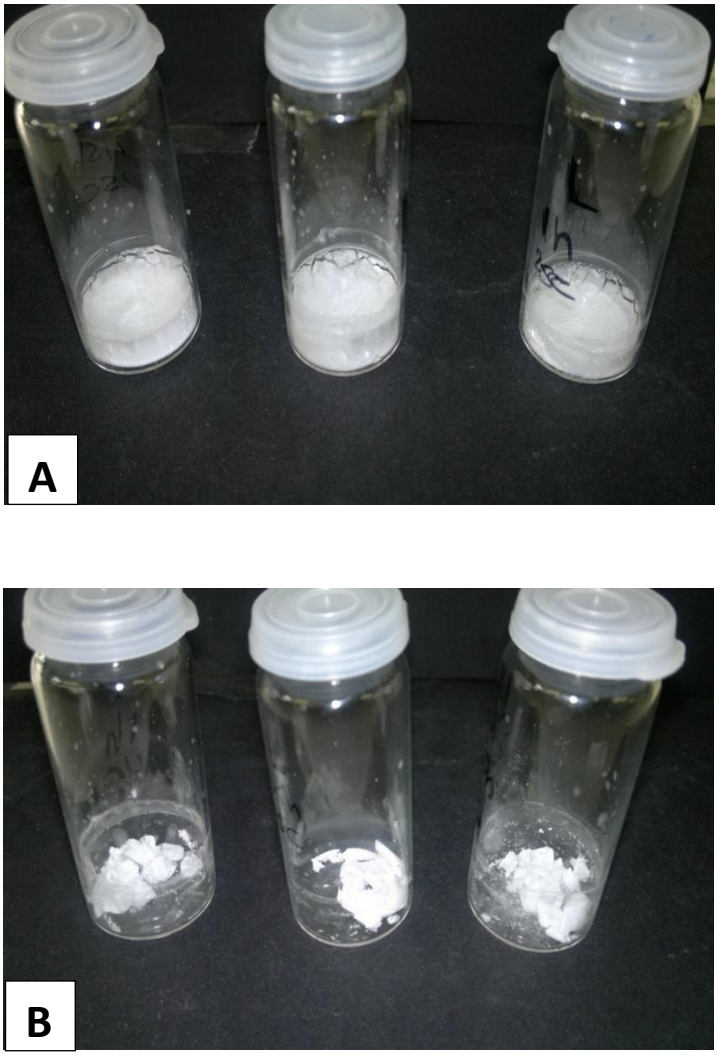

Figure 2.14. Freeze-dried samples of MCPA after coating with lactose: (**A**) MCPA freeze dried samples before vial opening, (**B**) MCPA freeze dried samples after vial opening and the formation of a gum.

2.3.3. Aquasomes with HA Cores

2.3.3.1. Preparation of HA Aquasomes

2.3.3.1.1. Preparation of HA cores

The HA powder was purchased from Sigma Aldrich, UK. The mean particle size of the powder, as the company claims, is (>200 nm). However, the size of the HA powder when measured (section 2.2.3.1) was between 925 nm-1100 nm.

Attempts were made to reduce the mean size of particles. For instance, hand grinding for a period of 15 min and sonication for a period of 1 hr at a sonication amplitude of 10.0. The attempts were unsuccessful in reducing the particle size. The failure in the reduction of size was expected, because HA powder has a high density (3.16 g/cm^3) and high calcium to phosphate ratio (1.67) (Combes, 2011; Kalita *et al*., 2007). The reasons to why the mean particle size of HA does not match what has been claimed, could be either due to manufacturing defect (batch defect) or an irreversible agglomeration (Merkus 2009). Therefore, the powder was used as received without further modification.

2.3.3.1.2. Size measurements

As mentioned previously, the mean particle size of HA did not match what has been claimed (>200 nm), and the measured mean particle size of HA varied between the samples. According to Table 2.5, it is clear that the mean particle size measurements of HA cannot be utilized for characterization purposes.

Table 2.5. HA mean particle size and zeta potential measurements.

Sample No.	Mean Particle Size (nm)	Zeta Potential
Solid cores	950 ±160	- 8.01 ±0.23
Coated cores	1100 ±130	- 8.30 ±0.57
Loaded cores	1200 ±190	-8.32 ±0.69

2.3.3.1.3. Zeta Potential Measurements

The zeta potential measurements of the aquasomes with HA cores are listed in Table 2.6. It is known that the zeta potential of lactose at pH 7.4 is neutral to slightly positive in charge, trehalose is slightly negative and BSA is negatively charged. (Malvern, 2005; Tymczyszyn 2007; Horiba, 2009).

In the case of mixing time, 2.5 hr coating times resulted in higher zeta potential values in both coating materials, lactose and trehalose, at the same coating conditions. In addition, higher loading conditions resulted in higher zeta potential values at the same loading temperatures. This is parallel to the fact that the rate of physical adsorption increased as the mixing time increases. Therefore, as the mixing time increases, more layers are adsorbed to the surface and higher zeta potential values are recorded. In terms of manufacturing temperatures, coating and loading at 4^{o}C resulted in higher zeta potential values, and thus, the more coating material or BSA is adsorbed.

However, the zeta potential values recorded indicates that less BSA is adsorbed on HA cores coated with trehalose at 4^{o}C, while more BSA is adsorbed on HA cores coated with trehalose at 25^{o}C when compared to HA cores coated with lactose. This could be related to viscosity of both lactose and trehalose at low temperatures. As the temperature increases, the viscosity of trehalose solution is increased, while the lactose solution increases in viscosity as the temperature decreases. High viscosity resulted in reduced particle motions in the solution, and thus increased the rate of physical adsorption (Miller *et al*., 1997; Maher *et al*., 2011).

2.3.3.1.4. DSC Analysis

HA cores have high melting and decomposition temperatures (1000^{o}C) which cannot be measured due to instrument limitation (maximum of 350^{o}C can be measured on the TA Q200). The DSC analysis of both coated and loaded cores did not reveal any peak at the melting or decomposition temperatures of lactose, trehalose or BSA (Figure 2.15).

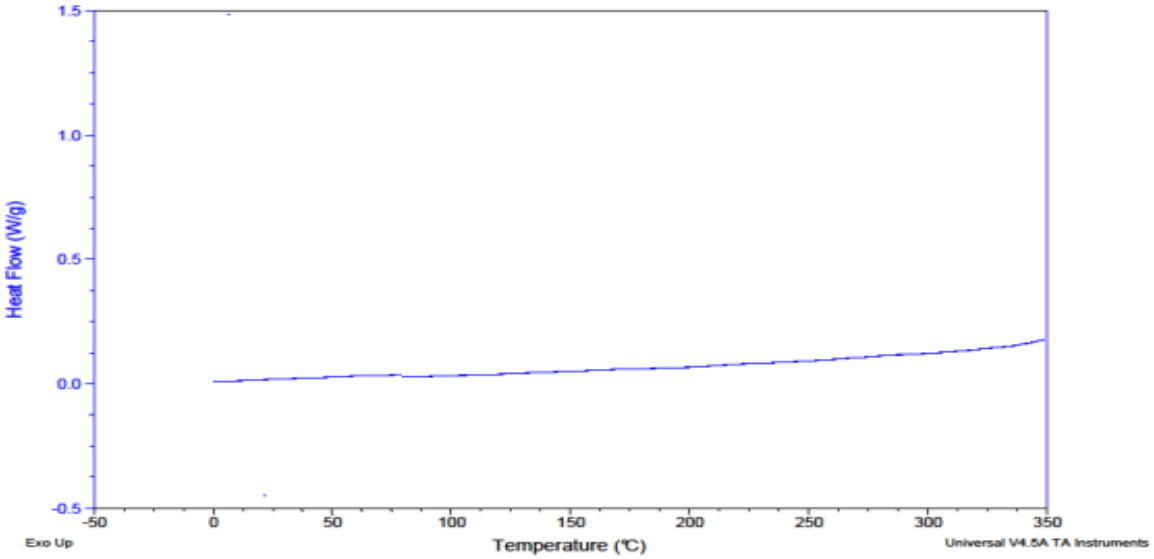

Figure 2.15. DSC analysis of Aquasomes with HA cores coated with lactose.

2.3.3.1.5. FTIR Analysis

The recorded FTIR data of the samples showed no identifying peaks of lactose and trehalose (Figure 2.16). This may be due to both coating materials being present at low concentrations compared to the HA, which has the predominant absorbance (3300 cm^{-1} - 3600 cm^{-1}, 1422 cm^{-1} - 1460 cm^{-1} and 1100 cm^{-1} for OH, CO_3 and PO_4 stretching vibrations which are indicated by red arrows) (Miller and Wilkins 1952). Moreover, the same occurred when measuring the presence of BSA after the loading step. Since the IR spectrum is the sum absorbance of the materials present in the sample, according to Beer-lambert law. FTIR spectrum of HA powder when compared to before or after loading, two low absorbance peaks of HA powder which is present at the wavelengths of (2360 cm^{-1} and 2337.60 cm^{-1}) are absent. This probably because the absorbance recorded form either lactose, trehalose or BSA is overlapping with the two peaks, which causes the absence of these peaks. Therefore, the presence of lactose, trehalose and BSA can be detected but by their overlapping effect with FTIR spectrum of the HA powder but not by their identifying peaks because they present in the sample in low concentrations compared to HA. An attempt was made to increase the sensitivity of FTIR detection by decrease the path between the detector and the sample. However, there was no change observed.

Figure 2.16. (**A**) IR spectrum of HA cores before coating, (**B**) IR spectrum of HA cores coated with trehalose and (**C**) IR spectrum of Aquasomes with HA cores coated with lactose.

2.3.3.1.6. SEM analysis

Microscopic analysis was performed to study the surface morphology of the HA powder particles and its distribution since it is known that the surface morphology has a great influence on adsorption and more generally on coating. SEM images show that HA particles have a round shape and a semi-smooth surface (Figure 2.17). Therefore, such morphology assists in good attachment of lactose or trehalose on the HA particles (Oviedo *et al*., 2007). The SEM images also show that the HA particles are not uniform in size (the presence of small and large particles), which confirms the sizing studies.

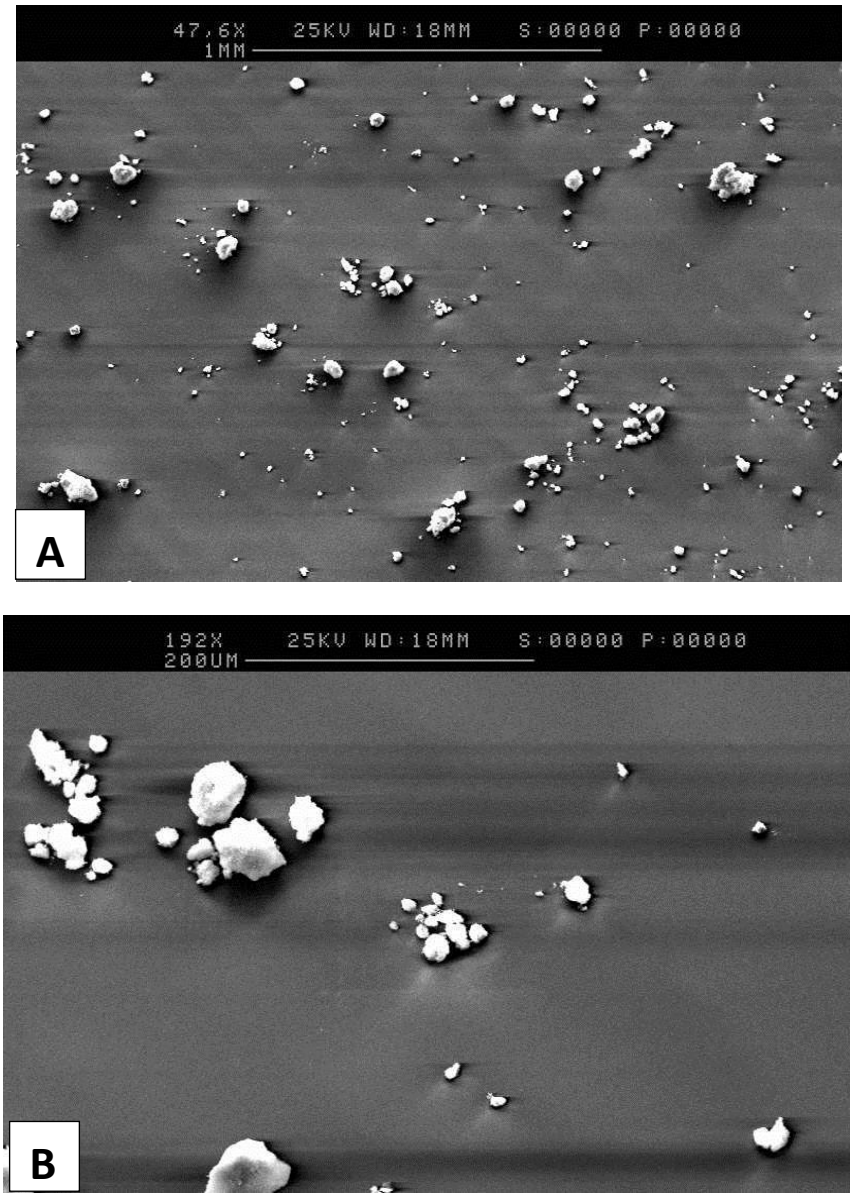

Figure 2.17. SEM images of HA powder: (**A**) shows HA cores with different particle sizes, (**B**) shows the morphology of the HA cores.

2.3.3.1.7. *In vitro* release studies of aquasomes with HA cores

The loading efficiency of the HA aquasomes were calculated and are summarized in Table 2.6 and 2.7. Results show that the total BSA loading of formulations coated with trehalose is higher for those coated with lactose. This comes in parallel to what has been suggested in the literature that trehalose has been used extensively in the preparation of aquasomes (Cherian *et al*., 2000; Oviedo *et al*., 2007).

In terms of mixing time, it is found that 2.5 hr produced higher BSA loadings when compared to a 1 hr mixing time. This is parallel to the zeta potential measurements, which confirms that higher coating and loading times resulted in more negatively charged molecules (more BSA attached on the surface). This may be because longer loading times allowed more layers of BSA to be adsorbed onto the surface (longer mixing times of BSA encouraged physical adsorption). BSA loading performed at 4ºC with lactose as coating resulted in aquasomes with higher BSA loading to that performed at 25ºC (p<0.01). This could be due to lower temperature which allow more BSA to be adsorbed onto the surface (lower temperature manufacturing conditions encourages physical adsorption) (Ferrieu *et al.,* 2009). However, in the case of trehalose as a coating, BSA loading at 25ºC was higher than that of 4ºC despite the time of coating.

In terms of total BSA loading, aquasomes coated with trehalose produced higher BSA loadings by approximately 7.5% to aquasomes coated with lactose (p<0.05). This may be due to trehalose attaching better to the HA cores because of its structure. However, aquasomes coated with trehalose at 25ºC produced similar BSA loadings to the aquasomes coated with lactose at 4ºC. This finding backs up the zeta measurements in that the viscosity of trehalose increases as the temperature increases and thus encourages physical adsorption (physical adsorption increases as particle motion decreases) (Thommes, 2012)

The results also reveal that the difference (approximately by 10%) between the BSA loading at the loading step was (20 hr at 25ºC and 2.5 hr at 4ºC) more apparent when trehalose was used as a coating material. This may be due to the use of trehalose as a preservative for biological materials. This sugar ability based on the hydration and solid-state properties of this sugar, which is based on the presence of the α, α-1,1-glycosidic linkage (Sakurai 2009). Moreover, the release pattern of BSA for the HA aquasomes coated with trehalose are more consistent to those loaded with lactose over 6 hr (Figures 2.18- 2.21).

Table 2.6. Zeta potential measurements of aquasomes with HA cores after coating and loading steps

Formulation No.	Coating material	Coating Conditions	Zeta Potential After Coating	Loading material	`Loading Conditions	Zeta Potential After Loading
1	Lactose	2.5 hr/4°C	4.1 ±0.3	BSA	2.5 hr/4°C	-10.4 ±0.2
2					20 hr/25°C	-12.6 ±0.3
3	Lactose	1 hr/4°C	2.5 ±0.8		2.5 hr/4°C	-13 ±0.1
4					20 hr/25°C	-12 ±0.8
5	Lactose	2.5 hr/25°C	3.0 ±0.6		2.5 hr/4°C	-9 ±0.5
6					20 hr/25°C	-10 ±0.4
7	Lactose	1hr/25°C	1.5 ±0.5		2.5 hr/4°C	-11.2 ±0.2
8					20 hr/25°C	-10.6 ±0.2
9	Trehalose	2.5 hr/4°C	-1.3 ±0.2		2.5 hr/4°C	-10.2 ±0.3
10					20 hr/25°C	11.5 ±0.1
11	Trehalose	1 hr/4°C	-1.22 ±0.3		2.5 hr/4°C	-8.2 ±0.4
12					20 hr/25°C	-12 ±0.1
13	Trehalose	2.5 hr/25°C	-1.15 ±0.2		2.5 hr/4°C	-10.4 ±0.3
14					20 hr/25°C	12.3 ±0.2
15	Trehalose	1hr/25°C	-1. ±0.2		2.5 hr/4°C	-10.1 ±0.33
16					20 hr/25°C	-12.1 ±0.33

Table 2.7. Loading capacity of HA aquasomes coated with lactose and trehalose.

Coating material	Formulation No.	% of BSA loading
Lactose	Formulation 1	39.32% ±1.5
	Formulation 2	46.34% ±1.2
	Formulation 3	50.05% ±1.4
	Formulation 4	42.01% ±1.4
	Formulation 5	36.82% ±1.5
	Formulation 6	50.56% ±1.9
	Formulation 7	40.12% ±1.8
	Formulation 8	39.72% ±1.7
Trehalose	Formulation 9	36.73% ± 2.5
	Formulation 10	59.24% ±1.9
	Formulation 11	34.14% ±1.5
	Formulation 12	56.97% ±1.3
	Formulation 13	31.79% ± 2.2
	Formulation 14	47.85% ± 2.1
	Formulation 15	38.00% ±1.0
	Formulation 16	52.43% ±1.1

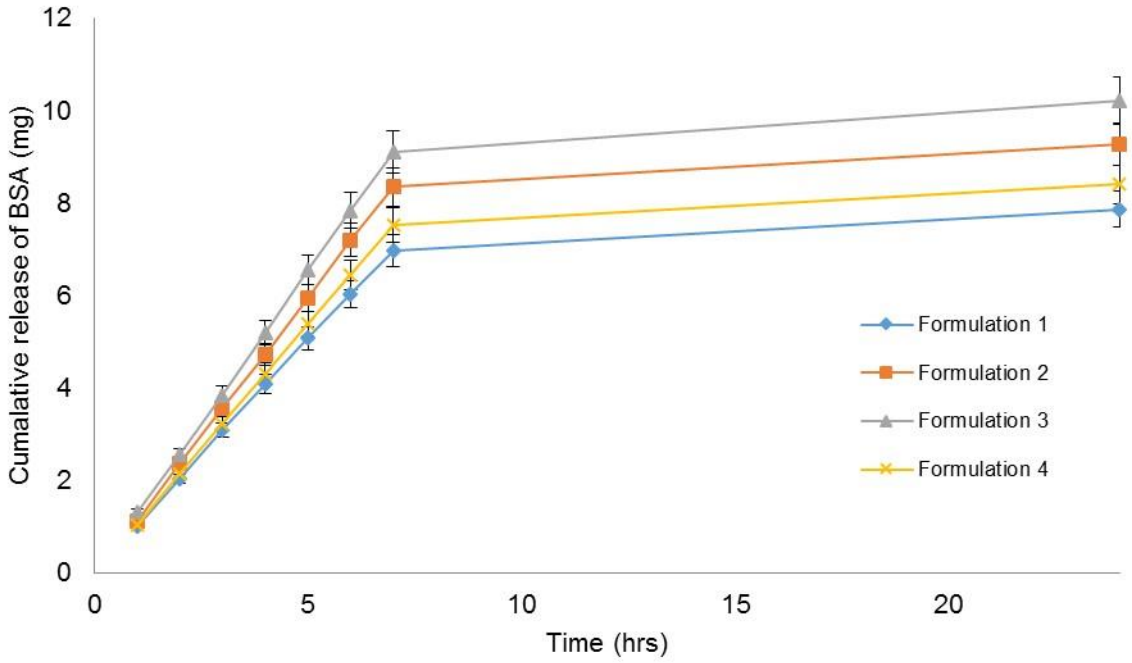

Figure 2.18. *In vitro* cumulative release of BSA (mg) from HA cores coated with lactose (formulations 1-4) over 24 hr.

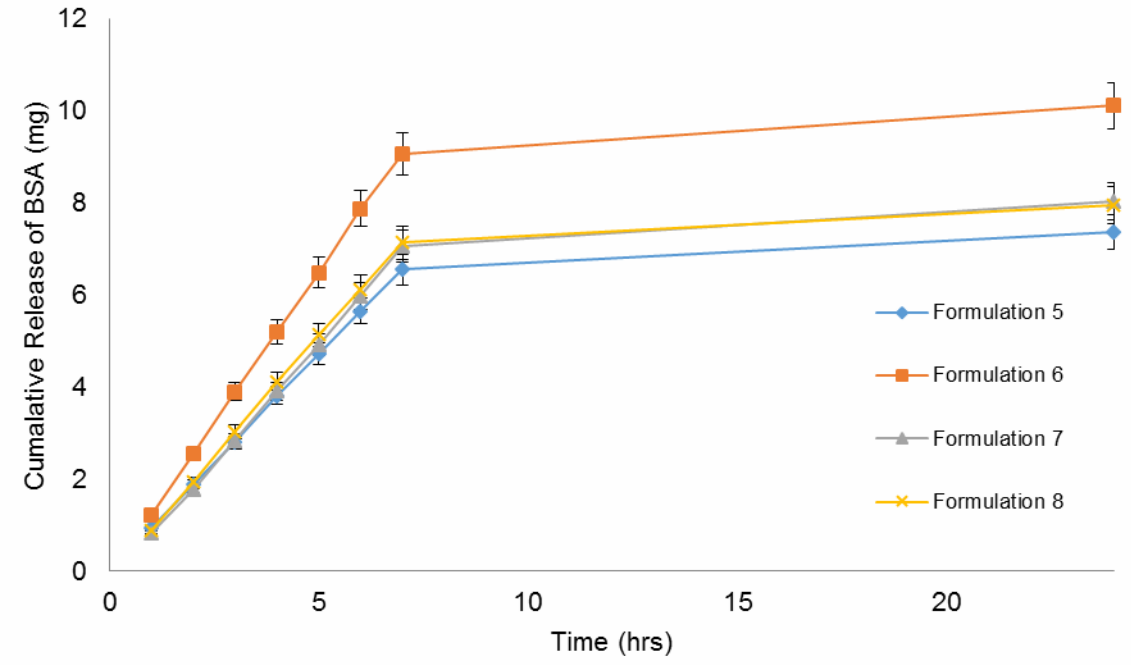

Figure 2.19. *In vitro* cumulative release of BSA (mg) from HA cores coated with lactose (formulations 5-8) over 24 hr.

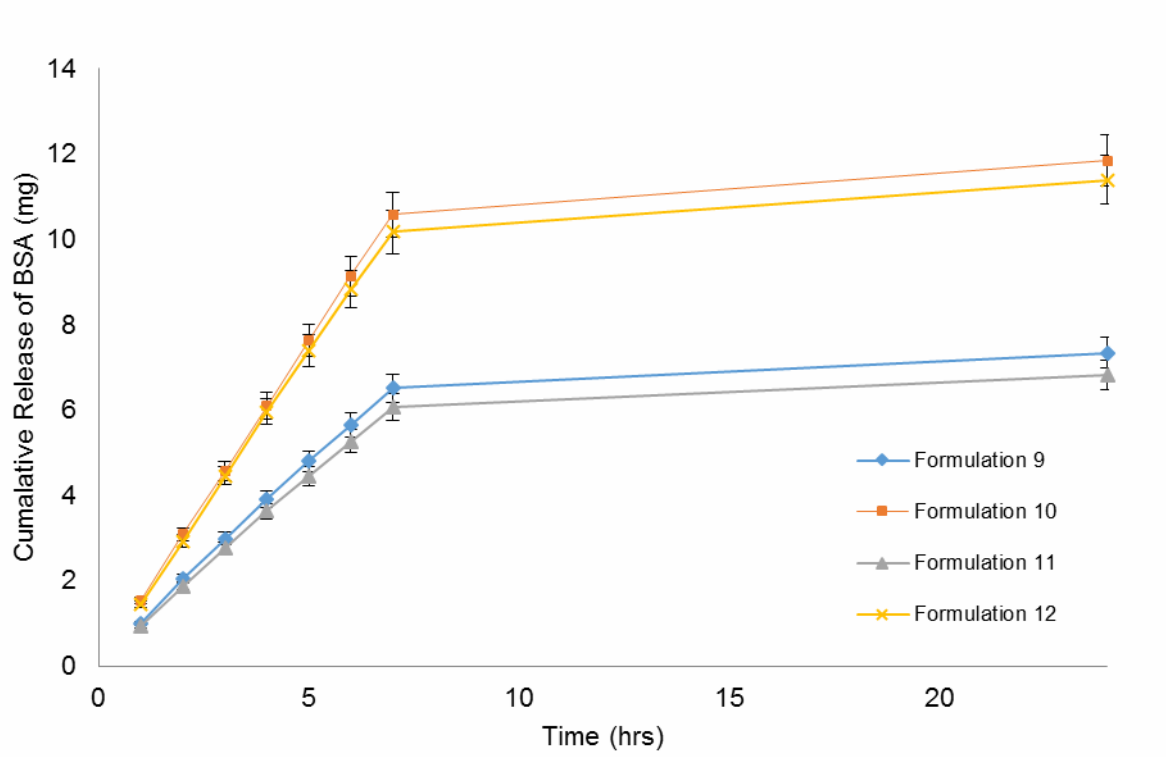

Figure 2.20. *In vitro* cumulative release of BSA (mg) from HA cores coated with trehalose (formulations 9-12) over 24 hr.

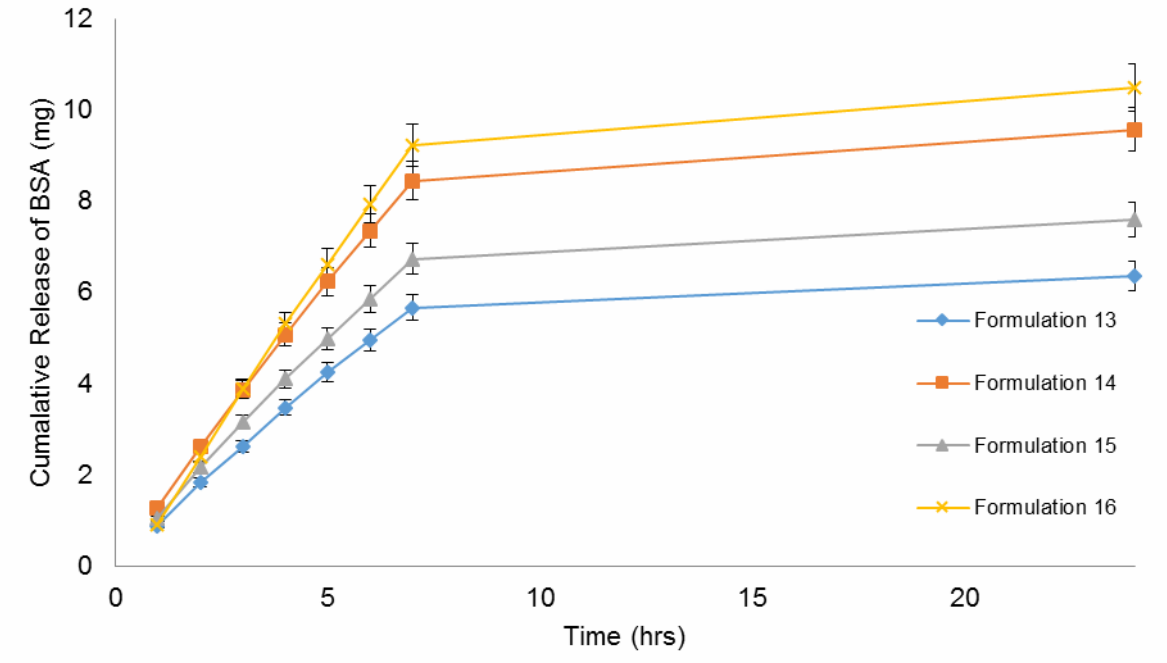

Figure 2.21. *In vitro* cumulative release of BSA (mg) from HA cores coated with trehalose (formulations 13-16) over 24 hr.

2.3.3.2. Manufacture of aquasomes with HA cores using various coatings

The method for aquasome preparation was followed as described by Oveido R. *et al*. (2007) with modification. In order to increase the loading and to enhance the sustained release of the BSA, different coatings were investigated. The HA cores and BSA was fixed in all formulations and a screening process was carried out using different sugars from different classes (mono, di and polysaccharides). It was noticed that monosaccharides formulations had the least loading efficiency (1-4%). To investigate more, the loaded cores were characterized with FTIR to confirm the presence of the sugar (Figure 2.22). The FTIR results show no identifying peaks of any of the monosaccharaides used. Therefore, its either present in very low concentrations (the interaction between the HA and monosaccharaides is weak which lead to low BSA molecules attached) or the sugar is probably not present (Table 2.8).

Figure 2.22. FTIR spectrum of BSA loaded aquasomes with HA cores coated with Fucose. Identical FTIR spectrums obtained from all monosaccharides and sucrose.

The case was different for sucrose, in the literature, sucrose was mentioned as a coating since it is in the same category with trehalose and Cellobiose (Umashankar *et al*., 2010). However, results show it has poor loading approximately 10%. Interestingly, Cellobiose resulted higher BSA loading, similar to trehalose). *In vitro* release studies show a steady release of BSA over 6 hr. The total BSA content per 100 mg of aquasomes was approximately 6-6.5 mg (p<0.05). High BSA loading of Cellobiose coating could be due to the number of OH groups present in the molecule, which encourages BSA attachment. The number of OH groups on each side is equal similar to trehalose OH distribution. Such distribution balances the favor of attaching to the core and BSA.

Table 2.8. Different BSA loaded aquasomes formulations and their characterization and loading (A=Arabinose, R=Rhibose, F=Fucose, M=Mannose, S=Sucrose, RH=Rhaminose, SA=Saccharine, C=Cellobiose).

Aquasomes	Zeta Potential Before Coating	Zeta Potential After Coating	Zeta Potential After Loading	Size Before Coating (nm)	Size After Coating (nm)	Size After Loading (nm)	% BSA Loading
HA/A/BSA	-10 ± 1	-8.2±1.6	-10±2	990± 120	1050±50	1030±62	1- 10 %
HA/R/BSA		-7.6±1.7	-7.6±2.1		1000±65	1100±26	
HA/F/BSA		-8±1.1	-8±2.3		1100±55	1095±15	
HA/M/BSA		-6±1.9	-6±3.1		1090±10	994±104	
HA/S/BSA		-6.7±2.1	-6.7±2.4		1154±44	998±38	
HA/RH/BSA		-5.1±2.2	-5.1±2.8		1150±12	1110±92	
HA/SA/BSA		-8.5±1.2	-8.5±2.1		1000±14	1150±33	
HA/C/BSA		2±0.5	-17±1.5		1350±15	1400±12	64±3 %

2.3.3.3. Modeling of aquasomes with HA cores

MD was performed to simulate the assembly of the layers of HA aquasomes. HA aquasomes were used because with either lactose or trehalose as a coating material, they had the highest BSA loading (40%- 60%) when compared to DSPA aquasomes.

2.3.3.3.1. HA cell and HA surface

Recently, HA has been studied for various purposes using molecular modelling. For instance, Hyp-Pro-Gly peptide modelling on a surface in an aqueous environment to simulate HA-protein interaction in HA implants (Laurencin *et al.,* 2010). Moreover, HA structural defects and uptake of carbonate has also been investigated using molecular modeling of HA (Proose *et al*., 2006). Furthermore, the effect of magnesium on HA during elemental replacement has also been explored using molecular modelling. However, HA molecular studies has used multiple softwares or force field packages to perform the simulations such as METADIS and SIESTA. AMBER 12 has never been reported to be used in HA simulations as the library of xLEAP was missing Ca and P atoms to identify HA structure.

An alternative method was used to build the xLeap library, which are detailed section 2.2.4.1. Post HA crystal structure transfer from AMBER (Figure 2.23), the HA super cell was then reduced to a cell unit and was beautified with Scigress workstation (Figure 2.24). The HA structure was processed for MM2 (geometry optimization). It was noticed that MM2 processing resulted in fragmented structure of the HA cell. To expand more, Scigress was treating each atom individually and not as a structure of the HA cell. This could be because of the nature of HA as all bonds are ionic. Therefore, the HA cell structure was used without further processing.

Surface analysis of the HA cell structure with Discovery Studio showed that HA has a high SAS (structure accessibility surface), which highlights that the surface of the nanoparticles is accessible. In addition, surface analysis show that HA can form hydrogen bonds by acting as an acceptor (Figure 2.25 and 2.26).

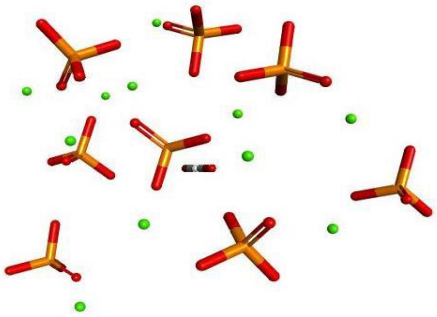

Figure 2.23. The crystal structure of hydroxyapatite super cell [$Ca_{10}(PO_4)_6(OH)_2$].

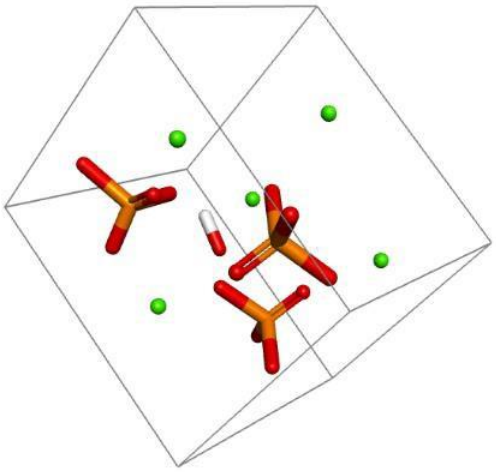

Figure 2.24. The cell unit of the hydroxyapatite which will be used to create the surface [$Ca_5(PO_4)_3OH$).

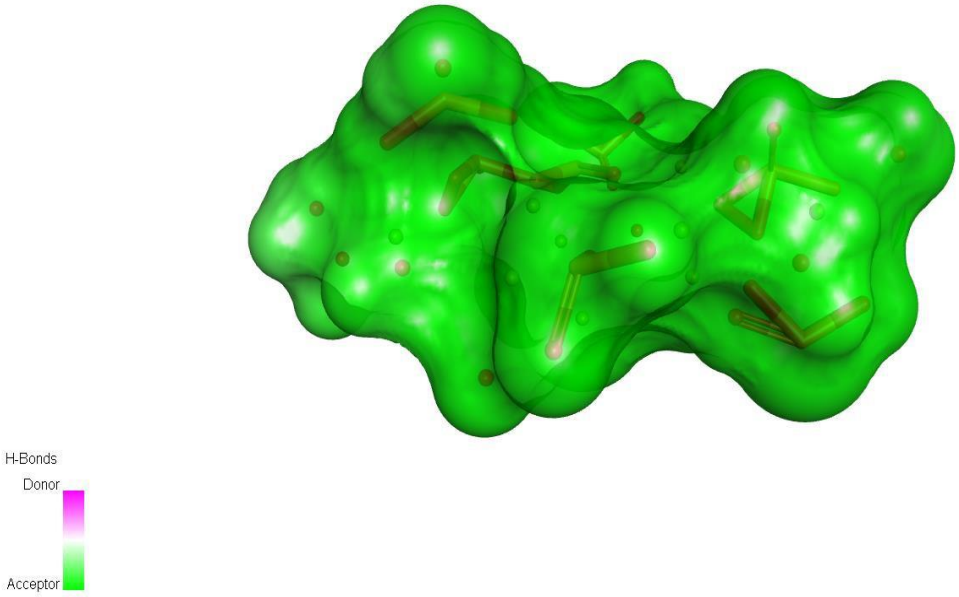

Figure 2.25. Hydrogen bond accessibility surface of hydroxyapatite.

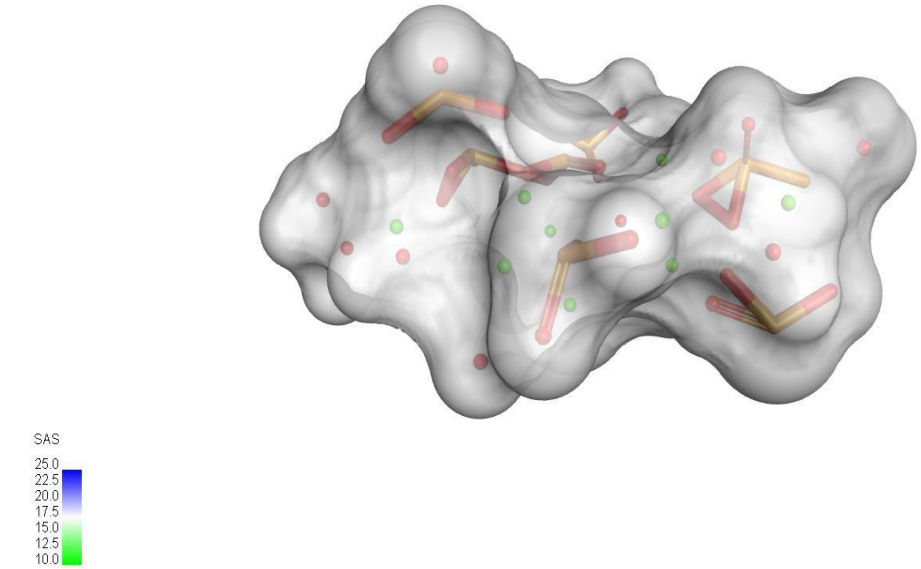

Figure 2.26. SAS of the surface of hydroxyapatite.

After setting xLeap libraries of the HA cell (Ca, P and OH), the HA surface was built by repeating cell units of HA (Figure 2.27). The process was performed manually and required a number of HA cells of 500. The 500 repeated HA cell units were required to build up an HA surface of dimensions of 30*30 A^0. Such dimensions were necessary to accommodate the large BSA protein of size of 7 A^0, which was measured by VMD.

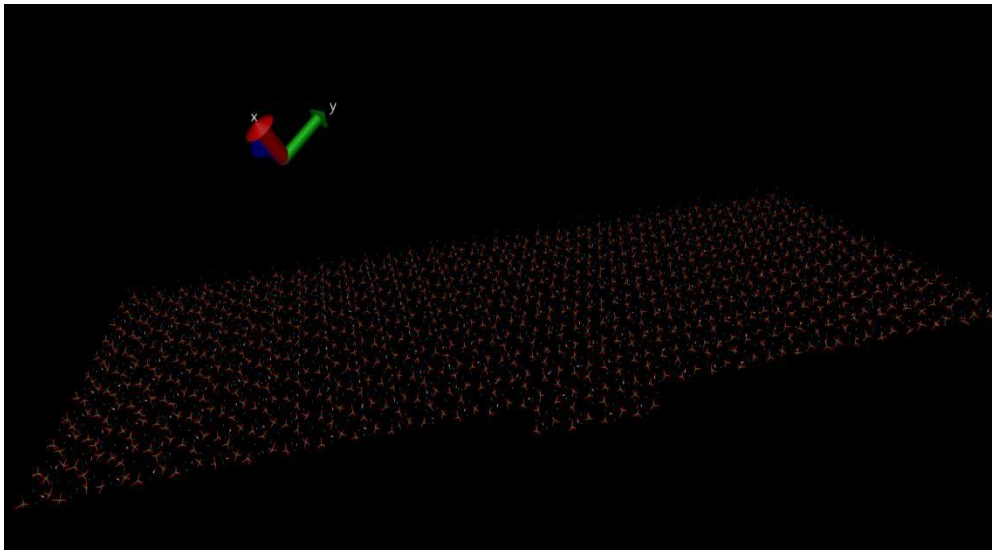

Figure 2.27. Surface of HA of dimensions of 30*30 A^0.

2.3.3.2. Trehalose modelling

Post trehalose structure beautification with Scigress explorer, MM2 geometry optimization was performed on the beautified structure (Figure 2.28). A total of 4 runs were performed and the energy value of 39.906 kcal/mol was recorded 3 out of the 4 runs (Table 2.9). No further processing on the trehalose was required and the structure was saved as a PDB file ready for docking/MD.

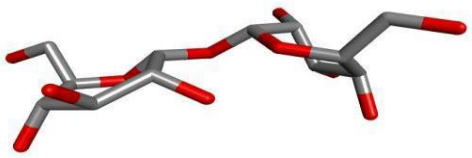

Figure 2.28. Trehalose structure after geometry optimization.

Table 2.9. Runs performed with trehalose structure on Scigress (MM2).

	Energy (kcal/mol)
Run 1	-160.01
Run 2	-39.906
Run 3	-39.906
Run 4	-39.906

2.3.3.3. BSA modelling

The crystal structure of BSA was downloaded from the Protein Data Bank (Majorek *et al*., 2012) (Figure 2.29). The structure was first analysed using Discovery Studio. The BSA molecule comprises from one chain of 583 amino acid residues. The BSA crystal structure was identified with x-ray diffraction with resolution of 2.70 Å with no missing residues. Although there are better crystal structures at high resolution of x-ray diffraction, missing residues are present in the pdb file (Bujacz *et al*., 2014; Bujacz, 2012).

A Rachamandran plot was used to map the ψ against φ of amino acid residues of the BSA molecule. A Ramachandran plot can be used to theoretically show, which conformations of the ψ and φ angles are potential for amino acid residues. Another use of a Ramachandran plot is to illustrate the experimental distribution of data observed in a single molecule structure, which later can be used as a validation method (Richardson, 1981). Rachamndran analysis of BSA chains shows acceptable bonds and amino acids distribution (Figure 2.30). In the literature, there are few examples of the MD simulations using the BSA molecule, and they all approach part of the BSA molecule (active site) for their MD simulation. In the BSA modelling, because the sugar molecule was not acting as a drug with an active site to attach to it, the entire chain was treated as an active site, which in return increases the MD simulation because of the numerous possibilities Scigress/AMBER needs to test for best fit (Huang *et al*., 2013; Gelamo and Tabak 2000; Gelamo *et al*., 2004)

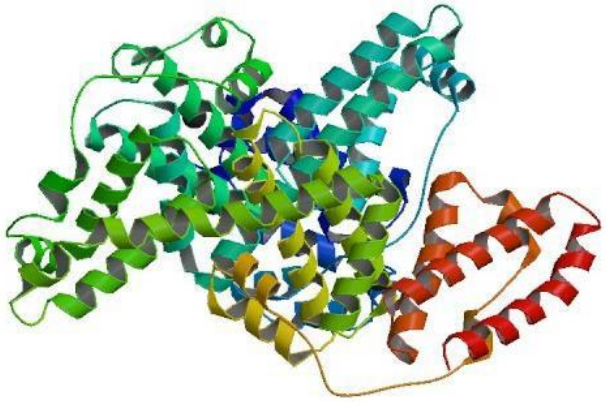

Figure 2.29. The crystal structure of BSA (Majorek *et al*., 2012).

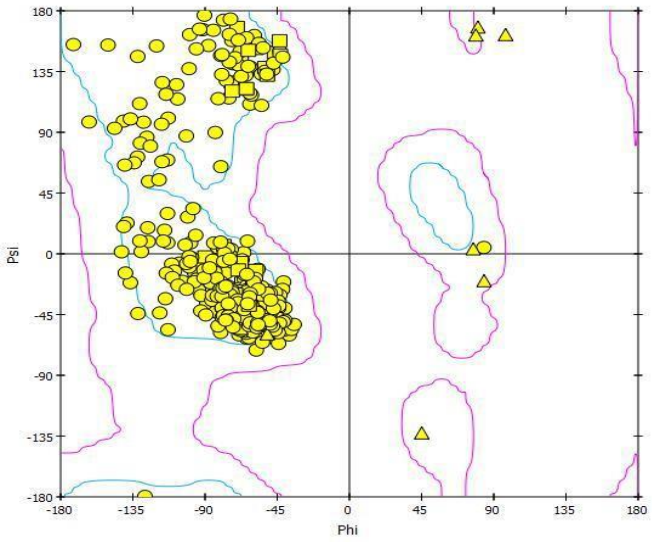

Figure 2.30. Ramachandran Plot of BSA chain.

BSA crystal structure was also analyzed for H-Bond, SAS, and charge. These findings gave the preliminary results about how the interaction of the sugar trehalose occurs on the surface of BSA (Figure 2.31-2.33).

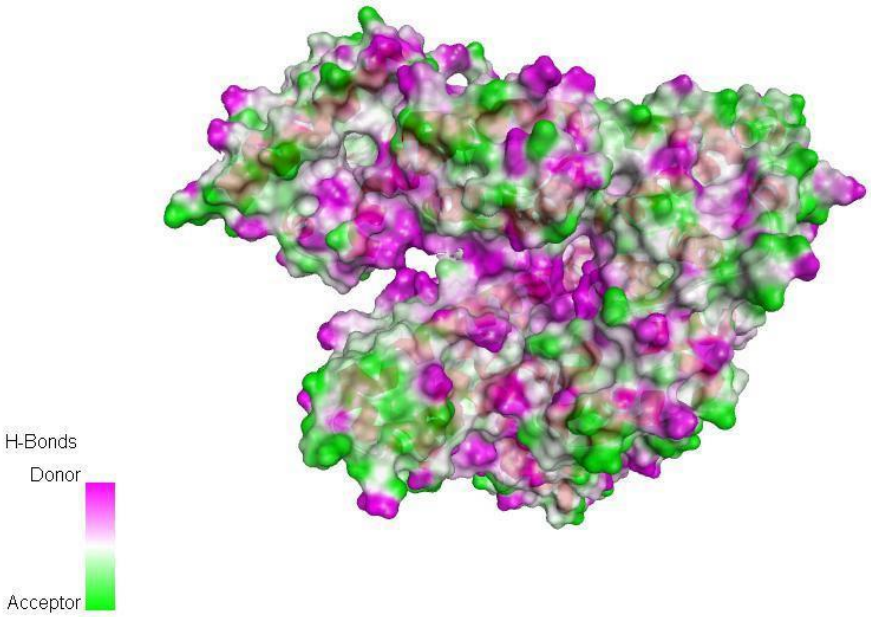

Figure 2.31. Hydrogen bond accessibility surface of BSA chain A.

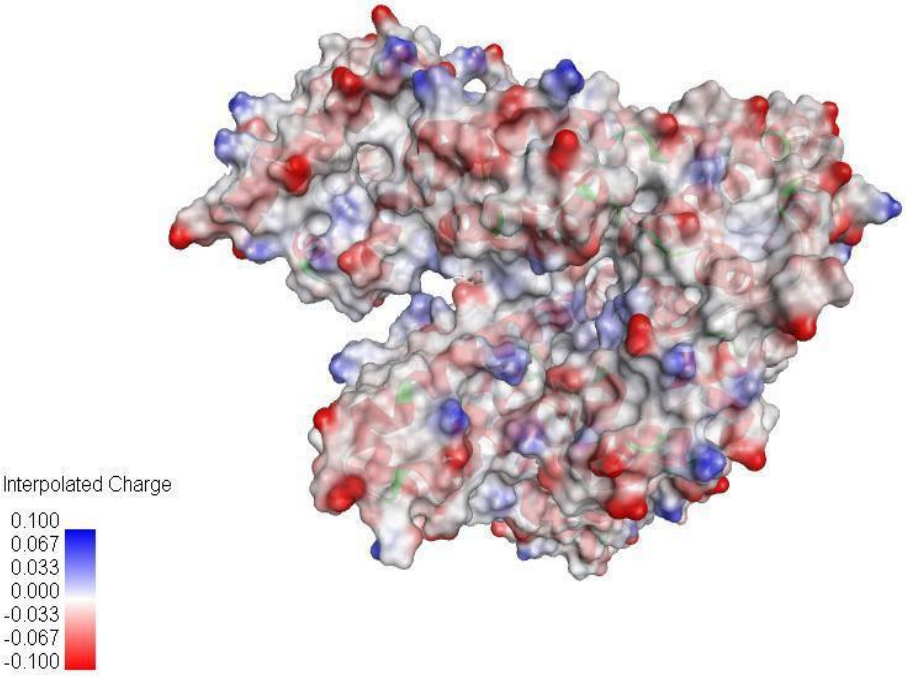

Figure 2.32. Charge on the surface of BSA chain A.

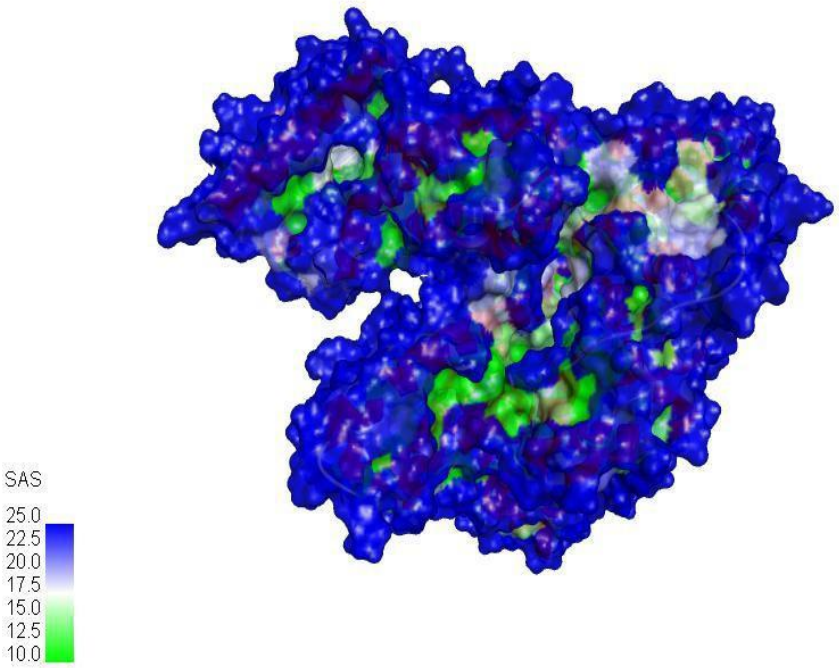

Figure 2.33. SAS on the surface of BSA chain A.

It can be noticed from the surface analysis of BSA crystal structure that BSA is capable of forming hydrogen bonds on the surface of the molecule, where the water accessibility is very high. Alongside the negativity of the BSA surface, BSA has many sites available for trehalose molecules to attach to it through hydrogen bonding. It is interesting to notice that zeta potential measurements of BSA, which were performed during manufacturing optimization of BSA loaded aquasomes, found a charge of -17, which correlates to the surface charge analysis performed with Discovery Studio.

2.3.3.4. BSA MD Simulation with AMBER 12

In order for successful AMBER MD simulation, certain files must be present in the input portal. These files were edited to match the input rules of the AMBER programme. One of the main files to be edited is the pdb file of BSA. In this step, all CYS-CYS bonds are replaced with CYX-CYX, removal of histidine (HIS) as AMBER does not recognize such bonds. It is noted here that there were 144 CYC-CYC bonds and 20 HIS amino acids present which were needed to be edited manually in the pdb file.

MD simulation of BSA was carried out in explicit water (programme add water molecules to the calculation rather than estimation) and at atmospheric pressure, Figure 2.34. The simulation was run for 5 nanoseconds using AMBER 12 and AMBER force field (99FFSB). The system was first relaxed at 300K or 280K prior for MD simulation to reach the minimum conformational energy. The results for total energy during the simulation run were extracted using '*pearl*'.

For BSA MD run at 300K, the total energy was low (~1.3e+05 eV) with a fluctuating range of less than (~±0.11eV). This indicates a high stable conformation produced in these conditions. However, the total energy for BSA MD run at 280K was significantly higher than that of BSA MD performed at 300K (Figure 2.35-38).

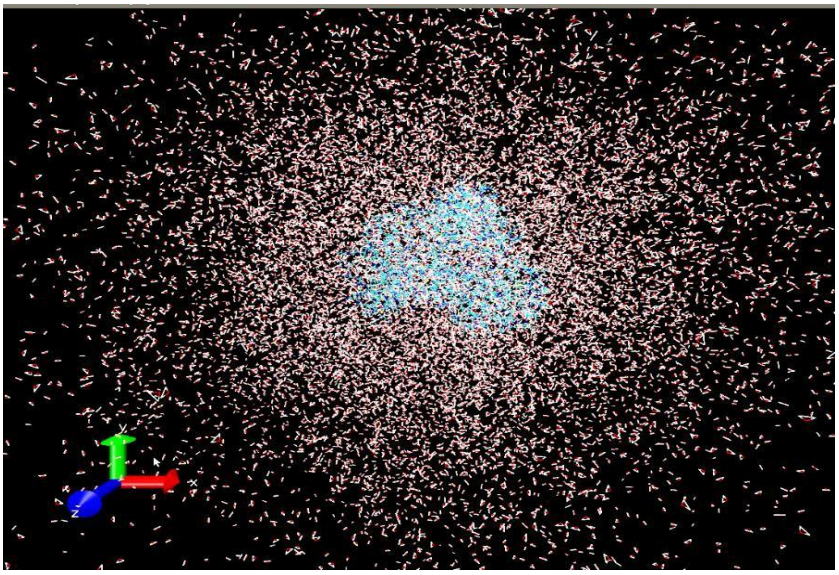

Figure 2.34. A snapshot of BSA molecule during MD simulation at 300K at 5 ns with explicit water molecules.

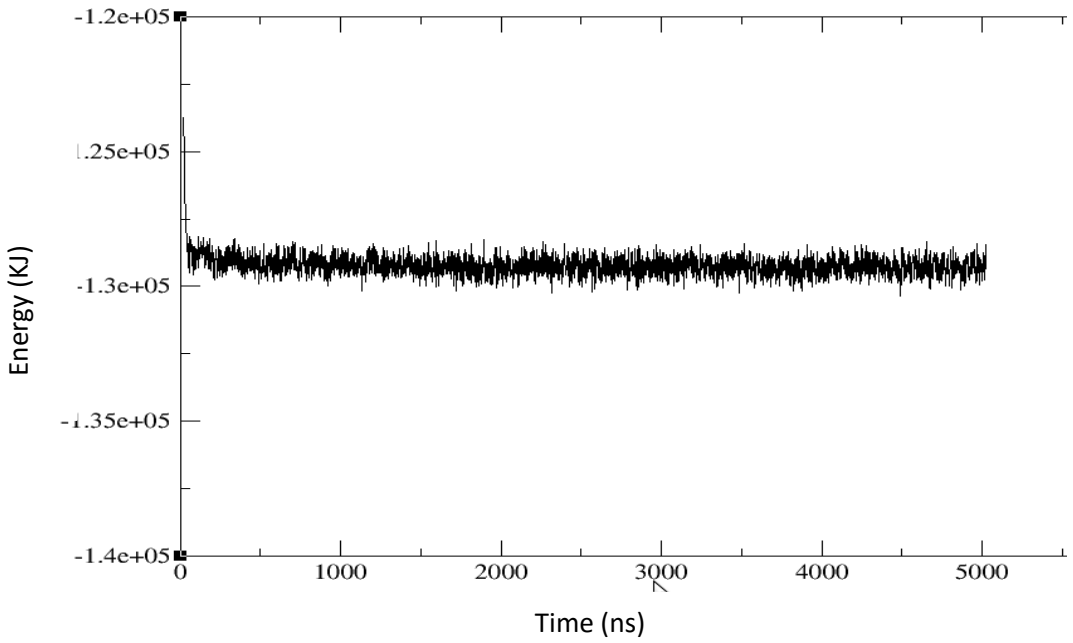

Figure 2.35. Total energy of BSA during MD simulation at md2 stage at 300K.

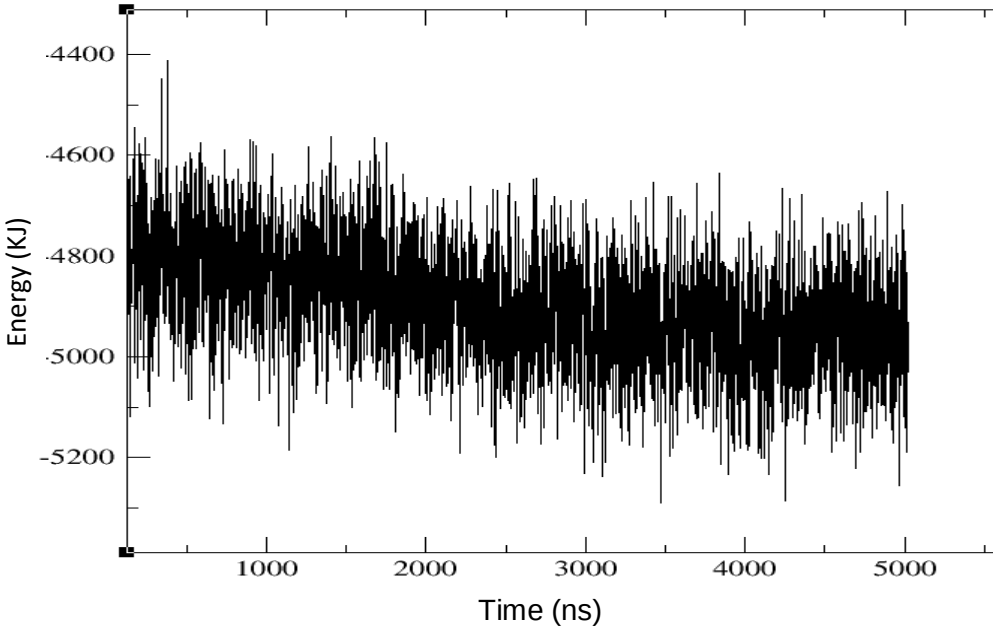

Figure 2.36. Total energy of BSA during MD simulation at md2 stage at 280K

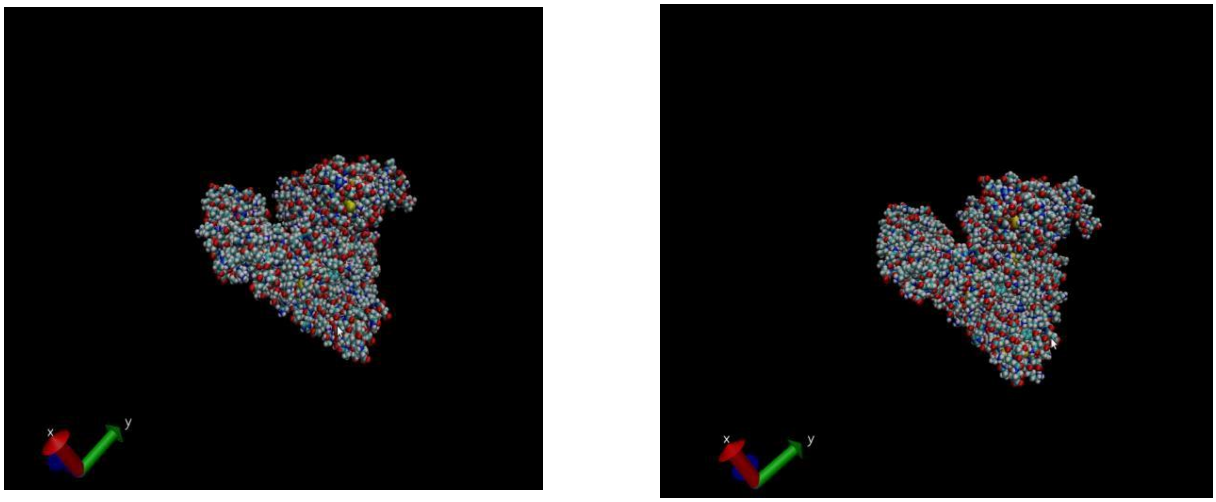

A B

Figure 2.37. BSA molecule during MD simulation at 280K, A (2ns) and B (5ns) (without explicit water molecules).

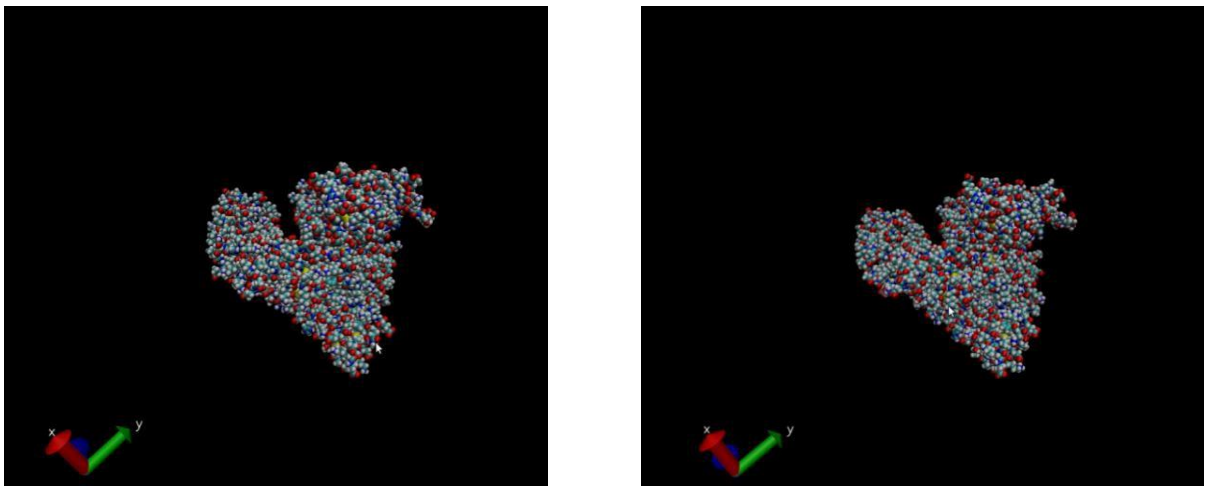

C D

Figure 3.38. BSA molecule during MD simulation at 300K, A (2ns) and B (5ns) and at 280K A (2ns) and B (5ns) with explicit water molecules has been ignored.

To measure the degree of similarity of the produced protein modules generated, the root-mean-square distance (RMSD) was used. The similarity measure is greatly based on the protein dimensions. This is matching to the number of equivalent pair atoms. The data gathered from MD simulations (.mdcrd) were analysed to calculate the RMSD as a function of time using *ptraj*. From the RMSF plots (root-mean-square of Fluctuation), it can be seen that the BSA is behaving similarly under the two different conditions (Figure 2.39-40). This confirms the total energy values of these two conditions that the BSA molecule is stable during MD simulations and producing comparable conformations within a short fluctuating range of less than 1.0 A^0.

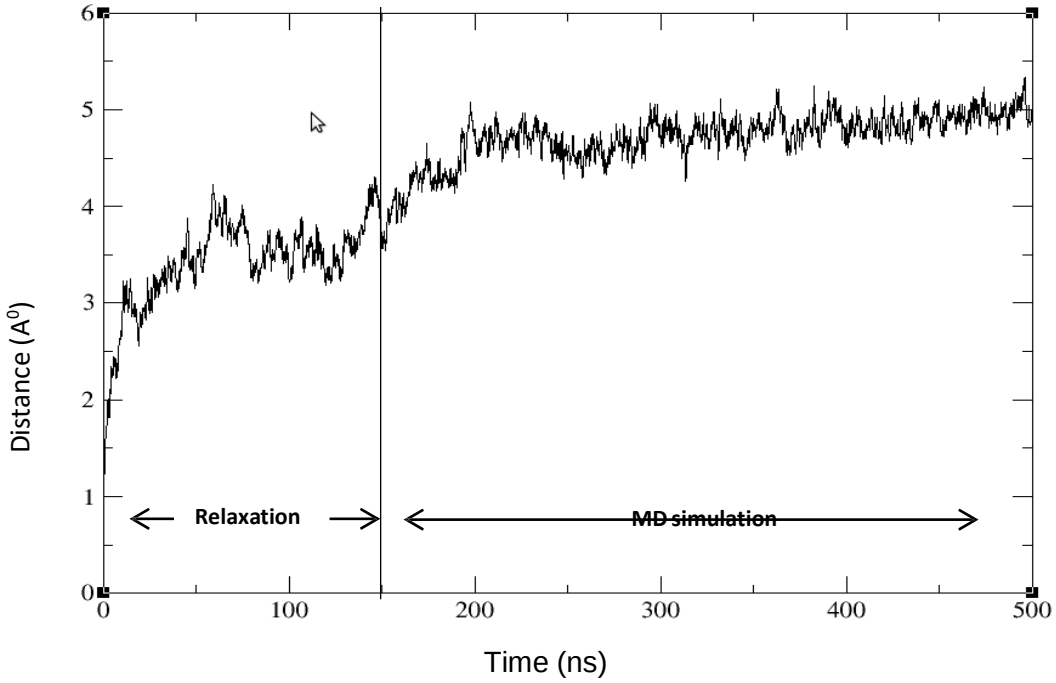

Figure 2.39. RMSF graph for MD simulation of BSA at temperature of 300K.

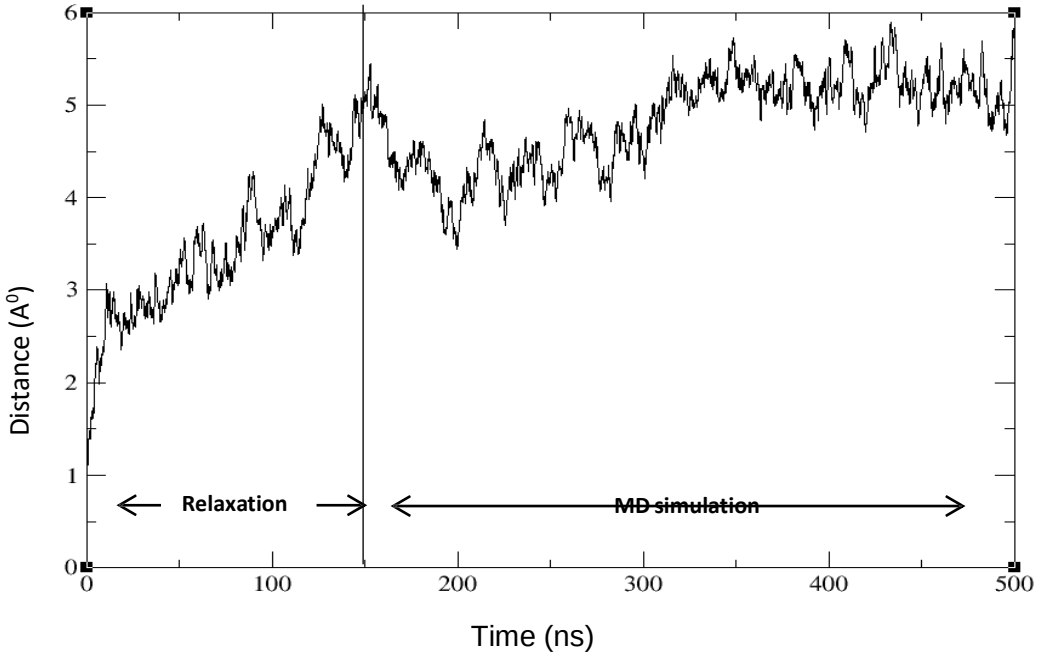

Figure 2.40. RMSF graph for MD simulation of BSA at temperature of 280K.

2.3.3.5. Docking studies of HA and trehalose

A docking study was performed on a HA surface of 3 hydroxyapatite cells units and a trehalose molecule using a Lamarckian genetic algorithm (Figure 2.41). The energy of the produced conformation was low (-134 kJ/mole), which indicates high stability of the complex (Table 2.10). It was also noted that the total number of hydrogen formed between trehalose and hydroxyapatite was 4, which also backs up the low energy of the complex and eventually the stability of the complex.

Table 2.10. Docking scores of HA and trehalose with Scigress.

	Energy (kJ/mole)
Run 1	-140
Run 2	-134
Run 3	-134
Run 4	-130

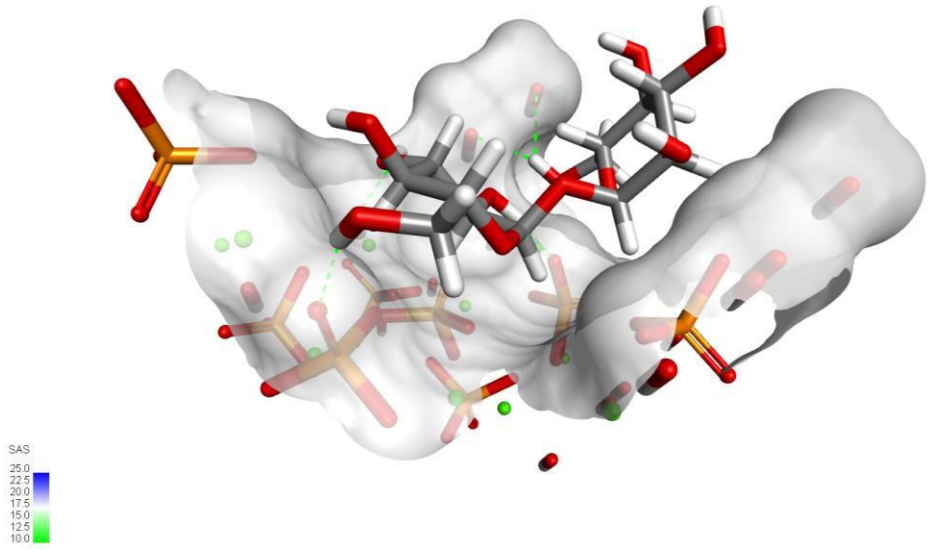

Figure 2.41. Trehalose molecule adsorbed on the surface of 3 cell units of hydroxyapatite. The hydrogen bonds are labeled with green arrows.

In the trehalose molecule, there are 8 OH groups available for hydrogen bonding. According to the docking results, 4 are formed with the HA surface, while the rest are available to form hydrogen bonding with BSA. It is also interesting to notice that only the trehalose molecule has an even distribution of OH groups on the two sides of the molecule and the presence of the o-o linkage compared to other sugar molecules tested, which relates to the higher loadings of BSA compared to the other sugar molecules (Figure 2.42).

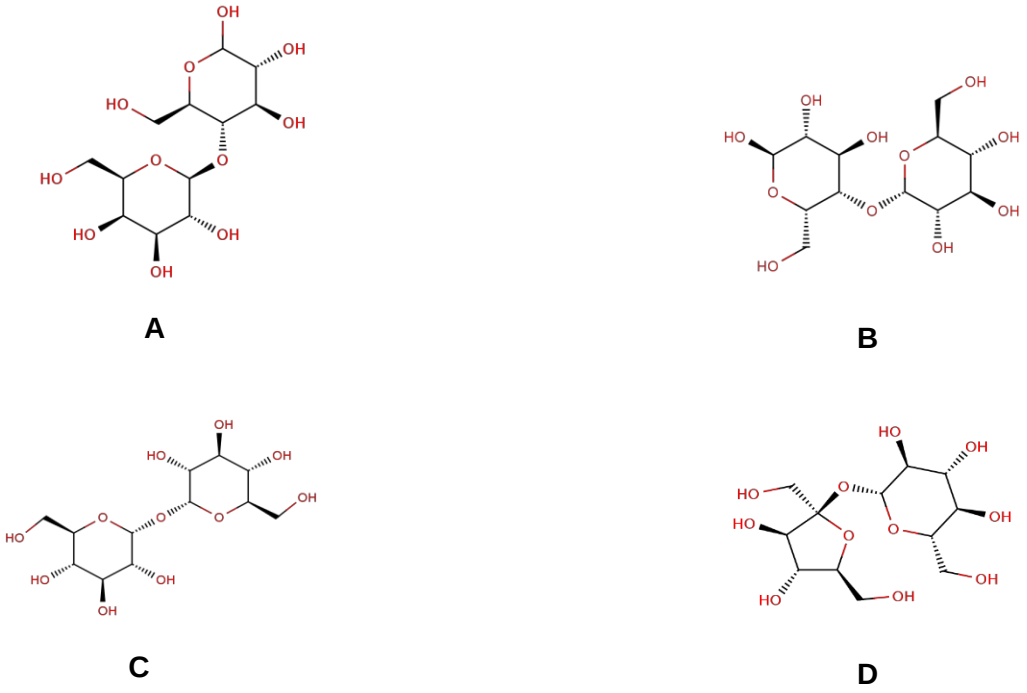

Figure 2.42. Chemical structure of sucrose (**A**), lactose (**B**), trehalose (**C**) and cellobiose (**D**) (modified from: Drug Bank 2015).

2.3.3.6. The relation between MD simulations and experimental results

The total energy values are considered crude data and can be misrepresentative since a small rotation to a subunit in the protein structure in relation to another subunit or a pivot motion can lead to a significant change (Menor, 2008). However, if experimental results are in line with total energy values, a conclusion could be made. The BSA loadings of aquasomes manufactured at 4^0C was significantly less than that of 25^0C (p<0.05). It is known that at low temperatures, physical adsorption increases due to fewer collisions with molecules due to energy transferred to the molecules in the form of heat is reduced. However, BSA loadings show the opposite, as at lower temperatures the BSA loadings were less than that obtained at high temperatures. Considering the total energy curves obtained from BSA MD simulations, the energy of the protein at 300K (25^0C) was higher than that obtained from MD simulations performed at 280K (4^0C). The kinetic energy theory states that when heat is introduced to a

material, the molecules and atoms of the material vibrate and therefore the space between the atoms increases. The spacing and motion of the atoms determines the state of the material. The net outcome of increased molecular motion is that the material enlarges and takes up more volume. In the case of proteins, the 3D structure is very crucial to its stability and to how it interacts with the surrounding environment. Therefore, as the heat is applied to a solution of proteins, the 3D structures start to unfold, due to increased kinetic energy, and proteins start to interact with each other (agglomerations/denaturation) or the amino acid chain breaks (loss of action) (Cain *et al*., 2006).

However, based on the experimental data and BSA MD simulations the opposite was noticed. Such variation was reported in the literature. Hopkins (1930) was the first to report ovalbumin precipitation due to protein denaturation by concentrated urea at various temperatures tested. It was observed that the denaturation rate was highest at 0°C compared to at 23°C. The adverse effect of temperature was unexpected, especially as it was known that the rate of denaturation increases as the temperature increases. Clark (1985), who later confirmed the conclusion of Hopkins, reported that the negative temperature effect on ovalbumin denaturation, but only at high concentrations of urea, while it is positive at low concentrations of urea. Induced denaturation by temperature effect on the GuHC1 was studied broadly on cytochrome c-552 by Nojima and co-workers (1987). The researcher found that this protein was stable at 27°C in 5.5 to 6.0 M GuHC1 solutions. The GuHC1 solutions were denatured when heating or cooling from 27^0C. Therefore, at low temperatures of manufacturing BSA loaded aquasomes, the protein might be unfolding or breaking which in both cases lowers the BSA loadings. This was also noticeable from the low energy values of BSA MD simulations performed at 300K and 280K.

2.3.4. Stability studies of BSA-loaded aquasomes

The stability of API formulations is important for patient's safety (the physical and chemical integrity of dosage form) as stability calculations of expiration date of the APIs formulation is based on it. Various degradation pathways can be adopted by pharmaceutical products such as hydrolysis, deamination, oxidation and cyclization. The prime target of accelerated stability studies is to calculate the long-term stability of formulations. These studies are performed by exposing API formulations to stress conditions of humidity, temperature, radiations and light. In general, companies conduct accelerated stability studies but the procedures that direct the practices may vary widely in terms of when and how these studies are to be performed (Waterman and Adami, 2005; Lee *et al*., 2010; Byrn *et al*., 2001; Fitzpatrick *et al*., 2002).

The stability studies of BSA-loaded aquasomes was conducted at three storage conditions of 4ºC ±1ºC/60% RH ±2%, 25ºC ±1ºC/60% RH ±2% and 40ºC ±2ºC/75% RH ±5%, Tables 2.11-13. The stability result of BSA loaded aquasomes at 4ºC ±1ºC/60% RH ±2% and 25ºC ±1ºC/60% RH ±2% conditions show no significant changes (p>0.05) in size, zeta potential and BSA content at storage conditions of 4ºC ±1ºC/60% RH ±2% and 25ºC ±1ºC/60% RH ±2% for 90 days. The *in vitro* release data for both conditions were similar and statistically comparable (p>0.05). At 40ºC ±1ºC/60% RH ±2% storage conditions BSA loaded aquasomes failed due to BSA degradation The release of BSA was sustained for 6 hr at 90 rpm/37^{0}C release conditions. The stability result of BSA loaded aquasomes at 40ºC ±1ºC/60% RH ±2% show a marked decrease in BSA content after 14 days' time point (1 month 80.9±5.3). The decrease was continued until 90 days' time point when it reached 55.61±9.5 (**p<0.001). There was also a decrease in zeta potential, but without significant change size.

Table 2.11. Stability study result of BSA-loaded aquasome powder for size, zeta potential, BSA content and visual inspection. Storage condition was at 4ºC ±1ºC/60 % RH ±2% RH. Values are represented as mean ± mean (n=3).

	0 Day	7 Days	14 Days	30 Days	60 Days	90 Days
BSA content (%)	99.3±0.2	99.1±0.6	99.6±0.2	99.1±0.3	99.3±0.4	98.1±0.7
Zeta potential	17±0.9	17.5±1.9	17.1±1.6	18.9±2.9	16.3±2.1	17.0±1.1
Size (µm)	923±75	920±85	940±60	970±98	920±75	933±45
Visual inspection (discoloration and agglomeration)	Pass	Pass	Pass	Pass	Pass	Pass

Table 2.12. Stability study result of BSA-loaded aquasome powder for size, zeta potential, BSA content and visual inspection. Storage condition was at 25ºC ±1ºC/60 % RH ±2% RH. Values are represented as mean ± mean (n=3).

	0 Day	7 Days	14 Days	30 Days	60 Days	90 Days
BSA content (%)	99.3±0.2	99.2±0.6	98.8±0.4	98.9±0.3	98.1±0.5	97.1±1.2
Zeta potential	17±0.9	16.2±1.6	16.1±2.4	15.9±1.8	15.9±1.8	17.3±0.8
Size (µm)	923±75	950±70	950±70	920±75	920±90	930±61
Visual inspection (discoloration and agglomeration)	Pass	Pass	Pass	Pass	Pass	Pass

Table 2.13. Stability study result of BSA-loaded aquasome powder for size, zeta potential, BSA content and visual inspection. Storage condition was at 40ºC ±1ºC/60 % RH ±2% RH. Values are represented as mean ± mean (n=3).

	0 Day	7 Days	14 Days	30 Days	60 Days	90 Days
BSA content (%)	99.3±0.2	98.1±1.6	95.8±1.9	80.9±5.3	55.61±9.5	55.61±9.5
Zeta potential	17±0.9	15.2±1.1	17.1±0.6	12.6±1.8	10.3±3.8	10.3±3.8
Size (µm)	923±75	951±63	941±69	980±55	966±70	966±70
Visual inspection (discoloration and agglomeration)	Pass	Pass	Pass	Pass	Agglomeration present	Agglomeration present

2.4. Conclusions

Different core and coating materials were used to manufacture under different manufacturing conditions to investigate the relationship between manufacturing conditions and loading capacity of the prepared aquasomes. Results show that aquasomes with DCPA cores coated with lactose resulted in higher loadings of BSA when compared to DCPA aquasomes coated with trehalose. The effect of manufacturing conditions on the prepared aquasomes could not be established due to size distribution variability. MCPA as a core material failed due to change in crystal form. Aquasomes with HA solid cores coated with lactose resulted in less BSA loadings when compared to HA aquasomes coated with trehalose. BSA loading of HA aquasomes was dependent on manufacturing conditions. High BSA loading was achieved at low temperatures and longer mixing times, which supports the fact that these conditions encourage physical adsorption. In terms of loading efficiency, HA aquasomes, with either lactose or trehalose as a coating material, have the highest BSA loading (40%- 60%) when compared to DCPA aquasomes. While DCPA aquasomes, with either lactose or trehalose as a coating material, have the lowest BSA loading (8%-16%).

It was concluded from the *in vitro* release studies that when the coating is performed at 4^0C and the loading step is performed at 25^0C this resulted in higher BSA loadings in the case of trehalose when compared to lactose as a coating material. This is interesting as it was hypothesised for aquasomes that low manufacturing conditions would result in high loading efficiency. It was noticed that monosaccharides produced low BSA loadings when HA cores were used. This could be because of the low OH groups per molecule (4 OH groups per molecule) compared to disaccharides (8 OH groups per molecule). In general, the conditions for preparation of aquasomes which was brought forward for the work concluded in this thesis was coating at 4ºC and loading at 25ºC for 2 hr with HA and trehalose as the solid core and coating materials respectively. Desirable BSA loadings were achieved (7 mg/100 mg) at these conditions.

Docking and MD simulations performed were essential to understand the forces that governs the assembly of the three layers of the aquasomes. Surface analysis performed by Discovery Studio show that HA and trehalose interact by hydrogen bonding with the later acting as a hydrogen acceptor, while BSA show almost complete SAS and that there are numerous targets for trehalose attachments (no specific active site). This was further confirmed by performing docking studies, which confirms hydrogen bonding formation between HA and trehalose, and that there are 4 hydrogen bonds formed (4 per trehalose

molecule per 3 HA cell units). MD simulations of BSA performed by AMBER 12 shows a stable MD simulation of BSA for 5 ns. Total energy analysis of BSA on the two conditions performed (300K and 280K) support the experimental data of lower BSA loadings of aquasomes manufactured at 4^0C compared to those manufactured at 25^0C (p<0.05). This could be because BSA might have either started to denature/unfold at 4^0C, which eventually resulted in low BSA loadings obtained for aquasomes manufactured at 40C.

CHAPTER 3

Pulmonary Delivery of Aquasomes

3.1. Introduction

The use of drug inhalation as therapy dates back to 1,500 BC when the ancient Egyptians inhaled vapours for ritual or healing purposes (Patton and Byron, 2007). Lung conditions such as chronic obstructive pulmonary disease (COPD) and asthma have been treated for years using pulmonary drug delivery. Pulmonary drug delivery allows local treatment of various diseases, whilst minimising side effects from systemic administration (Lenzer, 2006). The lungs also offer a non-invasive systemic administration method with low enzyme activity and no hepatic first pass effect, which is suitable for biomolecules such as proteins and peptides (Wolf, 1998). The anatomy of the lungs may compensate for the reduced bioavailability of macromolecules. This includes a thin membrane (0.1-0.2 μm) and a large surface area (100 m^2) which are both qualities that does not limit absorption (Tortora and Grabowdki, 2003). For drug delivery via the lungs to be therapeutically effective, the amount of an API required for therapy has to pass the oropharynx. An API with an aerodynamic diameter between 0.5 and 5 μm tends to be deposited in the lower region of the respiratory tract where in the alveoli there is a longer residence time and the API can diffuse into the blood stream (Zanan *et al*., 1996; Cherian *et al*., 2000). Ideally, a successful inhaled drug delivery device must provide reproducible drug dosing and generate an aerosol at enough speed to pass the oropharynx. A good example of such devices include pressurised metered dose inhalers (pMDIs) and dry powder inhalers (DPIs) (Steckel and Brandes, 2004).

3.1.1. Pulmonary deposition of inhaled particles

There are four mechanisms along with target and formulation factors that determine where in the lung the inhaled particles will be deposited. These mechanisms are impaction, sedimentation, interception and diffusion. Impaction describes the event when particles impact with the bifurcation of the lung (it is where the trachea is divided internally into left and right bronchi), because they follow their original path (inertia). The deposition of the particles with such mechanisms is affected by the aerodynamic diameter, which ultimately is affected by particle mass, for this reason the heavier the particles the more deposition that occurs. Therefore, the bronchial region is where most of the heavier particles deposit. The second mechanism is sedimentation, where particles are deposited in the lower lung airways because of decreased airflow and narrower airways. As with the impaction mechanism, it depends on aerodynamic diameter. In some cases, particles may grow in size, due to their hygroscopic nature, which eventually deposit earlier in the upper airways than anticipated. The third mechanism is interception, which occurs when the outer edges of particles contact the surface of the airways of the lung and deviate from their original path, hence it is more evident within the lower airways. This deposition of particles with interception is greatly affected by particle

shape and the diameter of the airways. The fourth mechanism is diffusion, which affects particles with diameters of below 500 nm. The aerodynamic diameter has less influence on the deposition of larger particles in the lower airways. In this region, the airflow is low and the particles exhibit Brownian movements, which move from an area of high concentration to a lower concentration area (Tena and Clara, 2012; Yeh, *et al*, 1976; Scott, 2016).

3.1.2. Cascade impactors

To study the deposition of particles, cascade impactors provide a platform for *in vitro* characterisation. Cascade impactors include the Anderson Cascade Impactor (ACI), Multi-stage Liquid Impactor (MSLI) and the Next Generation Impactor (NGI). There are other types of methods apart from cascade impactors, such as Phase-Doppler particle size analysis (PDA), the particle time of flight (TOF) and laser diffractometry (LD). However, these methods provide an average particle size rather than size distribution and does not include particle density into size calculations (Marple *et al*., 2003; Vacellio et al., 2001; Byron et al., 2004).

Cascade impactors work based on impaction (inertia) to determine particle size and distribution in the lung. The air is introduced at a fixed velocity (30, 60 or 90 L/min) into a series of meshes. As the air velocity is fixed, the particles will be deposited according to aerodynamic diameter (cut-off diameter). The NGI was introduced in 1997 by collaborative work of prominent pharmaceutical companies to bring an impactor, which is robust and closely resembles the lung airways (Figure 3.1 and 3.2) (Copley, 2007).

Figure 3.1. A diagram shows NGI, which is used in the characterisation of pMDI and DPI formulations (Adapted from: US Pharmacopia monograph (<601>).

Figure 3.2. A diagram shows the stages of NGI and the dimension of the nozzles (Adapted from: Adapted from: US Pharmacopia monograph (<601>).

3.1.5. Aim and Objectives

The aim of the work in this chapter is to investigate pMDI and DPI as a platform for aquasomes for pulmonary delivery. To achieve this aim, the following objectives was sought:

- Formulate BSA and metronidazole loaded aquasomes as pMDI and DPI formulations.
- Investigate the aerodynamic behaviour of the pMDI and DPI formulations using NGI to identify lung distribution of aquasomes.
- Perform *in vitro* release studies with simulated lung fluid to determine the release profile of aquasome formulations.
- Perform cell culture studies with BEAS-2B cell lines to demonstrate the controlled release effect of aquasomes in comparison to salbutamol sulphate which was used as a model drug.
- Perform stability studies to explore the stability of pMDI and DPI formulations.

3.2. Materials and Methods

3.2.1. Materials

Hydroxyapatite powder (99%), trehalose powder of (99%), cellobiose powder (99%), HPLC grade acetonitrile (99%), metronidazole (99%), salbutamol sulphate (99%), trifluoroacetic acid (TFA) (99%) and Bovine Serum Albumin (BSA) powder (99%) were purchased from Sigma Aldrich, UK. Modified Eagle's Minimum Essential Medium solution, Earle's Balanced Salt Solution (EBSS), L-glutamine, nonessential amino acids, sodium bicarbonate, sodium pyruvate, Fetal Bovine Serum (FBS), Penicillin-Streptomycin (pen/strep) antibiotic solution and 0.25% (w/v) Trypsin were purchased from Fisher Scientific, USA. Hydrofluoroalkane (HFA)-134a (pharmaceutical grade) was purchased from INEOS Fluor, UK. All materials were used as received unless otherwise specified. Ultra-pure grade water was used when required.

3.2.2. Preparation of Aquasomes

3.2.2.1. Freeze-drying protocol

In the preparation of aquasomes, freeze-drying process was used. The freeze-dryer used was Vir Tis Advantage Plus, USAa. A freeze-drying cycle of 24 hr was performed. The cycle consisted of four stages; pre-stage (60 min at -45ºC/atmospheric pressure), primary drying stage (720 min at -45ºC under vacuum of 400 mbar), secondary drying stage (460 min at -20ºC under vacuum of 400 mbar) and equilibrium stage (240 min at 25 ºC). The condenser temperature was set at -76ºC. Freeze-drying vials and lids were used where required.

3.2.2.2. Aquasomes preparation

Aquasomes were manufactured by modifying the method of Kossovsky *et al.* (1995). A quantity of 100 mg of hydroxyapatite powder (HA) was mixed with trehalose solution (0.1 M) for 2.5 hr at 25ºC. The resulting coated cores were then centrifuged (3000 rpm for 10 min), washed to remove unadsorbed trehalose and then freeze-dried. A quantity of 10 mL of BSA solution (1 mg/mL) was added to the freeze-dried sample under stirring for 2.5 hr at 25ºC. The sample was then centrifuged (3000 rpm for 10 min), washed to remove unadsorbed BSA and freeze-dried.

3.2.3. Powder Characterisation

3.2.3.1. HPLC analysis

Drug analysis from the *in vitro* release studies and the amount deposited in the NGI stages was analysed using an Agilent 1200 series HPLC System equipped with UV and fluorescence detectors (Germany). Analysis was performed at ambient temperatures.

3.2.3.1.1. BSA HPLC method

For HPLC analysis of BSA, a C18-ODS Jupiter column (4.6 mm x 250 mm / 5 µm / 300 Å (Phenomenex, USA) was used. The injection volume of the sample was set at 100 µL. Fluorescent detection method was used with excitation wavelength of 220 nm and emission wavelength was set at 312 nm. A gradient elution method was used during which the proportion of solution B (acetonitrile) in the eluent increased from 5% to 65% solution against solution A (0.01%, v/v trifluoroacetic acid in ultra-pure water). The flow rate of mobile phase was set at 1 mL/min. BSA eluted with a retention time of 17.0 min. A standard calibration curve was established by the use of BSA standard solutions (r^2 = 0.998), which was used for the determination of unknown BSA concentration samples. The HPLC method was adapted from Umerthia *et al*., (2010).

3.2.3.1.2. Metronidazole HPLC method

For HPLC analysis of metronidazole, a C18 Luna column (4.6 mm x 150 mm / 5 µm / 300 Å (Phenomenex, USA) was used. The injection volume of the sample was set at 100 µL. Fluorescent detection method was used with excitation wavelength was set at 275 nm and emission wavelength was set at 312 nm. An isocratic elution method was used during which the proportion of solution B (methanol) in the eluent was 60% against solution A (0.01%, v/v trifluoroacetic acid in ultra-pure water). The flow rate of mobile phase was set at 1 mL/min. metronidazole eluted with a retention time of 3.0 min. A standard calibration curve was established by the use of metronidazole standard solutions (r^2 = 0.997), which was used for the determination of unknown metronidazole concentration samples. The HPLC method was adapted from Tashtoudh *et al.* (2008).

3.2.3.1.3. Salbutamol sulphate HPLC method

For HPLC analysis of salbutamol sulphate, a C18 Luna column (4.6 mm x 150 mm / 5 µm / 300 Å (Phenomenex, USA) was used. The injection volume of the sample was set at 100 µL. Fluorescent detection method was used with excitation wavelength was set at 292 nm and emission wavelength was set at 312 nm. An isocratic elution method was used during which the proportion of solution B (acetonitrile) in the eluent was 50% against solution A (0.01%, v/v trifluoroacetic acid in ultra-pure water). The flow rate of mobile phase was set at 1 mL/min. Salbutamol sulphate eluted with a retention time of 2.5 min. A standard calibration curve was established by the use of salbutamol sulphate standard solutions (r^2 = 0.997), which was used for the determination of unknown salbutamol sulphate concentration samples. The HPLC method was adapted from Pai *et al.* (2009).

3.2.3.2. Preparation of pMDI formulations

BSA-loaded aquasome pMDI formulations were prepared by adding 100 mg of the BSA-loaded aquasomes powder into pMDI canisters (glass canister was used for stability studies and metal canister for any other studies). Pamasol crimper (Pamasol Willi Mäder AG, Pfäffikon, Switzerland) was used to crimp the valve (BK357 30 µL) onto the pMDI vials. Pamasol propellant filler (Pamasol Willi Mäder AG, Pfäffikon, Switzerland) was used to fill the pMDI vials with approximately 10 g of HFA-134a. The final pMDI formulation formed a suspension of an approximate concentration of 1.0% w/w. Crimping and filling of the canisters were carried out at ambient temperature.

3.2.3.3. Preparation of aquasomes DPI formulation

A quantity of 20 mg of aquasomes powder was loaded into size 3 hydroxypropyl methylcellulose (HPMC) capsules (Shionogi Qualicaps). The HPMC capsules were placed into a Cyclohaler®. The capsules are pierced before introducing the Cyclohaler® to the mouth tip of the NGI. Capsule loading was performed at ambient temperatures.

3.2.3.4. *In vitro* powder aerosolisation

The aerosolisation of aquasomes were investigated using an NGI, Copley Scientific, UK. In the case of the pMDI formulations of aquasomes, the pMDI canister was introduced to the 1-7 stages of the NGI by spraying into the mouthpiece, which was attached to the throat piece. In the case of the pMDI formulation, the Cyclohaler® is fixed into the mouthpiece. Prior analysis, a digital flow meter (Model DFM2, Copley Scientific, UK) was used to set the flow rate through the NGI at 60 ±1 L/min for 5. After introduction of the pMDI formulation, the NGI was disassembled and the powder in the trays was weighed. An adjustment was required to the NGI for DPI formulation assessment, a pre-stage is added between the NGI. The pre-stage is a stage consisting of a perforated disk with a 15 mL reservoir in the centre. The same procedure as pMDI were followed for DPI formulations in terms of aerodynamics and formulation recovery. The procedure was adopted from USP26 (601).

3.2.3.5. *In vitro* release studies

Simulated lung fluid (Gamble's solution) was prepared by dissolving the required components in 1L of ultra-pure grade water (Table 3.1). The solution was then left standing for 4-5 hr at ambient temperature to check for any salt precipitation, which if occurs, the solution was discarded and a fresh 1L was prepared. *In vitro* release studies were performed on the aquasomes collected from stages 3 and 5. The samples were redistributed in 10 mL of simulated lung fluid and placed in a shaking water bath at 37^{o}C/100 rpm. A quantity of 0.3 mL

was taken for HPLC analysis (section 3.2.3.1) at hourly time points up to 6 hr. The release medium was replaced with 0.3 mL of fresh pre-heated simulated lung fluid.

Table 3.1. The required components to prepare the simulated lung fluid (Gamble's solution) used for the in vitro release studies of pMDI and DPI aquasomes formulations.

Material	Amount (mg)/L
Potassium chloride	720
calcium chloride dehydrate	220
sodium chloride	600
potassium phosphate monobasic	680
sodium phosphate dibasic	866
potassium carbonate	1500
potassium thiocyanate	60
citric acid	30

3.2.3.6. Aerosolisation parameters of pMDI and DPI formulation

To assess the aerosolisation performance of the pMDI and DPI formulations, emitted dose (ED), fine particle dose (FPD) and fine particle fraction (FPF) were calculated. ED was calculated as the percentage of total loaded powder weight exiting the pMDI vial. FPD was calculated as the weight of drug less than 5 µm (NGI stages 2-6). FPF was calculated as the ratio of FPD to total loaded dose. The same procedure of calculation was followed for DPI formulations.

3.2.7. Procedure for BEAS-2B cell lines

3.2.7.1. Cell lines maintenance

BEAS-2B cell lines were received as a gift from Dr Lindsay Marshall, Aston University. The cells were maintained using medium comprised from Dublecco's modified Eagle's medium (DMEM), 0.5% penicillin-streptomycin, 10% fetal bovine serum (FBS), 2% glutamate solution and 1% nonessential amino acids (NEAA). The cells were incubated at 37°C temperature and 5% CO_2. The cells were feed every day and passaged every 2-3 days. The media, HBSS and trypsin were preheated to 37°C in a water bath prior to mixing. A quantity of 10 mL of HBSS solution was used to wash the flask containing the cells to remove traces of FBS and dead BEAS-2B cells. Trypsin was added (3 mL of 0.25% w/v) to the flask and Incubated for 5-10

min at 37°C. After the detaching of the cells, a quantity of 10 mL of media was added to quench trypsin effect. To prevent clumping of BEAS-2B cells, the mixture was pipetted 3-4 times. A quantity of Caco-2 cells was then placed in a new flask (1 mL to a 75cm^2 and 0.5 mL to a 25cm^2 flask). The media was then added to the flask (20 mL to a 75cm^2 and 10 mL to a 25cm^2 flask) and incubated at 37°C.

3.2.7.2. Cell Counting

To count the BEAS-2B cells, a haemocytometer was used. A haemocytometer is a slide made of thick glass with a rectangular indentation to create a chamber. The chamber is carved with perpendicular lines by laser-etched grid. After addition of trypsin to BEAS-2B cells, a quantity of 1 mL was placed in an Eppendorf tube in to which a quantity of 100 µL of trypan blue was added. After thorough mixing, a quantity of the mixture was then moved and added to the upper edge of the haemocytometer. Using an inverted light microscope and under a suitable objective (10-20x), the cells were counted in the four corners with exclusion of the cells outside the four rectangular indentation. To calculate the total number of the cells, the following equations were used:

$$\text{Cells count} = \frac{\text{total No. of cells counted}}{4} \text{x2} \ldots\ldots (2) \qquad \% \text{ of viability} = \frac{\text{number of live cells}}{\text{total number of cells}} \ldots\ldots\ldots (3)$$

3.2.7.3. Cell viability assay

A 96 well plates were used to seed the BEAS-2B cells at a concentration of 1x10^6 cells/well. Then, the cells were incubated for 24 hr. Afterwards, the media, and a quantity of metronidazole was added to the wells (C to H) and incubated for 24 hr (well A and B are controls). After the 24 hr, an amount of 10 µL of 3-(4, 5-dimethylthiazolyl-2)-2, 5-diphenyltetrazolium bromide (MTT) was added to each well and the cells were then incubated for a period of 4 hr. The cells were then shaken for 15 min using an electric shaker and measured for absorbance at a wavelength of 520 nm using Bio Rad microplate reader, model 3350, USA. All measurements were performed in triplicate (n=3). The values are reported as mean ± standard deviation.

Table 3.2. Concentrations of salbutamol, trehalose and HA used in the cell viability assays of BEAS-2B cell lines for the delivery of aquasomes via the pulmonary route.

Description	Concentrations used
Salbutamol sulphate solution	10, 20, 40, 80, 90 and 100 µg
Trehalose solution	10, 20, 40, 80, 90 and 100 µg.
HA suspension	10, 40, 80, 90, 100 and 150 µg

3.2.7.4. TEER measurements

For TEER measurements, the cells at a concentration of 2 x 10^5 cells/cm² were seeded on 6-well trans-well plates with polycarbonate-coated membranes (24mm; 4.7cm²; 0.33 cm^3). The cells were allowed to grow for 20 days. The media in the apical and basal compartments was replaced every 1-2 days. TEER were recorded every 2 days using an epithelial voltmeter, (World precision, USA). The measurements were performed in triplicate and each well was measured from three different sides to reduce reading errors. All measurements were performed in triplicate (n=3). The values are reported as mean ± standard deviation.

3.2.7.5. Permeability studies

The cells were grown on 6-well Transwell® as described in section 4.2.4.4. After replacing the exhausted media from the apical and basal compartments, 1.5 mL of plane media (MDEM) mixed with metronidazole at a concentration of 200 µg/mL was added to the apical compartment. At time intervals of 1, 2, 3, 4, 5 and 6 hr, an amount of 300 µL was taken from both compartments and analysed using HPLC (sections 4.2.3.4). For permeability studies, HBSS was used to wash the cells prior the addition of the drug and pre-equilibrated for 1 hr with blank media. Afterwards, blank media was removed and the concentrations of metronidazole mixed with blank media was added subsequently. All measurements were performed in triplicate (n=3). Permiability methods were adopted from Khan *et al*. (2011). The values are reported as mean ± standard deviation. The percentage of drug transported was calculated as shown in equation 4.

$$\%\ \text{of drug transported} = \frac{\text{Apical drug concentration} - \text{Basal drug concentration}}{\text{total drug loading}} \text{x}100 \quad \ldots\ldots\ldots(4)$$

3.2.8. Stability studies

BSA-loaded aquasomes pMDI and DPI formulations were stored at 4ºC ±1ºC/60% RH ±2% RH, 25ºC ±1ºC/60% RH ±2% RH and 40ºC ±1ºC/75% RH ±2% RH in accelerated stability

studies cabinet. At interval time points of 7, 14, 21 and 28 days, samples were taken for *in vitro* release studies (section 3.2.3.5). Visual inspection was performed on the samples, which include changes in colour and peeling. Stability methods were adopted from FDA guidelines Q1A (R2). All measurements were performed in triplicate (n=3). The values are reported as mean ± standard deviation.

3.2.9. Statistical analysis

A one-way analysis of variance with Tukey–Kramer multiple comparisons test was used statistically compared the results obtained from performed experiments. The significance level of analysis was $p<0.05$.

3.3. Results and Discussion

To assess the aerosolisation performance of pMDI and DPI aquasome formulations, there are certain parameters to examine. These parameters include ED, FPD and FPF (Table 3.3). In general, a successful pMDI and DPI formulations will score ED, FPD and FPF of >90%, >8% and >1 respectively.

Table 3.3. Aerosolisation parameters used in the assessing of pMDI/DPI formulations for the delivery of aquasome formulation.

	Acceptance level	Comments
ED	>90%	The higher the better as it indicates the amount of powder that exits the inhaler to the oral cavity (less waste).
FPD	>80%	The higher the better as indicates the fraction of the dispersed powder of less than 5 µm
FPF	>1	The higher the better.

To produce BSA-loaded aquasomes with enhanced powder aerosolisation, minor adjustments were performed to the freeze-drying method. It was noticed that BSA-loaded aquasomes have the tendency to form loose agglomerates when compared to metronidazole-loaded aquasomes. The tendency to form loose agglomerates could be related to Van der Waals forces or transitory forces as the protein is attached to the outer surface of the aquasomes (Senese, 2010). Such agglomerations can directly affect the aerodynamic performance of the BSA-loaded aquasomes (agglomerates were deposited in the first two stages of NGI). Therefore, to reduce the amount of agglomerates in the freeze-dried powder, the amount of water mixed with the formulation before the freeze-drying step was increased gradually in steps (0.2 mL, 0.4 mL and 0.6 mL) (Table 3.4). The aerosolisation performance of the powder, measured with the NGI, was enhanced as the amount of the water increased (Figure 3.3). It is known that as water temperature decreases, the volume of the water increases. This is because as the temperature of the water decreases the hydrogen bond strength decreases, which allow water molecule to expand in size. This also affects water density, as the density of water in frozen state is much less than in its liquid state (Chaplin, 2015; Deville *et al*., 2007). However, when higher volumes of water were added to the BSA-loaded aquasomes powder (>0.8 mL), the drug adsorbed onto the aquasomes started to be released (5% release which is equivalent 0.35±0.03 mg), which eventually reduced the loading efficiency.

Table 3.4. The deposition of BSA-loaded aquasomes DPI formulations in the stages of the NGI. The table shows the improvement in aerosolisation of the DPI formulations as the amount of water increases prior to freeze-drying. Values are represented as mean ± mean (n=3).

Stage	Cut-off diameter (µm)	Amount of water (mg) / 0.2 mL	Amount of water (mg) / 0.4 mL	Amount of water (mg) / 0.6 mL
Device	-	4.2 ± 1.1	1.8 ± 0.22	0.5 ± 0.05
Throat	-	1 ± 0.20	1.33 ± 0.20	1.33 ± 0.30
Pre-Stage	> 8.06	4.2 ± 0.44	2.9 ± 0.90	1.46 ± 0.37
Stage 1	8.06	3.5 ± 0.62	2 ± 0.12	< 1
Stage 2	4.40	4.5 ± 0.97	6.2 ± 1.41	1.5 ± 0.36
Stage 3	2.82	1.2 ± 0.55	1.2 ± 0.39	4.03 ± 0.85
Stage 4	1.66	< 1	3.5 ± 0.81	4.53 ± 0.58
Stage 5	0.94	< 1	< 1	4.63 ± 0.24

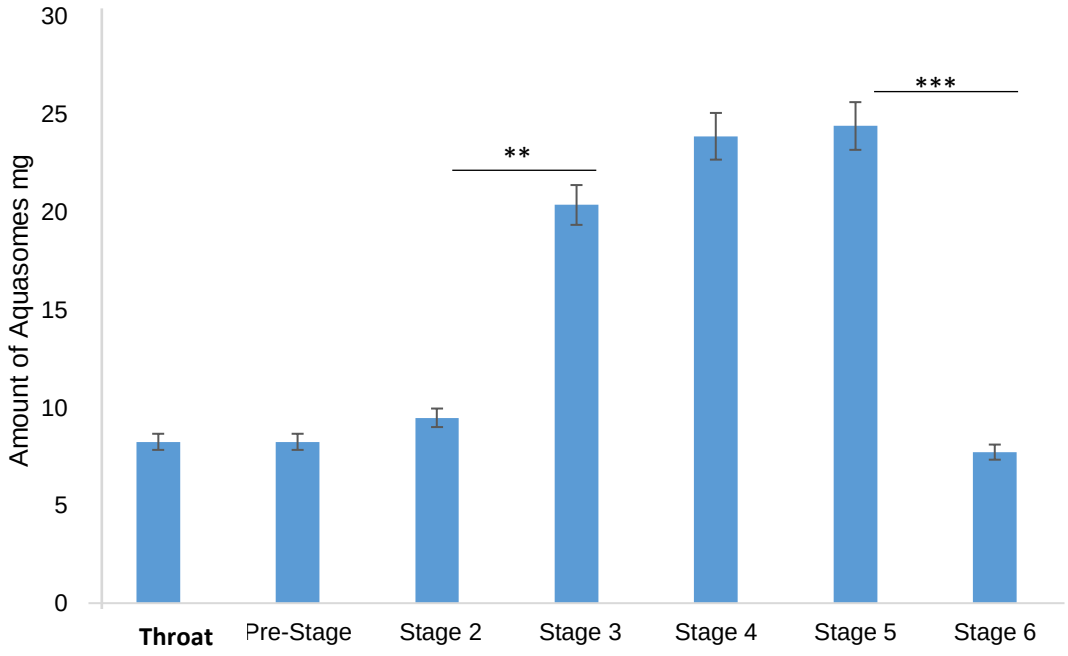

Figure 3.3. A bar chart shows the DPI formulation of BSA-loaded aquasomes deposited in the stages of the NGI (formulated with 0.6 mL ultra-pure water mixed with the powder after freeze-drying). BSA-loaded aquasomes show enhanced aerosolisation as most of the deposited powder were in NGI stages 3, 4 and 5. Values are reported as mean ± SD (n=3). Statistical analysis (one-way ANOVA/Tukey) between stages: $^{**}p < 0.01$, $^{***}p < 0.001$.

In both cases of pMDI and DPI formulations of metronidazole-loaded aquasomes, the drug loading during *in vitro* release studies were at or below the limit of quantification (LOQ) of the metronidazole HPLC method. The formulations were treated with 0.1 % Triton X to dissemble the system and then the total loading of the formulation was calculated. The reason that the loading of metronidazole is lower than that of BSA could be because metronidazole has a molecular weight of 171.153 g/mol, while BSA has a molecular weight of 66,463 g/mol. This results in higher attraction forces of BSA molecules (583 residues) to that of metronidazole per molecule, which eventually decreases the loading despite the concentrated solution of metronidazole used to prepare the metronidazole-loaded aquasomes. This is further explained in Chapter 2.

3.3.1. pMDI formulation of aquasomes

3.3.2.1. pMDI formulations of BSA-loaded aquasomes

The dispersant aiders are used to produce a dispensable powder, which eventually enhances the aerosolisation performance. L- Leucine is one of the known dispersant aiders that has widely been used in pMDI and DPI formulations to produce dispersible powders. It is interesting to indicate that aquasomes showed high dispersability (ED 94.86% ±2.6) without the use of dispersant aiders (Table 3.5). The aerosolisation performance of the particles was assessed using the NGI. Table 3.4 shows the amount of aquasomes and the percentage of the delivered dose of aquasomes to each stage of the NGI. It can be observed that (54.7% ±6.85) of the delivered dose has a cut-off diameter of 2.82 µm. It has been recognized that particle deposition in the lower respiratory region occur at aerodynamic diameter between 0.5-5 µm. For systemic circulation, this is the optimum location for the drug to diffuse into the blood stream. In addition, the BSA-loaded aquasomes showed high dispersability, which indicate that inhalation of these formulation powders would be associated with low incidence of local side effects which results from the low deposition of these powders in the oropharyngeal region (Koleswara, 2007; Rabe, 2006).

ED and FPD values of the aerosolised aquasome formulations were used to calculate FBF and the percentage of aquasomes delivered to each step of the NGI. FPD is an indication to what fraction of the delivered dose is less than 5 µm, which draw an indication to the deposition of the powder in the mid-lower lung region. It is noticeable that the majority of the deposited aquasomes were in stages 2, 3 and 4 which is in the terminal bronchiole region (Figure 3.4). The collected powder in stages 6 and 7 was unprocessable and hence the reduction was calculated from the delivered dose, which was anticipated to belong to those stages. The FBF

score of the BSA-loaded aquasome formulation was above 1, which shows that a large percentage of the aquasomes powder exited the pMDI vial and has deposited in the NGI stages with minimum waste. It is noted that the aerosolisation performance of the BSA powder was not performed as in its original state the powder causes blockage of the pMDI valve. To produce a respirable powder, it has to be dissolved in water, mixed with a dispersible aider and then spray dried to produce the final powder. Since the aim of the current study is to sustain the release of BSA (develop a controlled release system), BSA respirable powder was not produced as a control, instead, freeze-dried BSA powder was used as a control for the *in vitro* release studies of the aquasome pMDI formulations.

Table 3.5. The cut-off diameter of the NGI stages, ED, FBD, FBF, mass of aquasomes, actual amount of BSA and the theoretical amount of BSA at each stage of pMDI formulation of BSA-loaded aquasomes. Values are mean ± SD (n = 3).

Stage	Cut-off Diameter (µm)	Amount of Aquasomes (mg)	ED	FBD	FBF	Aquasomes Delivered (%)	Theoretical amount of Drug (mg)	Actual Amount of Drug (mg)
Unprocessed formulation	-	100				-		7.0 ±0.89
Device	-	4.9 ±1.39	94.86 ±2.6	80 ±1.5	1.18	-		-
Throat	-	6.1 ±1.35				-	0.043 ±0.09	-
Stage 1	8.06	3.7 ±0.6				4.6 ±0.75	0.259 ±0.04	0.45 ±0.12
Stage 2	4.40	18.7 ±2.13				22.7 ±2.86	1.27 ±0.15	1.6 ±0.40
Stage 3	2.82	44 ±5.29				54.7 ±6.58	3.08 ±0.37	2.24 ±0.09
Stage 4	1.66	12.6 ±2.51				15.7 ±3.13	0.88 ±0.17	0.95 ±0.10
Stage 5	0.94	5.5 ±0.5				6.8 ±0.62	0.385 ±0.03	0.65 ±0.03

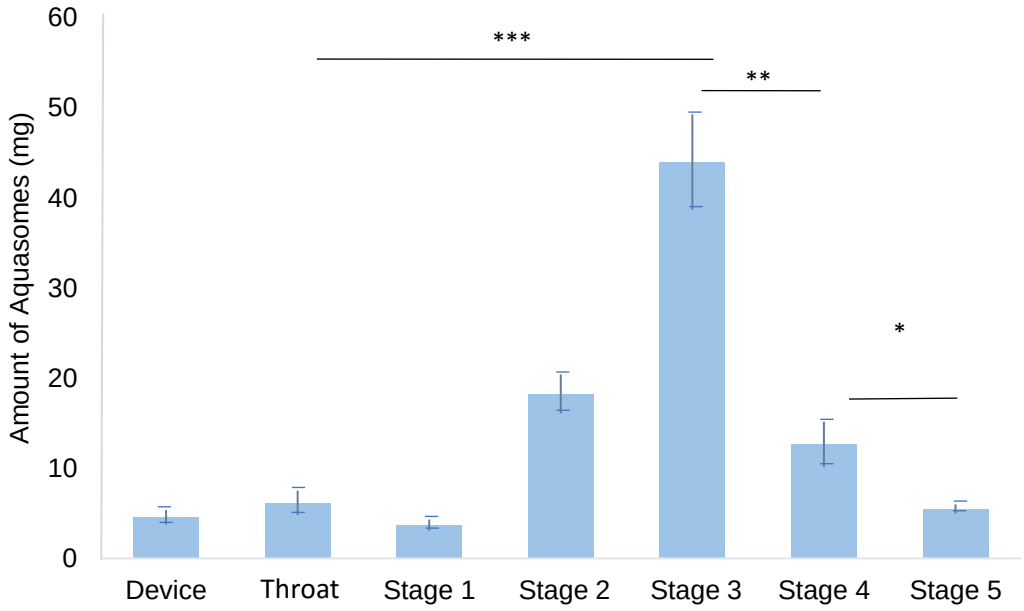

Figure 3.4. The amount of aquasomes deposited at different stages of the NGI of a pMDI formulation of BSA-loaded aquasomes. The majority of the deposited aquasomes were in stages 2, 3 and 4 which is in the terminal bronchiole region Values are reported as mean ± SD (n = 3). Statistical analysis (one-way ANOVA/Tukey) between stages: *$p < 0.05$, **$p < 0.01$, ***$p < 0.001$.

3.3.2.2. *In vitro* release studies of pMDI formulation of BSA-loaded aquasomes

Even though there is a vast amount of research within the area of pulmonary drug delivery, the release models for inhalable powders are rarely discussed. However, the absence of a suitable model for pulmonary *in vitro* release is interesting. This is because with inhalable drug delivery systems, the onset of action is critical to assess the formulation. To elaborate more, in the literature, unprocessed powders are used as a reference. However, it is with no doubt, the powder undergoes immediate release unless the drug has poor solubility or dissolves under certain pH conditions (which is not the case in the present study) (Learoyda *et al.,* 2010; Taylor *et al*., 2006; Learoyd *et al*., 2008).

Figure 3.6 shows the release of BSA from aquasomes with aerodynamic diameters of 2.82 and 0.94 µm (stages 3 and 5 respectively) and BSA-loaded aquasomes powder. Stage 3 was the stage where most of the deposition of aquasomes occurred (mid region of lung) and stage 5 represents the alveoli region. The BSA release from aquasomes was controlled over the 6 hr study with no burst effect noticed. A small burst was observed from aquasomes collected from stage 5, which was statistically significant compared to control ($p < 0.01$). This could be related to the large amount of the release media used (10mL) which may have contributed to

a higher number of water molecules being attracted to the system compared to the 100 mg of manufactured aquasomes (Kossovsky *et al*., 1995). On the other hand, these studies exhibit the potential to sustain drug release through aquasomes. It is interesting to observe that over the 6 hr study, BSA-loaded aquasomes with an aerodynamic diameter of 0.94 µm released 650±0.03 µg of BSA (9.2% ±0.5 of total loading). This is very encouraging for potential protein/peptide delivery using aquasomes via the pulmonary route. As to achieve maximum therapeutic effect dose not streamed from optimisation of inhaled delivery device only, but also from well-designed formulation or delivery systems (Onoue *et al.*, 2008).

BSA-loaded aquasomes released approximately 95% of the initial loading over the 6 hr of the release study (Figure 3.5 and 3.6). *In vitro* release studies for stages 3 and 5 show the amounts of BSA of 2.24±0.09 mg and 0.65±0.03 mg respectively (Table 3.4). However, these values are different to the theoretical loadings by 27% and 71% respectively. This deviation could arise because the size distribution width is high (990±120 µm), which could result in an uneven distribution of BSA-loaded aquasomes in stages 3 and 4. However, it would be interesting to investigate if such deviation can be overcome by sonicating the cores at higher sonication amplitudes to produce a more uniform particle size (Learoyd *et al*., 2009; Alessandra *et al*., 2008).

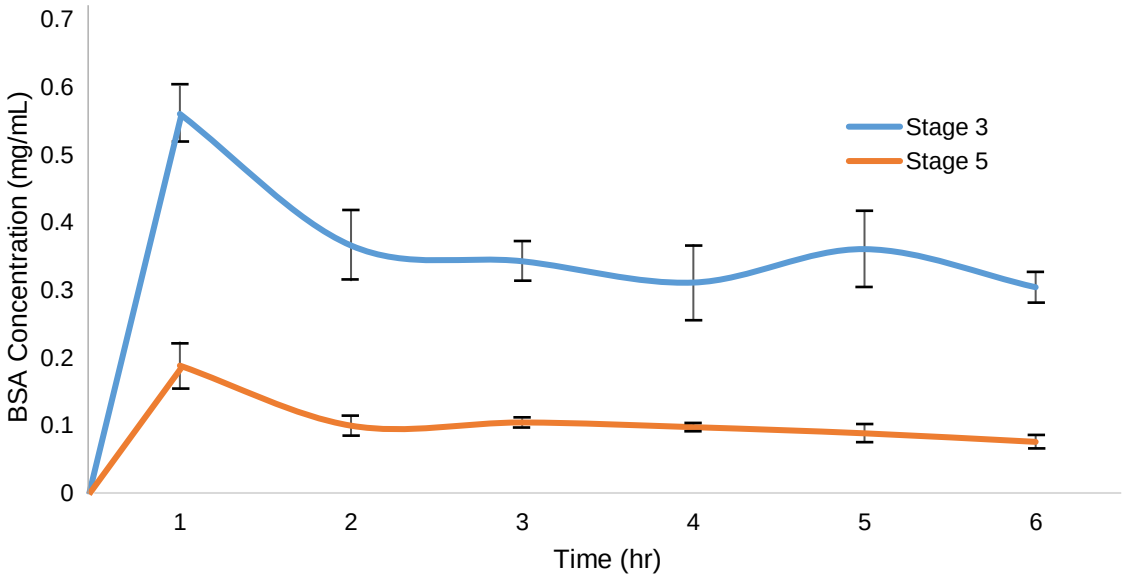

Figure 3.5. The hourly BSA concentration released from aquasomes taken from NGI stages 3 and 5 of pMDI formulation of BSA-loaded aquasomes. BSA-loaded aquasomes in both stages show a sustained release of BSA. Values are reported as mean ± SD (n = 3).

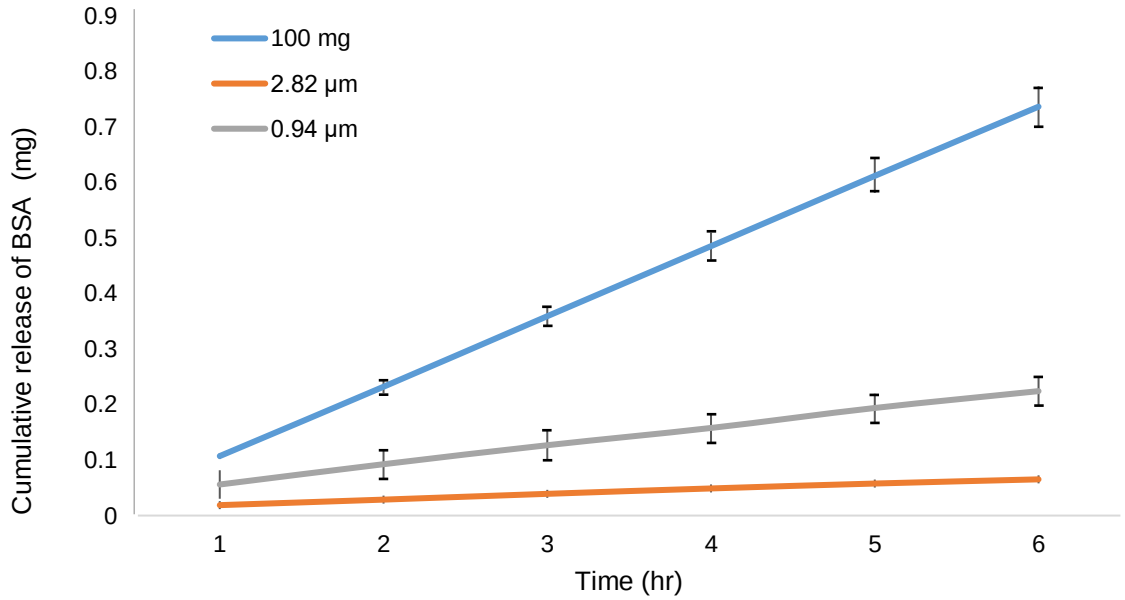

Figure 3.6. A figure shows the cumulative release of BSA from 100 mg aquasomes (r^2 0.999), aquasomes collected from stage 3 (r^2 0.998) and aquasomes collected from stage 5 (r^2 0.997) of pMDI formulation of BSA-loaded aquasomes. Values are reported as mean ± SD (n = 3).

3.3.2. pMDI formulation of metronidazole-loaded aquasomes

As with the BSA-loaded aquasomes pMDI formulation, dispersant aiders were not used in the process of formulation for metronidazole. The ED of the pMDI formulation of metronidazole-loaded aquasomes was 94.5 ±1.6%. The aerosolisation performance of metronidazole-loaded aquasome particles was evaluated using the NGI and the results are presented in table 3.6. A percentage of 66.2% ±4.9 of the delivered dose has a cut-off diameter of 2.82 µm. pMDI formulation of metronidazole-loaded aquasomes show similar trends to pMDI formulation of BSA-loaded aquasomes in terms of these particles will be expected to deposit in the lower respiratory tract and the alveoli and have high dispersability, which indicate low incidence of local side effects. The percentage of the metronidazole-loaded aquasomes in each stage of the NGI shows that the majority of the deposited aquasomes were in stages 2 and 3, which are in the terminal bronchiole region (Figure 3.7). As for the collected powder in stages 6 and 7, this was unprocessable and hence the reduction was calculated from the delivered dose, which was anticipated to belong to those stages. The FBF score of the metronidazole-loaded aquasome formulation was 1.17. This shows that a greater percentage of the aquasome powder exited the pMDI vial and has deposited in the NGI stages with minimum waste.

As was the case for the BSA-loaded aquasomes, metronidazole powder is not a respirable powder (section 3.3.2.1). Since the aim of the study is to sustain the release of metronidazole (develop a controlled release system), metronidazole respirable powder was not produced as

a control, instead, metronidazole powder was used as a control in the *in vitro* release studies of the aquasomes pMDI formulations.

Table 3.6. The cut-off diameter of NGI stages, ED, FBD, FBF, mass of aquasomes, actual amount of metronidazole and the theoretical amount of metronidazole at each stage of the pMDI formulation of metronidazole-loaded aquasomes. Values are reported as mean ± SD (n = 3).

Stage	Cut-off Diameter (µm)	Amount of Aquasomes (mg)	ED	FPD	FPF	Aquasomes Delivered (%)	Theoretical amount of Drug (mg)	Actual Amount of Drug (mg)
unprocessed Formulation	-	100				-		0.4 ±0.09
Device	-	3.9 ±1.2	94.5 ±1.6	80.5 ±1.1	1.17	-		-
Throat	-	4.1 ±1.1				-	-	-
Stage 1	8.06	3.2 ±0.6				3.7 ±0.4	0.01 ±0.002	un quantified
Stage 2	4.40	20.7 ±1.1				24.0 ±2.2	0.08 ±0.002	0.09 ±0.04
Stage 3	2.82	49.2 ±3.3				56.9 ±6.2	0.19 ±0.004	0.28 ±0.05
Stage 4	1.66	9.6 ±2.0				11.1 ±2.9	0.03 ±0.003	un quantified
Stage 5	0.94	3.5 ±0.5				4.0 ±0.3	0.01 ±0.002	un quantified

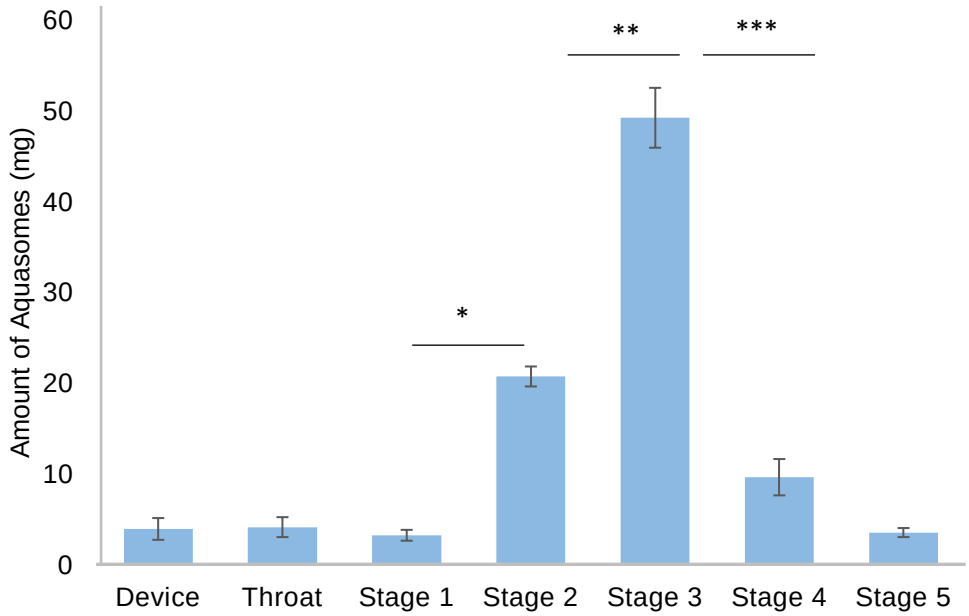

Figure 3.7. A bar chart shows the amount of aquasomes deposited at different stages of NGI of the pMDI formulation of metronidazole-loaded aquasomes. Values are reported as mean ± SD (n = 3). Statistical analysis (one-way ANOVA/Tukey) between stages: *$p < 0.05$, **$p< 0.01$, ***$p < 0.001$.

3.3.2.1. *In vitro* release studies of pMDI formulation of metronidazole-loaded aquasomes

As shown in Figure 3.8, the release of metronidazole from aquasomes with aerodynamic diameters of 2.82 (NGI stage 3) was controlled over the 6 hr of study. The release of metronidazole from aquasomes with aerodynamic diameters of 2.82 exhibit the potential to sustain drug release through aquasomes. Aquasomes collected from NGI stages 1, 2, 3, 4 and 5 was washed with simulated lung fluid and analysed using HPLC (3.2.3.3). The loading of the 100 mg of metronidazole-loaded aquasomes was less comparable to that of BSA (0.4 mg ±0.09), therefore, it was difficult to quantify metronidazole because these concentrations are less than the LOQ of the HPLC method.

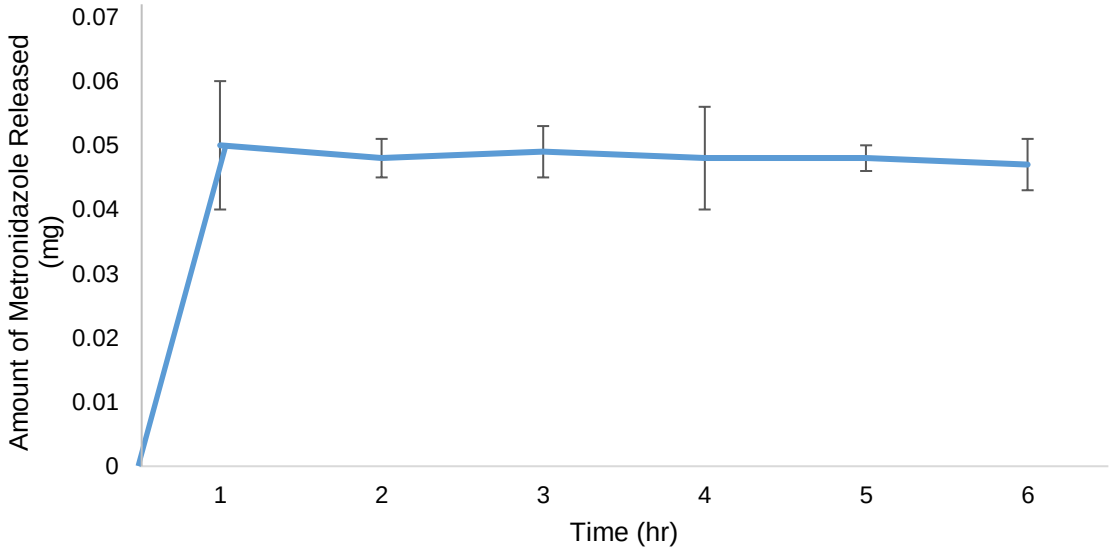

Figure 3.8. A figure shows the amount of metronidazole released from aquasomes collected from NGI stage 3 of the pMDI formulation of metronidazole-loaded aquasomes. Values are reported as mean ± SD (n = 3).

However, metronidazole was detected in stages 1, 4 and 5. Metronidazole-loaded aquasomes released 96% of the initial loading after 6 hr of release (Figure 3.9). *In vitro* release studies for stages 2 and 3 show that metronidazole loading was of 0.09 mg ±0.04 and 0.28 mg ±0.05 respectively. Though, these values are different to the theoretical loadings of metronidazole by 12.5% and 47.3% respectively (Table 3.5). The reason to why such deviation from the theoretical metronidazole loadings was explained in section 3.3.2.2.

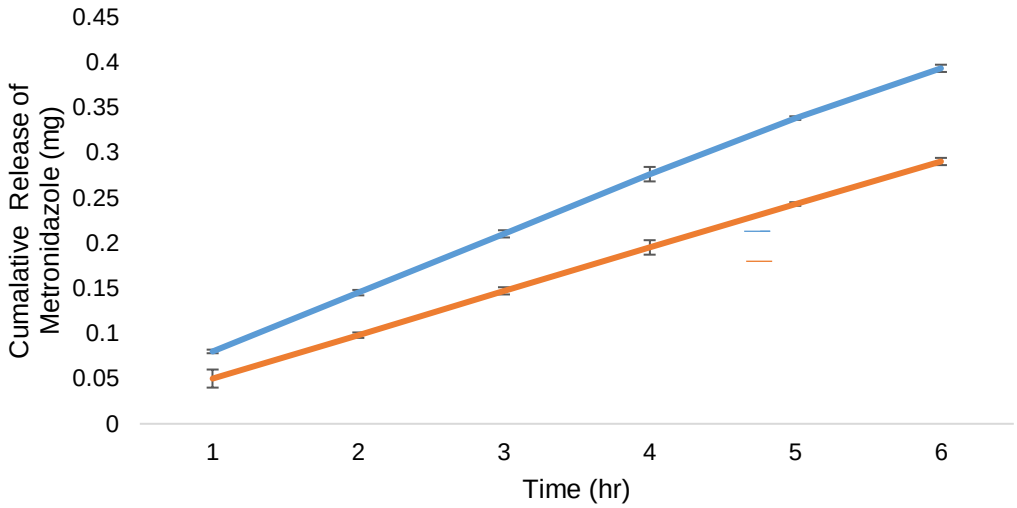

Figure 3.9. A figure shows the cumulative release of metronidazole from 100mg aquasomes (r^2 0.998), aquasomes collected from stage 3 (r^2 0.998) of the pMDI formulation of metronidazole-loaded aquasomes. Values are reported as mean ± SD (n = 3). Values are reported as mean ± SD (n = 3).

3.3.3. DPI formulations of aquasomes

3.3.3.1. DPI formulation of BSA-loaded aquasomes

The ED of the DPI formulation of BSA-loaded aquasomes was 96.0% ±2.3. The NGI was used to assess the DPI formulation of BSA-loaded aquasomes (Table 3.7). A percentage of 62.76% ±2.8 of the delivered dose has a cut-off diameter of 2.82 µm. Therefore, the BSA-loaded aquasomes showed high dispersability and low incidence of local side effects (e.g. mouth and throat). The FBF score of the BSA-loaded aquasome DPI formulations was 1.09, this shows that a great percentage of the aquasomes powder exited the capsule has deposited in the NGI stages with minimum waste. To produce a respirable powder, the same procedure mentioned in section 3.3.2.1 was performed. The percentage of the BSA-loaded aquasomes in each stage shows that the majority of the deposited aquasomes were in stages 2 and 3, which is in the terminal bronchiole region of the lung (Figure 3.10). The collected powder in stages 1, 6 and 7 was unprocessable and hence the reduction in the delivered dose was anticipated to belong to those stages.

Table 3.7. The cut-off diameter of NGI stages, ED, FBD, FBF, mass of aquasomes, actual amount of BSA and the theoretical amount of metronidazole at each stage of DPI formulation of BSA-loaded aquasomes. Values are reported as mean ± SD (n = 3).

Stage	Cut-off Diameter (µm)	Amount of Aquasomes (mg)	ED	FBD	FBF	Aquasomes Delivered (%)	Theoretical amount of Drug (mg)	Actual Amount of Drug (mg)
unprocessed Formulation	-	20				-		1.5 ±0.09
Device	-	-	96.0 ±2.3	88.1 ±1.9	1.09	-	-	-
Throat	-	1.33 ± 0.3				-	-	-
Pre-stage	> 8.06	3.50 ± 0.3				-	0.10 ±0.07	-
Stage 1	8.06	-				-	-	-
Stage 2	4.40	4.51 ± 0.2				23.4 ±1.8	0.33 ±0.05	0.28 ±0.09
Stage 3	2.82	7.50 ± 0.7				39.4 ±2.5	0.56 ±0.07	0.74 ±0.09
Stage 4	1.66	1.83 ± 0.4				9.13 ±2.1	0.65 ±0.07	0.31 ±0.07
Stage 5	0.94	-				-	-	un quantified

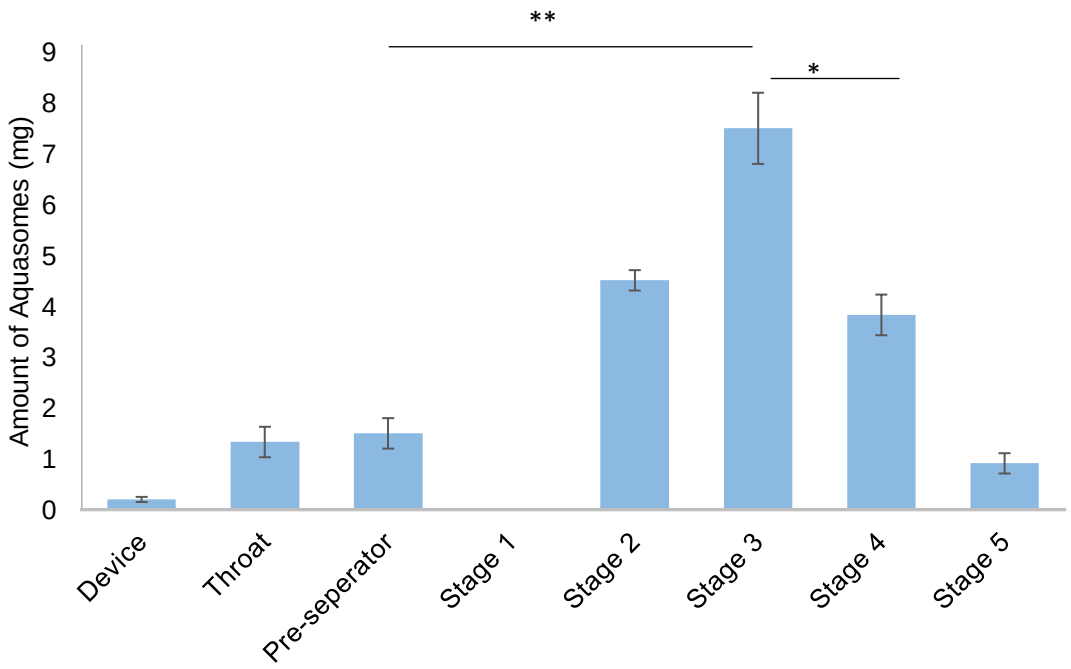

Figure 3.10. A bar chart shows the amount of aquasomes deposited at different stages of NGI of the DPI formulation of BSA-loaded aquasomes. Values are reported as mean ± SD (n = 3). Statistical analysis (one-way ANOVA/Tukey) between stages: *$p < 0.05$, **$p < 0.01$, ***$p < 0.001$.

3.3.3.2. *In vitro* release studies of DPI formulations of BSA-loaded aquasomes

Figure 3.11 compares the release of BSA from aquasomes with aerodynamic diameters of 2.82 (NGI stage 3) and the aquasome powder. The BSA release of aquasomes was controlled over the 6 hr of study. Aquasomes collected from the NGI stages 1, 2, 4 and 5 were washed with simulated lung fluid and analysed using the HPLC (2.3.3.3).

BSA was detectable in stages 1, 2, 4 and 5 of the NGI. BSA-loaded aquasomes released approximately 98% of the loading after 6 hr of release (Figure 3.9). *In vitro* release studies for stages 2, 3 and 4 show that BSA loading was of 0.28 ±0.09, 0.74 ±0.09 and 0.31 ±0.07 mg. However, these values are different from the theoretical loadings of BSA by 15.15%, 32.14% and 24.23% respectively because of the reasons explained in section 3.3.2.2.

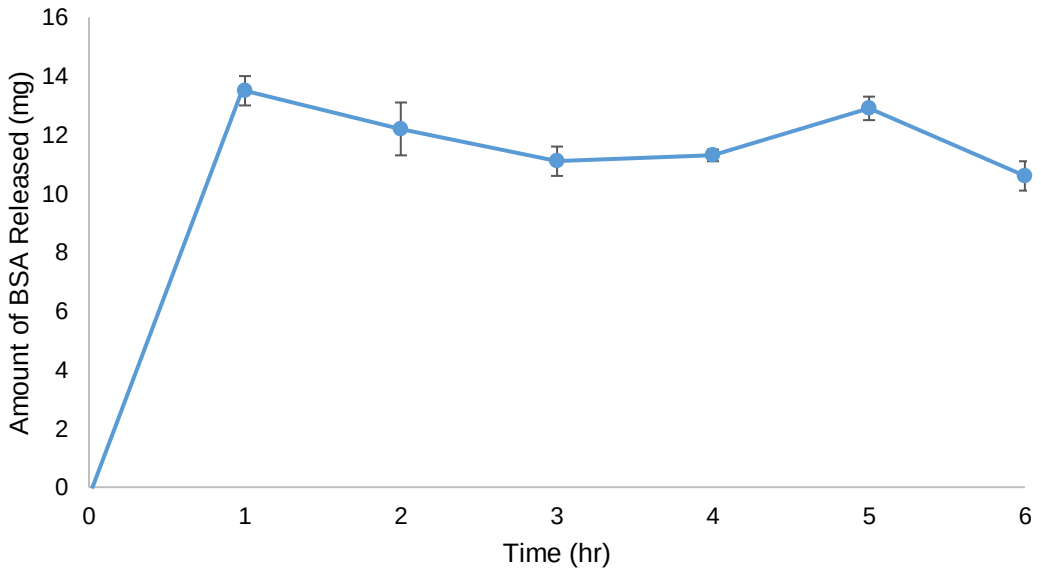

Figure 3.11. The figure shows the hourly amount of BSA released from aquasomes at NGI stage 3 of DPI formulation of BSA-loaded aquasomes (6 hr *in vitro* release study). Values are reported as mean ± SD (n = 3).

3.3.3.3. DPI formulation of metronidazole-loaded aquasomes

The ED of the DPI formulation of metronidazole-loaded aquasomes was 94.5 ±1.9, Table 3.8. A percentage of 80.5% ±1.1 of the delivered dose has a cut-off diameter of 2.82 µm. Therefore, metronidazole-loaded aquasomes DPI formulation will deposited in the lower respiratory region with minimal local side effect due to their high dispersability. The FBF score of the metronidazole-loaded aquasomes formulation was 1.17, this shows that a great percentage of the metronidazole-loaded aquasomes powder exited the DPI vial has deposited in the NGI

stages with minimum waste. To produce a respirable powder, since metronidazole in its original state is not a respirable powder, the same procedure mentioned in section 3.3.2.1 was performed. The percentage of the metronidazole-loaded aquasomes in each stage shows that the majority of the deposited aquasomes were in stages 2 and 3, which is in the terminal bronchiole region of the lung (Figure 3.12). As for of the collected powder in stages 1, 5, 6 and 7, this was unprocessable and hence the reduction was calculated from the delivered dose, which was anticipated to belong to those stages.

Table 3.8. The cut-off diameter of NGI stages, ED, FBD, FBF, mass of aquasomes, actual amount of metronidazole and the theoretical amount of metronidazole at each stage of the DPI formulation of metronidazole-loaded aquasomes. Values are reported as mean ± SD (n = 3).

Stage	Cut-off Diameter (µm)	Amount of Aquasomes (mg)	ED	FPD	FPF	Aquasomes Delivered (%)	Theoretical amount of Drug (mg)	Actual Amount of Drug (mg)
unprocessed Formulation	-	20	-					0.08 ±0.89
Device	-	-	94.5 ±1.9	80.5 ±1.1	1.17	-	-	-
Throat	-	1.90 ± 0.5				-	-	-
Pre-stage	> 8.06	2.80 ± 0.4				-	0.10 ±0.07	-
Stage 1	8.06	-				-	-	-
Stage 2	4.40	4.81 ± 0.6				25.2 ±1.6	0.01 ±0.01	0.02 ±0.01
Stage 3	2.82	7.00 ± 0.5				36.8 ±2.1	0.03 ±0.02	0.05 ±0.01
Stage 4	1.66	1.30 ± 0.3				6.9 ±1.6	0.005 ±0.002	un quantified
Stage 5	0.94	-				-	-	-

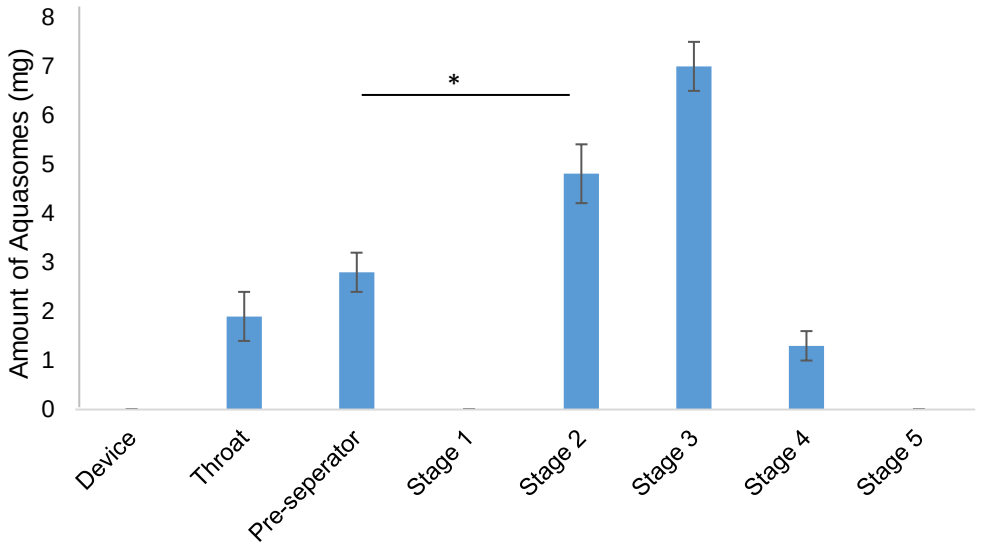

Figure 3.12. A bar chart shows the amount of aquasomes deposited at different stages of NGI of the DPI formulation of metronidazole-loaded aquasomes. Values are reported as mean ± SD (n = 3). Statistical analysis (one-way ANOVA/Tukey) between stages: *$p < 0.05$, **$p< 0.01$, ***$p < 0.001$.

3.3.3.4. *In vitro* release studies of DPI formulations of metronidazole-loaded aquasomes

Table 3.8 compares the release of metronidazole from aquasomes with aerodynamic diameters of 4.40 and 2.82 (NGI stage 2 and 3). The metronidazole release of aquasomes was controlled over the 6 hr of the study. The aquasomes collected from other stages were unquantifiable on the HPLC because the metronidazole concentration was below the LOQ of the metronidazole HPLC method. The amount of metronidazole deposited on stages 2 and 3 were 0.02 mg ±0.01 and 0.05 mg ±0.01 respectively.

3.3.4. Cell culture studies

In cell culture studies, salbutamol sulphate was used as a model drug. The use of salbutamol sulphate as a model drug for this study and not metronidazole was for two reasons. Salbutamol is a well suited as a model for the BEAS-2B cell lines as salbutamol sulphate is already used to treat asthma. Moreover, there is substantial research where salbutamol is used as a model drug, which provide a rich ground to progress with these studies (Lipworth and Clark, 1997; Lipworth and Clark, 1998). However, there is less research in terms of sustained release formulations for pulmonary drug delivery.

The cell line that was used for cell viability and permeability studies was BEAS-2B. BEAS-2B cells are derived from normal bronchial epithelium obtained from healthy individuals. The cells

were infected with a replication-defective SV40/adenovirus 12 hybrid to clone them. BEAS-2B have been used in studies of pneumococcal infection mechanisms. BEAS-2Bhas also been used to express keratins and SV40 T antigen. Despite that Calu-3 cell lines still remains the preferred choice of cell lines because of it early appearance, BEAS-2B is gaining a growing interest because its origin (human origin and not immortalised cancer cells) and for its rapid confluency (3-4 days) (Reddel, *et al*., 1995).

3.3.4.1. MTT assay for the effects of HA, trehalose and salbutamol sulphate

The MTT assay is a method that quantifies cell viability and cytotoxicity based on colour change (yellow to purple) of MTT due to the reduction of the agent inside the living cells. It is worth noting that the MTT assay cannot be used as an indication for cell proliferation, because the MTT is specifically metabolised by the mitochondria, hence, it is designed to measure cell viability via cell metabolism. To measure cell proliferation, assays such as the tetrazolium assay may be used (Berridge *et al*., 2005).

To measure cell viability in the presence of HA, concentrations of 0.1, 0.4, 0.6, 0.8, 0.9, 1 and 1.5 mg/mL of salbutamol were used. The analysis of the data gathered from the MTT assay indicates that the BEAS-2B cells were viable, in comparison with the control, at all the concentrations of HA apart form the highest concentration (1.5 mg/mL). The reduction in the percentage of cell viability was statistically significant ($p< 0.01$) when compared to the HA concentration of 0.8 mg/mL, and also significant statistical difference ($p<0.05$) when compared to the HA concentration 1.0 mL (Figure 3.13). Cell death may have occurred either because of the high concentration of the non-soluble HA covered the surface area and produced a barrier between the cells and the medium or because non-soluble HA particles introduced a stress and indirectly caused cell death. However, it is interesting to notice Xe *et al.* (2013) performed a study on the toxicity of HA using BEAS-2B cell lines and found that needle- and plate-shaped HA nanoparticles caused cell toxicity compared to spherical HA nanoparticles at concentrations of 10–300 μg/mL. Moreover, Zhao *et al.* (2011) performed *in vitro* assessment of rod shaped HA nanoparticles and found that reactive oxygen species (ROS) was highly generated in the case of longer and large surface area HA nanoroads compared shorter and small surface area ones. These studies come parallel to the MTT assay that show low toxicity of HA nanoparticles used and highly suggest that the HA cell toxicity is shape and size dependent rather than an inherit characteristic.

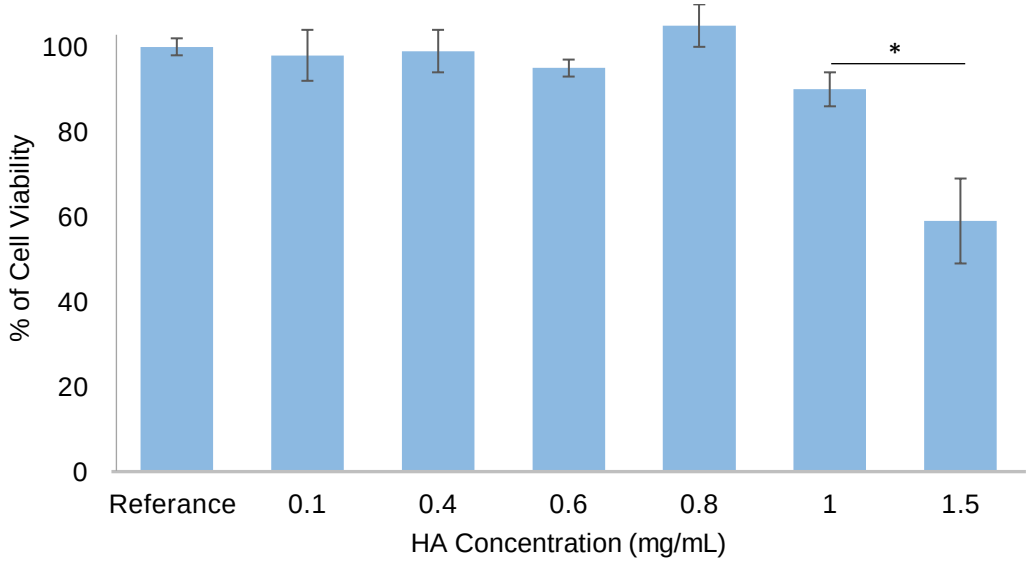

Figure 3.13. The bar chart shows the percentage of BEAS-2B cell viability in various HA concentrations. Values are reported as mean ± SD (n = 3). Statistical analysis (one-way ANOVA/Tukey) between stages: *p< 0.05.

To measure the percentage of cell viability in the presence of trehalose, concentrations of 0.1, 0.2, 0.4, 0.6, 0.8, 0.9, 1 mg/mL of trehalose were used. The analysis of the data gathered from MTT assays indicate that the BEAS-2B indicate that there is no significant difference (p>0.05) in viability compared to the reference (p>0.05) (Figure 3.14). Such results come parallel to what has been published in terms of the cell-preservative effect of trehalose. For instance, Cloonan *et al.* (2014) studied the effect of trehalose on rats during cigarette smoke induced COPD. They noticed that rats treated with 2% w/v solution trehalose (via mouth) was protected from induced COPD compared to control (treated with sucrose). They suggest that trehalose exhibited this effect via a marked increase in autophagy flux and increased expression of ubiquitin binding scaffold protein p62. Moreover, Geissler *et al.* (2013) found that trehalose (concentration of 300 mM) had unique characteristic in stabilising mitochondria of BEAS-2B cell during apoptosis cell studies using a fungal pathogen called gliotoxin.

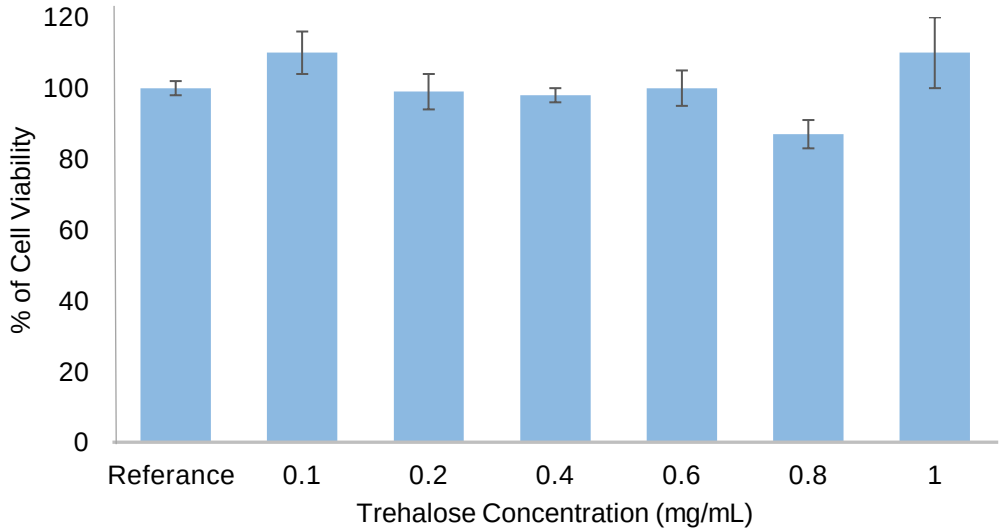

Figure 3.14. The bar chart shows the percentage of BEAS-2B cell viability in various trehalose concentrations. Values are reported as mean ± SD (n = 3).

3.3.4.2. MTT assay of the effect of salbutamol sulphate

To measure cell viability in the presence of salbutamol, concentrations of 0.1, 0.2, 0.4, 0.6, 0.8, 0.9, 1 mg/mL of salbutamol were used. The analysis of the data collected from MTT assays indicate that there is no significant difference (p>0.05) in viability compared to the reference, in comparison with the reference absorbance, at concentrations of 0.1, 0.2, 0.4 and 0.6 mg/mL of salbutamol (p>0.05) (Figure 3.15). However, with concentrations of 0.8 and 1 mg/mL of salbutamol there was a decrease in the mean absorbance. Despite the decrease in absorbance, there was no statistical difference when compared to the reference absorbance (p>0.05). These findings are parallel to the lethal dose studies performed on rats, which show salbutamol sulphate had a high margin of toxicity level. The lethal dose of subcutaneous salbutamol sulphate injection is approximately 2,000 mg/kg. By comparison, the maximum recommended daily inhalation dose for adults is less by 1400 times higher than that of rats. This highlights the safety profile of salbutamol sulphate, though lethal dose studies have not been identified in humans for ethical reasons (Drugs, 2015).

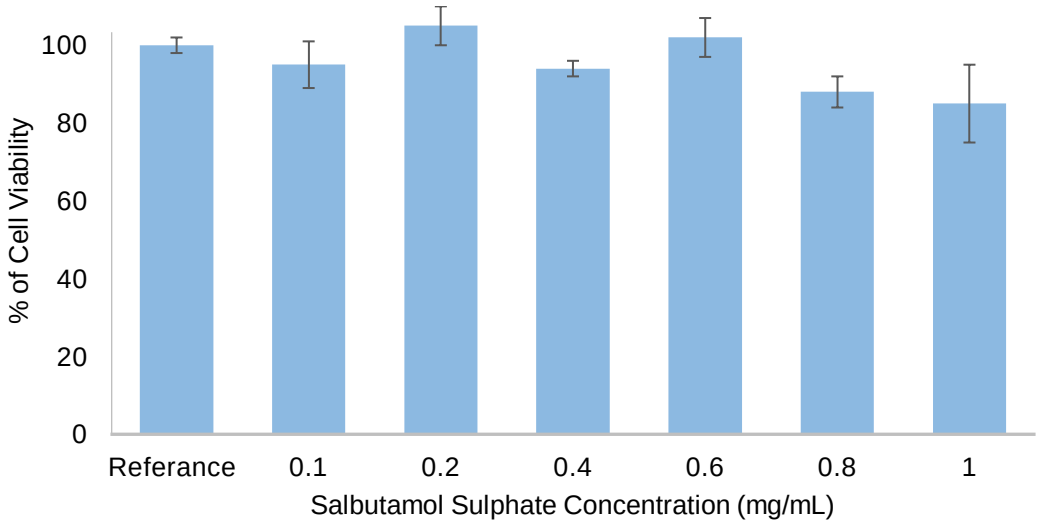

Figure 3.15. The bar chart shows the percentage of BEAS-2B cell viability in various salbutamol sulphate concentrations. Values are reported as mean ± SD (n = 3).

3.3.4.3. TEER measurements

MTT assays were performed to quantify cell viability in the presence of aquasome components (HA, trehalose and metronidazole). Although MTT assay in the literature was performed on HA, trehalose and metronidazole, the concentrations of the three materials have not been reported to fit the purpose (assembly of aquasomes aquasomes) (Ignjatović *et al*., 2013; Mathoera *et al*., 2002; Umashankar *et al*., 2010). To measure TEER, the cells were allowed to grow for a period of 20 days after seeding on 6-well Transwell® plates and the TEER was measured every 2 days. The TEER measurements for the BEAS-2B cells plateaued after day 15 (Figure 3.16). It is worth to indicate that measuring TEER of BEAS-2B cell line are challenging as the confluency rate is rapid compared to Caco-2 cell line, and on many occasions it is difficult to produce TEER measurements of higher than 100 ohm/cm^2 (Erhardt and Kim, 2007; Stewart *et al*., 2012).

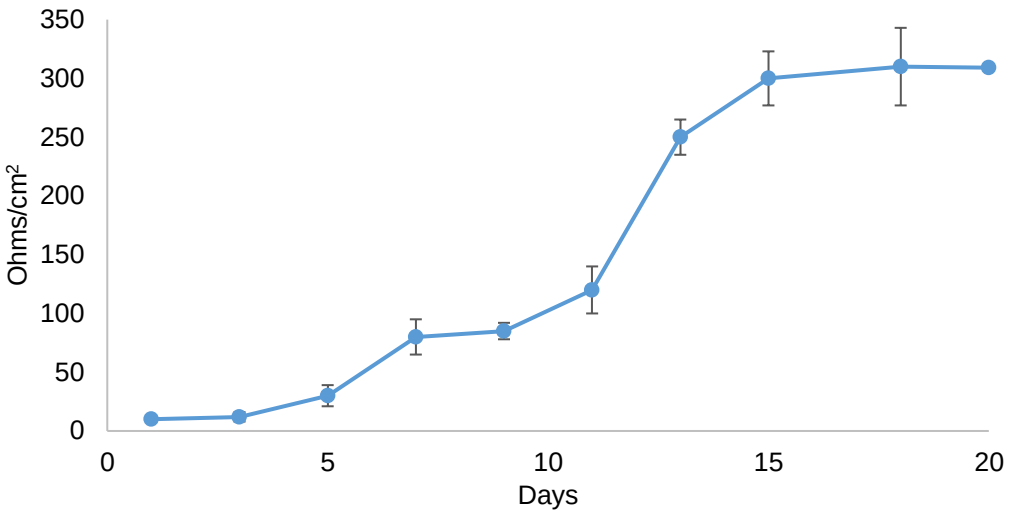

Figure 3.16. The figure shows the TEER measurement of BEAS-2B cells seeded on 6-well Transwell® plates with TEER measured every 2 days for 20 days. Values are mean ± SD, n = 3.

3.3.4.4. Permeability studies of Salbutamol sulphate loaded aquasomes

Salbutamol sulphate loaded aquasomes were administered to the monolayers of BEAS-2B cells in Transwell® and the permeability was compared to that of salbutamol sulphate solution of the same concentration to determine whether salbutamol-loaded aquasomes can show a delayed drug release effect. As shown in Figure 3.17, salbutamol loaded aquasomes had a delayed salbutamol release across the monolayers of cells compared to the free salbutamol sulphate solution. This was also confirmed with the lower total salbutamol released from both formulations. Within the first hour of release of salbutamol sulphate from aquasomes, there was an initial burst effect of 40% higher than that of salbutamol sulphate solution, despite the fact that there was no statistical difference. After 2 hr, the release of salbutamol sulphate from aquasomes started to slow gradually until it reached its highest difference at hour 6 (p<0.05). The salbutamol transported across the BEAS-2B monolayer was 46.12% ±2.9 after 6 hr. Rytting *et al.,* (2010) performed similar studies on negatively-charged polymer poly (vinyl sulfonate-co-vinyl alcohol)-g-poly (d,l-lactic-co-glycolic acid) which was loaded with salbutamol sulphate. They found that these nanopolymeric carriers delayed the release of the salbutamol sulphate compared to control free salbutamol. It is interesting to note that the encapsulation efficiency of these nanopolymeric carriers was 2.7% (2.7 mg salbutamol sulphate in every 50 mg of the nanopolymeric carrier). However, the applied concentration of these systems was at 2.5 mg/mL, which is a fraction to the concentration of the nanopolymeric carrier proposed by Rytting *et al*. (2010).

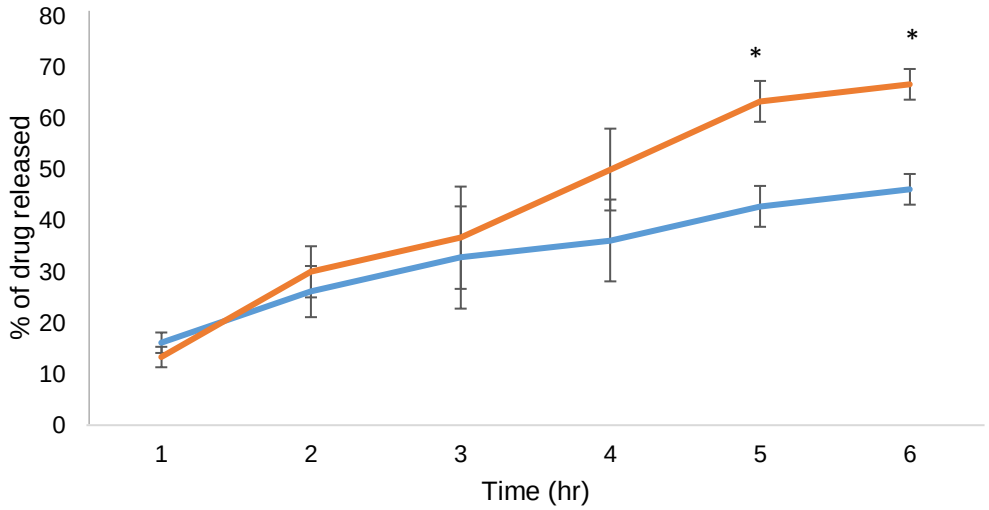

Figure 3.17. A figure shows the transport of salbutamol sulphate across BEAS-2B as free drug solution (orange line) or as loaded on aquasomes (blue line). Values are reported as mean ± SD (n=3). Statistical analysis (one-way ANOVA/Tukey) between stages: *p< 0.05.

3.3.5 Stability studies of DPI and pMDI formulations

The stability of BSA-loaded aquasome pMDI and DPI formulations were conducted in two storage conditions of 4ºC ±1ºC/60% RH ±2% RH and 25ºC ±1ºC/60% RH ±2% RH. The stability of BSA-loaded aquasomes of DPI and pMDI formulations were not investigated at 40ºC ±1ºC/75% RH ±2% RH because the stability studies of BSA-loaded aquasomes at storage conditions of 40ºC ±2ºC/75% RH ±5% RH failed (Chapter 2).

The stability studies of BSA-loaded aquasome DPI formulations were investigated for a period of 6 months at storage conditions of 4ºC ±1ºC/60% RH ±2% RH and 25ºC ±1ºC/60% RH ±2% RH, Table 3.9 and 3.10. However, the stability studies of BSA-loaded aquasome pMDI formulations was investigated for a period of 2 months at storage conditions of 4ºC ±1ºC/60% RH ±2% RH and 25ºC ±1ºC/60% RH ±2% RH, Table 3.11.

The stability studies of BSA-loaded aquasome DPI formulations was investigated for a period of 6 months at storage conditions of 4ºC ±1ºC/60% RH ±2% RH and 25ºC ±1ºC/60% RH ±2% showed no change in aerosolisation performance and percentage of loadings of BSA (p>0.05). The samples were also checked for discoloration after NGI studies, where the samples showed no change in colour. This highlights aquasomes as a stable platform for the delivery of proteins and peptide. The minimum time required by guidelines for stability studies performed at 4ºC ±1ºC/60% RH ±2% RH, 25ºC ±1ºC/60% RH ±2% RH and 40ºC ±1ºC/75% RH ±2% RH is for 12, 6 and 6 months respectively (Faisal *et al.,* 2013; SADC, 2014; Singh *et al.,* 2012). The stability studies of BSA-loaded aquasomes DPI formulation was investigated

for a period of 6 months at storage conditions of 4ºC ±2ºC/60% RH ±5% RH was performed for 6 months which was inadequate to establish an accepted shelf life. However, at storage condition of 25ºC ±2ºC/60% RH ±5%, aquasomes were able to withstand storage conditions up to 6 months. According to FDA guidelines, shelf life is calculated as the amount of time of accelerated stability studies to the power of two (n^2). In this case, the predicted shelf life for BSA-loaded aquasomes at 25ºC ±1ºC/60% RH ±2% is 12 months. It is important to highlight that such predictions should always be accompanied by real stability studies to confirm the predicted shelf life.

The stability studies of BSA-loaded aquasome pMDI formulations was investigated for a period of 6 months at storage conditions of 4ºC ±1ºC/60% RH ±2% RH and 25ºC ±1ºC/60% RH ±2% for 2 months show no change in aerosolisation performance and percentage of loadings of BSA (p>0.05). The samples were also checked for clarity, discoloration and presence of agglomeration, which the samples show none for the duration of the stability studies. As the case with BSA-loaded aquasomes DPI formulation, the study was performed less than 6 months at 4ºC ±1ºC/60% RH ±2% RH and 25ºC ±1ºC/60% RH ±2% RH storage conditions.

Table 3.9. Stability studies of BSA-loaded aquasomes DPI formulation for 6 months at 25ºC ±1ºC/60% RH ±2% RH. The table shows the deposition of BSA-loaded aquasomes in each stage and the amount of BSA loading. Values are reported as mean ± SD (*n* = 3).

Stage	Aquasomes deposited (mg) 14 days	Amount of BSA (mg) 14 days	Aquasomes deposited (mg) 1 month	Amount of BSA (mg) 1 months	Aquasomes deposited (mg) 2 months	Amount of BSA (mg) 2 months	Aquasomes deposited (mg) 3 months	Amount of BSA (mg) 3 months	Aquasomes deposited (mg) 4 months	Amount of BSA (mg) 4 months	Amount of Aquasomes (mg) 5 months	Amount of BSA (mg) 5 months	Aquasomes deposited (mg) 6 months	Amount of BSA (mg) 6 months
Device	-	-	-	-	-	-	-	-	-	-	-	-	-	-
Throat	1.33 ± 0.3	-	1.32 ± 0.4	-	1.30 ± 0.4	-	1.34 ± 0.3	-	1.40 ± 0.3	-	1.30 ± 0.6	-	1.33 ± 0.3	-
Pre-stage	3.50 ± 0.3	-	3.47 ± 0.5	-	3.45 ± 0.6	-	3.48 ± 0.4	-	3.45 ± 0.5	-	3.48 ± 0.5	-	3.50 ± 0.3	-
Stage 1	-	-	-	-	-	-	-	-	0.7± 0.2	UQ	-	-	-	-
Stage 2	4.51 ± 0.2	0.28 ±0.09	4.64 ± 0.3	0.30 ±0.1	4.46 ± 0.4	0.28 ±0.08	4.50 ± 0.4	0.30 ±0.1	4.48 ± 0.4	0.25 ±0.05	4.50 ± 0.4	0.30 ±0.1	4.51 ± 0.2	0.25 ±0.09
Stage 3	7.50 ± 0.7	0.74 ±0.09	7.61 ± 0.9	0.78 ±0.07	7.51 ± 0.6	0.68 ±0.1	7.52 ± 0.6	0.75 ±0.07	7.51 ± 0.5	0.70 ±0.1	7.55 ± 0.5	0.75 ±0.09	7.50 ± 0.7	0.70 ±0.05
Stage 4	1.83 ± 0.4	0.31 ±0.07	1.62 ± 0.6	0.29 ±0.1	1.80 ± 0.5	0.30 ±0.09	1.79 ± 0.4	0.29 ±0.09	1.66 ± 0.5	0.25 ±0.07	1.82 ± 0.5	0.31 ±0.09	1.83 ± 0.4	0.39 ±0.09
Stage 5	-	UQ	-	UQ	-	UQ	-	UQ	-	UQ	-	UQ	-	UQ
Discoloration	none	none	none	none	none	none	none	none	none	none	none	none	none	none

Table 3.10. Stability studies of BSA-loaded aquasomes DPI formulation for 3 months at 4ºC ±1ºC/60% RH ±2% RH. The table shows the deposition of BSA-loaded aquasomes in each stage and the amount of BSA loading. Values are reported as mean ± SD (*n* = 3).

Stage	Aquasomes deposited (mg) 14 days	Amount of BSA (mg) 14 days	Aquasomes deposited (mg) 1 month	Amount of BSA (mg) 1 months	Aquasomes deposited (mg) 2 months	Amount of BSA (mg) 2 months	Aquasomes deposited (mg) 3 months	Amount of BSA (mg) 3 months
Device	-	-	-	-	-	-	-	-
Throat	1.29 ± 0.4	-	1.39 ± 0.7	-	1.33 ± 0.5	-	1.43 ± 0.6	-
Pre-stage	3.56 ± 0.4	-	3.29 ± 0.7	-	3.50 ± 0.9	-	3.60 ± 0.7	-
Stage 1	-	-	-	-	-	-	-	-
Stage 2	4.60 ± 0.4	0.30 ±0.07	4.54 ± 0.4	0.30 ±0.01	4.51 ± 0.5	0.29 ±0.1	4.52 ± 0.7	0.30 ±0.09
Stage 3	7.59 ± 0.5	0.75 ±0.1	7.70 ± 0.9	0.73 ±0.09	7.80 ± 0.9	0.76 ±0.1	7.55 ± 0.6	0.74 ±0.09
Stage 4	1.50 ± 0.5	0.29 ±0.09	1.51 ± 0.9	0.25 ±0.09	1.63 ± 0.9	0.34 ±0.09	1.85 ± 0.8	0.39 ±0.1
Stage 5	-	UQ	-	UQ	-	UQ	-	UQ
Discoloration	none	none	none	none	none	none	none	none

Table 3.11. Stability studies of BSA-loaded aquasomes DPI formulation for 2 months at 4ºC ±1ºC/60% RH ±2% RH and 25ºC ±1ºC/60% RH ±2% RH. The table shows the deposition of BSA-loaded aquasomes in each stage and the amount of BSA loading. Values are reported as mean ± SD (*n* = 3).

Stage	Aquasomes deposited (mg) 14 days	Amount of BSA (mg) 14 days	Aquasomes deposited (mg) 1 month	Amount of BSA (mg) 1 months	Aquasomes deposited (mg) 2 months	Amount of BSA (mg) 2 months	Aquasomes deposited (mg) 14 days	Amount of BSA (mg) 14 days	Aquasomes deposited (mg) 1 months	Amount of BSA (mg) 1 months	Amount of Aquasomes (mg) 2 months	Amount of BSA (mg) 2 months
Storage conditions	4ºC ±1ºC/60% RH ±2% RH						25ºC ±1ºC/60% RH ±2% RH					
Device	-	-	-	-	-	-	-	-	-	-	-	-
Throat	1.30 ± 0.4	-	1.33 ± 0.6	-	1.33 ± 0.7	-	1.30 ± 0.5	-	1.25 ± 0.3	-	1.31 ± 0.5	-
Pre-stage	3.52 ± 0.5	-	3.47 ± 0.8	-	3.50 ± 0.5	-	3.40 ± 0.4	-	3.40 ± 0.9	-	3.54 ± 0.6	-
Stage 1	-	-	-	-	-	-	-	-	-	-	-	-
Stage 2	4.51 ± 0.6	0.29 ±0.08	4.64 ± 0.4	0.30 ±0.1	4.79 ± 0.8	0.32 ±0.09	4.61 ± 0.5	0.29 ±0.1	4.31 ± 1	0.22 ±0.11	4.61 ± 0.7	0.30 ±0.09
Stage 3	7.45 ± 0.4	0.72 ±0.1	7.61 ± 0.4	0.70 ±0.1	7.55 ± 0.5	0.74 ±0.07	7.40 ± 0.6	0.75 ±0.1	7.60 ± 0.7	0.72 ±0.12	7.20 ± 0.9	0.61 ±0.06
Stage 4	1.75 ± 0.6	0.30 ±0.09	1.62 ± 0.9	0.28 ±0.07	1.80 ± 0.4	0.29 ±0.1	1.80 ± 0.8	0.27 ±0.1	1.73 ± 0.5	0.30 ±0.09	1.79 ± 0.4	0.30 ±0.11
Stage 5	-	UQ	-	UQ	-	UQ	-	UQ	-	UQ	-	UQ
Clarity of solution	clear	clear	clear	clear	clear	clear	clear	clear	clear	clear	clear	Clear
Agglomerations	none	none	none	none	none	none	none	none	none	none	none	none
Discoloration	none	none	none	none	none	none	none	none	none	none	none	none

3.4. Conclusions

BSA-loaded aquasomes were successfully formulated as pMDI and DPI formulations. The aerodynamic behaviour of the pMDI and DPI formulations was investigated to identify lung distribution of aquasomes. Both DPI and pMDI formulations show large amounts of aquasomes deposited in stages 2, 3 and 4 of the NGI. These stages represent mid-lower lung area, which relate to less chances of being removed by cilia movement and also better drug targeting. *In vitro* release studies with simulated lung fluid were performed to examine the release profile of the aquasomes. The release studies on the selected size fractions show a sustained release of BSA over a period of 6 hr. In order to complement the *in vitro* release data, cell culture studies were performed to demonstrate the controlled release effect of aquasomes with BEAS-2B cell lines. The release of salbutamol sulphate from aquasomes started to slow gradually after 2 hr until it reached its highest difference at hour 6 ($p<0.05$).

The transported salbutamol across the BEAS-2B monolayer in aquasomes formulation was 46.12 ± 2.9% after 6 hr. The stability studies of BSA-loaded aquasomes pMDI and pMDI formulations were investigated. The stability studies of BSA-loaded aquasomes pMDI formulation was performed for a period of 6 months at storage conditions of 4ºC ±1ºC/60% RH ±2% RH and 25ºC ±1ºC/60% RH ±2% for 2 months show no change in aerosolisation performance and percentage of loadings of BSA ($p>0.05$). The stability studies of BSA-loaded aquasomes DPI formulation was investigated for a period of 6 months at storage conditions of 4ºC ±1ºC/60% RH ±2% RH and 25ºC ±1ºC/60% RH ±2% for 6 and 2 months respectively show no change in aerosolisation performance and percentage of loadings of BSA ($p>0.05$). The stability studies of BSA-loaded aquasome DPI formulations was investigated for a period of 6 months at storage conditions of 4ºC ±1ºC/60% RH ±2% RH was performed for 6 months which 6 months less to be adequate to establish an accepted shelf life. However, at storage conditions of 25ºC ±1ºC/60% RH ±2%, aquasomes were able to withstand storage conditions up to 6 months. In this case, the predicted shelf life for BSA-loaded aquasomes at 25ºC ±1ºC/60% RH ±2% is 12 months.

In general, both pMDI and DPI formulation of aquasomes exhibited an acceptable aerodynamic performance with the majority of the powder deposited in the mid-lower regions of the lung. Furthermore, the both pMDI and DPI formulation, show encouraging stability study data, which show a formulation stability of pMDI and DPI for 6 and 3 months respectively at the tested conditions.

CHAPTER 4

Oral Delivery of Aquasomes

4.1. Introduction

To obtain a tablet with API content uniformity, the components of the tablet mixture have to be dry (low moisture content), powdered or granular, uniform particle size and has good flowability. For instance, a tablet mixture of different particle sized powders could segregate during the manufacturing process due to different densities, and eventually lead to poor API content uniformity. This is crucial as content uniformity ensures that the correct dose of API is delivered. One of the simplest methods of tablet manufacturing is direct compression. In addition to the simplicity of formulation and tablet manufacture, direct compression has other advantages such as reduced labour and energy costs of manufacturing. For successful tableting with direct compression, three key factors have to be accomplished flowability, compactability of the compression mixture and API content uniformity. The properties and the percentage of API in the tablet mixture have an impact on the three factors formerly mentioned. For instance, a tableting mixture of low dose API, the flow and compaction of the tableting mixture are dependent on the type of excipients used. For a tableting mixture of a medium API dose, the compression mixture flowability may become a critical factor. However, the tableting mixture with high API dose, the flow and compaction of the mixture are both significantly depend on the properties of the API (Table 4.1). Formulations made by direct compression can be developed with minimum numbers of excipients such as a diluent (filler/binder), a disintegrant and a lubricant. Extra additives can be added to serve various purposes (Table 4.2) (DFE pharma, 2014; Gohel and Jogani, 2005; Parmar and Rane, 2009; Huang W. *et al*., 2013; McCormick, 2005).

Table 4.1. The table shows the effect of API concentration in the tablet mixture on flowability, compactability and content uniformity using direct compression (modified from: DFE pharma, 2014).

	Low API dose (mg)	Medium API dose (mg)	High API dose (mg)
API (%)	<10	10-50	>50
250 mg	<4%	4-20%	>20%
Content uniformity	Principal concern	Generally not an issue	Least concern
Flowability	Excipients needed to improve	Minor interference	Drug properties dependant
Compactability	Excipients needed to improve	Unlikely to be an issue	Drug properties dependant

Table 4.2. A list of the most widely used excipients in the manufacture of tablets and their description (modified from: Drug Topics, 2008).

Function	Description and examples
Diluent	Diluents increase the bulk of tablets and are responsible for compaction and flow tablet properties. Direct compression diluents are frequently referred to as filler-binders. Examples include MCC and lactose.
Disintegrant	Super disintegrants are materials that disintegrate a tablet at low concentrations (2% to 6% w/w). Commonly used super disintegrants include cross carmellose sodium and sodium starch glycolate.
Lubricant	Magnesium stearate is used in the vast majority of direct compression tablets. A common problem with metal stearates is their potential to reduce the strength of tablets and to cause slow disintegration and dissolution if overused or over blended.
Glidant	Glidants are only needed when API is present in sufficient concentration to enhance flowability.
Surfactant	Wetting agents may be included if the API is hydrophobic. An example of surfactant is sodium lauryl sulphate (SDS).

Some APIs may be unsuitable for direct administration by the oral route. For instance, stomach acids denature protein based-drugs such as insulin. With this range of APIs that cannot be formulated into tablets and administered directly, a coating is applied to form a barrier and prevent the acidic effect of the stomach (Table 4.3) (Grosser *et al*., 2012; Ansel *et al*., 1995)

Table 4.3. The table shows examples with description of the three main types of coatings for tablets (modified from: Ankit G *et al*., 2012; DFE, 2014; Bose and Bogner, 2007).

Type of coating	Description
Film coated (FC)	Most commonly used to alter the appearance of the tablets, protect the tablet to remain stable and mask the taste of APIs. To apply the film coating, the coating is deposited on the tablets surface to form a thin uniform film. An example of film coating material is ethyl cellulose.
Enteric coating (EC)	Some APIs degrades in acidic media or cause irritation. These APIs are coated with pH dependent coating (the coating disintegrate at specific pH). These tablets must not be crushed or chewed, due to APIs exposure. Examples of enteric coating materials are Methyl acrylate-methacrylic acid copolymers and shellac.
Compression coating	The use of this type of coating has increased recently due to its ease of application and cost effectiveness. It involves the DC of granular coating (dry) using a special coating equipment. Examples of compression coating materials used are polyethylene oxide and micronized ethyl cellulose.

Extensive studies have been performed to explore the mechanism of coating formation. As for coatings that dissolve in solvent, once the coating solution droplets deposited on the surface of the tablet, the droplets join to form a thin liquid layer. As the solvent starts to evaporate, the liquid layer transforms to a gel layer thin into a solid film. Conversely, for coating dispersion, they require the process of coalescence to form the film. The polymer spheres closely join on the surface of the tablet after spraying due to evaporation of water. Then, the spheres distort to fill in the voids remain after water evaporating. With continuous drying, the spheres fuse together and the polymer chains interpenetrate to form the film. (Steward *et al*., 2000; Bauer, 1998; Massoud and Bauer, 1989; Felton, *et al.*, 2013)

4.1.1. Aim and objectives

The aim of the work in this chapter is to investigate tablets as a platform for aquasomes for oral delivery. To achieve this aim, the following objectives were explored:

- Preparation of BSA-loaded aquasomes tablets with MCC as a filler/disintegrant and magnesium stearate or talc as lubricants under various compression forces.
- Investigate the effect of compression forces (0.5, 1, 2 and 3 tons) on BSA-loaded aquasomes to examine the BSA layer under increased compression forces.
- Film coat the aquasome tablets with pH dependent coating (pH >5.5) to produce enteric coated tablets to protect BSA on the outer layer of the aquasomes from acidic secretions of the stomach.
- Perform cell culture studies and compare the release obtained from *in vitro* studies to demonstrate the controlled release effect of aquasomes.
- Perform stability studies to explore the compatibility of the excipients and the formulation stability.

4.2. Materials and Methods

4.2.1. Materials

Hydroxyapatite powder (99%), trehalose powder (99%), metronidazole (99%), microcrystalline cellulose ph-112 (99%), HPLC grade acetonitrile and trifluoroacetic acid (TFA) (>99%) and Bovine Serum Albumin (BSA) powder (99%) were purchased from Sigma Aldrich, UK. Talc (99%), magnesium stearate (99%), Modified Eagle's Minimum Essential Medium solution, Earle's Balanced Salt Solution (HBSS), Penicillin-Streptomycin antibiotic solution, nonessential amino acids, sodium pyruvate, Fetal Bovine Serum (FBS), L-glutamine and 0.25% w/v Trypsin were purchased from Fisher Scientific, USA. Acrylic b-based polymer (Eudraget L100) and ethyl acetate were received as gifts from Colorcon, UK. HPMCAS were received as gifts from Shin-Etsu, Japan. All materials were used as received unless otherwise specified. Ultra-pure grade water was used when required.

4.2.2. Preparation of Aquasomes Tablets

4.2.2.1. Preparation of BSA-loaded aquasomes

BSA-loaded aquasomes were manufactured by modifying the method of Kossovsky *et al.,* 1995. A quantity of 100 mg of HA was added to a trehalose solution (10 mL/0.1 M) and mixed for 2.5 hr at 25ºC. Afterwards, the coated cores were then centrifuged (3000 rpm/10 min), washed with ultra-pure water to remove unadsorbed trehalose and then freeze-dried. A quantity of 100 mg of the coated cores were added to a BSA solution (10 mL/0.015 M) and mixed for 2.5 hr at 25ºC. Then, aquasomes were centrifuged (3000 rpm/10 min), washed with ultra-pure water to remove unadsorbed BSA and then freeze-dried. The same procedure was used to load aquasomes with metronidazole.

4.2.2.2. Freeze-drying Protocol

In the preparation of aquasomes, freeze-drying process was used. The freeze-dryer used was Vir Tis Advantage Plus, USA. A freeze-drying cycle of 24 hr was performed. The cycle consisted of four stages; pre-stage (60 min at -45ºC/atmospheric pressure), primary drying stage (720 min at -45ºC under vacuum of 400 mbar), secondary drying stage (460 min at -20ºC under vacuum of 400 mbar) and equilibrium stage (240 min at 25 ºC/atmospheric pressure). The condenser temperature was set at -76ºC. Freeze-drying vials and lids were used where required.

4.2.2.3. Tablet preparation

Tablets were made using BSA-loaded aquasomes powder, MCC powder grade ph-112 as a multifunctional excipient (filler/binder/disintegrant). Powders of magnesium stearate and talc (1% w/w) were used as lubricants. Five powder blends with varying amounts of BSA-loaded aquasomes were prepared (Table 4.4). The target weight of the tablet was 400 mg. The tablets were made using a manual direct compression presser under 0.5, 1, 2 and 3 tons of compression force followed by 30 seconds dwelling time. All measurements were performed in sextuplicate (n=6) at ambient room temperature.

Table 4.4. The description of powder blends used for the preparation of aquasome tablets using direct compression method.

Powder blend No.	Powder composition		% of aquasomes in 400 mg tablet
1	100 mg of aquasomes / 296 mg of MCC-ph 112	4 mg Talc	25
2	150 mg of aquasomes / 246 mg of MCC-ph 112		37.5
3	200 mg of aquasomes / 196 mg of MCC-ph 112		50
4	250 mg of aquasomes / 146 mg of MCC-ph 112		62.5
5	296 mg of aquasomes / 100 mg of MCC-ph 112		75

4.2.2.4. Measurement of angle of repose (**Ɵ**)

The cone method was used to measure the angle of repose. The specified funnel was attached to the funnel holder. The powder was then dispensed through the funnel until a conical pyramid was obtained. The diameter and height of the heap were measured. To calculate the angle of repose, the internal angle between the horizontal surface and the powder surface was measured, and the angle of repose was calculated from the equation: Tanθ = 2xheight/diameter. The method were adopted from US Pharmacopia monograph (<1174>). All measurements were performed in sextuplicate (n=6) at ambient room temperature. The values are reported as mean ± standard deviation.

4.2.2.5. Hardness test

Hardness of tablets was measured after dwelling time of tablets with 4M hardness tester, Schleuniger, (Thun) Switzerland. The method were adopted from US Pharmacopia monograph (<1217>). All measurements were performed in sextuplicate (n=6) at ambient room temperature. The values are reported as mean ± standard deviation.

4.2.2.6. Disintegration test

To measure the disintegration time of tablets, ZT3 from Erweka, (Heusenstamm) Germany disintegration test machine was used. The method were adopted from US Pharmacopia monograph (<701>). A tablet was positioned in the disintegration basket which was cycling at a constant frequency of 30 cycles/min in DI water (800 ml) at 37°C (floating disk was not needed). The time at which the tablet was fully disintegrates and passed through the sieve was noted. All measurements were performed in sextuplicate (n=6). The values reported as mean ± standard deviation.

4.2.2.7. Friability test

To measure the tablets friability, a Roche friabilator from J. Engelsmann AG, (Ludwigshafen) Germany. The method were adopted from US Pharmacopia monograph (<1216>). The tablets (n=6) were placed in the friability chamber at 25 rpm for 4 min. The tablets were then de-dusted and weighed and the friability expressed as the percentage loss in weight as shown in the equation 5. All measurements were performed at ambient room temperature. The values are reported as mean ± standard deviation.

$$\text{The percentage of friability} = \frac{(pre\ friability\ weight - post\ friability\ weight)}{pre\ friability\ weight}\ x100 \quad \ldots\ldots\ldots(5)$$

4.2.2.8. Porosity test

To measure tablet porosity, a helium multipycnometer from Quantachrome Instruments, (Syosset) USA was used. The true volume of the tablet was calculated based on the Archimedes principle of fluid (helium gas) displacement. Helium is used because it does not cause oxidation to the sample being tested, so it does not affect sensitive APIs and because the helium atom is small in size, it can penetrate and fill the voids within the bulk of the tablet. All measurements were performed in sextuplicate (n=6) at ambient room temperature. The values are reported as mean ± standard deviation.

4.2.2.9. Coating of aquasome tablets

For the coating of aquasome tablets, two coatings were trialled. The first coating was HPMC-AS at a concentration of 2-20% w/w of solids. The second coating was Eudragit®L100 at concentration of 20% w/w of solids (the powder was sieved with 150 µm sieve to remove agglomerations). Both coatings are pH dependent and provide protection against the acidic environment of the stomach (at pH >5.5 the coating disintegrate). All the coatings were mixed with 11% w/w triethyl citrate (TEC) as a plasticiser and 0.05% w/w of sodium lauryl sulphate (SLS) as anti-foaming agent. The coating conditions for the two coatings were 30 min at 70-80% air inlet; temperature was of 37^0C at 4.00 rpm of feed using a Caleva mini coater, USA. All measurements were performed in sextuplicate (n=6). The values are reported as mean ± standard deviation.

4.2.3. Powder Characterization

4.2.3.1. Particle size and size distribution

Size measurements were performed using a Sympatek particle size analyser (Brookhaven Instruments). A quantity of 100 µL of diluted aquasomes with ultra-pure water were placed in the specified cuvette (4 clear sides cuvette). All measurements were performed in triplicate (n=3) at ambient room temperature. The values are reported as mean ± standard deviation.

4.2.3.2. Scanning electron microscopy (SEM)

The samples were attached onto an aluminium pin stubs with adhesive surface (radius=12.5 mm). A thin layer of gold was applied on the samples on the pin stubs using a gold coater Polaron SC500, Polaron Equipment, UK. The samples on the pin stubs were then examined using a Stereoscan 90, Cambridge Instrument. In an atmosphere of argon gas, a high vacuum with an accelerating voltage of 20 KV was used to operate the SEM and at 12 mm of working distance, Polaron Equipment, UK.

4.2.3.3. HPLC analysis

Drug analysis from the *in vitro* release studies were measured using an Agilent 1200 series HPLC System with UV and fluorescence detectors (Germany). The analysis was performed at ambient temperature.

4.2.3.3.1. BSA HPLC method

For HPLC analysis of BSA, a C18-ODS Jupiter column (4.6 mm x 250 mm / 5 µm / 300 Å (Phenomenex, USA) was used. The injection volume of the sample was set at 100 µL.

Fluorescent detection method was used with excitation wavelength was set at 220 nm and emission wavelength was set at 312 nm. A gradient elution method was used during which the proportion of solution B (acetonitrile) in the eluent increased from 5% to 65%solution against solution A (0.01%, v/v trifluoroacetic acid in ultra-pure water) at 1 mL/min flow rate of. BSA eluted with a retention time of 17.0 min. A standard calibration curve was established with the use of BSA standard solutions ($r^2 = 0.998$), which the concentration of BSA in unknown solutions was determined.

4.2.3.4.2. Metronidazole HPLC method

For HPLC analysis of metronidazole, a C18 Luna column (4.6 mm x 150 mm / 5 µm / 300 Å (Phenomenex, USA) was used. The injection volume of the sample was set at 100 µL. Fluorescent detection method was used with excitation wavelength was set at 275 nm and emission wavelength was set at 312 nm. An isocratic elution method was used during which the proportion of solution B (methanol) in the eluent was 60% against solution A (0.01%, v/v trifluoroacetic acid in ultra-pure water). The flow rate of mobile phase was set at 1 mL/min. metronidazole eluted with a retention time of 3.0 min. A standard calibration curve was established by the use of metronidazole standard solutions ($r^2 = 0.997$), which was used for the determination of unknown metronidazole concentration samples. The HPLC method was adapted from Tashtoudh *et al.* (2008).

4.2.3.5. *In vitro* release studies of aquasome tablets

Fasting state simulated gastric fluid (FaSGF) and fasting state simulated intestinal fluid (FaSIF) were prepared by dissolving the required components (Table 4.5) in 1L of ultra-pure grade water (Marques *et al*., 2011). The solutions were kept standing for 4 to 5 hr at ambient temperature to check for any salt precipitation, which if occurs, the solutions are discarded and a fresh 1L are prepared. *In vitro* release studies were performed on the BSA/metronidazole-loaded aquasome tablets in continuous phase. The samples were redistributed in 40 mL of simulated media (FaSGF/FaSIF) and placed in a shaking water bath at 37^{o}C/100 rpm. A quantity of 0.3 mL was taken for HPLC analysis at hourly time points up to 6 hr. The release medium was replaced with 0.3 mL of fresh simulated lung fluid.

Table 4.5. Materials required to prepare 1L of FaSGF and FaSIF for *in vitro* release studies of aquasome tablets.

Material	Amount (mg)
FaSGF Potassium chloride	122.6
Orthophosphoric acid	5.5
Sodium dihydrogen phosphate	32
Hydrochloric acid	To the required pH
FaSIF sodium taurocholate	4.5
lecithin	0.5
maleic acid	58.09
sodium hydroxide	72
sodium chloride	51
glyceryl monocholate	1
sodium oleate	0.8
Sodium hydroxide or hydrochloric acid	To the required pH

4.2.4. Cell culture studies

4.2.4.1. Cell lines maintenance and passaging

Caco-2 cell lines were received as a gift from Dr Afzal Mohammed, Aston University. The cells were maintained using medium comprised from Dublecco's Modified Eagle's medium (DMEM), 0.5% penicillin-streptomycin, 10% fetal bovine serum (FBS), 2% glutamate solution and 1% nonessential amino acids (NEAA). The cells were incubated at 37°C temperature and 5% CO_2. The cells were fed every day and passaged every 2-3 days. The media, HBSS and trypsin were preheated to 37°C in a water bath prior addition. A quantity of 10 mL of HBSS solution was used to wash the flask containing the cells to remove traces of FBS and dead Caco-2 cells. Trypsin was added (3 mL of 0.25% w/v) to the flask and Incubated for 5-10 min at 37°C. After the detaching of the cells, a quantity of 10 mL of media was added to quench trypsin effect. To prevent clumping of Caco-2 cells, the mixture was pipated 3-4 times. Then, a quantity of Caco-2 cells was then placed in a new flask (1 mL to a 75 cm^2 and 0.5 mL to a 25 cm^2 flask). The media was then added to the flask (20 mL to a 75 cm^2 and 10 mL to a 25 cm^2 flask) and incubated at 37°C.

4.2.4.2. Cells counting procedure

To count the Caco-2 cells, a haemocytometer was used. A haemocytometer is a slide made of thick glass with a rectangular indentation to create a chamber. The chamber is carved with perpendicular lines by laser-etched grid. After lysing of the Caco-2 cells with trypsin, a quantity of 1 mL was placed in an eppendorf tube in to which a quantity of 100 µL of trypan blue was added. After thorough mixing, a quantity of the mixture was then moved and added to the upper edge of the haemocytometer. Using an inverted light microscope and under a suitable objective (10-20x), the cells were counted in the four corners with exclusion of the cells outside the four rectangular indentation. To calculate the total number of the cells, the following equations were used:

$$\text{Cells density} = \frac{\text{total No. of cells counted}}{4} \text{ x2} \ldots\ldots (6) \qquad \% \text{ of viability} = \frac{\text{Number of live cells}}{\text{total number of cells}} \ldots\ldots (7)$$

4.2.4.3. Cell viability assay

A 96 well plates were used to seed the cells at a concentration of $1x10^6$ cells/well. Then, the cells were incubated for 24 hr. Afterwards, the media, and a quantity of metronidazole was added to the wells (C to H) and incubated for 24 hr (well A and B are controls). After the 24 hr, an amount of 10 µL of 3-(4, 5-dimethylthiazolyl-2)-2, 5-diphenyltetrazolium bromide (MTT) was added to each well and the cells were then incubated for a period of 4 hr. The cells were then shaken for 15 min using an electric shaker and measured for absorbance at a wavelength of 520 nm using Bio Rad microplate reader, model 3350, USA. All measurements were performed in triplicate (n=3). The values are reported as mean ± standard deviation.

Table 4.6. Concentrations of metronidazole, trehalose and HA used in the cell viability assay of Caco-2 cell lines for the delivery of aquasomes via the pulmonary route.

Description	Concentrations used
Metronidazole solution	10, 20, 40, 80, 90 and 100 µg
Trehalose solution	10, 20, 40, 80, 90 and 100 µg.
HA suspension	10, 40, 80, 90, 100 and 150 µg

4.2.4.4. TEER measurements

As for TEER measurements, the cells at a concentration of 2 x 105 cells/cm² were seeded on 6-well trans-well plates with polycarbonate-coated membranes (24mm, 4.7cm²; 0.33 cm^3). The cells were allowed to grow for 20 days. The media in the apical and basal compartments was replaced every 1-2 days. TEER were recorded every 2 days using an epithelial voltmeter, (World precision, USA). The measurements were performed in triplicate and each well was measured from three different sides to reduce reading errors. All measurements were performed in triplicate (n=3). The values reported as mean ± standard deviation.

4.2.4.5. Permeability studies

The cells were grown on 6-well Transwells® as described in section 4.2.4.4. After replacing the exhausted media from the apical and basal compartments, 1.5 mL of media (MDEM) mixed with metronidazole at a concentration of 200 µg/mL was added to the apical compartment. At time intervals of 1, 2, 3, 4, 5 and 6 hr, an amount of 300 µL was taken from both compartments and analysed using HPLC (sections 4.2.3.4). For permeability studies, HBSS was used to wash the cells prior the addition of the drug and pre-equilibrated for 1 hr with blank media. Afterwards, blank media was removed and the concentrations of metronidazole mixed with blank media was added subsequently. Permiability methods were adopted from Khan *et al*. (2011). All measurements were performed in triplicate (n=3). The values are reported as mean ± standard deviation. The percentage of drug transported was calculated as follows:

$$\%\ \text{of drug transported} = \frac{\text{Apical drug concentration} - \text{Basal drug concentration}}{\text{drug loading}}\ x100 \quad \ldots\ldots(8)$$

4.2.5. Stability studies

Aquasome tablets were stored at 4ºC ±1ºC/60% RH ±2% RH, 25ºC ±1ºC/60% RH ±2% RH and 40ºC ±1ºC/75% RH ±2% RH in accelerated stability studies cabinet (ATG, UK). At interval time points of 7 days, 14, 21 and 28 days, samples were taken for *in vitro* release studies (section 4.2.3.5). Visual inspection was performed on the samples, which includes changes in colour and peeling. Stability methods were adopted from FDA guidelines Q1A (R2). All measurements were performed in triplicate (n=3). The values are reported as mean ± standard deviation.

4.2.6. Statistical analysis

A one-way analysis of variance with Tukey–Kramer multiple comparisons test was used statistically compared the results obtained from performed experiments. The significance level of analysis was $p<0.05$.

4.3. Results and Discussion

There are many different delivery systems of solid oral dosage forms, most commonly used are tablets and capsules. Tablets as a solid dosage form are economical in manufacturing, stable and most suitable for transportation, packaging and shipping. Tablets can also be modified to release API into different sections across the GIT by applying different types of coatings. To investigate the possibility of manufacturing tablets with BSA-loaded aquasomes for oral delivery, it was essential to investigate the integrity of BSA-loaded aquasomes under compression forces and the stability of BSA-loaded aquasomes in the presence of excipients during the preparation of tablets. To investigate the integrity of BSA-loaded aquasomes, fluorescent-labelled BSA was used and was loaded on the aquasomes and tablets were prepared by direct compression subsequently (Figure 4.1). The fluorescent-labelled BSA was used instead of a standard fluorescent agent to facilitate further investigation using confocal microscopy as well as using the same model protein (comparable loading and release profile can be achieved using the same condition for manufacturing, characterization and release studies). BSA is used widely as a model for proteins and peptide studies. For instance, He *et al*., (2013) used BSA as a model for proteins and peptides in their research to facilitate a strategy for the fabrication of protein-functionalized quantum dots (QDs) at ambient temperature with single step. Likewise, Tantisripreecha *et al*. (2012) used BSA to develop delayed-release tablets from proliposomes of BSA granules by direct compression method. However, in the literature, there was no evidence found for the use of fluorescent-labelled BSA to investigate how proteins can handle compression forces using confocal microscopy. For instance, Tantisripreecha *et al.* (2012) used phosphorous nuclear magnetic resonance spectroscopy (^{31}P-NMR) to study BSA interactions after compression.

As a nanocarrier system, aquasomes have not been investigated through the oral route in a solid dosage form (Umashankar *et al*., 2010; Narang, 2012; Monica *et al*., 2015). Because the drug is attached on the outer layer of these systems, it was essential to investigate whether BSA will be attached to the system at high compression forces required to manufacture the tablets. It is documented that compression forces can affect the API integrity either directly due to the forces of compression or indirectly due to physical/chemical interaction with the tablet excipients during the tablet manufacture. For instance, (E)-4-[1-[4-[2-(Dimethylamino)ethoxy]phenyl]-2-(4-isopropyl) phenyl]-1-butenyl]phenyl monophosphate (TAT-59) is a new anticancer drug for the treatment of breast cancer. The physical and chemical stability of a mixture of TAT-59 and MCC at various powder blend concentrations directly compressed at 0, 300, 600 and 1400 kg/cm2 were assessed. It was found that the

increase in compression force increased the contact area between TAT-59 and MCC. The degradation of TAT-59 was enhanced as the proximity between TAT-59 and moisture presented at the surface of MCC increased (Matsunaga *et al*., 1994).

In another study, 6-benzyl-3-(5-methoxy-1,3,4-oxadiazol-2-yl)-5,6,7,8-tetrahydro-1,6-naphthyridin-2(1H)-one, is a new receptor agonist produced from benzodiazepine and was proposed to be formulated as a tablet. It was demonstrated that due to decreased crystallinity, chemical instability occurred which was caused by direct compression. Therefore, it was challenging to manufacture tablets with stable API using direct compression method (Fujita *et al*., 2010). However, in other cases compression can improve the formulation to that of unprocessed powder. A study investigated solid dispersions of drug-polymer mixture (NAP in PVP-VA) under compression force of 1.5 tons to prepare tablets. It was found that compression improved drug-polymer interactions compared to uncompressed powder and was studied using DSC and PXPRD. It was also proposed by the researcher that T_g width, the PXRD halo patterns and vibrational spectroscopic techniques can be used predict physical stability of the solid dispersions of drug-polymer mixture (Worku *et al*., 2013).

Figure 4.1. Preparation workflow of and testing of BSA-loaded aquasome tablets

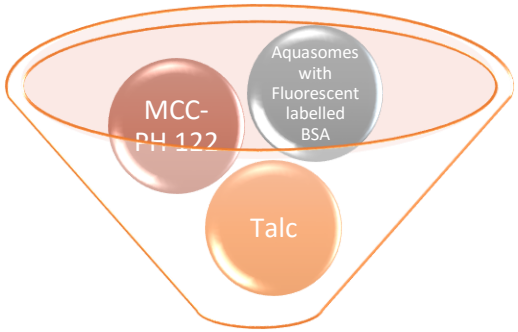

Manual mix for 5 min.

Compression of the mixture under different compression forces (0.5, 1, 2 and 3 tonnes) with 30 seconds keep time.

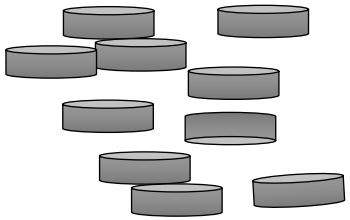

The upper surface (where the compression is highest compared to the bulk) is gently sampled to collect fine powder particles, which then viewed with confocal microscopy.

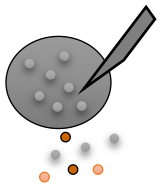

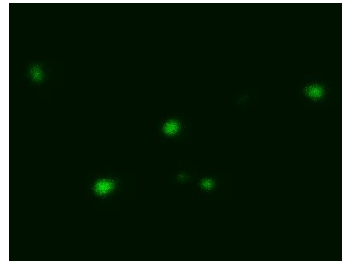

The BSA-loaded aquasomes tablet are then characterised for hardness, porosity, friability and disintegration time.

Tablets are then coated using acrylic based polymer (Eudraget 100) for 30 min until 10% weight gain was achieved.

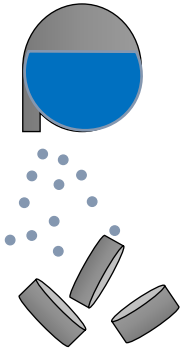

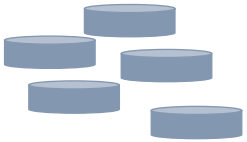

The coating of the BSA-loaded aquasomes tablets was checked for coating uniformity and resistance to 2 hr in acidic medium by placing them in FaSGF 0.1 HCL/100 rpm/37^{0}C.

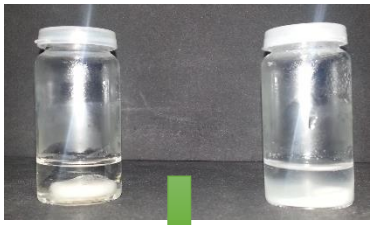

In vitro dissolution studies were then performed on the BSA-loaded aquasome coated tablets (90 rpm/37^{0}C).

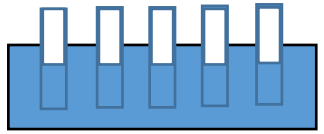

4.3.1. Preparation of aquasome tablets

To prepare the powder blends for direct compression, two excipients were used initially, MCC and magnesium stearate. Both excipients are widely used in the manufacturing of tablets and have established safety profiles (Matsunaga *et al*., 1994). MCC was used as a multifunctional excipient (filler/binder/disintegrant) while magnesium stearate and talc were used as lubricants. The grade of MCC used was ph-112 because it has a high bulk density (0.28-0.34 g/cc) and large particle size (100 µm) so it may provide protection to aquasomes against compression forces and enhances flowability (Gohel, 2005; FMC biopolymer, 2015). MCC also has the lowest amount of moisture (<1.5%), which is superior to the other types in providing stability to moisture sensitive APIs (FMC biopolymer, 2015).

Various mixtures of both excipients and fluorescent-labelled BSA aquasomes were prepared (Table 4.1). The tablets were produced under increasing compression forces (0.5. 1, 2 and 3 tons) to examine the effect of compression forces on the integrity of BSA-loaded aquasomes. It was noticed that during the first trials of tablet preparation, black dots appeared on the surface of the tablets (Figure 4.2). As MCC was the main excipient, the suggestion was to first replace the lubricant magnesium stearate with talc to investigate the cause of these black spots. After the use of talc as a lubricant instead of magnesium stearate, the black spots disappeared. There are various reasons which may explain the appearance of black dots. For instance, if the formulation contains large amounts of calcium phosphate and/or hydroxyapatite, the chances of these spots appearing are high due to the abrasive nature of these powders. This is why calcium tablet supplements made from calcium phosphate have a greyish colour and not a white colour as the uncompressed powder appears. The other reason may be due to moisture, whether the formulation has high moisture content or the API is hygroscopic in nature. Moreover, high quantities of fine powder in the product can enter between the feed frame and turret and cause friction and lead to the appearance of the black dots. Improper mixing could lead to powder pockets, which upon compression form discoloration. Furthermore, compression forces could trigger the melting of API (APIs with low melting points) due to heat generated during compression (Bundenthal, 2014; Patel *et al*., 2010; Roy, 2011).

In the case of BSA-loaded aquasome tablet preparations, the powder blend was mixed by hand for about 5 min to achieve a visually uniform mixture. In addition, the amount of HA is less than 25% w/w of the powder blend, therefore black spots could not be due to HA cores being compressed. Although proteins have a tendency to absorb moisture, BSA is not

considered a hygroscopic material. In addition, the aquasome powder was freeze-dried and the moisture content of MCC used was 1.5% w/w. Furthermore, the melting point of BSA, trehalose and hydroxyapatite is above 70^0C (as measured by DSC), which makes it unreasonable to reach it at 0.5 tons of compression force. The fact that after changing the lubricant lead to the disappearance of the black spots highly suggests that under compression of the tablet blend a sort of physical/chemical interaction occurred between the BSA-loaded aquasomes and magnesium stearate. Such interactions, especially with magnesium stearate has been reported in the literature. As a principal example, magnesium stearate interacted with acetylsalicylic acid in tablet manufacture and lead to the degradation of the later. The mechanism of how magnesium stearate causes the degradation of acetylsalicylic acid is not clearly understood. Kornblum and Zoglio (1967) found that acetylsalicylic acid rate of decomposition in suspensions with containing lubricants, such as magnesium stearate, was related to the high solubility of the magnesium salt of acetylsalicylic acid. This was resulted in the formation of a buffer with dissolved acetylsalicylic acid, generating a pH that was negative on the stability of the API. It has also been proposed that the existence of magnesium stearate impurities in magnesium stearate may increase the degradation by forming an alkaline pH environment (Kornblum and Zoglio, 1967; Miller, 1988; Bharate, *et al*., 2010).

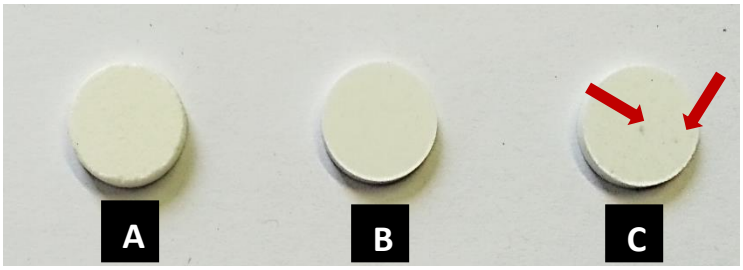

Figure 4.2. Three aquasome tablets prepared by direct compression method. (**A**) Coated aquasome tablets, the surface is less shiny because of the coating (at 1 tons of compression force), (**B**) uncoated aquasomes tablet with 1% w/w talc (at 0.5 tons of compression force) (**C**) uncoated aquasome tablet with 1% w/w magnesium stearate (at 0.5 tons of compression force). The black dots are marked with red arrows.

A total of five powder blends with varying BSA-loaded aquasomes quantities were prepared and compressed under increasing compression forces of 0.5, 1, 2 and 3 tons (Table 4.1). Compressed blends 3, 4 and 5 failed to produce a tablet. The tablets produced with these formulations were fragmented when trying to release them from the dye and this was the case

with the different compression forces used. MCC is well known for its filler and binder properties and it is also known that MCC has high compressibility (Carlin, 2008; Ohwoavworhua and Adelakun, 2010). Compressed powder blends 3 and 4 had the lowest MCC and this could be related to the failure of these formulations, as there was not enough MCC present. Another reason could be that when 400 mg of BSA-loaded aquasome powder was compressed, it produced fragmented tablets (chipping was also noticed), which indicate the poor mechanical properties of aquasomes (Sina Y, 2009; Nicklasson *et al*., 1999). Furthermore, hydroxyapatite (the prominent component of aquasomes) alone is not useful as an excipient, but by adding substantial quantities of carob flour to the hydroxyapatite, a directly compressible material can be produced (US patent 20100150806 A1, 2010).

The failure of aquasomes to produce compressed tablets with compressed blends 1 was investigated using SEM (Figure 4.3 and 4.4). At compression forces of 1 ton, the compressed powder blends were sampled and viewed with SEM. It can be noticed that as the percentage of BSA-loaded aquasomes increases, the MCC under increased compression transformed from fibres to fragmented sheets (heterogeneous mixture). These fragmented sheets are produced from the compressed BSA-loaded aquasomes, as it can be clearly understood from the compressed BSA-loaded aquasomes without any additives when compared to compressed MCC without any additives (Figure 4.4 A and B). This correlates to the poor mechanical properties of HA.

The tablets produced with compressed blend 2 failed to produce tablets at compression forces of 0.5 and 1 ton, while at compression forces of 2 and 3 tons tablets were produced. In the pharmaceutical industry, the preferred compression forces are at 1 ton and less. The reasons to such preference is that high compression forces increase the chances of physical/chemical interactions. Moreover, compression forces on dyes are low, which eventually extends their lifespan. Furthermore, low compression forces prevent tablet defects such as chipping and picking which are increased at higher compression forces (Knopp, 2013; Matsunaga *et al*., 1994). Therefore, compressed blend 2 was not brought forward to the next stage (coating and evaluation of BSA). As for compressed blend 1, it produced tablets with satisfactory properties at the different compression forces investigated.

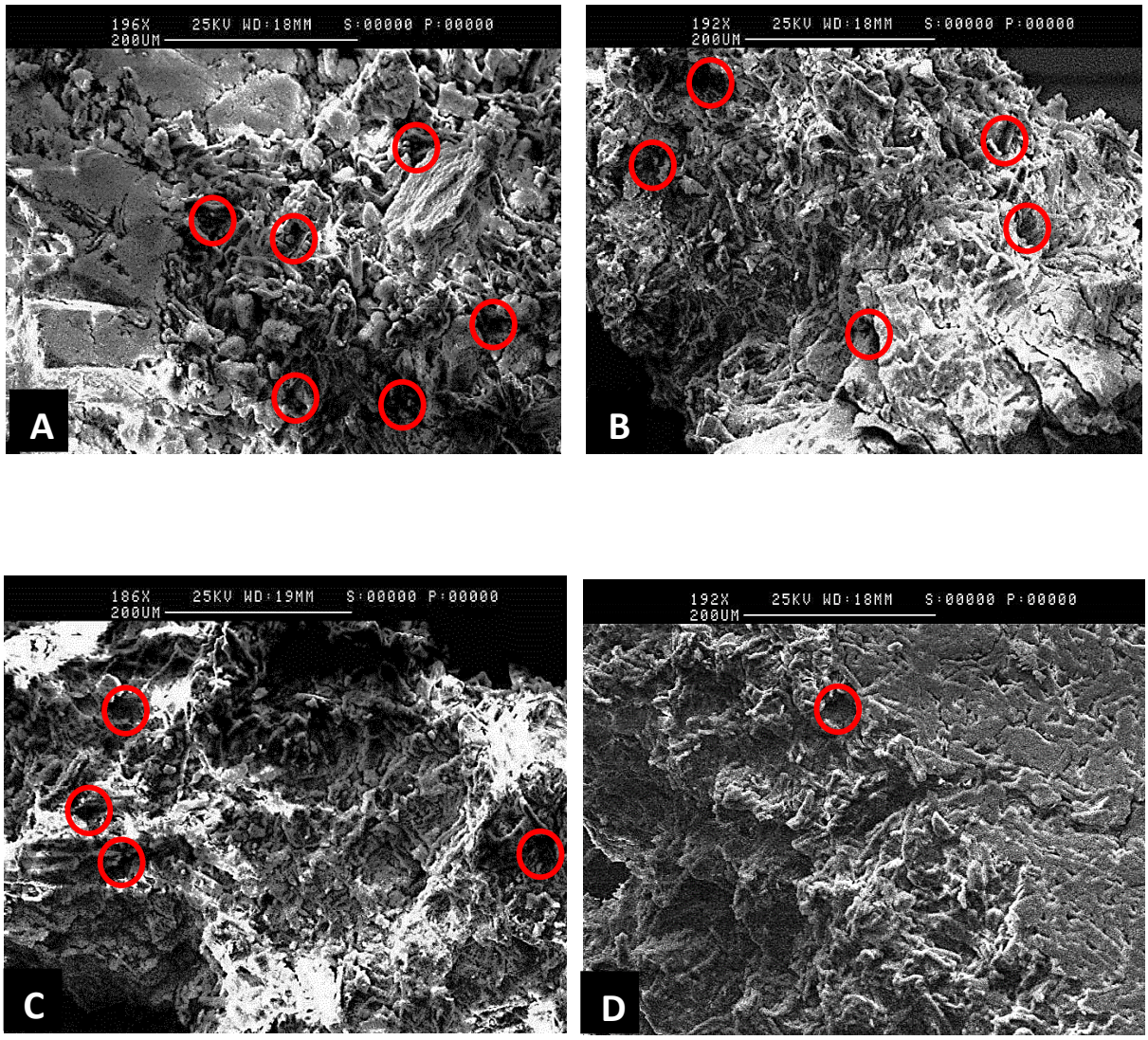

Figure 4.3. SEM images of tablets' bulk prepared with BSA-loaded aquasomes at compression force of 0.5 (A), 1 (B), 2 (C) and 3 (D) ton. The voids (marked with red circles) in the bulk decreases as compression force increases, which correlates to the decrease in porosity and the increase of disintegration time of these tablets. SEM images were taken at 186-196x of magnification and at 25 KV.

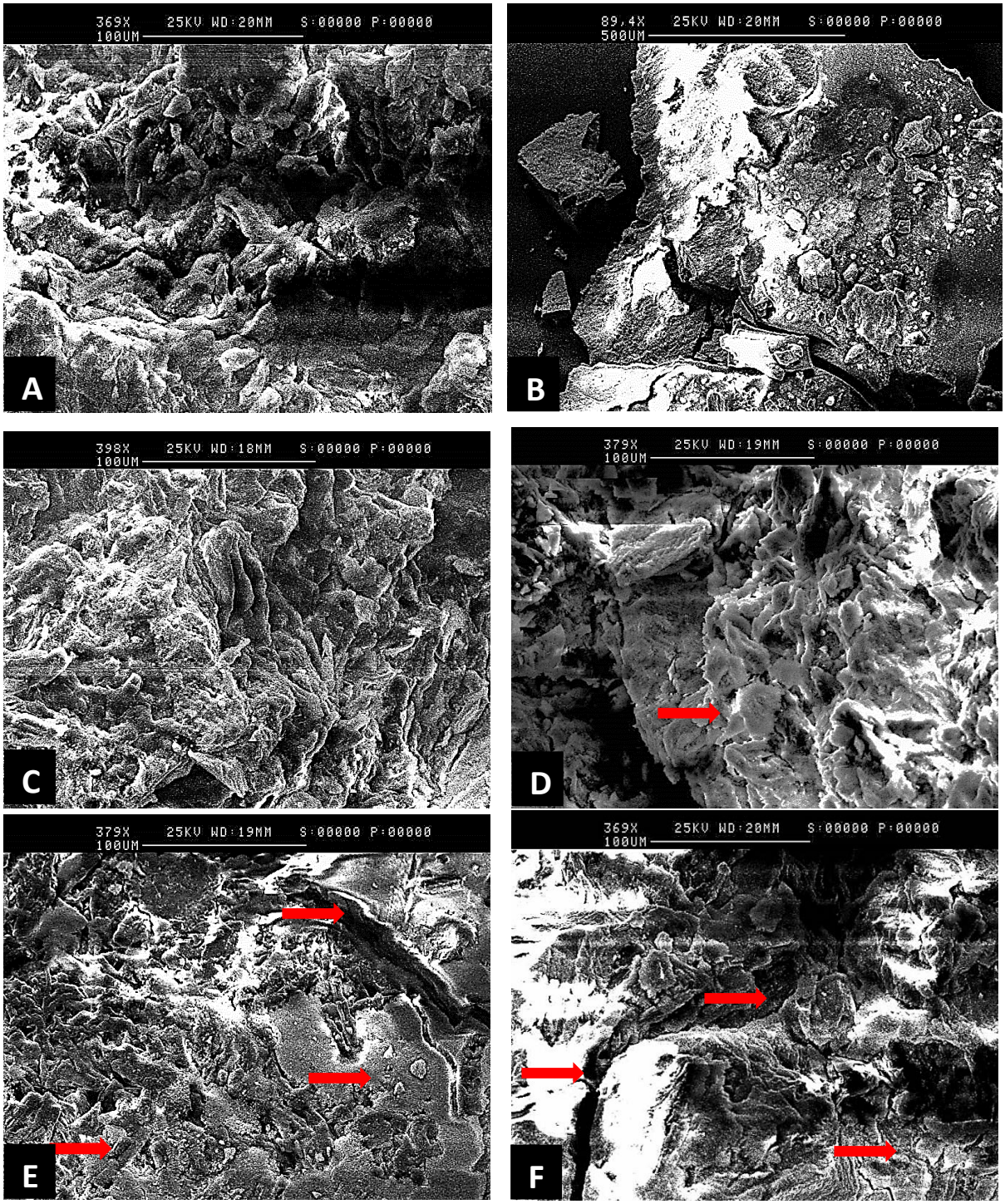

Figure 4.4. SEM images of tablets' bulk prepared with BSA-loaded aquasomes at increasing amounts of BSA-loaded aquasomes [MCC powder (A), BSA-loaded aquasomes powder (B), 37% BSA-loaded aquasomes (C), 50% BSA-loaded aquasomes (D), 62% BSA-loaded aquasomes (E) and 75% BSA-loaded aquasomes (F)] at 1 ton of compression force. As the amount of BSA-loaded aquasomes increases, the mixture under compression transformed from heterogeneous appearance due to MCC fibres to fragmented flat sheets (marked with red arrows). SEM images were taken at 369-398x of magnification and at 25 KV.

4.3.2. Characteristics of aquasome tablets

To investigate the behaviour of MCC/BSA-loaded aquasomes mixtures under various compression forces, the results of hardness and porosity were plotted against each other (Table 4.7 and 4.8). compressibility profile of the powder blend can be produced by plotting tablet porosity against compaction pressure. Compressibility is defined as the ability of the materials in the powder blend to undergo a volume reduction on exposure to compression (Joiris *et al*., 1998). The compressibility profile of the aquasome tablets show moderate compressibility at 0.5 and 1 tons of compression force and high compressibility at 2 and 3 tons of compression force (Figure 4.5). This could be related to the effect of the MCC, as at higher compression forces it tends to undergo plastic deformation with less voids (low porosity) (Amin *et al*., 2012; Hx *et al*., 1999; Shlieout *et al*., 2002). Comparing MCC compressibility without aquasomes to reported polydex and crosspovidone, MCC show high compressibility especially at high compression forces (Al khatawi *et al*., 2012). In comparison, the compressibility profile of MCC powder has similar trends to the MCC/BSA-loaded aquasomes mixture. This could be because MCC is the dominant powder fraction of the MCC/BSA-loaded aquasome mixture (approximately 74% of powder blend).

To understand the reduction in volume of a powder blend, several mathematical equations were developed to evaluate the effect of applied pressure on the porosity changes of the tablets. Some of the known mathematical equations are the Heckel, Kawakita and Cooper-Eaton equations. These equations evaluate the effect of applied pressure on the porosity changes of the tablets. The Heckel plot is used to demonstrate powder profile under compression and is normally distinguished by three regions. The first region is an initial nonlinear region (section I), then a linear region where the data obey the expression (section II), and a third non-linear region (section III) (Denny, 2002; Ramberger and Burger, 1985; Mani, 2004; Heckel, 1961). The P_y value on the heckle plot of MCC is lower than that of MCC/aquasomes mixture. This indicates that aquasomes have low elasticity, which was evident from the SEM images (aquasome powder turns into fragmented plates, which possess no elasticity) (Figure 4.4 and 4.3). Moreover, according to the Heckel profile (Figure 4.5 and 4.6), the first part (marked with a dotted line) is where particle arrangement occurs. MCC exhibited a steep straight ascending line, which indicates deformation mechanism of particle arrangement, which correlates with the SEM images of compressed MCC, BSA-loaded aquasomes and mixture of both at elevated compression forces. Whereas MCC/aquasomes exhibited a more gradual ascending line, which indicates high degree of particle arrangements, which could be due to the difference of particle size of both mixture and to the high compressibility of MCC particles.

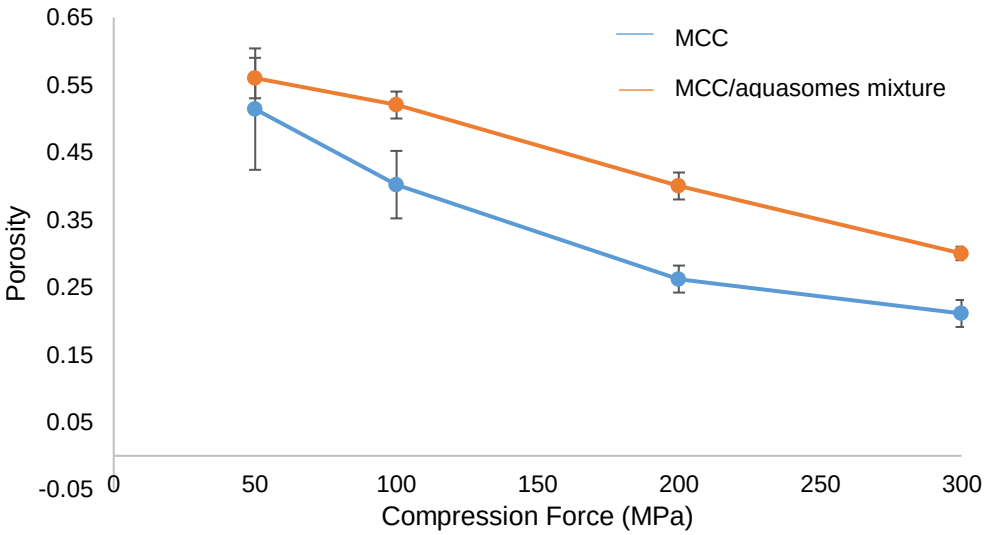

Figure 4.5. A graph shows the compressibility profile of MCC and MCC/aquasomes mixture shows higher compressibility (lower porosity) of MCC than MCC/aquasomes (higher porosity) at the different compaction pressures used. Values are reported as mean ± SD (n=6).

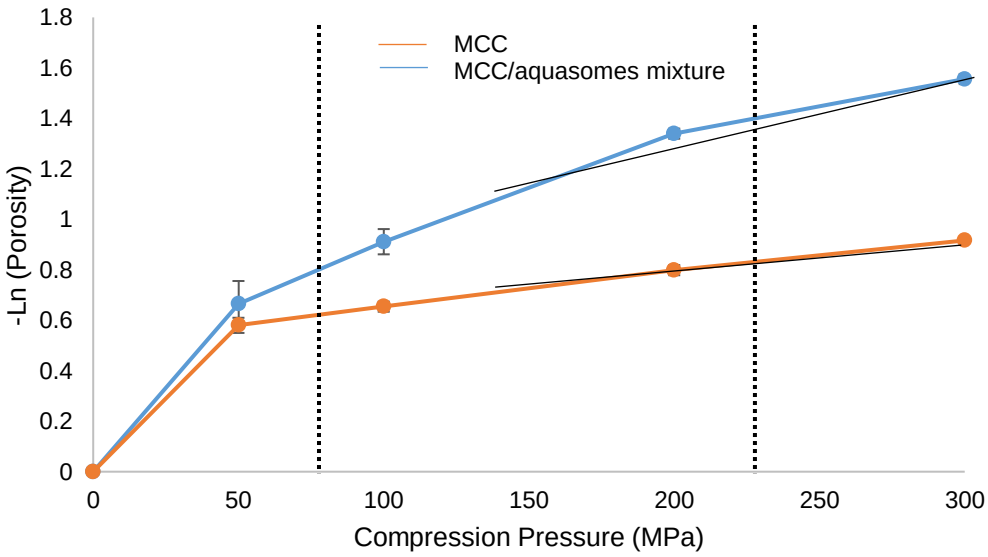

Figure 4.6. Heckel plot of MCC (orange line, R^2 0.976) and MCC/aquasomes (blue line, R^2 0.963) mixture compressed under 50, 100, 200 and 300 MPa. The linear portions of the graph were used to obtain P_y values 520 and 658 MPa for MCC and MCC/aquasomes mixture respectively. Values are reported as mean ± SD (n=6).

Table 4.7. Table of results of hardness before and after coating, friability, porosity, disintegration of compressed powder blend 1 before and after coating and visual inspection. Values are reported as mean ± SD (*n* = 6).

	Compression Force (Tons) (variable factor)	***Friability***	***Disintegration Time (min)***	***Porosity***	***Hardness (N)***	***Visual Inspection[1]***	***Hardness After Coating (N)***	***Disintegration After Coating (Min)***	***Visual Inspection[2] After Coating***
Formulation 1	0.5	2.1±0.3	4±1	0.514±0.02	80±9	Pass	112±6	12±1	Pass
Formulation 2	1	1.3±0.2	8±0.5	0.402±0.01	120±7	Pass	145±8	17±1.5	Pass
Formulation 3	2	0.8±0.2	9±0.5	0.262±0.01	180±6	Pass	200±5	20±1	Pass
Formulation 4	3	0.5±0.2	13±0.5	0.211±0.01	210±9	Pass	245±6	32±1.5	Pass

- Visual Inspection[1] includes checking if the tablets are undamaged, smooth, cracks or capping, chipping, swelling, mottling, discoloration, fusion between tablets
- Visual Inspection[2] includes checking if the three are picking or sticking, capping, peeling, chipping and twinning.

Table 4.8. Data of hardness before and after coating, friability, porosity, disintegration of compressed powder blend 2 before and after coating and visual inspection. Values are reported as mean ± SD (*n* = 6). Failed formulations marked with F.

	Compression Force (Tn) (variable factor)	***Friability***	***Disintegration Time (min)***	***Porosity***	***Hardness (N)***	***Visual Inspection[1]***
Formulation 1	0.5	F	F	F	F	Failure to form a tablet
Formulation 2	1	F	8±0.5	0.352±0.01	69±5	Pass
Formulation 3	2	F	9±1.2	0.312±0.05	90±5	Pass
Formulation 4	3	F	10±1	0.230±0.09	100±4	Pass

- Visual Inspection[1] includes checking if the tablets are undamaged, smooth, cracks or capping, chipping, swelling, mottling, discoloration, fusion between tablets.

4.3.3. Coating of aquasome tablets

The aquasome tablets prepared under compression forces of 1 ton were selected for coating with HPMCAS-M. HPMCAS-M is a polymeric coating that disintegrates at pH>6. It has been used widely as a coating of tablets (Tanno *et al*., 2004; Sarood *et al*., 2014). When HPMCAS-M was initially used for the coating of BSA-loaded aquasome tablets, it was found that even at very low concentrations (2% w/w), the coating solution solidified in the machine tubing within 5-10 min. It is important to highlight that the minimum level to produce a uniform film of HPMCAS-M should be at least 15%w/w. One of the reasons to why this could be happening is that the pump speed was not sufficient to pump the coating dispersion even when placed at maximum output (4 ml/min). Even though when the distance of the tube that connects between the spray head and fed-in container (contains the coating dispersion) was reduced as an attempt to overcome this issue, the solution solidified after the first 5 min into the coating process. Consequently, acrylic based coating was used as an alternative. The procedure to prepare the coating dispersion was recommended by the coating manufacturer as the standard method to reach optimum coating using the spray coating technique (section 4.2.2.9). As for the coating parameters, the temperature was kept at 30^{o}C, so the protein was exposed to lower temperatures to minimise protein degradation (Table 4.9). The pump speed was kept at maximum to prevent solidification of the coating solution inside the tubes. The agitator remained on to prevent tablets attaching to the coating chamber and the air flow speed was kept at 70-80% as it was found that when lower air flows were used the tablets sank into the coating chamber and if higher flow speed was used the tablets exited the coating chamber.

Table 4.9. The parameters of the coating procedure and their description used to coat aquasome tablets prepared under compression forces of 1 ton. (modified from: Lan *et al,* 2004; Kout and Muller, 2009; Caleva 2015).

Parameter	Description	Conditions
Temperature	The temperature of the air, which controls the drying speed of the coating. The higher the temperature the less sticking of tablets and less after coating defects such as peeling	Rang of temperature (25-100 ^{0}C) Selected temperature (30 ^{0}C)
Agitation	Agitation prevent the tablets from sticking to the coating chamber.	Rang of functioning (on/off) Selected functioning (on)
Air flow speed	Controls the speed of the air going into the coating chamber, which eventually controls the drying speed and the tumbling of the tablets in the coating chamber, which eventually affects the effectiveness of the coating. The higher the airflow sped the better the efficiency of tablet.	Rang of air flow speed (10-100 %) Selected air flow speed (70-80 %)
Pump speed	Controls the speed of the coating solution going to the spry head. The higher the pump speed the better coverage area and less the defects due to empty pockets.	Rang of pump speed (1-4 mL/min) Selected pump speed (4 mL/min)
Air pressure	To control how much of the coating solution being pumped into the coating chamber. Air pressure and airflow speed has an important role in smoothness of the tablets. The higher the pressure sped the better the smoothness of the coating.	Rang of air flow speed (0.5-2 psi) Selected air flow speed (0.5 psi)

The duration of the coating process lasted for 30 min, which achieved a percentage weight gain of 9%±0.5 mg. The coating was then visually inspected for picking or sticking, capping, peeling, chipping, and twinning or incomplete coating. Initially, the amount of tablets which were placed in the coating chamber was seven. However, after inspection, 2 tablets were sticking to each other after 15-20 min of coating. To overcome this issue, the number of tablets was reduced to five. This issue could be related to the low temperature of drying (30^{o}C), which increases the chance of sticking due to over wetting, and also that when the amount of tablets was seven the chances that the tablets could collide with each other before drying is also higher. As stated previously, a temperature increase could not be used as with the 30 min coating time BSA could be degraded.

Inverted fluorescent microscopy was used to examine the coating of the BSA-loaded aquasome tablets. This was performed by mixing the coating solution with the fluorescent agent and viewing the tablets using the florescent microscope. SEM is generally used in the literature to examine the coating of the tablets. However, SEM provide images with limited information as the images are black and white. The images taken with the inverted fluorescent microscope show the build-up of the coating on the upper surface of the tablets after 5, 10, 15, 20 and 30 min of coating (Figure 4.7). It can also be noticed that as the coating increases the roughness of the coating on the tablet surface decreases as the coating accumulates gradually and produces smother surfaces. The false image technique was also used to demonstrate that there is a build-up of the coating, which occurs gradually as the coating time increases. As shown in the images (Figure 4.7), as the concentration of the coating increases the colour changes from orange (lowest fluorescence/low concentration of coating) to blue (high fluorescence/high concentration of coating) after 5, 10, 15, 20 and 30 min of coating respectively.

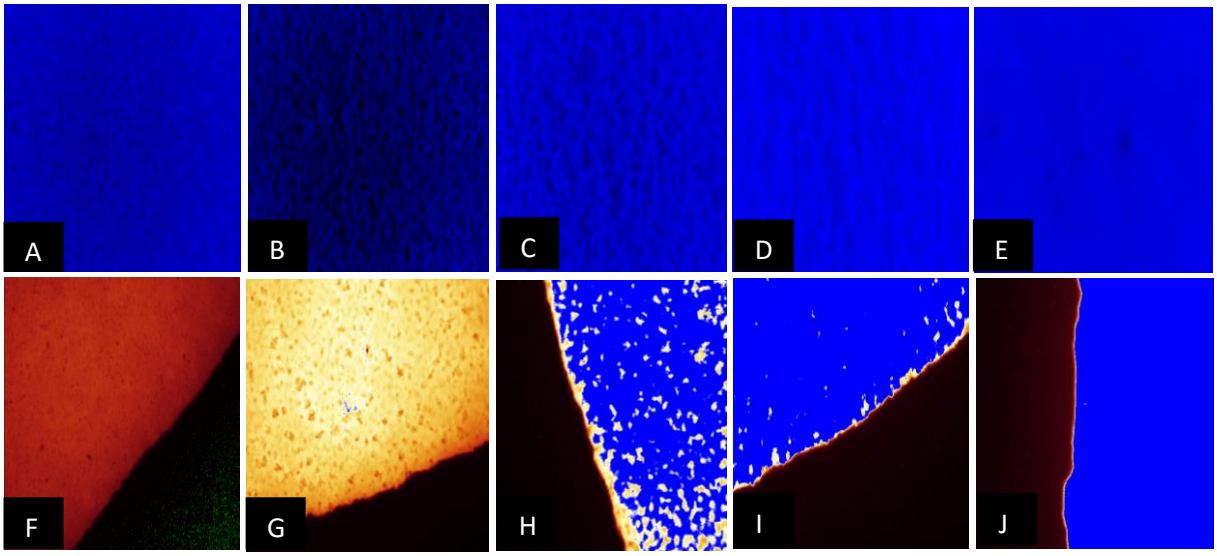

Figure 4.7. Images taken by the inverted fluorescent microscope. Images from A-E show the build-up of the coating on the upper surface of the tablets after 5, 10, 15, 20 and 30 min of coating respectively. Images from F-J are for the edge of the tablet and show the change in colour from orange (low concentration of coating) to blue (high concentration of coating) after 5, 10, 15, 20 and 30 min of coating respectively. In all images, the false colour technique was employed using Leica LAS AF light software.

4.3.4. *In vitro* release studies of aquasomes tablets

The *in vitro* release studies of tablets are normally performed in 900-1000 mL volume of media using the USP II/III dissolution apparatus at 50/75 rpm paddle speed and at 37ºC. However, there are some exemptions according to the FDA, where dissolution can be performed in smaller volumes of dissolution media (Hydromorphone HCl extend release tablets dissolution is performed in 50 mL of media). The volumes can be as low as 50 mL or even lower if the reason is justified. In the case of aquasome tablets, the reason to choose 40 mL volume of dissolution media to perform the *in vitro* release studies that BSA concentration in volume above 40 mL presents below the LOQ. Therefore, to keep BSA below sink conditions and also to maintain concentrations above the LOQ, the release studies were performed in 40 mL volume of media at 100 rpm/37ºC.

The coated tablets under compression forces of 1 ton were brought forward for *in vitro* release studies. The reason not to choose the tablet produced at 0.5 ton of compression forces was because it is recommended that for tablets to be coated to have high hardness in order to withstand coating conditions (pan coating as it is the preferred method for coating tablets in industry and require sufficient hardness for the tablets to withstand the tumbling) (Augsburger and Hoag 2008). The tablets produced at 0.5 ton of compression force scored marginal hardness of 80±9 N and it is more likely to fail during pan coating conditions.

The coated tablets under compression forces of 1 ton were placed in 40 mL volume of media ready to perform *in vitro* release study to represent what happens to a tablet inside the body as it travels through the GI tract (Figure 4.8). The initial medium was FaSGF (pH 1.2) for 2 hr at 37ºC/100 rpm followed by immersing the tablet in FaSIF (pH 5.1) for 1 hour followed by FaSIF (pH 6.7) for 6 hr. Samples were taken at the end of the 2 hr of SGF (pH1.2) and at the end of the first hour of FaSIF (pH 5.1) to investigate whether BSA had been released. HPLC results show no BSA was detected (at SGF pH 1.2 and FaSIF pH 5.3) which indicates that the coating layer and the coating procedure is effective. The release of BSA over the 6 hr in FaSIF (pH 6.7) was steady and results in a release of 14% ±1.9 in the first hour and approximately 90% ±4.2 after 5 hr. As a result, the coating performed as expected as the coating completely disintegrates at pH >5.5 without affecting the release of BSA from aquasomes. In comparison, BSA released from the tablets after the first hour was 2.9% ±0.6 less than that released from aquasomes powder, but the difference not statistically significant (p>0.05). This could be related to the time

required for the coated tablet to disintegrate (17 min ±0.6) and BSA to start to release from aquasomes.

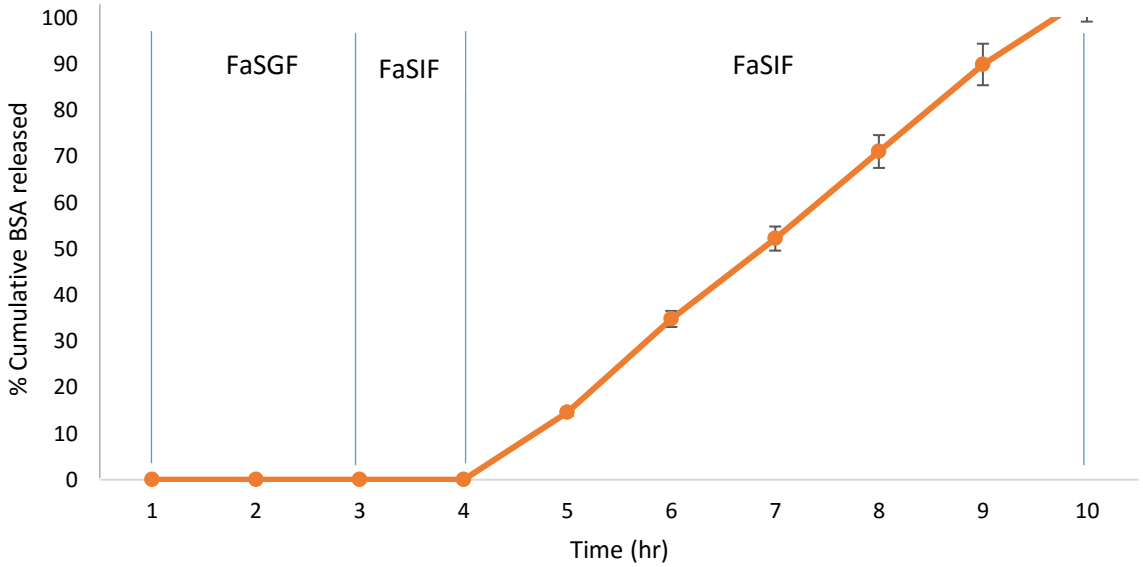

Figure 4.8. The percentage of cumulative BSA released from BSA-loaded aquasome tablets over 14 hr of release (2 hr at SGF pH 1.2, 1 hr at FaSIF pH 5.3 and 6 hr in FaSIF pH 7.4). BSA was not released from coated BSA-loaded aquasome tablets for the first 4 hr as expected due to the effect of the coating. However, once the pH was increased after 4 hr, the coating started to disintegrate and BSA started to release as expected. Values are reported as mean ± of SD (n=3).

4.3.5. Effect of compression on aquasome tablets

Confocal microscopy was used to investigate BSA-loaded aquasome tablets under the compression forces used (compressed powder blend 1). The tablets were prepared with fluorescent-labelled BSA loaded on to the aquasomes so it can be viewed with the confocal microscopy. Fluorescent-labelled BSA aquasomes where collected from the outer surface and not from the bulk of these tablets as it is recognised that the surface of the tablet experiences the highest effect of compression compared to the bulk.

As can be seen from the confocal microscopy images that fluorescent-labelled BSA aquasomes of compressed powder blend 1 at compression force of 0.5 and 1 tons appear as green dots (the fluorescence is concentrated in one point) (Figure 4.9 C and D). In comparison, fluorescent-labelled BSA aquasomes of compressed powder blend 1 at compression force of 2 and 3 tons appear as green spots, the fluorescence is not concentrated in one point (Figure 4.10 A and B). loaded BSA of aquasomes of

compressed powder blend 1 at compression force of 2 and 3 appear to be spread out of the cores to the surrounding area. This suggest that BSA aquasomes of compressed powder blend 1 at compression forces of 1 and 2 tons failed even though their tablets have sufficient tablet properties (hardness, porosity). Research, which has been performed by Edwards and Slater (2009), investigated the delivery of live bacteria via the oral route as tablets. Tablets were prepared by compressing live bacterial vaccine strain S. typhimurium SLDAPD/pUC18I. At the compression conditions they used, the live bacteria were tested for activity after compression and found that compression did not affect their activity.

At high compression forces (2 and 3 tons), the system could coagulate or fragment which results in the distribution of fluorescent-labelled BSA (Figure 4.9 A). In order to roll out such an assumption, the same samples were viewed with confocal images (non-fluorescent state) (Figure 4.9 B). The images show greyish dots, which represent the cores, and the cores look intact and show similar sizes before direct compression. This demonstrates that fluorescent BSA spreads out of the cores under high compression forces and the cores are not fragmented/coagulated.

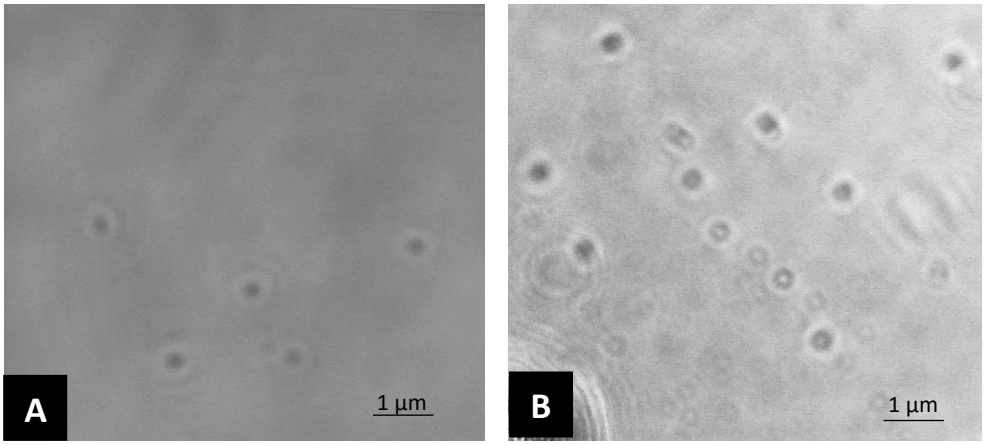

Figure 4.9. Confocal images (non-fluorescent state) of BSA-loaded aquasomes under compression forces of 0.5 (A) and 3 tons (B). It can be seen that the cores under high compression are intact and they are not fragmented.

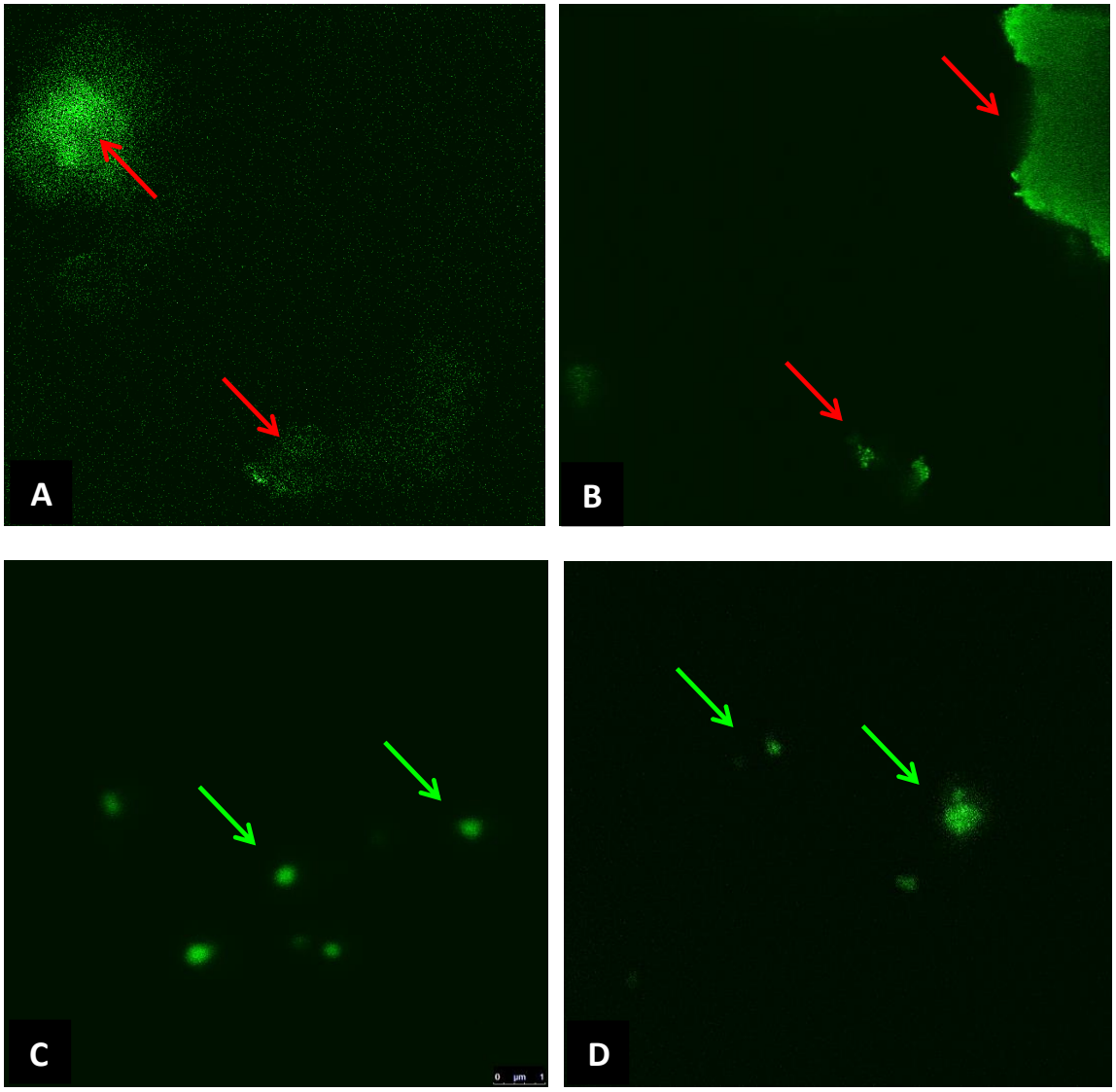

Figure 4.10. Confocal Images of fluorescent-labelled BSA-loaded aquasomes under 3 (A), 2 (B), 1 (C) 0.5 (D) tons of compression force. At higher compression forces (2 and 3 tons), the BSA spreads out of aquasomes (marked with red arrows). At low compression forces (0.5 and 1 tons) aquasomes were intact (BSA concentrated in one spot) (marked with green arrows).

4.3.6. Cell culture studies

Caco-2 cells are the most commonly used cell line to measure drug permeability of medicines for human use because of their ease of management and accessibility. The Caco-2 cells spontaneously differentiate at incubation conditions to form continuous monolayers of cells. Because Caco-2 cells are derived from the human colon, therefore, the permeability is higher *in vivo* perfusion studies conducted in humans to that of Caco-2 cells (Artursson and Karlson, 1991). Nevertheless, the absorptive capabilities of Caco-2 cell monolayers are comparable to small intestinal cells (Hidalgo *et al*., 1989). The prime disadvantage of Caco-2 cell monolayers are the variability of expression of efflux systems, active transporters and variability in the expression of metabolizing enzymes, including CYP 3A4. To account for such deficiency, induction of up regulation of these variables or transfection of the cell cultures with the cDNA has been used to evaluate the variability in expression (Cummins *et al*., 2001; Crespi *et al*., 1996). Additional limitations of the Caco-2 cell monolayers include the lack of a mucus layer, which is normally present in the human intestine, and cell culture homogeneity. Caco-2 cells do not have the ability to produce mucus, which can obstruct the absorption of APIs, in particular rapidly permeable ones. In spite of these disadvantages, good correlations have been established between the relative oral absorption in humans and the permeability of Caco-2 cells (Ingels and Augustijns, 2003). Therefore, standardized guidelines have been established to correlate Caco-2 permeability as a model.

4.3.6.1. MTT assay of metronidazole, trehalose and HA

To measure cell viability in the presence of HA, concentrations of 0.1, 0.4, 0.6, 0.8, 0.9, 1 and 1.5 mg/mL of HA were used. The analysis of the data gathered from the MTT assay indicates that the cells were viable, in comparison with the reference absorbance, apart from the highest concentration used (1.5 mg/mL). The reduction in the percentage of cell viability was statistically significant ($p<0.001$) when compared to the HA concentration of 1 mg/mL, and also statistically significant ($p< 0.05$) when compared to the HA concentration 1.5 mL (Figure 4.11). Cell death may have occurred either because the high concentration of the non-soluble HA covered the surface area and provided a barrier between the cells and the media and/or CO_2 and the cells eventually died. Another possible reason is that HA particles induced oxidative stress which eventually may have caused indirect cell death. HA has been reported by Meena *et al* (2011) to cause cell death via increased ROS in the human breast cancer cells (MCF7). However, the size of the HA nanoparticles tested in the study was between 10-20 nm and the significant

changes where observed at 100mg/L compared to the control (p<0.01). In addition, Kamal *et al*. (2013) studied the effect of HA scaffold with direct/indirect cell contact studies on bone marrow cells (MSC) and have found that HA bear no direct cell toxicity for the duration of the testing (24 hr). Equally, MTT reflects metabolic changes due to cell death. Further studies are required to measure inter leucine 8 (IL-8), which is released in higher amounts when the cells undergo stress. Stressed cells do not necessarily die, but could undergo morphological changes (benign or malignant). IL-8 test provides an in-depth view on how the cells are reacting towards a specific agent/stress rather than MTT (Baggiolini and Clark-Lewis, 1992; Smirnova *et al*., 2003).

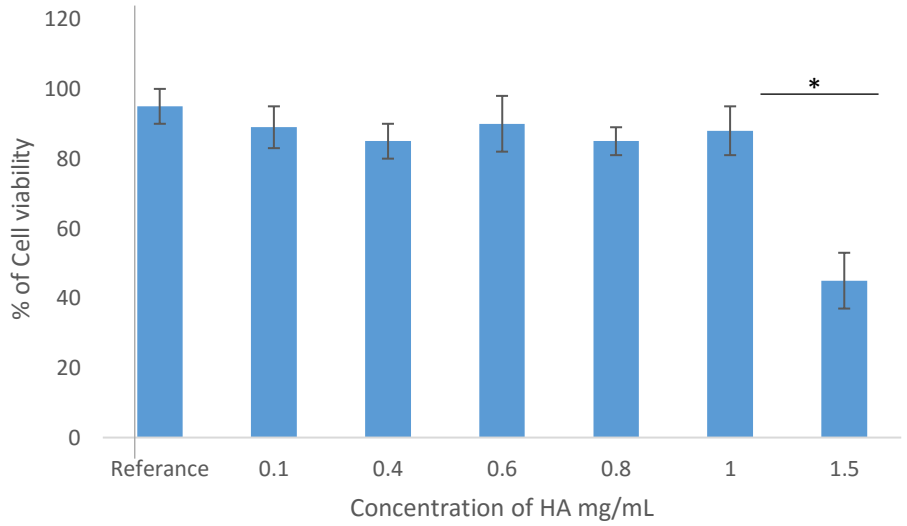

Figure 4.11. A bar chart shows the percentage of Caco-2 cell viability in various HA concentrations. Values are reported as mean ± SD (n = 3). Statistical analysis (one-way ANOVA/Tukey) between stages: *p< 0.05.

To measure the percentage of cell viability in the presence of trehalose, concentrations of 0.1, 0.2, 0.4, 0.6, 0.8 and 1 mg/mL of trehalose were used. The analysis of the data gathered from MTT assay indicates that the cells were viable, in comparison with the reference absorbance, at all concentrations of trehalose investigated (Figure 4.12). This highlights the importance of trehalose in maintaining/preserving cells from death in plants. Relatively high concentrations of trehalose can be found in Anhydrobiotic organisms (sometimes including disaccharides and oligosaccharides). When the nematode *Aphelenchus avenae* was dehydrated slowly, trehalose was synthesised internally by an amount up to 20% of it is weight (Madin and Crowe, 1975). This is also

evident from the toxic dose of trehalose in rats which is >500 mg/Kg via oral route (Inchem, 2016).

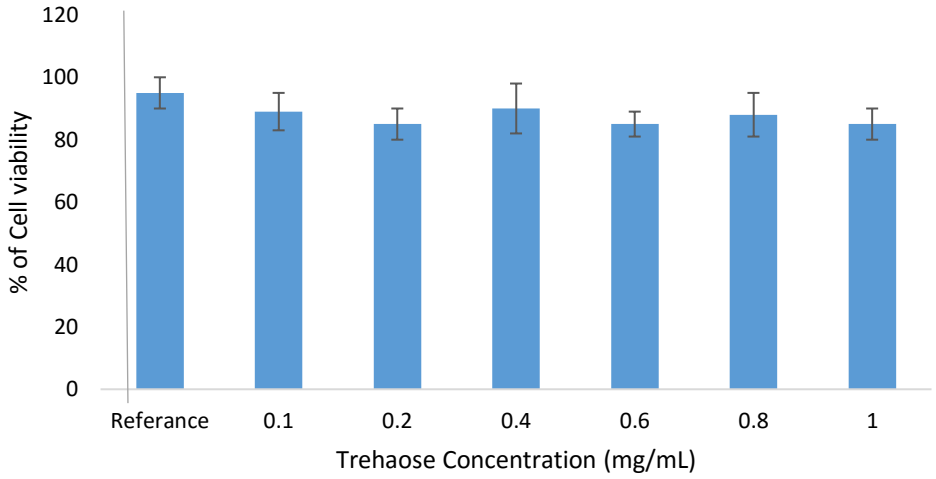

Figure 4.12. A bar chart shows the percentage of Caco-2 cell viability in various trehalose concentrations. Values are reported as mean ± SD (n = 3).

To measure cell viability in the presence of metronidazole (used as a model drug), concentrations of 0.1, 0.2, 0.4, 0.6, 0.8, and 1 mg/mL of metronidazole were used. The analysis of the data gathered from MTT assay indicates that the cells were viable, in comparison with the reference absorbance, at concentrations of 0.1, 0.2 and 0.4 mg/mL of metronidazole, (Figure 4.13). However, with concentrations of 0.6. 0.8 and 1 mg/mL of metronidazole there was a decrease in the mean absorbance. Despite the decrease in absorbance, there was a statistical difference when compared to the reference absorbance (p<0.05). Previous MTT studies on metronidazole state that cell toxicity occurs at concentrations above 0.65 mg/mL. In order to perform the permeability studies, metronidazole concentration that was used did not exceed 0.4 mg/mL (Vanic *et al*., 2013; Drug Bank, 2013).

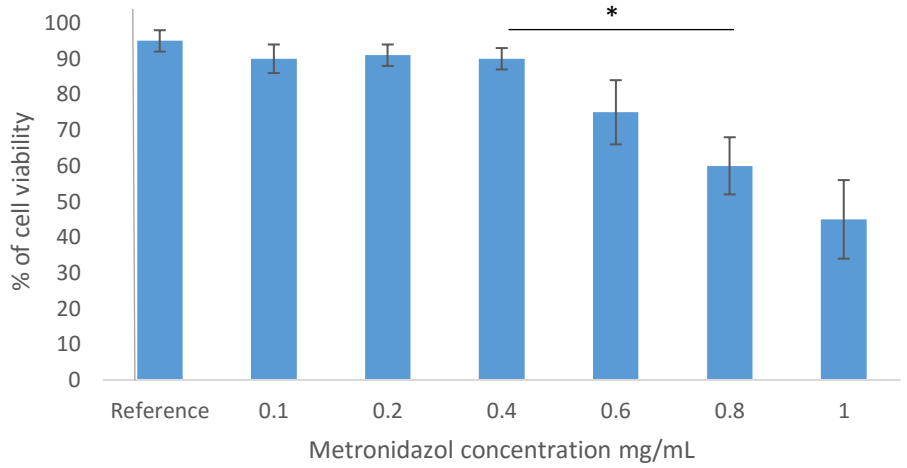

Figure 4.13. A bar chart shows the percentage of Caco-2 cell viability in various metronidazole concentrations. Values are reported as mean ± SD (n=3). Statistical analysis (one-way ANOVA/Tukey) between stages: *p< 0.05.

4.3.6.2. TEER measurements

TEER measurement is an important technique to measure the confluency of the cells seeded on a transwells® membrane (the cells are forming tight junction). TEER measurements of Caco-2 has been performed widely in the literature as a valuable tool in the evaluating/development on nanoparticles (Pereira *et al*., 2013; Thompson *et al*., 2011; Zhang *et al*., 2010; Pereira *et al*, 2013). To measure TEER, the cells were allowed to grow for a period of 20 days and were seeded on 6-well transwells® plates with polycarbonated-coated membranes and the cells checked for TEER every 2 days. The TEER measurements plateaued after day 18 (Figure 4.14). The results of TEER measurements obtained are parallel to what has been published in the literature (Ahmed *et al*., 2009; Ranaldi *et al*., 2013; HPA, 2016). As for Caco-2 TEER measurements, TEER tends to plateau after day 17-18 depending on the number of seeding and incubation conditions.

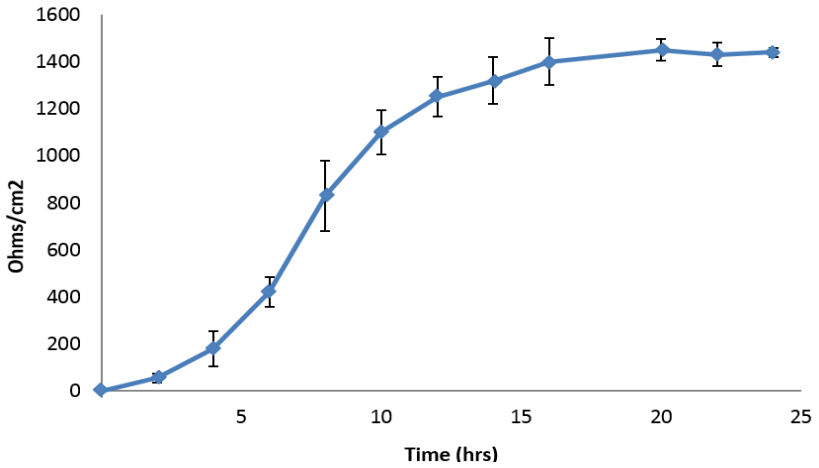

Figure 4.14. A graph shows the TEER measurement of Caco-2 cells seeded on 6-well trans-wells plates every 2 days for 20 days. Values are reported as mean ± SD (n=3).

4.3.6.3. Permeability studies of Metronidazole-loaded aquasomes

Metronidazole-loaded aquasomes were administered to a monolayer of Caco-2 cells and compared to a metronidazole solution of equal drug concentration in order to determine whether a delayed drug release effect could be noticed (Figure 4.15). The permeability studies show that the metronidazole-loaded aquasomes displayed a delayed transport of metronidazole across the monolayer of cells compared to the metronidazole solution. This was also confirmed with the lower total metronidazole released from both formulations. Within the first hour of release of metronidazole from aquasomes, there was an initial burst effect of approximately 4% higher than that of metronidazole solution, despite the fact that there was no statistical difference (p>0.05). Metronidazole was used as a model instead of BSA to perform permeability studies because BSA is a large protein (66,463 Da) and there are no receptors present on Caco-2 cells to facilitate its permeability (Shukla *et al*., 2000; Tuovinen *et al*., 2002).

The release of metronidazole from aquasomes after 2 hr in the permeability study started to slow gradually until it reached its highest difference at hour 6 (p< 0.05). The metronidazole transported across the Caco-2 monolayer was 60.92 ±3.5% after 6 hr. The data was not plotted using apparent permeability coefficient, as the purpose of the study was not related to measure, alter or enhance the permeability of metronidazole. In contrast, the purpose of the study was to observe if the aquasomes are delaying the release of metronidazole compared to the control (metronidazole solution).

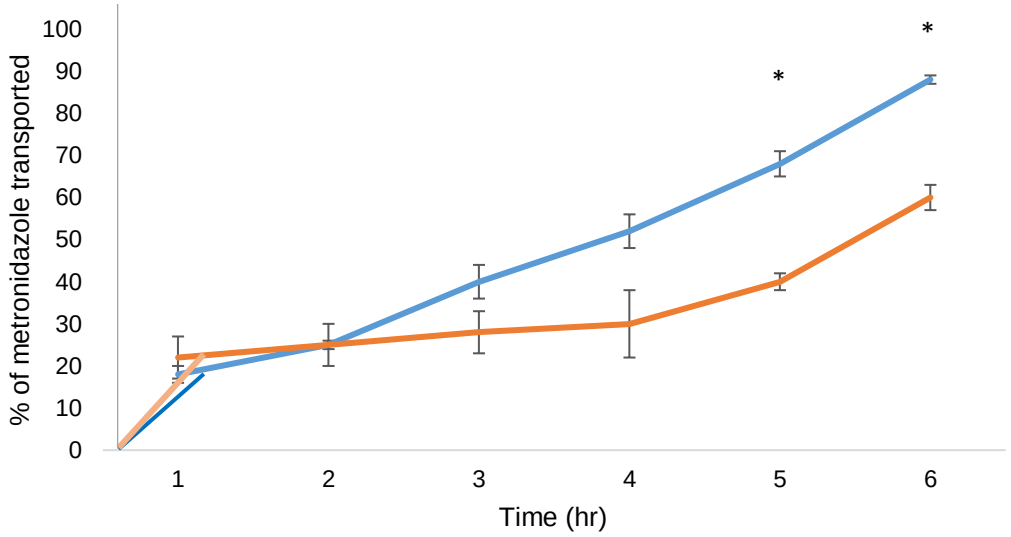

Figure 4.15. Transport of metronidazole across Caco-2 from metronidazole solution (blue line) and metronidazole-loaded on aquasomes (orange line). The graph shows that there is a significant delayed release from aquasomes during the last two hr. Values are reported as mean ± SD (n = 3). Statistical analysis (one-way ANOVA/Tukey) between stages: *p< 0.05.

4.3.7. Stability Studies of aquasome tablets

The stability studies of BSA-loaded aquasome tablets were conducted in three storage conditions of 4ºC ±1ºC/60% RH ±2% RH, 25ºC ±1ºC/60% RH ±2% RH and 40ºC ±1ºC/75% RH ±2% RH (Tables 4.10, 4.11 and 4.12 respectively). The stability result of BSA-loaded aquasome tablets at the tested conditions show no significant changes (p>0.05) in hardness, disintegration time and BSA content. Although such results are encouraging, extended stability studies are required to reach a solid conformation about the stability of BSA-loaded aquasome tablets. Due to the limited time points, degradation profile and estimated shelf times cannot be established. It is worth noting that the minimum time required by guidelines for stability studies performed at 4ºC ±1ºC/60% RH ±2% RH, 25ºC ±1ºC/60% RH ±2% RH and 40ºC ±1ºC/75% RH ±2% RH is for 12, 6 and 6 months respectively (Faisal *et al*., 2013; SADC, 2014; Singh V. *et al*., 2012).

Table 4.10. Stability study result of BSA-loaded aquasome tablets for hardness, disintegration time, BSA content and visual inspection. Storage condition was at 4ºC ±1ºC/60% RH ±2% RH. Values are reported as mean ± SD (n = 3).

	Day 0	Day 7	Day 14	Day 21	Day 28
Hardness	145±8	143±6	150±4	148±6	151±5
Disintegration Time (min)	16±1.2	17±1.6	18±1.3	18±1.7	18±1.1
BSA content (%)	98.97±1.4	97.90±1.2	99.97±0.9	97.95±1.9	100.09±1.8
Visual inspection (discoloration and peeling)	**Pass**	**Pass**	**Pass**	**Pass**	**Pass**

Table 4.11. Stability study result of BSA-loaded aquasome tablets for hardness, disintegration time, BSA content and visual inspection. Storage condition was at 25ºC ±1ºC/60% RH ±2% RH. Values are reported as mean ± SD (n = 3).

	Day 0	Day 7	Day 14	Day 21	Day 28
Hardness	145±8	142±5	151±5	150±4	148±5
Disintegration Time (min)	16±1.5	18±1.3	18±1.0	18±1.1	18±1.5
BSA content (%)	99.97±1.2	96.69±1.6	100.80±1.4	99.55±1.2	98.59±1.7
Visual inspection (discoloration and peeling)	**Pass**	**Pass**	**Pass**	**Pass**	**Pass**

Table 4.12. Stability study result of BSA-loaded aquasome tablets for hardness, disintegration time, BSA content and visual inspection. Storage condition was at 40ºC ±1ºC/75% RH ±2% RH. Values are reported as mean ± SD (n = 3).

	Day 0	Day 7	Day 14	Day 21	Day 28
Hardness	145±8	146±6	149±6	152±4	153±4
Disintegration Time (min)	16±1.2	19±1.8	19±1.9	19±1.2	20±1.7
BSA content (%)	99.97±1.2	98.46±1.5	96.37±2.1	96.53±1.9	95.98±1.6
Visual inspection (discoloration and peeling)	**Pass**	**Pass**	**Pass**	**Pass**	**Pass**

4.4. Conclusions

BSA-loaded aquasome tablets were successfully formulated with MCC as a multifunctional excipient and talc as a lubricant. It was noticed that magnesium stearate showed physical/chemical incompatibility with aquasomes, hence it was replaced with talc. Various powder blends of varying BSA-loaded aquasomes amounts (25, 37.5, 50, 62.5 and 75% w/w) were prepared and compressed at increasing compression forces (0.5, 1, 2 and 3 tons). It was discovered that under high compression forces of 2 and 3 tons BSA was spreading out of BSA-loaded aquasomes as was evident from confocal microscopy images. BSA-loaded aquasomes tablets compressed under 1 ton of compression force was chosen for coating as it showed preferable tablet characteristics (hardness, disintegration etc.). Acrylic based coating was used to spray coat the tablets. The coated tablets were tested for *in vitro* release (2 hr at SGF pH 1.2, 1 hr at FaSIF pH 5.5 and 6 hr in FaSIF pH 7.4). The tablets were found to disintegrate in pH >5.5 and steadily release for 6 hr. Cell culture studies were conducted to demonstrate the controlled release effect of aquasomes on Caco-2 cell lines. The release of metronidazole from aquasomes after 2 hr in the permeability study started to slow gradually until it reached its highest difference at hour 6 ($p< 0.05$) when compared to the 6 hr point of metronidazole solution. The metronidazole transported across the Caco-2 monolayer was 60.92 ±3.5% after 6 hr. The stability of BSA-loaded aquasome tablets were performed in three storage conditions of 4ºC ±1ºC/60% RH ±2% RH, 25ºC ±1ºC/60% RH ±2% RH and 40ºC ±1ºC/75% RH ±2% RH. The stability result of BSA-loaded aquasome tablets showed no significant changes ($p>0.05$) in hardness, disintegration time and BSA content. In general, BSA-loaded aquasome tablets show encouraging results of *in vitro* and cell culture studies over the 6 hr release studies. Extended stability studies (>1 month) are required to reach a solid conformation about the stability of BSA-loaded aquasome tablets.

CHAPTER 5

General Discussion and Conclusions

Proteins and peptides based drugs widely exist for therapy. Owing the nature of proteins of being sensitive to various stress (pH of media, temperature etc), only a limited number has been approved by the regulatory bodies. The advances in DNA recombinant technologies have resulted in the steep increase in the proteins or peptide-based drugs to manage various illnesses. Moreover, large-scale productions of proteins or peptide-based drugs were also possible due to such advances (Umashankar *et al*., 2010; Veuillez *et al*., 2001; Meredith Et al., 2015)

The main issue with the delivery of proteins or peptide-based drugs with a suitable delivery system that preserve them from external stress remains an area of research. There are various routes for the delivery of drugs to the body such oral, pulmonary and parenteral route. However, the oral route remains the dominant route for delivery and the most preferable in terms of delivery platforms available to it (tablets, capsules and liquid based formulations). Despite such advantages, the oral rout has various disadvantages such as poor permeability of the intestinal mucosa and degradation by gastrointestinal enzymes (Aulton, 2007; Aulton and Taylor, 2013; Benjamin *et al*., 2013; Jwala *et al*., 2013). Less popular routes of delivery have also been investigated for the delivery of proteins or peptide-based drugs (nasal, buccal, vaginal and rectal routes). Interestingly, the current research for the delivery of proteins or peptide-based drugs via those routes are encouraging and promising despite the inherit limitations such as enzymatic activity, patient accebtability and dose delivery (Sharma *et al.*, 2011; Johansson *et al*., 2001; Swarbrick and Boylan, 2000; Du Plessis *et al*., 2010).

In another study, degradation of luteinizing hormone–releasing hormone in buccal, nasal, and liver tissues was reported (Mingda and Jagdish, 1998). To avoid the enzymatic activity of the oral, buccal, nasal, rectal, and vaginal routes, proteins or peptide-based drugs are administered via the parenteral route (such as intravenous and intramuscular). However, even with the administration via the parenteral route, the short duration of action and rapid clearance of proteins or peptide-based drugs remain a challenge, in addition to the structural complexity these biomolecules have.

Therefore, the need to for new delivery systems to deliver proteins or peptide-based drugs not only to preserve them from external stress, but also to sustain their duration of action where needed. Other non-proteins or peptide-based drugs factors also can affect the therapeutic action of these molecules. Such factors can include particle size, immunogenicity, biological half-life, conformational stability, rate of administration, pharmacokinetics/pharmacodynamics and dose requirement that represent an added challenge to as aspect of formulation. There is a wide range

of nanocarrier systems that are proposed for the delivery of proteins or peptide-based drugs such liposomes, polymers and carbon-based materials (Safari and Zarnigar, 2014; Umashankar *et al*., 2010; Singh et al., 2008). Recently, a new class of nanocarrier systems have been emerged, aquasomes, proposed by Nir Kossovsky. Aquasomes consist of three distinct layers; an inner solid core, a polyhydroxy carbohydrate film and a layer of the active molecule with or without modification (Kossovsky *et al.,* 1995). The unique ability of aquasomes to carry therapeutically active proteins and peptides non-covalently and it superior stability have highlighted them as potential nanocarriers for proteins and peptides (Masatoshi and Yongning, 1998; Kim and Kim, 2002; Khopade *et al*., 2002; Kossovsky *et al.,* 1995). Aquasomes preserve the conformation of molecules and their pharmacological activity. It is essential to highlight that an active molecule have the following qualities which aquasomes preserve during the delivery, a unique 3D conformation, a freedom of internal molecular rearrangement induced by molecular interactions and a freedom of bulk movement. Such preservation also extends to stress environment such as acidic/basic pH., solvents and high temperature which causes denaturation. Various core and materials are available to manufacture aquasomes, such as ceramics, gold and diamond. The current research on aquasomes highlight the system as promisable carrier in many field that are not limited to drug delivery, such as food chemistry, microbiology and solid phase synthesis. (Kossovsky *et al.,* 1995; Jain, 2001; Priyanka *et al*., 2012)

In the present study various core and coating materials were used to prepare aquasomes under different conditions to study the relationship between manufacturing conditions and BSA loading. In terms of manufacturing conditions, coating or loading times for 2.5 hrs/25^{o}C resulted in high BSA loading compared to 1 hrs/4^{o}C (*p<0.05) for the different coating and solid core materials tested. DCPA and MCPA cores were unsuitable as solid core materials for aquasomes preparation because DCPA resulted in low BSA loading efficiencies whereas MCPA formed lumps post freeze drying. HA aquasomes with trehalose as a coating material, had the highest BSA loading (7 mg/100 mg) which resulted in a sustained release of BSA over a period of 6 hours. To explore aquasomes suitability for pulmonary delivery, pMDI and DPI formulations were prepared. Both formulations showed large amounts of aquasomes deposited in stages 2, 3 and 4 of the NGI (mid-low respiratory region). The pMDI and DPI formulations also showed high disposability, which indicates low incidence of local effect. *In vitro* release studies performed with SIF showed a sustained release of BSA over a period of 6 hrs. *Ex vivo* studies were performed to demonstrate the controlled release effect of aquasomes with BEAS-2B cell lines. The release of salbutamol sulphate from aquasomes from hour 2 started to slow gradually until it reached its highest difference at hour 6 (*p<0.05). BSA-loaded aquasome tablets were formulated with MCC

as multifunctional excipient and talc as a lubricant. It was noticed that under high compression forces of 2 and 3 tons BSA was spreading out of BSA loaded aquasomes as was presented with confocal microscopy images.

To explore aquasomes suitability for oral delivery, DC tablets were prepared. Compression force of 1 ton was chosen for coating as it showed preferable tablet characteristics. Acrylic coating was used to prepare enteric coated tablets. The coated tablets were tested for *in vitro* release (2 hrs at SGF pH 1.2, 1 hrs at SIF pH 5.5 and 6 hrs in SIF pH 7.4). The tablets were found to disintegrate in pH >5.5 and steadily release BSA for 6 hours. In e*x vivo studies,* the release of metronidazole from aquasomes after 2 hours in the permeability study started to slow gradually until it reached its highest difference at hour 6 (**p*< 0.05) when compared to the 6 hrs point of control.

Docking and MD simulations performed were essential to understand the forces that govern the assembly of the three layers of the aquasomes. HA and trehalose interact by hydrogen bonding, with trehalose acting as a hydrogen acceptor, while BSA shows almost complete SAS and that there are numerous targets for trehalose attachments (no specific active site). This was further confirmed by performing docking studies, which confirms hydrogen bonding formation between HA and trehalose, and that there are 4 hydrogen bonds formed (4 per trehalose molecule per 3 HA cell units surface). Total energy analysis of BSA on the two conditions performed (300 K and 280 K) support the experimental data of lower BSA loadings of aquasomes manufactured at 4^{o}C compared to those manufactured at 25^{o}C (**p*<0.05). This could be related to the fact that BSA might have either started to denature/unfold or begin breaking up at 4^{o}C.

In order to investigate the stability of aquasomes, stability studies were performed on aquasomes tablets, pMDI and DPI formulations at storage conditions of 4^{o}C ±1^{o}C/60% RH ±2%, 25^{o}C ±1^{o}C/60% RH ±2% and 40^{o}C ±1^{o}C/75% RH ±2%. The results showed no significant changes (**p*>0.05) in BSA content or release patterns. Although the stability studies were not performed for more than 6 months, with exception of pMDI formulations, further prolonged stability studies will be required for long term assessment of aquasomes. In this study, aquasomes has been optimised in terms of manufacturing conditions, which yielded a loading of approximately 7 mg per 100 mg of aquasomes, which is higher than what is reported in the literature. Pulmonary formulation of aquasomes (pMDI and DPI) were prepared and showed an *in vitro* sustained release over a period of 6 hours whereas cell culture studies using BEAS-2B cells showed a significant difference of release at hour 6 (**p*<0.05). Similarly, oral formulations of aquasomes (directly compressed tablets) showed in *vitro* sustained release over a period of 6 hours of tablets

prepared at 1 tonne of compression force. Cell culture studies using Caco-2 cell lines showed a significant difference of release at hour 6 (*p<0.05). These results are promising and interesting, especially given the fact that aquasomes has not been investigated orally or pulmonary as nanocarriers for protein and peptides. These results as well as inherit aquasomes qualities of being biodegradable and resistance towards clearance by the reticuloendothelial system or degradation by other environmental challenges highlight the system as promising nanocarriers for proteins and peptides.

In general, aquasomes are a novel carrier for bioactive molecules that deals with the principle of self-assembly. Better biological activity can be seen even in the case of conformationally sensitive drug candidates due to the presence of the unique carbohydrate coating the ceramic. The carbohydrate prevents the destructive of drug-carrier interactions and helps to preserve the spatial qualities. The stability of structure and overall integrity is controlled by the crystalline nature of the core. This strategy may be beneficially scaled up to the novel delivery of other bioactive molecules. Aquasomes have given a new optimism for the pharmaceutical sciences to deliver bioactive molecules. Within the large pool of peptide drugs there are a considerable number of candidates with the potential for delivery via these carriers including viral antigens, haemoglobin and insulin.

References

Aditya NP, Patankar S, Madhusudhan B, Murthy RSR, Souto EB, 2012. Arthemeter- Loaded Lipid Nanoparticles Produced by Modified Thin-Film Hydration: Pharmacokinetics, Toxicological and In Vivo Anti-Malarial Activity. *European Journal of Pharmaceutical* Sciences, 40 (5), 448-455.

Ahmed S, Giazzon M, Favre M, Angeloni S, Matthey N, Liley M, 2009. Transepithelial Electrical Resistance as an Evironmental sensor. LiveSense Presentation. Available at: http://www.nano-tera.ch/pdf/posters2012/LiveSense168.pdf. [Accessed on 05 MAY 14].

Alessandra L. Poli, Tatiana Batista, Carla C. Schmitt, Fergus Gessner, Miguel G. Neumann, 2008. Effect of sonication on the particle size of montmorillonite clays. *Journal of Colloidal Sciences*, 325 (2), 386-390.

Al-Khattawi A, Iyire A, Dennison T, Dahmash E, Bailey CJ, Smith J, Rue P and Mohammed AR, 2014. Systematic Screening of Compressed ODT Excipients: Cellulosic Versus Non- Cellulosic. *Journal of Current Drug Delivery*, 11, 486-500.

Allen LV, Popovich NG, Ansel H.C, 2011. Ansel's Pharmaceutical Dosage Forms and Drug Delivery Systems. Lippincott Williams & Wilkins.

Almora-Barrios, N, de Leeuw, N H, 2010. Modelling the interaction of a Hyp-Pro-Gly peptide with hydroxyapatite surfaces in aqueous environment. *Journal of Crystengcomm*, 12 (3), 960-967.

Amin MCIM, Albawani SM, Amjad WM, 2012. A Comparative Study of the Compaction Properties of Binary and Bilayer Tablets of Direct Compression Excipients. *Journal of Pharmaceutical Research*, 11 (4), 585-594.

Ankit G, Ajay B, Kumar KM, Neetu K, 2012. Tablet Coating Technologies: Concept and Recent Trends. *International Research Journal of Pharmacy*, 3 (9), 50-58.

Ansel HC., Nicholas G. Popovich, Loyd V. Allen, 1995. Pharmaceutical Dosage Forms and Drug Delivery Systems. Williams & Wilkins.

Artursson P, Karlsson J, 1991. Correlation Between Oral Drug Absorption in Humans and Apparent Drug Permeability Coefficients in Human Intestinal Epithelial (Caco-2) Cells. *Journal of Biochemistry and Biophysical research communications*, 175(3):880-885.

Arunan E, Mani D, 2015. Dynamics of the chemical bond: inter- and intra-molecular hydrogen bond. *Journal of faraday Discussions*, 177, 51-64.

Augsburger LL., Hoag SW, 2008. Pharmaceutical Dosage Form: Tablets, Volume 1. CRC Press.

Aulton ME, Taylor KMG, 2007. Aulton's Pharmaceutics: The Design and Manufacture of Medicines. Churchil Livingstone.

Aulton ME, Wells TI, 1998. Pulmonary drug delivery; Pharmaceutics the science of dosage form design. Churchill Livingstone.

Austin LB and Pieter RC, 1997. Liposomes Fusion. *Current Topics in Membranes*, 44, 359-373.

Axelsson B, 1989. Liposomes as carriers for anti-inflammatory agents. *Advanced Drug Delivery Reviews*, 3 (3), 391-404.

Baggiolini M, Clark-Lewis I, 1992. Interleukin-8, A Chemotactic and Inflammatory Cytokine. *Journal of FEBS Letters*. 307 (1), 97–101

Bangham, AD, Horne RW, 1965. Negative Staining of Phospholipids and Their Structural Modification by Surface-Active Agents As Observed in the Electron Microscope. *Journal of Molecular Biology*, 8 (5): 660–668.

Barkay Z., Rivkin I., Margalit R., 2009. Three-Dimensional Characterization of Drug- Encapsulating Particles Using STEM Detector in FEG-SEM. *Micron*, 40 (4), 480-485.

Bauer KH, 1998. Coted Pharmaceutical Dosage Forms. CRC Press, New York, Washington, D.C., medpharm Scientific Publishers, Stuttgart.

Baumann H., Gauldie J., 1994. The acute phase response. *Immunology Today*, 15, 74-80.

Behrens I, Stenberg P, Artursson P, Kissel T, 2001. Transport of lipophilic drug molecules in a new mucus-secreting cell culture model based on HT29-MTX cells. *Journal of Pharmaceutical Research*, 18,1138–1145.

Benjamin JB, Geoffrey DM, Carol SL, 2013. Basics and recent advances in peptide and protein drug delivery. *Future Sciences*, 4 (11), 1443-1467

Bermudez O, Boltong MG, Driessens FCM, Planell JA, 1994. Development of Some Calcium Phosphate Cements from Combinations of Alpha -TCP, MCPM and Cao. *Journal of Materials Science, Materials in Medicine*, 5 (3), 160-163.

Berridge MV, Herst PM, and Tan AS, 2005. Tetrazolium dyes as tools in cell biology: new insights into their cellular reduction. *Journal of Biotechnology Annual Review*, 11, 127-152.

Bertoluzza A, Cacciari S, Tinti A, Vasina M, Morelli MA, 1995. FTIR and Raman Spectra of Bioceramics Obtained by an Innovative Method. *Journal of Material Sciences: Materials in Medicine*, 6 (2), 79-79.

Bharate SS, Bharate SB, Bajaj AN, 2010. Interactions and incompatibilities of pharmaceutical excipients with active pharmaceutical ingredients: a comprehensive review. *Journal of Excipients and Food Chemistry*, 1 (3), 3-26.

Bohner M, Lemaitre J, Ohura K, Hardouin P, 1995. Effects of Sulfate Ions on The in Vitro Properties of B-TCP - MCPM - Water Mixtures. *Preliminary in vivo results. Ceramic Transactions*, 48, 245-259.

Borchard, G, Cassará, ML, Roemelé, PEH, Florea, BI, Junginger HE, 2002. Transport and local metabolism of budesonide and fluticasone propionate in human bronchial epithelial cell line (Calu-3), *Journal of Pharmaceutical Sciences*, 91, 1561-1567.

Borges O, Borchard G, Verhoef JC, de Sousa A, Junginger HE, 2005. Preparation of coated nanoparticles for a new mucosal vaccine delivery system. *International Journal of Pharmaceutics,* 299 (1-2), 155-156.

Bose S, Bogner RH, 2007. Solventless Pharmaceutical Coating Process. Journal of *Pharmaceutical Development and Technology*, 12, 105-113.

Britanica, 2016. Van Der Waals Forces. Available at: https://www.britannica.com/science/van-der-Waals-forces. [Accessed on 22 MAR 15].

Bujacz A, 2012. Structures of bovine, equine and leporine serum albumin. *Journal of Acta Crystallogrphica section D Biological Crystallogrphica*, 68 (10), 1278-89.

Bujacz A, Zielinski K, Sekula B, 2014. Structural studies of bovine, equine, and leporine serum albumin complexes with naproxen. *Journal of Protein: structure, function and bioinformatics*, 82(9), 2199-208.

Bundenthal M, 2014. Pinpointing the source of Tablet spots and specks. *Pharmaceutical Technology*, 38 (12).

Byrn SR, Xu W and Newman AW, 2001. Chemical Reactivity in Solid-State Pharmaceuticals: Formulation Implications. *Journal of Advanced Drug Delivery Reviews*, 48(1), 115 -136

Byron PR, Cummings RH, Nichols SC, Poochikian G, Smurthwaite MJ, Stein SW, Truman KG, 2004. Election and Validation of Cascade Impactor Test Methods. *Respiratory Drug delivery*, IX, 169-178.

Cabral ECM, Zollner RL, Santana MHA, 2004. Preparation and Characterization of Liposomes Entrapping Allergenic Proteins. Brazilian. *Journal of Chemical Engineering*, 21 (02), 137-146.

Cain ML, Damman H, Lue R, Yoon CK, Morel R, 2006. Discover Biology, 3 ed. Norton & Co. and Sumanas, Inc.

Cape SP, Villa JA, Huang ETS, Yang TH, Carpenter JF, Sievers RE, 2008. Preparation of Active Proteins, Vaccines and Pharmaceuticals as Fine Powders Using Supercritical or Near-Critical Fluids. *Pharmaceutical Research*, 25, 1967-1990.

Carlin B, Augsburger LL, 2008. Pharmaceutical Dosage Forms: Tablets. Informa.

Carlin, B., 2008. Direct compression and the role of filler-binders. In: Augsburger, L. L., Hoag, S.W. (Eds.), Pharmaceutical Dosage Forms: Tablets. *Informa*, 173– 216.

Case DA, Darden TA, Cheatham TE, Simmerling CL, Wang J, Duke RE et al., 2012. AMBER 12. San Francisco: University of California.

Caygill C.P.J., Stein W.D., 1969. Binding of Insulin by Liposomes Incorporating Protein. *Journal of Life Sciences,* 8 (16), 809-812.

Ceschel GC, Badiello R, Ronchi C, Maffei P, 2003. Degradation of components in drug formulations: a comparison between HPLC and DSC methods. *Journal of Pharmaceutical and Biomedical Analysis*, 32 (4-5).

Çetin M, Vural M, ÇAPAN Y, Hincal AA, 2007. Preparation and Characterization of BSA-Loaded Alginate Microspheres. *Journal of Pharmaceutical Sciences*, 32, 103-107.

Chan KLA, Kazarian SG, 2005. Detection of Trace Materials with Fourier Transform Infrared Spectroscopy Using a Multi-Channel Detector. *The Royal Society of Chemistry*, 131, 126-131.

Chaplin M, 2015. Explanation of the Density Anomalies of Water, [Online]. Available at: http://www1.lsbu.ac.uk/water/density_anomalies.html. [Accessed on 05 MAR 15].

Cherian AK, Rana AC, Jain SK, 2000. Self-Assembled Carbohydrate-Stabilized Ceramic Nanoparticles for The Parenteral Delivery of Insulin. *Drug Delivery Indian Pharmaceuticals*, 26, 459-463.

Choi S, Lee J, Igawa K, Suzuki S, Mochizuki M, Nishimura R, Chung UI, Sasaki N, 2011. Effect of Trehalose Coating on Basic Fibroblast Growth Factor Release from Tailor- Made Bone Implants. *Journal of Veterinary Medical Sciences*, 73 (21), 1547-1552.

Choudhary S, 2014. Factors affecting design of Controlled Release Drug Delivery Systems. Available at: http://www.slideshare.net/suraj_mindgamer/factors-affecting-design-of-controlled-release-drug-delivery-systems. [Accessed on 12 APR 15].

Clark JH, 1945. The temperature coefficient of the urea denaturation of egg albumin. Journal of Gen. *Journal of Physiology*, 28, 539.

Clark T, 1985. A Handbook of Computational Chemistry. John Wiley & Sons.

Cloonan SM, Lam HC, Bhashyam AR, Haspel JA, Cervo M, Parameswaran H, Caroline A. Owen, Mahmood A, Choi AMK, 2014. The Modified Disaccharide Trehalose Reverses Cigarette Smoke-Induced COPD. *Respiratory and critical care Medicine*, B45.

Coderch L, Fonollosa J, De Pera M, Estelrich J, De La Maza A, Parra JL, 2000. Influence of Cholesterol on Liposome Fluidity by EPR. relationship with Percutaneous Absorption. *Journal of Controlled Release*, 68 (1), 85-95.

Connor J, Sullivan S, Huang L, 1985. Monoclonal Antibody and Liposomes. *Pharmaceutical Therapy*, 28, 341-365.

Cortie MB, 2004. The Weird World of Nanoscale Gold. *Gold Bulletin*, 37 (1), 12-19.

Crespi CL, Penman BW, Hu M, 1996. Development of Caco-2 Cells Expressing High Levels of cDNA-Derived Cytochrome P4503A4. *Journal of Pharmaceutical Research*, 13(11), 1635-41.

Crowe JH, Madin KAC, 1975. Anhydrobiosis in Nematodes: Evaporative Water Loss and Survival. *Journal of Experimental Zoology*, 193, 323–334.

Crowe LM, Reid DS, Crowe JH, 1996. Is Trehalose Special for Preserving Dry Biomaterials. *Biophysical Journal*, 71, 2087-2093.

Cummins CL, Mangravite LM, and Benet LZ, 2001. Characterizing the expression of CYP3A4 and efflux transporters (P-gp, MRP1, and MRP2) in CYP3A4-transfected Caco-2 cells after induction with sodium butyrate and the phorbol ester 12-O-tetradecanoylphorbol- 13-acetate. *Journal of Pharmaceutical Research*, 18, 1102-1109

Curoservice, 2015. Lung and Circulation [Online]. Available on: http://www.curoservice.com/parents_visitors/lungs_circulation/structure_alveoli.php. [Accessed on: 13 MAR 2013].

Dail DH, Hammar SP, 2013. Dail and Hammar's Pulmonary Pathology. Springer Science & Business Media.

Deangelis NJ, Papariello GJ, 2006. Differential scanning calorimetry. Advantages and limitations for absolute purity determinations. *Journal of Pharmaceutical Sciences*, 57 (11), 1868-1873.

Degim IT, Celebi N, 2007. Controlled Delivery of Peptides and Proteins. *Current Pharmaceuticals*, 13, 99-117.

Demana PH, Davies NM, Berger B, Rades T, 2004. Incorporation of Ovalbumin into Iscoms and Related Colloidal Particles Prepared by The Lipid Film Hydration Method. *International Journal of Pharmaceutics*, 278 (2), 263-274.

Denny, PJ, 2002. Compaction equations: A comparison of the Heckel and Kawakita equations. *Powder Technology*, 127, 162-172.

Deville S, Saiz, E, Tomsia AP, 2007 Ice-templated porous alumina structures. *Acta Materiala,* 55, 1965–1974.

DFE Pharma, 2014. Introduction to tableting by direct compression, [Online]. Available at: www.dfepharma.com/. [Accesssed on 14 MAR 2015].

Dixit N, Maurya SD, Sagar BPS, 2013. Sustained Release Drug Delivery System. *Indian Journal of Research in Pharmacy and Biotechnology,* 1 (3), 305-310.

Dodoo AN, Bansal SS, Barlow DJ, Bennet F, Hider RC, Lansley AB, Lawrence MJ, Marriot C, 2000. Use of alveolar cell monolayers of varying electrical resistance to measurepulmonary peptide transport. *Journal of Pharmaceutical Sciences*, 89, 223-231.

Dormant LM, Adamson AW, 1968. Physical Adsorption Behaviour of molecular Solids. *Journal of Colloidal and Interface Science*, 28 (3-4), 459-465.

Drug Topics, 2008. Overview of pharmaceutical excipients used in tablets and capsules, [Online]. Available at: http://drugtopics.modernmedicine.com/drug-topics/news/modernmedicine/modern-medicine-news/overview-pharmaceutical-excipients-used-tablets. [Accessed on: 07 JUN 2014].

Drug bank, 2013. Metronidazole, [Online]. Available at: http://www.drugbank.ca/drugs/DB00916. [Accessed on 23 MAY 15].

Drugs, 2015. Albuterol Inhalation Solution, [Online]. Available at: http://www.drugs.com/pro/albuterol-inhalation-solution.html. [Accessed on 09 MAR 15].

Du Plessis LH1, Kotzé AF, Junginger HE, 2010. Nasal and rectal delivery of insulin with chitosan and N-trimethyl chitosan chloride. *Drug Delivery*, 17 (6), 399-407.

Edwards AD, Slater NKH, 2009. Protection of Live Bacteria from Bile Acid Toxicity Using Bile Acid Adsorbing Resins. *Journal of Vaccine*, 27 (29), 3897-3903.

El-Nesr OH, Yahiya Ab, El-Gazayerly ON, 2010. Effect of Formulation Design and Freeze-Drying on Properties of Fluconazole Multilamellar Liposomes. *Saudi Pharmaceutical Journal*, 18, 217-224.

Eom HJ, Choi J, 2011. Sio2 Nanoparticles Induced Cytotoxicity by Oxidative Stress in Human Bronchial Epithelial Cell, Beas-2b. *The journal of Environmental Health Toxicology*, 26, e2011013.

Ehrhardt C, Kim KJ, 2007. Drug Absorption Studies: In Situ, In Vitro and In Silico Models. Springer Science & Business Media.

Faisal U, Ibrahim J, Rasheed S, Ranjha NM, Hussain L and Massud A, 2013. Accelerated Stability Studies of Flurbiprofen Film Coated Tablets of Five Different National Brands in Pakistan. *Journal of Drug Delivery and Therapeutics*, 3 (2), 9-11.

Felton LA, 2013. Mechanisms of Polymeric Film Formation. *Journal of Pharmaceutics*, 457, 423-427.

Fernandez E., Gil F.J., Ginebra M.P., Driessens, F.C.M. Planell J.A., Best S.M., 1999. Calcium Phosphate Bone Cements for Clinical Applications. Part I: Solution Chemistry. *Journal of Materials Science: Materials in Medicine*, 10 (3), 169-176.

Ferrieu F, Piel JP, Stehlé L, 2009. Physical surface adsorption and Molecular Surface Fractal Analysis (MFSA) detected with Spectroscopic Ellipsometry. *Applied Surface Sciences*, 256 (3), S96-S100.

Finlay WH, 2001. The mechanics of inhaled pharmaceutical aerosols. Elsevier.

Fitzpatrick S, Mc Cabe JF, Petts CR and Booth SW, 2002. Effect of Moisture On Polyvinyl-Pyrrolidone in Accelerated Stability Testing. *International Journal of Pharmaceutics*, 246 (1)

Florea BI, van der Sandt ICJ, Schrier SM, Kooiman K, Deryckere K, de Boer AG, Junginger HE, Borchard G, 2001. Evidence of P-glycoprotein mediated apical to basolateral transport of flunisolide in human broncho-tracheal epithelial cells (Calu-3). *British Journal of Pharmacology* 134, 1555-1563.

FMC, 2015. Avicel for Solid Dosage Forms, [Online]. Available at: http://www.fmcbiopolymer.com/Pharmaceutical/Home.aspx. [Accessed on 30 May 2015].

Foster K A, Avery ML, Yazdanian M, Audus KL, 2000. Characterization of the Calu-3 cell line as a tool to screen pulmonary drug delivery, *Experimental Cell Research*, 243, 359-366.

FQS, 2016. Scigress. Available at: http://www.fqs.pl/chemistry_materials_life_science/products/scigress. [Accessed on: 25 JAN 2014].

Frenkel D, Smit B, 1996. Understanding Molecular Simulation: From Algorithms to Applications.

Freund RM, 2004. The Steepest Descent Algorithm for Unconstrained Optimization and a Bisection Line-search Method, [Online]. Available at: http://ocw.mit.edu/courses/sloan-school-of-management/15-084j-nonlinear-programming-spring-2004/lecture-notes/lec5_steep_desce.pdf. [Accessed on: 20 FEB 2014].

Fujita M, Himi S, Handa T, 2010. Effects of compression and grinding on chemical stability of a benzodiazepine receptor agonist. *Journal of Chemical and Pharmaceutical Bulletin*, 58(1):51-5

Furlong RJ, Osborn JF, 1991. Fixation of hip prostheses by hydroxyapatite ceramic coatings. *The Journal of bone and joint surgery British volume*, 73 (5), 741-745.

Chien Y.W., (1992), Novel drug delivery systems, In Swarbrick J. ed. Oral drug delivery and delivery systems. NewYork, Marcel Dekker., 139-196.

Gale JD, Faraday JCS 1997. GULP - a computer program for the symmetry adapted simulation of solids. *Journal of Translation*, 93, 629

Gancia E, Montana JG, Manallack DT, 2001. Theoretical Hydrogen Bounding Parameters for Drug Design. *Journal of Molecular Graphics and Modelling*, 19 (3-4), 349- 362.

Gangwar M, Singh R, Goel RK, Nath G, 2012. Recent advances in various emerging vescicular systems: An overview. S1176-S1188.

Garret A. FitzGerald, 2012. Drug Resistance and Pseudoresistance: An Unintended Consequence of Enteric Coating Aspirin. *Journal of circulation*, 112.117283.

Gbureck U, Dembski S, Thull R, Barralet JE, 2005. Factors Influencing Calcium Phosphate Cement Shelflife. *Journal of Biomaterials*, 26 (17), 3691-3697.

Geissler A, Haun F, Frank DO, 2013. Apoptosis induced by the fungal pathogen gliotoxin requires a triple phosphorylation of Bim by JNK. *Cell Death and Differentiation*, 20 (10),1317-1329.

Gelamo EL, Itri R, Alonso A, da Silva JV, Tabak M, 2004. Small-angle X-ray scattering and electron paramagnetic resonance study of the interaction of bovine serum albumin with ionic surfactants. *Journal of Colloid Interface*, 277 (2), 471-82.

Gelamo EL, Tabak M, 2000. Spectroscopic studies on the interaction of bovine (BSA) and human (HSA) serum albumins with ionic surfactants. *Journal of Spectrochim Acta and Molecular Biomolecular Spectroscopy*, 56A (11), 2255-71.

Gelin BR and Karplus M, 1977. Mechanism of tertiary structural change in hemoglobin. *The Proceedings of the National Academy of Sciences*, 74, 801-805.

Gharsallaoui A, Roge B, Mathlouthi M, 2008. Water–Disaccharides Interactions in Saturated Solution and The Crystallisation Conditions. *Food Chemistry*, 106, 1329-1339.

Gohel M, Jogan P, 2005. A review of co-processed directly compressible excipients. *Journal of Pharmacy and Pharmaceutical Sciences*, 8(1):76-93.

Gothoskar AV, 2016. Drug Delivery Systems.

Goyal P, Goyal K, Gurusamy S, Kumar V, Singh A, Katare O, Mishra DN, 2005. Liposomal Drug Delivery Systems – Clinical Applications. Acta Pharmacieutica, 55, 1-25.

Grosser T, Fries S, Lawson JA, Kapoor SC, Grant GR, FitzGerald GA, 2012. Drug Resistance and Pseudoresistance: An Unintended Consequence of Enteric Coating Aspirin. *Journal of Circulation*, 127(3):377-385.

Gullberg E, Leonard M, Karlsson J, Hopkins AM, Brayden D, Baird AW, Artursson P,2001. Expression of Specific Markers and Particle Transport in a New Human Intestinal M-Cell. *Journal of Biochemical and Biophysical Research Communications*, 281, 1063.

Guo HX, Heinämäki J, Yliruusi J, 1999. Characterization of particle deformation during compression measured by confocal laser scanning microscopy. *International Journal of Pharmaceutics*, 186(2):99-108.

Guo N, Puhlev I, Brown DR, Mansbridge J, Levine F, 2000. Trehalose expression confers desiccation tolerance on human cells. *Nature Biote*[Accessed on 26 May 2012].*chnology*, 18 (2),168-171.

Hamilton KO, Backström G, Yazdanian MA, Audus KL, 2001a. P-glycoprotein efflux pump expression and activity in Calu-3 cells. *Journal of Pharmaceutical Sciences*, 90, 647-658.

Hamilton KO, Yazdanian MA, Audus KL, 2001b. Modulation of P-glycoprotein activity in Calu-3 cells using steroids and β-ligands, *International Journal of Pharmacology*, 28, 171-179.

He Q, Micheal A, Morcol T, Bell SJD, 2000. Calcium Phosphate Nanoparticles Induce Mucosal Immunity and Protection against Herpes Simplex Virus Type 2. *Clinical and Vaccine Immunology*, 9 (5), 1021-1024.

He Q, Mitchell AR, Johnson SL, Bartak CW, Morcol T, Bell SJD, 2000. Calcium phosphate nanoparticle adjuvant. *Clin. Diagn. Lab. Immunology*, 7(6), 899–903.

He X, Gao L, Ma N, 2013. One-Step Instant Synthesis of Protein-Conjugated Quantum Dots at Room Temperature. *Journal of Scientific Reports*, 3, 2825.

Health, Medicine and Anatomy Reference Pictures, 2013. Available at: http://healthfavo.com. [Accessed on 14 APR 16].

Heckel RW, 1961. Density-pressure relationships in powder compaction. Trans. Metall. Soc. AIME., 221, 671-675.

Hickey AJ 1996. Inhalation Aerosols, Physical and Biological Basis for Therapy, Marcel Dekker.

Hidalgo IJ *et al*., 1989. Characterization of the human colon carcinoma cell line (Caco-2) as a model system for intestinal epithelial permeability. *Gastroenterology*, 96 (3), 736-749.

Hirnle P, Schubert R, 1990. Liposomes Containing Blue Dye for Preoperative Lymph Node Staining: Distribution and Stability in Dogs After Ndolymphatic Injection. *International Journal of Pharmaceuticals,* 72 (3), 259-269.

HMBD, 2016. Cellobiose. Available at: http://www.hmdb.ca/metabolites/HMDB00055. [Accessed on 06 Jun 2012].

Hopkins FG, 1930. Denaturation of proteins by urea and related substances. *Journal of Nature*, 126, 328-330.

Horiba, 2005. Zeta Potential of Bovine Serum Albumin (Bsa) Protein, [Online]. Available at: http://www.horiba.com. [Accessed on 26 May 2012].

HPA, 2016. Trans-epithelial electrical resistance (TEER) measurements of CACO-2 cells. Available at: http://www.phe-culturecollections.org.uk/media/54714/TEER_measurements_CACO-2.pdf. [Accessed on 20 JUN 2016].

Huang W, Shi Y, Wang C, Yu K, Sun F and Li Y, 2013. Using Spray-Dried Lactose Monohydrate in Wet Granulation Method for A Low-Dose Oral Formulation of a Paliperidone Derivative. *Journal of Powder Technology*, 246, 379-394.

Ignjatović N, Ajduković Z, Najman SV, Mihailović D, Vasiljević P, Stojanović Z, Uskoković V and Uskoković D, 2013. Nanoparticles of cobalt-substituted hydroxyapatite in regeneration of mandibular osteoporotic bones. *Journal of Material Sciences Materials Medical*, 24(2): 343–354.

Inchem, 2016. Who Food Additives Series 46: Trehalose. Available at http://www.inchem.org/documents/jecfa/jecmono/v46je05.htm. [Accessed on 26 May 2016].

Ingels FM, Augustijns PF, 2003. Biological, Pharmaceutical and Analytical Considerations with Respect to Transport Media Used in the Absorption Screening System, Caco-2. *Journal of Pharmaceutical Sciences*, 92, 1545-1558.

Inner Body, 2016. Respiratory System. Available at: http://www.innerbody.com/anatomy/respiratory. [Accessed on 14 MAR 16].

Inner Body, 2016. Small Intestine. Available at: http://www.innerbody.com/image_digeov/dige10-new3.html. [Accessed on 20 MAR 16].

Israelachvili J, Marra J, 2003. Direct Methods for Measuring Conformational Water Forces (Hydration Forces) Between Membrane and Other Surfaces. *Methods in Enzymology*,127, 353-360.

Jain NK, Umamaheshwari RB, 2006. Control and Novel Drug Delivery Systems. New Delhi: CBS Publishers & Distributors.

Jain SS, Jagtap PS, Dand NM, Jadhav KR, Kadam VJ, 2012. AQUASOMES: A Novel Drug Carrier. Journal of *Applied Pharmaceutical Sciences*, 2 (1), 184-192.

Jensen F, 1999. Introduction to Computational Chemistry, J. Wiley & Sons.

Jitendra, Sharma PK, Bansal S, Banik A, 2011. Noninvasive Routes of Proteins and Peptides Drug Delivery. *Indian Journal of Pharmaceutical Sciences*, 73 (4), 367-375.

Joiris E, Martino PD, Berneron, C, Guyot-Hermann A. and Guyot. JC, 1998. Compression Behaviour of Orthorhombic Paracetamol. *Journal of Pharmaceutical Research*, 15, 1122- 1130.

Johansson E-L, Wassén L, Holmgren J, Jertborn M, Rudin A, 2001. Nasal and Vaginal Vaccinations Have Differential Effects on Antibody Responses in Vaginal and Cervical Secretions in Humans. *Clements JD, ed. Infection and Immunity*, 69 (12), 7481-7486.

Jun JY, Nguyen HH, Paik SY, Chun HS, Kang BC, Ko S, 2011. Preparation of Size- Controlled Bovine Serum Albumin (BSA) Nanoparticles by A Modified Desolvation Method. *Food chemistry*, 127 (4), 1892-1898.

Jwala R, Aswani DV, Ashaben P, Sai HSB, Ashim KM, 2013. Approaches for Enhancing Oral Bioavailability of Peptides and Proteins. *International Journal of Pharmaceutics*, 447 (0), 75-93

Kalita SJ, Bhardwaj A, Bhatt HA, 2007. Nanocrystalline Calcium Phosphate Ceramics in Biomedical Engineering. *Materials Science and Engineering*, 27 (3), 441-449.

Kamal AF, Iskandriati D, Dilogo IH., Siregar NC, Hutagalung EU, Susworo R, Yusuf AA, Bachtiar A, 2013. Biocompatibility of various hydoxyapatite scaffolds evaluated by proliferation of rat's bone marrow mesenchymal stem cells: an *in vitro* study. *Medical Journal of Indonesia*, 22 (4).

Kamps JAA, Moreselt HMW, Meiler DKF, Scherphof G, 1997. Massive Targeting of Liposomes, Surface-Modified with Anionized Albumins, To Hepatic Endothelial Cells. *Proceedings of the National Academy of Sciences*, 94, 11681-11685.

Kaneda Y, 2012. Virosome: A Novel Vector to Enable Multi-Modal Strategies for Cancer Therapy. *Advanced Drug Delivery Reviews*, 64 (8), 730-738.

Karhale AA, Chaudhari HS., Ughade PL, Baviskar DT, Jain DK, 2012. Pulmonary Drug Delivery System. *International Journal of Pharmaceutical Technology Research*, 4 (1), 293-305.

Keck C.M., 2010. Particle Size Analysis of Nanocrystals: Improved Analysis Method. *Journal of Pharmaceutical Technology,* 1 (5), 3-12.

Keenan CR, Mok JSL, Harris T, Xia Y, Salem, S Stewart AG, 2014. Bronchial epithelial cells are rendered insensitive to glucocorticoid transactivation by transforming growth factor-β1. Journal of Respiratory Research, 15, 55.

Kernéis S, Bogdanova A, Kraehenbuhl JP, Pringault E, 1997. Conversion by Peyer's patch ymphocytes of human enterocytes into M cells that transport bacteria. *Journal of Science,* 277 (5328), 949-952.

Khopade AJ, Khopade S, Jain NK, 2002. Development of Haemoglobin Aquasomes from Spherical Hydroxyapatite Cores Precipitated in The Presence of Poly (Amidoamine) Dendrimer. *Drug Delivery Indian Pharmaceuticals*, 241, 145-54.

Khan MS, Sundararajan PR, 2011. Effects of Carbon Atom Parity and Alkyl Side Chain Length on the Crystallization and Morphology of Biscarbamates, A Set of Model Compounds for Polyurethanes., *Journal of Physical Chemistry*, B. 115, 8696–8706.

Kim, I.S., Kim, S.H., 2002. Development of polymericnanoparticulate drug delivery system. In vitrocharacterization of nanoparticles based on sugar containingconjugates. *International Journal of Pharmaceutics*. 245, 67–73.

Kirby C, Clarke J, and Gregoriadis G, 1980. Effect of The Cholesterol Content of Small Unilamellar Liposomes on Their Stability in Vivo and In Vitro. *Biochemistry Journal*, 168 (2), 591-598.

Knopp M, 2013. Resolving Tableting Defects, [Online]. Available at: www.tabletscapsules.com. [Accessed on 02 APR 15].

Kobayashi H, Watanabe R, Choyke PL, 2014. Improving Conventional Enhanced Permeability and Retention (EPR) Effects; What Is the Appropriate Target?. *Theranostics*., 4 (1), 81-89.

Koleswara G.S.N., Pharm Info, 2007. [Available at: http://www.raghupharmacy.com]. Accessed on 20 APR 2013.

Kondoh H, Lleonart ME, Gil J, Wang J, Degan P, Peters G, Martinez D, Carnero A, Beach D, 2005. Glycolytic Enzymes Can Modulate Cellular Life Span. *Cancer Research*, 65 (1), 177-185.

Kornblum SS, Zoglio MA, 1967. Pharmaceutical heterogeneous systems I. Hydrolysis of Aspirin in Combination with Tablet Lubricants in an Aqueous Suspension. *Journal of Pharmaceutical Sciences*, 56, 1569-1575.

Kossovsky N, Gelman A, Sponsler E, Rajguru S, Torres M, Mena E, Ly K, Festekjian A, 1995. Preservation of surface-dependent properties of viral antigens following immobilization on particulate ceramic delivery vehicles. *J. Biomed. Mater. Res*, 29 (5), 561–573.

Kossovsky N, Bunshah RF, Gelman A, Sponsler ED, Umarjee DM, 1990. A non-denaturing solid phase pharmaceutical carrier comprised of surface modified nanocrystalline materials. *Journal of Applied Biomaterial*, 1, 289-294.

Kost J, Langer R, 2001. Responsive polymeric delivery systems. *Journal of Advances in Drug Delivery Reviews*, 46, 125-148.

Kout A, Muller H, 2009. Parameter optimization for spray coating. *Journal of Advances in Engineering Softwares*, 40 (10), 1078–1086.

Kroh LW, 1994. Caramelization in Food Beverages. *Food Chemistry*, 51, 373-379.

Kushal M, Monali M, Durgavati M, Mittal P, Umesh S, Pragna S, 2013. Oral Controlled Drug Delivery Systems: Overview. *International Journal Research of Pharmacy*, 4 (3), 70- 76.

Lagarce F and Roger E, 2011. Nanocarrier Absorption Studies with Caco 2 Cells. Nova Science.

Lan Y, Butler P, Ali S, Langley N, 2002. Influence of Process Parameters on Properties of Instant Release of Coated Tablets, [Online]. Available at: https://industries.basf.com/bin/bws/documentDownload.en.8805716896213. [Accessed on: 22 APR 2014].

Laurencin D, Almora-Barrios N, de Leeuw NH, Gervais C, Bonhomme C, Mauri F, Chrzanowski W, Knowles JC, Newport RJ, Wong A, Gan ZH, Smith ME, 2011. Magnesium incorporation into hydroxyapatite. *Journal of biomaterials*, 32 (7), 1826 - 1837

Law SL, Huang KJ, Chiang CH, 2000. Acyclovir Containing Liposmes for Potential Occular Delivery, Corneal Penetration and Absoption. *Journal of controlled Release*, 631 (1-2), 135-140.

lbert, KJ, Schafer UF, Schafers HJ, Kim KJ, Lee VHL., Lehr CM, 1999. Monolayers of human alveolar epithelial cells in primary culture for pulmonary drug delivery and transport studies. *Pharmaceutical Research*, 16, 601-608

Learoyd TP, Burrows JL, French E, Seville PC, 2008. Modified Release of Beclomethasone Dipropionate from Chitosan-based Spray-dried Respirable Powder. *Powder technology*. 2008, 187 (3), 231-238.

Learoyd, TP, Burrows JL, French E, Seville PC, 2009. Sustained delivery by leucine-modified chitosan spray-dried respirable powders. *International Journal of pharmaceutics*, 187 (3), 97-104.

Leberl M, Kratzer A, Taraseviciene-Stewart L, 2013. Tobacco smoke induced COPD/emphysema in the animal model—are we all on the same page. *Frontiers in Physiology*, ; 4, 91.

Lee H, Wu P, Lee Y, 2010. An R Package for Drug Stability Data Analysis. *Journal of Computer Methods and Programs in Biomedicine*, 100 (2), 140-148

Lee VHL, 1988. Enzymatic barrier to peptide and protein CRC *Critical review therapeutic Drug Delivery Carrier Systems*, 5, 68-97

Leech, 1996. Molecular Modelling. Pearson.

Lefort R, De Gusseme A, Willart JF, Danède F, Descamps M, 2004. State NMR and DSC Methods for Quantifying the Amorphous Content in Dosage Forms: An Application to Ball-Milling of Trehalose. *International Journal of Pharmaceutics*, 280, 209-219.

Leibovitz A, Stinson JC, McCombs WB 3rd, McCoy CE, Mazur KC, Mabry ND, 1976. Classification of human colorectal adenocarcinoma cell lines. *Cancer Research,* 36 (12), 4562-4569.

Lenzer J, 2006. Inhaled insulin is approved in Europe and United States. *British Medical Journal*, 332, 21.

Li CL, Martini LG, Ford JL and Roberts M, 205. The Use of Hypromellose in Oral Drug Delivery. *Journal of Pharmacy and Pharmacology*, 57 (5):533-46.

Lin YH, Sonaje K, Lin KM, Juang JH, Mi FL, Yang HW, Sung HW. 2008. Multi-ion- crosslinked nanoparticles with pH-responsive characteristics for oral delivery of protein drugs. *Journal of Controlled Release*, 132, 141–149

Lipworth BJ, Clark DJ, 1997. Effects of Airway Calibre On Lung Delivery of Nebulised Salbutamol. *Journal of Thorax*, 52 (12), 1036-1039.

Lipworth BJ, Clark DJ, Lung, 2007. Delivery of Non-CFC Salbutamol Via Small Volume Metal Spacer and Large Volume Plastic Spacer Devices Compared with an Open Vent Jet Nebulizer. *British Journal of Pharmacology*, 45 (2), 160-163.

Luo D, Han E, Belcheva N, Saltzman, 2004. A self-assembled, modular DNA delivery system mediated by silica nanoparticles. *Journal of Controled Release*, 95, 333-41.

Lyklema J., 1995. Fundamentals of Interface and Colloid Science. Academic Press.

Maher PG, Fenelon MA, Zhou Y, Kamrul Haque M, Roos YH, 2011. Optimization of B- Casein Stabilized Nanoemulsions Using Experimental Mixture Design. *Journal of Food Science*, 76 (8), 1108-1117.

Majorek KA, Porebski P J, Dayal A, Zimmerman MD, Jablonska K, Stewart AJ, Chruszcz M, Minor W, 2012. Structural and immunologic characterization of bovine, horse, and rabbit serum albumins. *Journal of molecular immunology*, 52 (3-4), 174-82.

Malvern, 2005. Protein-Polyelectrolyte Complexes and The Characterisation of Protein-Polyelectrolyre Complexes Using The Malvern Zetasizer ZS. Available at: http://www.azonano.com/article.aspx?ArticleID=1236. [Accessed on 01 May 2012].

Mani, S, Tabil LG, Sokhansanj S, 2004. Evaluation of compaction equations applied to four biomass species. *Canadian Biosystems Engineering/Le génie des biosystèmes au Canada*, 46, 3.55- 3.61.

Marakanam SU, Rajesh KS, 2010. Aquasomes as a Promising Carrier for Proteins and Peptides Delivery. *Nanomedicine*, 6 (3), 419-426

Marple VA, Olson BA, Santhanakrishnan K, Mitchell JP, Murray S, Hudson-Curtis B. Next Generation Pharmaceutical Impactor, Part II: Calibration. *Journal of Aerosol Medicine*, 16, 301-324.

Marques MRC, Loebenberg R, and Almukainzi M, 2011. Simulated Biological Fluids with Possible Application in Dissolution Testing. *Journal of Dissolution Technologies*, 15-28.

Masatoshi, I., Yongning, Z., 1998. Influence of saccharides on thestabilization of frozen hemeprotein. *Journal of Chemistry Abstract*, 45, 539–544.

Massoud A and Bauer KH, 1989. Auswahl and dence of Bridging of Intagilations on Film Coated Tablets. *Journal of Pharmacology*, 33, 174-175.

Mathias, NR, Timoszyk J, Stetsko PI, Megil l, JR, Smith RL,Wall DA, 2002. Permeability characteristics of calu-3 human bronchial epithelial cells: in vitro-in vivo correlation to predict lung absorption in rats. *Journal of Drug Target*, 10 (1), 31-40.

Mathoera RB, KoK DJ, Verduin CM, Nijman RJM, 2002. Pathological and Therapeutic Significance of Cellular Invasion by Proteus mirabilis in an Enterocystoplasty Infection Stonne Model. *Journal of Infection and Immunity*, 70 (12), 7022-7032.

Matsukawa Y, Lee VHL, Crandall ED, Kim KJ, 1997. Size-dependent dextran transport across rat alveolar epithelial cell monolayers, *Journal Pharmaceutical Sciences*, 86, 305-309.

Matsukawa, Y, Yamahara H, Lee VHL., Crandall ED, Kim KJ, 1996. Horseradish peroxidase transport across rat alveolar epithelial cell monolayers. *Pharmaceutical Research*, 13, 1331-1335.

Matsunaga Y, Bando N, Yuasa H, Kanaya Y, 1994. Effects of compression pressure on physical and chemical stability of tablets containing an anticancer drug TAT-59. *Journal of Chemical and Pharmaceutical Bulletin*, 42(12):2582-7.

Maurer N, Fenske D, Cullis, P, 2001. Development in Liposomal Drug Delivery Systems. *Emerging Biotherapeutic Technologies*, 1 (16), 923-947.

McCormick D, 2005. Evolutions in direct compression. *Journal of Pharmaceutical Technology*, 52–65.

Meena R, Kessari K, 2012. Effect of Hydroxyapatite Nanoparticles On Proliferation and Apoptosis of Human Breast Cells (MCF-7). *Journal of Nanoparticle Research*, 14, 712.

Menor, 2008. Modelling and analysing the backbone of biomolecules.

Meredith ME, Salameh TS, Banks WA, 2015. Intranasal Delivery of Proteins and Peptides in the Treatment of Neurodegenerative Diseases. *AAPSJ*, 17 (4), 780-787.

Merkus GH, 2009. Particle Size Measurements: Fundamentals, Practise, Quality. *Springer*, 383-385.

Mi FL, Wu YY, Lin YH, Sonaje K, Ho YC, Chen CT, Juang JH, Sung HW, 2008. Oral delivery of peptide drugs using nanoparticles self-assembled by poly (γ-glutamic acid) and a chitosan derivative functionalized by trimethylation. *Journal of Bioconjugicate. Chemistry*, 19, 1248–1255.

Miller DP, de Pablo JJ, Corti H, 1997. Thermophysical Properties of Trehalose and Its Concentrated Aqueous Solutions. *Pharmaceutical Research*, 14 (5), 578-590.

Miller FA, Wilkins CH, 1952. Infrared Spectra and Characteristic Frequencies of Inorganic Ions. Analytical Chemistery, 24 (8), 1253-1249.

Miller TA, York P, 1988. Pharmaceutical Tablet Lubrication. *International Journal of Pharmaceutics*. 41, 1-19.

Mingda Bi, Jagdish S, 1998. Degradation of luteinizing hormone releasing hormone in buccal, liver, nasal and skin tissues, *International Journal of Pharmaceutics*, 175 (2), 269-273.

Mitchel J, Newman S, Chan HK, 2007. In Vitro and In Vivo Aspects of Cascade Impactor Tests and Inhaler Performance: A Review. *Journal of AAPS Pharmaceutical Sciences Technology*, 8 (4), 237-248.

Mitchell J, Newman S, Chan H-K 2007. In vitro and in vivo aspects of cascade impactor tests and inhaler performance: A review. *AAPS Pharmaceutical Scientists Technology*, 8 (4), 237-248.

Miyazaki T, Sivaprakasam K, Tantry J, Suryanarayanan R, 2009. Physical Characterization of Dibasic Calcium Phosphate Dihydrate and Anhydrate. *Journal of pharmaceutical sciences,* 98 (3), 905-916.

Moghimi SM, Hamad I, 2008. Liposome-Mediated Triggering of Complement Cascade. Journal of *Liposome Research*, 18, 195-209.

Morimoto K, Yamahara H, Lee VH, Kim KJ 1993. Dipeptide transport across rat alveolar epithelial cell monolayers. *Pharmaceutical Research,* 10, 1668-1674.

Morin D, 2015. Introduction to quantum mechanics.

Naito M, Nakahira K, Hotta T, Ito A, Yokoyama T, Kamiya H, 1997. Microscopic analysis on The Conation Process Granules Beds. *Powder Technology*, 95 (3), 214-219.

Newman SP, 2005. Principles of MeteredDose Inhaler Design. Respiratory care, 50 (9), 1177-1190.

Nickerson TA, 1979. Lactose Chemistry. *Journal of Food and Agriculture Chemistry*, 27, 672-677.

Nicklasson F1, Johansson B, Alderborn G, 1999. Tabletting Behaviour of Pellets of a Series of Porosities--A Comparisonbetween Pellets of Two Different Compositions. European *Journal of Pharmaceutical Sciences*, 8 (1), 11-7.

Nojima, H, Hon-nami, K, Oshima, T, and Noda, H, 1987. Reversible thermal unfolding of thermostable cytochrome c-552. *Journal of Molecular Biology*, 122, 33.

Nokhodchi A, 2005. Effect of Moisture on Compaction and Compression. *Pharmaceutical Technology*, 29 (1), 46-66.

Nokhodchi A, Raja S, Patel P, Asare-Addo K, 2012. The Role of Oral Controlled Release Matrix Tablets in Drug Delivery Systems. *BioImpacts, BI*.2 (4), 175-187.

Nounou MM., El-Khordagui LK., Khalafallah NA., Khalil SA., 2006. In Vitro release of Hydrophilic and Hydrophobic Drugs from Liposomal Dispersions and Gels. *Acta Pharmaceutica*, 56, 311-324.

Nouri E, Shahmiri M, Rezaie HR, Talayian F, 2012. A comparative study of heat treatment temperature influence on the thickness of zirconia sol–gel thin films by three different techniques: SWE, SEM and AFM. *Surface and Coatings Technology*, 19, 3809-3815.

Ochekpe NA, Olorunfemi PO, Ngwuluka NC, 2009. Nanotechnology and Drug Delivery Part 1: Background and Applications. *Tropical Journal of Pharmaceutical Research,* 8 (3), 265-274.

Ohwoavworhua FO and Adelakun TA, 2010. Non-wood Fibre Production of Microcrystalline Cellulose from Sorghum caudatum: Characterisation and Tableting Properties. Indian *Journal of Pharmaceutics*, 72(3): 295–301.

Onoue S, Hashimoto H, Yamada S, 2008. Dry Powder Inhalation Systems for Pulmonary Delivery of Therapeutic Peptides and Proteins. *Journal of Expert Opinion on Therapeutic Patents*, 18 (4), 429-442.

Osborne M.P., Richardson V.J., Jeyasing K., Ryman B.E., 1979. Radionuclide-Labelled Liposomes—A New Lymph Node Imaging Agent. *International Journal of Nuclear medicine and Biology*, 6 (2), 75-83.

Oviedo RI, Lopez SAD., Gasga RJ, Barreda CTQ, 2007. Elaboration and structural analysis of aquasomes loaded with indomethacin. *European Journal of Pharmaceutical Sciences*, 32, 223-230.

Pai PNS, Rao GK, Murthy MS, Agarwal A, Puranik S, 2009. Simultaneous Determination of Salbutamol Sulphate and Bromhexine Hydrochloride in Tablets by Reverse Phase Liquid Chromatography. *Indian Journal of Pharmaceutical Sciences*, 71(1), 53-55.

Parmer J, Rane M, 2009. Tablet formulation Design and Manufacture: Oral Immediate Release Application. *Journal of Pharmaceutical Times*, 41 (4), 21-24.

Patel SR, Patel PR, Vora CN, Patel ND, Patel JK, 2010. Formulation, Process Parameters Optimization and Evaluation of Delayed Release Tablets of Rabeprazole Sodium. *Journal of Pharmacy and Pharmaceutical Sciences*, 2 (3), 144-156.

Patel HM, 1992. Serum Opsonins and Liposomes: Their Interaction and Opsonophagocytosis: Critical Review in Therapeutic. *Drug Carrier Systems*, 9, 39-90.

Patil JS, Sarasija S, 2012. Pulmonary drug delivery strategies: A concise, systematic review. *Lung India : Official Organ of Indian Chest Society*, 29 (1), 44-49.

Patil S, Pancholli SS, Agrawal S, Agrawal GP, 2004. Surface-modified mesoporous ceramics as delivery vehicle for haemoglobin. *Drug Delivery*, 11, 193- 199.

Patton JS, Byron PR, 2007. Inhaling Medicines: Delivering Drugs to the Body Through Lungs. Nature Reviews Drug Discovery, 6, 67-74.

Paul W, Sharma CP, 2001. Porous Hydroxyapatite Nanoparticles for Intestinal Delivery of Insulin. *Trends in Biomaterials and Artificial Organs*, 14, 37-38.

Paulsen RL and Ornstein MD, 1993. Substrate Mobility in the Thiocamphor-bound cytochrome P450: An explanation of the Conflict Between the Observed Product Profile and the X-ray Structure. *Journal of Protein Engineering*, 6, 359-365.

Pavelic´ ZS, kalko-Basnet N, Jalsˇenjak I, 1999. Liposomescontaining drugs for treatment of vaginal infections. *Eurpoian Journal of Pharmaceutical Sciences*, 8, 345–351.

Pensak D A, 1989. Pure and Applied Chemistry.

Pereira DIA, Mergler BI, Faria N, Bruggraber SFA, Aslam MF, Poots LK, *et al*. (2013) Caco-2 Cell Acquisition of Dietary Iron(III) Invokes a Nanoparticulate Endocytic Pathway. *PLoS ONE,* 8 (11), e81250.

Peroos S, Du Z M., Leeuw N H., 2006. A computer modelling study of the uptake, structure and distribution of carbonate defects in hydroxy-apatite. *Journal of biomaterials*, 27 (9), 2150 - 2161.

Peroosa, Dub Z, Nora HDL, 2005. A computer modelling study of the uptake, structure and distribution of carbonate defects in hydroxy-apatite. *Biomaterials*, 27, 2150-2161.

Pezron I, Mitra R, Pal D, Mitra AK, 2002. Insulin aggregation and asymmetric transport cross human bronchial epithelial cell monolayers (Calu-3), *Journal Pharmaceutical Sciences,* 91, 1135-1146.

Pharm Tips, 2011. Manufacturer Translations. Available at: http://pharmatips.doyouknow.in/Articles/Pharmaceutics/Tablet/Introduction-Of-Tablet-Manufacturing-Process.aspx. [Accessed on 12 APR 15].

Pharmaceutical Formulations, [Online]. Available at: http://www.azonano.com/article.aspx?ArticleID=1234. [Accessed on 25 may 2012].

Philschatz, 2016. Anatomy and Physiology. Available at: http://philschatz.com/anatomy-book/. [Accessed on 12 APR 15].

Picker, KM, 2002. Influence of tableting on the enzymatic activity of different α-amylases using various excipients. *European Journal of Pharmaceutics and Biopharmaceutics,* 53 (2), 181-185.

Pidgeon C, Apostol G, Malkovich R, 1989. Fourier Transform Infrared Assay of liposomal Lipids. *Journal of Analytical Biochemistry,* 181 (1), 28-32.

Pillai O, Nair V, Panchagnula R., 2004. Transdermal Iontophoresis of Insulin: Influence of Chemical Enhancers. *International Journal of Pharmaceutics*, 269, 109-120.

Pontiroli AE, 1990. Intranasal Administration of Calcitonin and of Other Peptides: Studies with Different Promoters. *Journal of Controlled Release*, 13, 247-251.

Porter SC, 1980. The effect of additives on the properties of an aqueous film coating. *Pharmaceutical Technology*, 67-75.

Prausnitz MR, 2004. Microneedles for Transdermal Drug Delivery. *Advance Drug Delivery Review*, 56, 581-587.

Priyanka R, Shipra D, Gaurav S, 2012. Aquasomes: A Promising Nanobiopharmaceutical Drug Delivery System for Proteins and Peptides. *International Journal of Pharmacy and Technology*, 4 (1), 1875-1888

Protean M., 2010. Determine protein three-dimensional structure. [photograph] (Martin- Protean LLC).

Rabe K.F, Atienza T, Magyar P, Larsson P, Jorup C, Lalloo UG, 2006. Effect of budesonide in combination with formoterol for reliever therapy in asthma exacerbations: a randomised controlled, double-blind study. *Lancet*, 368 (9537), 744- 753.

Ramberger R, Burgrer A, 1985. On the application of the Heckel and Kawakita equations to powder compaction. *Powder Technology*, 43 (1), 1-9.

Ramteke KH, Gunjal SS, Sharma YP, 2012. Formulation and Quality Control of Metered Dose Inhaler: A Review.*Journal of Pharmaceutical and Scientific Innovation,* 1 (2), 44-49.

Ranaldi G, Consalvo R, Sambuy Y, Scarino ML, 2003. Permeability characteristics of parental and clonal human intestinal Caco-2 cell lines differentiated in serum-supplemented and serum-free media. *Toxicology In Vitro*, 17(5-6):761-7.

Rasenack KN, Muller BW, 2004. Micron-size drug particles: common and novel micronization techniques. *Pharmaceutical Development and Technology*, 9, 1-13.

Ravi SP, Satish S, MS, Sudheesha JM, Manoj K, Vinod KD, 2011. *Internet Imunopharm*, 11 (8), 925-931.

Rawat M, Singh D, Saraf S, Saraf S, 2008. Development and in Vitro Evaluation of Alginate Gel-Encapsulated, Chitosan-Coated Ceramic Nanocores for Oral Delivery of Enzyme. *Drug Delivery Indian Pharmaceuticals*, 34, 181-188.

Reddel RR, De Silva R, Duncan EL, Rogan EM, Whitaker NJ, Zahra DG, Ke Y, McMenamin MG, Gerwin BI, Harris CC, 1995. SV40-Induced Immortalization and Ras- Transformation of Human Bronchial Epithelial Cells. *International Journal of Cancer*, 61 (2), 199- 205.

Rey C, Combes C, Drouet C, Grossin D, 2011. Bioactive Ceramics: Physical Chemistry. *Comprehensive Biomaterial,* 1, 187–281

Riaz M, 1996. Liposomes Preparation Methods. *Pakistan Journal of Pharmaceutical Sciences*, 19 (1), 65-77.

Richardson, JS, 1981. Anatomy and Taxonomy of Protein Structures. *Journal of Advances in Protein Chemistry*, 34, 167–339.

Richon LB, 1994. An Introduction to Molecular Modeling. *Mathematech*, 1, 83.

Roger RR, Ke Y, Gerwin BI, McMenamin MG, Lechner FJ, Su RT, Brash DE, Park JB, Rhim JS, Harris CC, 1988. Transformation of Human Bronchial Epithelial Cells by Infection with SV40 or Adenovirus-12 SV40 Hybrid Virus, or Transfection via Strontium Phosphate Coprecipitation with a Plasmid Containing SV40 Early Region Genes. *Cancer Research*, 48, 1904-1909.

Rokicki W, Rokicki M, Wojtacha J, Dżeljijli A, 2016. The role and importance of club cells (Clara cells) in the pathogenesis of some respiratory diseases. *Kardiochirurgia i Torakochirurgia Polska = Polish Journal of Cardio-Thoracic Surgery*, 13 (1), 26-30.

Rowe RC, Sheskey PJ, Quin ME, 2012. Handbook of Pharmaceutical Excipients, 7ed. London Pharmaceutical Press.

Roy J, 2011. Introduction to Pharmaceutical Sciences. Woodhead Publishing.

Rujivipat, S, Bodmeier R., 2010. Modified release from hydroxypropyl methylcellulose compression-coated tablets. *Journal of Pharmaceutics*, 402, 72-77.

Rytting E, Bur M, Cartier R, Bouyssou T, Wang X, Krüger M, Lehr CM, Kissel T, 2010. In Vitro and in Vivo Performance of Biocompatible Negatively-Charged Salbutamol-Loaded Nanoparticles. *Journal of Controlled Release*, 141 (1), 101-107.

SADC, 2014. Guideline For Stability Testing, [Online]. Available at: www.ema.europa.eu. [Acessed in 25 FEB 2014].

Safari J, Zarnegar Z, 2014. Advanced drug delivery systems: Nanotechnology of health design A review. *Journal of Saudi Chemical Sociaty*, 18 (2), 85-99.

Saha, P, Kim KJ, Yamahara H, Crandall ED, Lee VHL, 1994. Transport of Beta-blockers across Alveolar Epithelial Cell Monolayers. *Journal of Controlled Release*, 32, 191-200.

Sakuma S, Suzuki N, Kikuchi H, Hiwatari KI, Arikawa K, Kishida A, Akashi M, 1997. Oral peptide delivery using nanoparticles composed of novel graft copolymers having hydrophobic backbone and hydrophilic branches. *Journal of International Pharmaceutics*, 149, 93–106.

Sakurai M, 2009. Biological Functions of Trehalose as a Substitute for Water. *SpringerLink*, 229-235.

Samuni AM, Lipman A, Barenholz Y, 1999. Damage to Liposomal Lipids: Protection by Antioxidants and Cholesterol-Mediated Dehydration. Jo*urnal of Chemistry and Physics of Lipids*, 105, 121-134.

Sánchez FJC, 1999. Introduction to molecular modelling.

Sanchez R and Sali A, 1999. A Database of Competitive Protein Structure Models. Bioinformatics, 15 (12), 1060-1061.

Sarode AL, Obara S, Tanno FK, Sandhu H, Iyer R, Shah N, 2014. Stability Assessment of Hypromellose Acetate Succinate (HPMCAS) NF for Application in Hot Melt Extrusion (HME). *Journal of Carbohydrate Polymers*, 30;101:146-53.

Scherphof G, Roerdink F, Waite M, Parks J, 1987. Disintegration of Phosphatidylcholine Liposomes in Plasma as a Result of Interaction with High-Density Lipoproteins. *Biochimica et Biophysica Acta*, 542, 296-307.

Schlichter J, Friedrich J, Herenyi L, Fidy J, 2001. Trehalose Effect on Low Temperature Protein Dynamics: Fluctuation and Relaxation Phenomena. *Biophysical Journal*, 80 (4), 2011-2017.

Schroeder A, Kost J, Barenholz Y, 2009. Ultrasound, Liposomes, and Drug Delivery: Principles for Using Ultrasound to Control the Release of Drugs from Liposomes. Chemistry and Physics of Lipids, 162, (1-2), 1-16.

Scott BR, 2016. How Particles Deposit in the Respiratory Tract. Available at: http://www.radiation-scott.org/deposition/particles.htm. [Accessed on 05 FEB 15].

Semple SC, Chonn A, Cullis P, 1998. Interactions of Liposomes and Lipid-Basedcarrier systems with blood proteins: Relation to clearance behaviour in vivo. *Advanced Drug Delivery Reviews*, 32 (1-2), 3-17.

Semple SC, Chonn A, Cullis PR, 1996. Influence of Cholesterol on The Association of Plasma Proteins with Liposomes. Journal of *Biochemistry*, 35, 2521-2525.

Senese F, 2010. What are van der Waals forces, [Online]. Available at: http://antoine.frostburg.edu/chem/senese/101/liquids/faq/h-bonding-vs-london-forces.shtml. [Accessed on 21 FEB 15].

Shaikh S, Nazim S, Khan T, Shaikh A, Zameeruddi M, Quazi A, 2010. Recent Advances In Pulmonary Drug Delivery System: A Review. *Internation Journal of Applied Pharmaceutics*, 2 (4), 27-31.

Shehata T, Ogawara K, Kazutaka H, Kimura T, 2008. Prolongation of Residence Time of Liposomes by Surface-Modification with Mixture of Hydrophilic Polymers. *International Journal of Pharmaceutics*, 359 (1-2), 272–279.

Shen J, Elbert KJ, Lehr CM, Yamashita FK, KJ, Lee VHL, 1997. Cultured rabbit alveolar epithelial barrier for organic cation transport studies, Journal of *Pharmaceutical Research* 14, S-134.

Shephard EG., Joubert JR., Finkelstein MC., Kühn SH, 1981. Phagocytosis of Liposomes by Human Alveolar Macrophages. *Life Sciences*, 29 (26), 2691-2698.

Shewchuk RJ, 1994. An Introduction to the Conjugate Gradient Method Without the Agonizing Pain, 11ed.

Shlieout G, Laich T, Zessin, G, 2002. Evaluating the Elastic Behavior of Pharmaceutical Excipients. *Journal of Pharmaceutical Technology*, 14 (6), 21-28.

Shukla R, Balakrishnan M, Agarwal GP, 2000. Bovine serum albumin-hemoglobin fractionation: significance of ultrafiltration system and feed solution characteristics. *Journal of Bioseperation*, 9(1):7-19.

Sina Y, 2009. Hydroxyapatite. Available at: http://www.slideshare.net/guest13294b/hydroxyapatite-by-younes-sina. [Accessed on 21 MAR 15].

Singh R, Singh S, Lillard JW, 2008. Past, Present, and Future Technologies for Oral Delivery of Therapeutic Proteins. *Journal of pharmaceutical sciences*, 97 (7), 2497-2523.

Singh V, Alam N, Sharma M, Alam S, Ali S, Alam I, 2012. Development, Evaluation and Stability Studies of Zidovudine and Lamivudine (ZILA) Tablet Dosage Form. *Journal of Applied Pharmaceutical Sciences*, 2 (9), 149-154.

Smirnova MG, Kiselev SL, Gnuchev NV, Birchall JP, Pearson JP, 2003. Role of The Pro-Inflammatory Cytokines Tumor Necrosis Factor-Alpha, Interleukin-1 Beta, Interleukin-6 And Interleukin-8 In The Pathogenesis of the Otitis Media with Effusion". *European Journal of Cytokine Network*, 13 (2), 161-72.

Smith PL, 1997. Peptide Delivery Via the Pulmonary Routeee: A Valid Approach for Local and Systemic Delivery. *Journal of Controlled Release*, 46, 99-106.

Sonali SB, Sandip BB and Amrita NB, 2010. Interactions and Incompatibilities of Pharmaceutical Excipients with Active Pharmaceutical Ingredients: A Comprehensive Review. *Journal of Excipients and Food Chemistry*, 1 (3), 1-26.

Song NN, Zhang SY, Liu CX, 2004. Overview of Factors Affecting Oral Absorption. *Asian Journal of Drug Metabolism and Pharmacokinetics*, 4 (3), 167-176.

Song NN, Zhang SY, Liu CX, 2004. Overview of factors affecting oral drug absorption. Asian *Journal of Drug Metabolism and Pharmacokinetics*, 4 (3), 167-176.

Stahl H, 2014. A Comparison of Granulation Technologies. Available at: http://www.gea.com/en/stories/comparing-granulation-techniques.jsp. [Accessed on 20 APR 15].

Steckel H, Brandes HG, 2004. A novel spray-drying technique to produce low density particles for pulmonary delivery. *International Journal of Pharmacy*, 278, 187-195.

Steinbach PJ, 2010. Energy minimization, [Online]. Available at http://cmm.cit.nih.gov/intro_simulation/. [Accessed on 22 MAR 15].

Steinhoff G, 2013. Regenerative Medicine: From Protocol to Patient. Springer Science & Business Media.

Steward PA, Hearn J, Wilkinson MC, 2000. An Overview of Latex Film Formation and Properties. *Advances in colloid and Interface Sciences*, 86, 195-267.

Stewart CE., Torr EE, Jamili M, Bosquillon C, Sayers I, 2012. Evaluation of Differentiated Human Bronchial Epithelial Cell Culture Systems for Asthma Research. *The journal of Allergy*, ID 943982.

Stylios GK, Giannoudis PV, Wan T, 2005. Applications of nanotechnologies in medical practice. *Journal of Injury*, 36 (4), S6-S13.

Swain K, Giri M, Gupta RN, Arora VK, Saha S, 2012. Dry Powder Inhaler a Review. *Research Journal of Pharmaceutical, Biological and Chemical Sciences,* 3 (3), 1346-1356.

Swarbrick J, Boylan JC, 2000. Encyclopedia of Pharmaceutical Technology: Volume 20 - Supplement 3. CRS Press.

Szebeni J, Moghimi SM, 2009. Liposome Triggering of Innate Immune Responses: A Perspective On Benefits and Adverse Reactions. *Journal of Liposomes Research*, 19, 85- 90.

Takanobu H, 2002. Novel Functions and Applications of Trehalose. *Pure Applied Chemistry,* 74 (7): 1263–1269.

Tam E, Lhernould SM, Lambert P, Delchambre A, Delplancke-Ogletree M, 2009. Electrostatic Forces in Micromanipulation: Experimental Characterization and Simulation Including Roughness. *Applied Surface Science*, 225 (18), 7898-7904.

Tanno F, Nishiyama K, Yuichi H, Obara S, 2004. Evaluation of Hypromellose Acetate Succinate (HPMCAS) as a Carrier in Solid Dispersions. *Drug Development and Industrial Pharmacy*, 30 (1), 9-11.

Tantisripreecha C, Jaturanpinyo M, Panyarachun B, Sarisuta N, 2012. Development of delayed-release proliposomes tablets for oral protein drug delivery. *Journal of Drug Delivery and Industrial Pharmacy*, 38 (6), 718-27.

Tashtoush BM, Jacobson EL, Jacobson MK, 2008. Validation of a Simple and Rapid HPLC Method for Determination of Metronidazole in Dermatological Formulations. Drug Development and Industerial Pharmacy, 34 (8), 840-844.

Tavares FW, Bratko D, Blanch HW, Prausnitz JM, 2004. Ion-Specific Effects in The Colloid-Colloid or Protein-Protein Potential of Mean Force: Role of Salt-Macroion Van Der Waals Interactions. *Journal of Physical Chemistry*, B108, 9228–9235.

Taylor MK.; Hickey AJ, Vanort M, 2006. Pharmaceutical Delivery and Technology, 11, 321-336.

Telko MJ, Hickey A.J., 2005. Dry powder inhaler formulation. *Respiratory Care*, 50 (9), 1209-12

Tena AF, Clarà PC, 2012. Deposition of Inhaled Particles in the Lungs. *Journal of Arch Bronconeumologia*, 48, 240-6.

Thassu D, Deelers M, Pathak Y, 2008. Nanoparticulate Drug Delivery Systems. *Drug Development and Industerial Pharmacy*, 34 (1), 116.

The Medica, 2009. The US Generic Drugs Industry Overview. Available at: http://www.themedica.com/articles/2009/04/the-us-generic-drugs-industry.html. [Accessed on 22 MAR 15].

Thommes M, 2012. Physical Adsorption Characterization of Nanoporous Materials. *Chemie Ingenieur Technik*, 82 (7), 1059-1073.

Thompson C, Cheng WP, Gadad P, Skene K, Smith M, Smith G, McKinnon A and Knott R, 2011. Uptake and Transport of Novel Amphiphilic Polyelectrolyte-Insulin Nanocomplexes by Caco-2 Cells--Towards Oral Insulin. *Journal of Pharmaceutical Research*, 28 (4), 886-896.

Tortora GJ, Grabowski SR, 2003. Principles of Anatomy and Physiology.

Touesy MD, 2002. The Granulation Process: Basic Technologies for Tablet Making. *Journal of Pharmaceutical Research*, 8-13.

Learoyda TP, Burrowsc JL, Frenchb E, Seville PC, 2010. Sustained delivery of salbutamol and beclometasone from spray-dried double emulsions. *Journal of Microencapsulation: Micro and Nano Carriers,* 187 (3), 231-238.

Tuovinen LM, Peltonnen SH, Suortti TM, Crowther NJ, Elomaa MA, Järvinen KP, 2002. Enzymatic degradation of and bovine serum albumin release from starch-acetate films. *Journal of Biomacromolecules*, 3 (2), 284-290.

Tymczyszyn EE, Del Rosario Díaz M, Gómez-Zavaglia A, Disalvo EA, 2007. Volume Recovery, Surface Properties and Membrane Integrity of Lactobacillus Delbrueckii Subsp. Bulgaricus Dehydrated in The Presence of Trehalose or Sucrose. *Journal of Applied Microbiology*, 103 (6), 2410-2419.

Umashankar MS, Sachdeva RK, Gulati M, 2010. Aquasomes: a promising carrier for peptides and protein delivery. *Nanomedicine: Nanotechnology, Biology and Medicine*, 6 (3), 419 – 426.

Umrethia M, Kett VL, Andrews GP, Malcolm RK, Woolfson AD, 2010. Selection of an analytical method for evaluating bovine serum albumin concentrations in pharmaceutical polymeric formulations. *Journal of Pharmaceutical and Biomedical Analysis*, 51 (5), 1175-1179.

Vanic Z, Hafner A, Bego M, Basnet NZ, 2013. Characterization of Various Deformable Liposomes with Metronidazole. *Drug Development and Industrial Pharmacy*, 39 (3), 481- 488.

Vecellio NL, Grimbert D, Becquemin MH, Boissinot E, Le PA, Lemarié E, Diot P. Validation of laser diffraction method as a substitute for cascade impaction in the European Project for a Nebulizer Standard. *Journal of Aerosol Medicine*, 14 (1), 107-114.

Vengala P, Shwetha D, Sana A, Pekha G, Kumaraswamy P, 2012. Aquasomes: A Novel Drug Carrier System. *International Research Journal of Pharmacy*, 3 (4), 123-127.

Veuillez F, Kalia YN, Jacques Y, Deshusses J, Buri P, 2001. Factors and strategies for improving buccal absorption of peptides. *Europian Journal of Pharmaceutics and Biopharmaceutics*, 5 (12), 93-109.

Wan, HI, DiAntonio A, Fetter RD, Bergstrom K, Strauss R, Goodman CS, 2000. Highwire regulates synaptic growth in Drosophila. *Neuron* 26 (2), 313--329.

Waterman KC, Adami RC, 2005. Accelerated Aging: Prediction of Chemical Stability of Pharmaceuticals. *International Journal of Pharmaceutics*, 293 (1-2), 101-25.

Werle M, Takeuchi H., 2008. Chitosan-aprotinin coated liposomes for oral peptide delivery: Development, characterisation and in vivo evaluation. International Journal of Pharmaceutics, 370 (1-2), 26-32.

William H, Andrew D, Klaus S, 1996. VMD: Visual molecular dynamics. *Journal of Molecular Graphics,* 14 (1), 33–38

Winton, HL, Wan H, Cannell MB, Gruenert DC, Thompson PJ, Garrod DR, Stewart GA, Robinson C, 1998. Cell lines of pulmonary and non-pulmonary origin as tools to study theeffects of house dust mite proteinases on the regulation of epithelial permeability, *Clinical Experimental Allergy* 28, 1273-1285.

Wolff RK, 1998. Safety of inhaled proteins for therapeutic use. *Journal of Aerosol Medicine* 11, 197–219.

Work Z, Aarts J and Van den Mooter G, 2013. Influence of Compression forces on the Physical and Structural Stability of Solid Dispersions. Pharmaceutical Solid State Research Cluster, [Online]. Available at: http://www.pssrc.org/research-highlights/cambridge/94/influence-of-compression-forces-on-the-physical-and-structural-stability-of-solid-dispersions. [Accessed on: 11 JAN 2013].

Wormald SA, Coupland J, 2009. Particle Image Identification and Correlation Analysis in Microscopic Holographic Particle Image Velocimetry. *Optics InfoBase*, 48 (33), 4600-4607.

Xue A, 2011. Nanotechnology Funding: Corporations Grab the Reins.

Yamashita, F, Mathias NR, Kim KJ, Lee VHL, 1996. Dipeptide transport properties of rabbit tracheal epithelial cell monolayers culturedat an air-interface, *Respiratory Drug Delivery*, 5, 432-4.

Yeh HC, Phalen RF, and Raabe OG, 1976. Factors Influencing the Deposition of Inhaled Particles. *Journal of Environmental Health prospect*, 15, 147-156.

Zaman M, Qureshi J, Ijaz H, Sarfraz RM, Khan MH, Chughtai FRS, Ur Rahman MS, 2016. Oral controlled release drug delivery system and Characterization of oral tablets; A review. *Pakistan Journal of Pharmaceutical Research*, 2 (1), 67-76.

Zanan P, Go LT, Lammers, JW, 1996. Optimal particle size for beta 2 agonist and anticholinergic aerosols in patients with severe airflow obstruction. *Journal of Thorax*, 51, 977-980.

Zhang W1, Kalive M, Capco DG, Chen Y, 2010. Adsorption of hematite nanoparticles onto Caco-2 cells and the cellular impairments: effect of particle size. *Journal of Nanotechnology*, (35):355103.

Zhao X, Heng BC, Xiong S, Guo J, Tan TT, Boey FY, Ng KW, Loo JS., 2011. In vitro assessment of cellular responses to rod-shaped hydroxyapatite nanoparticles of varying lengths and surface areas. *Nanotoxicology*, 5 (2), 182-194.

Zhou Q, Qu L, Larson I, Stewart PJ, Morton DAV, 2011. Effect of Mechanical Dry Particle Coating on the Improvement of Powder Flowability for Lactose Monohydrate: A Model Cohesive Pharmaceutical Powder. Journal of Powder Technology, 207 (103), 414-421.